University of Bath

PHD

Organophilic pervaporation: engineering science analysis and design tool

Ten, Po-Kiong

Award date:
2001

Awarding institution:
University of Bath

[Link to publication](#)

Alternative formats

If you require this document in an alternative format, please contact:
openaccess@bath.ac.uk

ORGANOPHILIC PERVAPORATION:

ENGINEERING SCIENCE ANALYSIS AND

DESIGN TOOL

By

Po-Kiong Ten

A thesis submitted to the University of Bath in accordance with the requirements for the degree of Doctor of Philosophy in the Faculty of Engineering and Design, School of Chemical Engineering, August, 2001

UMI Number: U533019

UMI

Dissertation Publishing

UMI U533019

ProQuest

DEDICATION

to *My Dearest Parents*

ABSTRACT

The main objective of this thesis is to present an advanced but simple to use performance modelling tool for organophilic pervaporation. The transport theory and processes of a commercial pervaporation membrane unit is reviewed and examined in three stages namely, (i) feed side boundary layer, (ii) selective layer and (iii) support layer. The effect of two dimensional flow in the support layer was also examined and was found to be negligible in commercial GKSS PDMS-Polysulfone composite membrane and composite membrane from Bath University. Based on the assumptions of negligible convective flow in feed side boundary layer and coupling effect in the composite membrane, a comprehensive transport model for commercial composite membrane that is based on solution-diffusion model is developed. The partial flux of component i is predicted by the following equation: $J_i = K_i (p_{f,i} - \Theta_i p_{p,i})$ where K_i, Θ_i, $p_{f,i}$ and $p_{p,i}$ are the overall mass transfer coefficient, the sorption-desorption coefficients ratio based on Henry's law, partial pressures at feed side and permeate side respectively. A novel approach has also been developed for determining intrinsic selectivity and the sorption-desorption coefficients ratio. The effect of permeate pressure upon performance has been investigated based on the comprehensive model. Different characteristics of response on performance has been derived and these characteristics has been validated by experimental data and data from literature. A performance classification diagram for various pervaporation systems that resembles the Geldart's powder classification diagram is also developed with co-ordinates E and y_i^*. E is related to the enhancement factor at the ultimate vacuum whilst y_i^* is the permeate composition at ultimate vacuum. By assuming the sorption-desorption coefficient ratios equal to unity, a crude evaluation of both E and y_i^* can be obtained from a single pervaporation experimental data and thus the effect of the permeate pressure upon performance profile can be predicted. Beside a model for performance, a novel analytical solution for sizing a pervaporation module unit is developed. Hence, the sizing tool has retained the characteristic of E but is expanded to a novel design concept for pervaporation, namely ATU (Area per Transfer Unit) and NTU (Number per Transfer Unit) by analogy to absorber unit design. The sizing tool can be applied to both continuous and batch modes. Factors that affect ATU's and NTU's for a particular system have been investigated. It has been found that the ATU and NTU concepts give insight in selecting and optimizing an appropriate membrane and module type and operation mode. For batch mode pervaporation, different process strategies are also developed to counter act variation in feed flowrate. Engineering analysis techniques developed for organophilic pervaporation also found to be useful in hydrophilic pervaporation

ACKNOWLEDGEMENTS

DECLARATION

This thesis entitled: Organophilic Pervaporation:-Engineering Science Analysis and Performance Modelling Tool, is submitted for the Degree of Doctor of Philosophy, in the Faculty of Engineering and Design, at the University of Bath.

The research, on which this thesis based was carried out between October 1996 and September 1999 under the joint supervision of Prof. Robert. W. Field, Prof. Brian. J. Brisdon and Dr. Richard England. It is due entirely to the author except where otherwise acknowledged in text and has not formed the basis of a submission for any other degree.

Signed.

Date...16/ 8/01

CONTENTS

Title page

Dedication

Abstract

Acknowledgements

Declaration

Contents

List of Figures

List of Tables

Notation

Part I   Introduction

LIST OF FIGURES

LIST OF TABLES

NOTATION

A	Arbitrary constant in equation (4.24) or	cmHg
	Total membrane area	m^2
a	Infinitesimal of membrane area	m^2
$\hat{a}$	Arbitrary constant in equation (6.15)	
a_i	Activity of component i	
B	Arbitrary constant in equation (4.26)	
$\hat{b}$	Arbitrary constant in equation (6.16)	
$C_{b,i}$	Bulk concentration of component i in the feed	$kmolm^{-3}$
C_m	Average total concentration of membrane	$kmolm^{-3}$
$C_{m1,i}$	Concentration of component i sorpted into the membrane adjacent to the feed side	$kmolm^{-3}$
$C_{m2,i}$	Concentration of component j sorpted into the membrane adjacent to the downstream side	$kmolm^{-3}$
$C_{mb,i}$	Concentration of component i adjacent to the feed side membrane surface	$kmolm^{-3}$
$C_{p,i}$	Concentration of component i in vapour permeate	$kmolm^3$
C_{tot}	Average molar density of feed liquid, $\cong \rho_j/M_j$	$kmolm^{-3}$
D_i	Dimensionless pressure ratio $= f_i/P_p$	
$D_{k,i}$	Knudsen diffusivity of component in the pore of support layer	m^2h^{-1}
$D_{l,i}$	Diffusivity of component i at the liquid feed	m^2h^{-1}
$D_{m,i}$	Diffusivity of component i in the membrane	m^2h^{-1}
$\overline{D}_{m,i}$	Mean diffusivity of solute	m^2h^{-1}
$D_{m0,i}$	Diffusivity of component i in the membrane at infinite dilution	m^2h^{-1}
E	Product of ultimate enhancement factor and the ratio of partition coefficients ratio $= K_i/K_j \cdot \Theta_i/\Theta_j$	
E^*	Ultimate enhancement factor = enhancement factor determined in ultimate vacuum = the ratio of mass transfer coefficient of component i to j $= K_i/K_j$	
E^*_{mem}	Intrinsic enhancement factor applied at ultimate vacuum and in absence of a boundary layer $= \hat{P}_{m,i}/\hat{P}_{m,j}$	

E'	Enhancement factor $= \alpha_{PV} / \alpha_{VLE}$	
F_f	Feed molar flow rate into a membrane unit	kmol h^{-1}
f_i	Pseudo-vapour pressure of component i or the ratio of the saturated vapour pressure to the partition coefficient ratio $= p_{f,i} / \Theta_i$	cmHg
F_R	Retentate molar flow rate exiting from the membrane unit	kmol h^{-1}
I_{cp}	Degree of concentration polarization	
J_i	Partial flux of component i	kmolm^{-2}h^{-1}
J_j	Partial flux of component j	kmolm^{-2}h^{-1}
$J_{p,i}$	Molar flux of the component through the pores of support	kmolm^{-2}h^{-1}
$J_{sm,i}$	Molar flux of the component through the support matrix	kmolm^{-2}h^{-1}
J_{tot}	Total flux $= J_i + J_j$	kmolm^{-2}h^{-1}
$K_G a$	Overall mass transfer coefficient in gas	kmol h^{-1}
K_i	Overall mass transfer coefficient of component i , see equation (3.144)	kmolm^{-2}h^{-1}cmHg^{-1}
K_j	Overall mass transfer coefficient of component j	kmolm^{-2}h^{-1}cmHg^{-1}
k_l	Diffusive velocity $= D_{l,i} / \delta_l$	mh^{-1}
L_i	Phenological coefficient account for mobility due to individual component	kmolm^{-2}h^{-1}
L_{ij}	Phenological coefficient account for mobility due to mutual drag	kmolm^{-2}h^{-1}
m	Total moles in the process tank of batch pervaporation	kmol
m_1	Initial total moles in the process tank of batch pervaporation before processing	kmol
m_2	Final total moles in the process tank of batch pervaporation after processing	kmol
$\dot{m}_G$	Molar feed flow rate of a gas stream to be stripped by gas stripper	kmol h^{-1}
M_i	Molar mass of component i	kg kmol^{-1}
M_j	Molar mass of component j	kg kmol^{-1}
Pe	Peclet number $= \bar{u} / k_l$	
p_f	Feed pressure in gas separation	cmHg
$p_{f,i}$	Partial pressure of component i at the feed	cmHg
P_i^*	Partial pressure of component I adjacent to the downstream surface of the membrane	cmHg
P_i^{sat}	Saturated vapour pressure of pure component i	cmHg

P_j^{sat}	Saturated vapour pressure of pure component j	cmHg
$p_{mb,i}$	Partial vapour pressure of component i adjacent to the feed side membrane surface	cmHg
$\hat{P}_{kud,i}$	Permeability of component i in the unfilled pores of the support due to Knudsen diffusion	kmolm^{-2}h^{-1} cmHg^{-1} m^{-1}
$\hat{P}_{m,i}$	Permeability of component i in membrane	kmolm^{-2}h^{-1} cmHg^{-1} m^{-1}
$\hat{P}_{m,i}^{G}$	Permeability of gaseous component i in membrane	kmolm^{-2}h^{-1} cmHg^{-1} m^{-1}
$\overline{P}_{pore}$	Mean permeability of component i in the pores of support	kmolm^{-2}h^{-1} cmHg^{-1} m^{-1}
P_p	Permeate pressure or downstream pressure	cmHg
$p_{p,i}$	Partial vapour pressure of component i in the permeate	cmHg
Q	Permeate product rate drawn from the membrane unit	kmol h^{-1}
q	Local permeate product rate drawn from the membrane unit	kmol h^{-1}
R	Universal gas constant	kJ kmol^{-1}K^{-1}
R_{bl}	Liquid boundary layer resistance of component i	hm^{2}cmHg kmol^{-1}
r_p	Mean pore radius of the support	m
$R_{sup,i}$	Support layer resistance of component i	hm^{2}cmHg kmol^{-1}
$R_{top,i}$	Top selective layer resistance of component i	hm^{2}cmHg kmol^{-1}
S_i^a	Partition coefficient based on the activity of component adjacent to the feed side	
S_i^d	Partition coefficient based on the activity of component adjacent to the permeate side	
S_i^f	Partition coefficient based on the partial pressure adjacent to the feed side	kmolm^{-3}cmHg^{-1}
S_i^p	Partition coefficient based on the partial pressure adjacent to the permeate side	kmolm^{-3}cmHg^{-1}
T	Thermodynamic temperature	K
$\overline{u}$	Convective velocity	mh^{-1}
v_i	Local velocity of component i	mh^{-1}
W	Permeate product collected at the end of batch pervaporation process	kmol
$w_{f,i}$	Mass fraction of component i at the feed inlet of the membrane unit	
$w_{R,i}$	Mass fraction of component i at the retentate of the membrane unit	

X	Effective diffusion distancce	m
$x_{l,i}$	Mole fraction of component i at process tank of batch pervaporation before processing	
$x_{2,i}$	Mole fraction of component i at process tank of batch pervaporation after processing	
$x_{b,i}$	Mole fraction of component i at the bulk feed	
$x_{b,j}$	Mole fraction of component i at the bulk feed	
$x_{f,i}$	Mole fraction of component i at the feed inlet of the membrane unit	
x_i	Feed mole fraction of component i in the feed	
x_j	Feed mole fraction of component j in the feed	
$x_{mb,i}$	Mole fraction of component i adjacent to the feed side of membrane surface	
$x_{R,,i}$	Mole fraction of component i at the retentate of the membrane unit	
$y_{f,i}$	Permeate concentration corresponds to feed concentration at the inlet of membrane unit	
y_i^*	Mole fraction of component i in the permeate at ultimate vacuum	
y_i	Mole fraction of component i in the permeate	
$\bar{y}_i$	Mean component mole fraction in the permeate product	
y_{in}	Mole fraction of gas in the inlet stream of a gas stripper	
y_i^{VLE}	Mole fraction of component i in vapour phase due to vapour equilibrium	
y_j	Mole fraction of component j in the permeate	
y_j^{VLE}	Mole fraction of component j in vapour phase due to vapour equilibrium	
y_{out}	Mole fraction of gas in the outlet stream of a gas stripper	
$y_{R,i}$	Permeate concentration corresponds to retentate concentration at the inlet of membrane unit	
z	Distance in the direction of the flux	m

Greek letters

α_{mem}	Intrinsic selectivity of gas separation membrane or the ratio of the permeabilities of the components through the membrane.
α_{PV}	Separation factor or selectivity due to pervaporation

α^{*}_{PV}	Separation factor due to pervaporation at permeate pressure = 0 $= E^{*}\alpha_{VLE}$	
α_{VLE}	Separation factor (selectivity) of vapour liquid equilibrium	
β	Dimensionless parameter = $\alpha^{*}_{PV}/(\alpha^{*}_{PV}-1)$	
β_i	Solute enrichment factor = $y_i/x_{b,i}$	
δ_{sup}	Effective support layer thickness	m
δ_m	Effective diffusion transport distance of a component in the selective part of the membrane.	m
δ_l	Boundary layer thickness	m
δ_{sup}	Support layer thickness	m
δ_{top}	Top selective layer thickness of a composite membrane	m
ε_s	Surface porosity of the support	
ε_{bl}	Effectiveness factor due to boundary layer resistance	
ϕ	Volume fraction or Cut-stage of a membrane unit	
ϕ_{batch}	Cut-stage for batch pervaporation	
$\phi_{m,i}$	Volume fraction of component i in the membrane	
$\phi_{ml,i}$	Volume fraction of component i in membrane that adjacent to the feed side	
$\phi_{m2,i}$	Volume fraction of component i in membrane that adjacent to the permeate side	
γ_i	Activity coefficient of component i	
γ_j	Activity coefficient of component j	
μ	viscosity of the liquid	Pa s
$\mu_{m,i}$	Chemical potential of the component in the membrane	kJ
Θ_i	Partition coefficient ratio of component i, $= S^{p}_{i}/S^{f}_{i}$	
Θ_j	Partition coefficient ratio of component j, S^{p}_{j}/S^{f}_{j}	
ρ_L	Liquid density	kgm^{-3}
$\tilde{\rho}_l$	Average molar density of the liquid $\cong \rho_j/M_j$	kmolm^{-3}
ρ_m	Membrane density	kgm^{-3}

$\tilde{\rho}_{m,i}$	Molar density of component i in the membrane or $= \rho_m / M_i$	kmolm^{-3}
$\tilde{\rho}_{m,j}$	Molar density of component j in the membrane or $= \rho_m / M_j$	kmolm^{-3}
υ_i	Molar volume of component i	m^{3}kmol^{-1}
ψ	Filling fraction in the pore of the support layer	

Subscript

b	Bulk condition of liquid feed
bl	Boundary layer
GS	Gas separation
i	Solute or the targeted organic component in the separation
j	Solvent or some time refers to water
L	Liquid
m	Membrane
m1	Within membrane surface adjacent to feed side
m2	Within membrane surface adjacent to permeate
mb	Adjacent to feed side of membrane surface
mem	Membrane
pore	pore of the support
PV	pervaporation
skin	Skin layer of the phase inversion porous support
sup	Support layer
T	Total
VLE	Vapour liquid equilibrium

Superscript

f	Sorption interface
p	Desorption interface
VLE	Vapour liquid equilibrium
*	Ultimate vacuum

Chapter 1

Project Objectives and Thesis Layout

1.1   Project Objectives

The project was undertaken in order to achieve the following objectives:-

1. develop an advanced transport model for determining the intrinsic membrane transport properties[1] ;

2. make comparison between pervaporation and vapour permeation, develop analogies and identify the important parameters that influence the performance[2,4];

3. investigate the influence of downstream pressure upon performance by using the advanced developed transport model and deduce an advanced classification method to account for system behaviour[4,6];

4. develop a novel design tool for determination of area, energy requirement and process development by using the advanced model developed[3,5];

5. assess potential of functionalised pervaporative membranes for the removal of organic contaminants from aqueous streams by using the novel design tool developed[3,5].

The scientific contributions from this project at various citations are shown below:

1.   Ten, P. K., Field, R. W., Brisdon, B. J, England, R. and Bennett, M. "A Simplified Method for the determination of intrinsic selectivity in Pervaporation." *IChemE Research Event 1998, Newcastle, IChemE, UK,* (1998)

2.   Ten, P. K. and Field, R. W. "Organophilic Pervaporation" in Membrane Workshop "Membrane processes call on expanded limits." *Nordic Network in Membrane Technology,* 1998, Trondheim, Norway, (1998)

3.   Ten, P. K. and Field, R. W. " Removal of VOCs by Pervaporation: A Design Tool for Process Development" Oral Presentation at the *International Conference on Membrane and Technology,* Beijing, China., p99-100, (1998)

4.   Ten, P. K. and Field, R. W. "Organophilic Pervaporation: An engineering analysis of component transport and the classification of behaviour with reference to the effect of permeate pressure" *Journal of Chemical Engineering Science,* Vol. 50 (2000) p1425 - 1445

5. Ten, P. K. and Field, R. W. "Analytical Analysis of Pervaporation Unit Design" *American Institution of Chemical Engineering Journal*, (2000) (Submitted)

6. Lipnizki, F., Hausmann, S., Ten, P. K., Field, R. W., Lauffenburg, G. " Organophilic Pervaporation: Prospect and Advances" *Journal of Chemical Engineering*, 73 (1999) p113-129

7. Lipnizki, F., Field, R. W., Ten., P. K. " Pervaporation-based hybrid process: a review of process design, applications and economics" *Journal of Membrane Science*, 153 (1999) p183-210

1.2   Background

Interest in pervaporation as a process for separating liquid mixtures can be traced back to the 19th century (Slater and Hickey 1989). It was not until the pioneering work of Binning and Lee, in the 1950's, that pervaporation was studied systematically as a means of separating organic liquids (Binning et al, 1961). These early studies did much to advance the understanding of the fundamentals of the pervaporation process, but no commercial applications were developed because of the lack of high performance membranes and module technology (Fleming and Slater, 1990). In the 1980s, GFT developed hydrophilic membranes for the removal of water from mixtures with organic liquids, which led to the commercialization of pervaporation for dehydration of alcohol and other organic solvents (GFT, 1993). GFT's demonstration of the energy efficiency and the relatively low cost of pervaporation at the industrial scale increased the interest in the development of pervaporation for other separations (Baker, 1992).

The application of pervaporation to the removal and recovery of volatile organic compounds (VOCs) from water is an emerging technology. There are many potential applications for this technology in the pharmaceutical, and food and beverage industries, both in the manufacturing process and as an environmental treatment technology (Wijmans et al, 1990; Barber and Miller, 1994). In the United States, Membrane Technology and Research Inc. (MTR) has been actively developing pervaporation technology for the removal of VOCs from water since 1983 (Blume and Baker 1987; Kaschemekat et al 1988). In 1992, MTR and the Pervaporation System Group of Hoechst Celanese formed Alliance to jointly develop and commercialise organophilic pervaporation technology for the removal and recovery of VOCs. (Membrane and Separation Technology Newsletter, June 1997). Their spiral wound membrane modules (PERVAP™ series) have shown success in various industrial wastewater applications (Athayde et al 1995). Other companies such as Zenon Environmental Inc.,

GKSS and Bend Research Inc., have also aggressively developed competitive organophilic pervaporative membranes, modules and processes (Shanley and Ondrey, 1994; McCray et al 1995). Recently the School of Chemical Engineering and Chemistry at the university of Bath have jointly developed a range of competitive and novel organophilic membranes via functionalisation of polydimethylsiloxane (PDMS) materials (Bennett, 1996; Bennett, 1997).

The major objective of this research is to develop a comprehensive and improved organophilic pervaporative transport model for determining the intrinsic membrane transport properties. This has lead to the ability to make comparisons between pervaporation and vapour permeation and useful analogies. The important parameters that influence the performance have been identified and the influence of downstream pressure upon performance has been investigated by using the developed transport model. A classification method to account for the system behaviour was developed. Finally a novel design tool for the determination of area requirement was produced and used to assess the process potential of the functionalised pervaporative membrane for the removal of organic contaminants from aqueous streams.

1.3   Layout of the thesis

In this thesis, theories of pervaporative transport are presented, a comprehensive transport model and a membrane area sizing tool are developed to enable the identification of important process parameters for engineering science analysis and assessment of the effect of functionalisation upon permeate pressure response behaviour. Thus, the thesis is in four parts: introduction, engineering science analysis, and performance modelling tool and conclusions.

In Chapter 1, the objectives of the research are stated and the background of the research is given.

Chapter 2, starts with an introduction of organophilic pervaporation, classification of various organophilic pervaporative membranes and modules are made. In this chapter, the importance of permeate pressure and predictive approaches are also discussed.

In Chapter 3, the current theories for pervaporative transport are reviewed.

The engineering science analysis and the performance modelling tool development are set out in Chapters 4, 5, 6 and 7.

In Chapter 4 an improved and comprehensive transport model for organophilic pervaporation is developed, a 2-D transport analysis of a composite membrane is also carried out, the engineering science analysis with respect to permeate pressure and the classification of system behaviour are also presented.

In Chapter 5 application of the engineering analysis is undertaken after an experimental section. The model and analysis was also tested by using literature data.

In Chapter 6 the membrane-sizing tool is developed and transfer units for pervaporation units are defined and discussed.

In Chapter 7 implications of the developed model and analytical tool for hydrophilic pervaporation are discussed.

In Chapter 8, the conclusions of the thesis are drawn and some recommendations for further research are suggested.

Part I   *Introduction*

Chapter 2

Introduction

2.1 Chapter Objectives

- To give an introduction to pervaporation, particularly organophilic pervaporation.
- To examine the current availability of organophilic pervaporation membranes and modules.
- To give a literature review on the analysis of organophilic pervaporation performance with particular regard to varied permeate pressure.

2.2 Introduction

New chemical separation techniques are becoming increasingly important as the regulatory focus shifts from end-of-pipe treatment to pollution prevention and resource recovery. As industries strive to meet the rising standards set by the environmental agency and counter the threat of fuel taxes from the "green orientated" government, new opportunities are being created for membrane separation. Companies that are positioned to use this technology for pollution prevention will reap the greatest reward (Cartwright, 1994). Among the membrane technologies, an emerging technology named organophilic pervaporation has created a growing interest among chemical and pharmaceutical industries. This emerging technology has been proven effective in removing volatile organic compounds (VOCs) from water for recycle and reuse (Lipnizki et al, 1999).

2.2.1 Why organophilic pervaporation?

Contamination of industrial effluent waters with dissolved organic solvents, such as methanol, ethanol, chloroform, methyl ethyl ketone (MEK), methyl-iso-butyl-ketone (MIBK), phenol, pyridine, benzene, toluene, and trichloroethane, has posed an important environmental problem. These solvents make water unfit for reuse or direct discharge to

municipal sewers, and are difficult to remove, even at low concentrations (UK Environment Agency, 1995).

Commonly used methods for removing volatile organic compounds include air-stripping, biological treatment, carbon adsorption and incineration. Air-stripping, in which water is circulated against a current of air in a contacting tower, is the least expensive process. However, air stripping merely exchanges water pollution for air pollution. Air-stripping is therefore seldom used if the solvent concentration exceeds 0.1%, and even then only for small streams where the total organic emission is less than 4.5-45kg/day (Baker and Wijmans, 1992). Carbon adsorption, a principal effluent technology for very dilute streams, is typically 1,000ppm or less, and more usually 100ppm or less (Blume and Baker, 1987). At these very low concentrations, carbon adsorption is a preferred technique, because the size of the plant scales in proportion to the amount of solvent removed. Thus, when the solvent concentration is very low, the amount of wastewater that can be treated by a small carbon adsorption system is high. However, once the feed solution concentration exceeds 1,000 ppm, carbon adsorption systems become very large per cubic metre of wastewater treated. In addition, carbon adsorption systems cannot handle some chlorinated and fluorinated solvents, and generate secondary waste, in the form of spent contaminated carbon, that may be sent to landfill. Biological treatment systems work well only for organics that can be fully metabolized by biomass, and where the process is not compromised by high or fluctuating solvent concentrations. At the high concentration end of the scale, incineration is reliable and effective for very concentrated streams, where the heat value of the solvent reduces the amount of supplemental fuel required. Typically, incineration is impossibly expensive at concentrations below 5% (Blume and Baker, 1987).

Thus there is a dissolved organic concentration range for which no conventional wastewater treatment method is really suited. Currently this range is avoided by pooling or diluting the waste to the point where it can be treated by carbon adsorption or biological processes, or concentrating it so that incineration can be used. There remains a real and long-felt need for a low cost method for directly treating contaminated streams, with an organic content of about 0.1% up to about 8 or 10%, to produce an effluent suitable for direct discharge or biological treatment, and a low-volume concentrated stream containing the bulk of dissolved organics, from which the organic component can be recovered. This long-felt need is now being fulfilled by an emerging technology, namely the **organophilic**

pervaporation technology (Baker and Wijmans, 1993). According to an investigation from Smithklime Beecham Plc (Freitas and Biundo, 1999), the annual cost of organophilic pervaporation is among the lowest and if recycle of organics is necessary, organophilic pervaporation is the choice for cost effective recovery of VOCs from wastewater (See table 1.1).

Table 2.1: Comparison of Capital and Operating Cost Estimates for Alternative VOC Removal Technologies in Wastewater Treatment
(Freitas and Biundo, 1999)

Technologies	Capital Cost (thousand)	Operating Cost (thousand)	Annualized cost ($£/m^3$)	Additional treatment
Carbon adsorption	£300	£40 (with regeneration) £80 (without regeneration)	12.5 17.5	Yes
Steam stripping	£150	£25	6.8	Yes
Air-stripping + Bioscrubbing	£125-150	£15	5.6	Yes
Extractive Membrane Reactor	£120	£15[*]	4.8	No
Organophilic Pervaporation	£110	£32	2.5	Yes[**]

* No labour cost included   ** The permeate product can be recycled for reuse

2.3 Organophilic pervaporation

Pervaporation is a *rate controlled process* that is characterised by the imposition of a barrier (membrane) layer between a liquid and a gaseous phase, with mass transfer occurring selectively across the barrier to the gas side. The unique phenomenon of a phase change being required of the liquid solutes diffusing across the membrane (i.e. permselective transport and "evaporation" of the liquid molecules), has given the process the name as "pervaporation" (Neel, 1991). It is graphically illustrated in Figure 2.1. Consider pervaporating an aqueous stream. If the preferential permeant is the organic component, the process can be termed as **organophilic** pervaporation, otherwise it is termed as **hydrophilic** pervaporation. Organophilic pervaporation is mainly applied to the removal of organics from

7

aqueous streams while the hydrophilic pervaporation is applied to the dehydration of organics. It should be noted that an organic-organic pervaporative separation is also labelled as organophilic pervaporation in the literature. In this thesis, the term *organophilic pervaporation* will be used throughout as referring to the removal of organics from aqueous streams and not organic-organic separation.
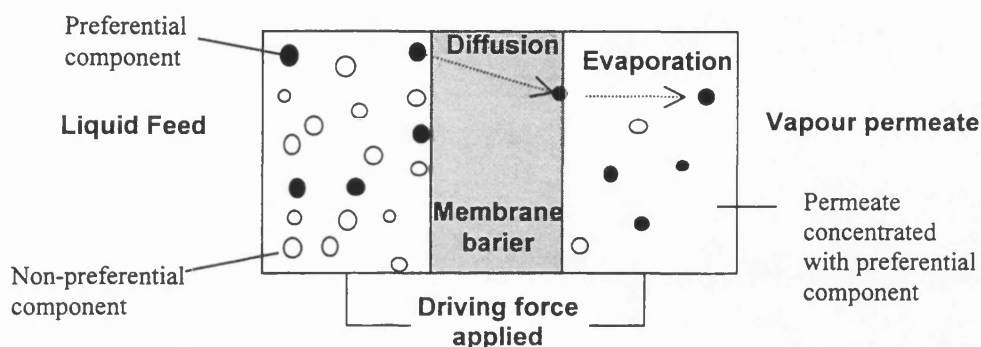
Fig 2.1 Components separation by pervaporation

The driving force of mass transport in pervaporation is actually the chemical potential gradient across the barrier (membrane). Hence, three modes of pervaporation (PV) have been realised (Fig. 2.2).

a. Pressure driven PV   b. Thermal driven PV   c. Inert sweep gas driven PV
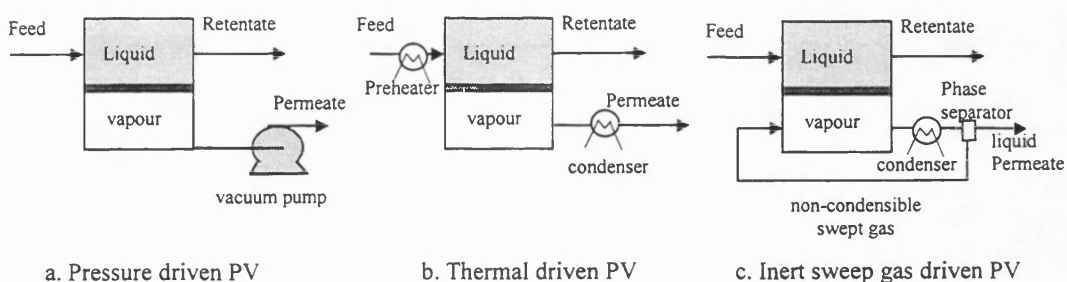
Fig 2.2: Various modes of PV operation (Fleming and Slater, 1992)

1. <u>Vacuum driven pervaporation</u>: A vacuum pump on the permeate side creates a partial pressure gradient.

2. Thermopervaporation: A difference in partial pressures (chemical potentials) may also be realised by temperature gradient provided the non-condensable gases are excluded from the permeate side. This type of pervaporation process is sometimes called thermopervaporation. However, such an operation mode requires the exclusion of non-condensable gases via a vacuum pump at the permeate side prior to the pre-heating of feed mixture to a temperature that is substantially above the permeate. Thus, thermopervaporation should be addressed as vacuum pervaporation (Boddeker, 1990).

3. Inert gas sweeping driven pervaporation: Pervaporation can be also be driven simply by an inert sweep gas on the permeate side. A condenser is necessary downstream to remove the condensing permeates from the sweep gas.

2.4   Classification of pervaporative membrane

Although only two types of pervaporation membrane have been extensively used commercially, (polyvinylalcohol (PVA) membrane, for hydrophilic and polydimethylsiloxane (PDMS) membrane, for hydrophobic separations) many other polymer materials have been investigated, as pervaporative membranes, on a laboratory and in a few cases, pilot plant scale. It is useful to classify these polymers into a number of groups. Roughly speaking all polymers can be classed as either glassy or rubbery polymers and a number of sub classes exist within these two groups, as discussed below (Koops and Smolders, 1991).

2.4.1 Glassy Polymers

These have a glass transition temperature above room temperature. Within this group, three types can be distinguished, crystalline, semi-crystalline and amorphous polymers. Generally it is the amorphous and semi-crystalline polymers that are most useful as pervaporation membranes. Membranes manufactured from these polymers tend to be hydrophilic and are used primarily for organic dehydration.

2.4.2 Rubbery Polymers

Rubbery, or elastomeric, polymers have a glass transition temperature below room temperature. They are very flexible, the main chain consisting of C-C, Si-O or C-O bonds. Due to the absence of polar groups in their flexible chains, elastomers preferentially absorb organic liquids with respect to water. This property makes them excellent candidates for being employed in the removal of organics from aqueous solutions.

2.4.3 Copolymers

These are polymers with two or more repeating units, i.e. different monomers that can be coupled together in various ways. Three types of copolymers can be distinguished:-

- Random copolymers - where the structural units are completely randomly distributed:

  -AAAABBBBBAAAAAAAAABBAAABBBBBBBB

- Block copolymers - where the copolymer is built up of blocks of monomers of fixed size:

  -AAAABBBBBAAAABBBBBAAAABBBBBAAAA-

- Graft copolymers - where a main chain built of the same repeating unit, has different monomer blocks, as side chains, irregularly distributed along the main chain:

```
      B
      B                                B
-AAAAAAAAAAAAAAAAAAAAAAAAAAAAAAAA-
                  B
                  B
                  B
```
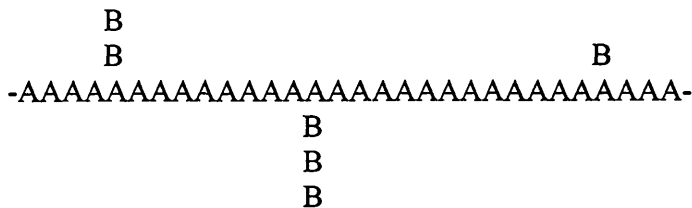
1.4.4 Polymer Blends

These are mixtures of two or more polymers that are not covalently bonded to one another. Two kinds of blend are distinguishable, homogeneous blends, in which the polymers are

miscible on a molecular scale and heterogeneous blends, in which the polymers are not completely miscible.

2.4.5 Ionic Polymers

These are polymers containing ionic groups which are covalently bonded to the polymer chain. Dependent on the sign of the charge of the ionic groups the membranes made of such materials are classed as either anionic or cationic exchange membranes. The charge of the fixed ionic group is neutralised by a counter ion. The counter ion may be either mobile or fixed, but the disadvantage with mobile counter ions is that they are washed out during pervaporation and need to be periodically replaced. All ion exchange membranes are hydrophilic and this makes them very suitable for the dehydration of organics. The membrane in this catagory that has been studied extensively at Bath is caesium poly(acrylate) (Burslem et al, 1992).

2.5   Organophilic pervaporative membrane

Most of the organophilic pervaporative membranes are rubbery membranes because of their hydrophobic nature. To assess the performance among various pervaporative membranes, the commonly adopted performance parameters are the separation factor (selectivity) and flux. The assessment is based upon the mass transfer of the preferential permeating species, irrespective of whether the depleted retentate (residue) or the enriched permeate is the target product of the process (Boddeker 1990). By definition, the separation factor (selectivity), α_{PV}, of the membrane towards a preferential permeating species, i, with respect to the non-preferential species, j, is the ratio of the analytical compositions of the permeate to the feed as shown in Fig. 2.3

Separation factor (Selectivity): $\alpha_{PV} = \dfrac{y_i / y_j}{x_i / x_j}$ (1.1)

11
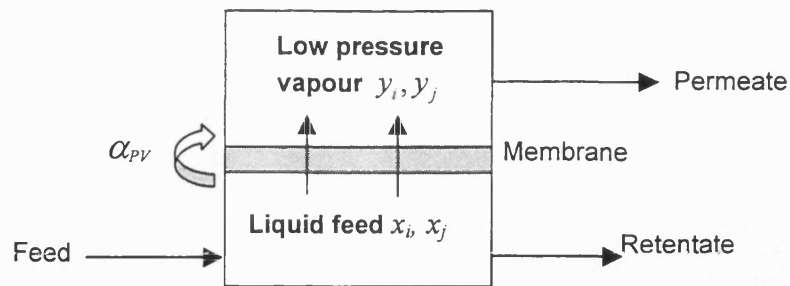
Fig. 2.3 : Definition of separation factor (selectivity) of pervaporation

It should be noted that, the separation factor is independent from the measure of concentration applied (e.g. mole fraction, mass fraction). The flux through a membrane is defined as the permeation rate per unit area of membrane. The units of permeate flux are usually expressed as $kg\ m^{-2}\ h^{-1}$ or $kmol\ m^{-2}\ h^{-1}$.

Table 2.2 Selectivities of PDMS membranes for pervaporation of organic compounds from wastewater (Boddeker and Bengston, 1989; Lipnizki et al, 1999)

Organic compound	Separation factor α_{PV}
Acetic acid	3
Ethanol	7
Phenol	27[a] (18)[b]
Acetaldehyde	48
Acetone	50
Pyridine	70 (56)[b]
Methyl-isobutylketone	705[b]
n-hexane	1300
Ethyl ether	1600
n-Butyl acetate	2300
1,2-Dichloroethane	4300
Chloroform	6800 (8510)[b]
Vinyl Chloroform	9000
Cyclohexane	9300
Toluene	10000
Benzene	11000
Styrene	13000

[a] based on Raghnunath and Hwang, 1992   [b] based on Bennett, 1996

An assessment made by Bruschke (1991) of GFT concluded that PDMS provides the best combination of properties with respect to flux, selectivity and stability for the removal of most organics. Table 2.2 shows the selectivity of this popular organophilic pervaporative membrane, towards various kind of organics with respect to water:

A further assessment by Bennett (1996) has found the performance of pervaporation for aqueous organics separation could be enhanced by the introduction of appropriate functional groups into normal PDMS membranes. Alternatively incorporation of a small portion of zeolite into PDMS has been found to be beneficial. In the following section, a brief review on PDMS membranes and modified PDMS will be presented

2.5.1 PDMS Membranes

PDMS membranes are characterised as containing a backbone of repeating dimethylsiloxane, $-Si(CH_2)_2-O-$, units. They are formed by cross-linking long, liquid, chains of PDMS with suitable short chained, silicone based, cross-linking agents. Membrane structures, typical of those generally achieved, are displayed pictorially in Fig 2.4. There may be substantial differences in membrane structure, particularly in the nature of membrane cross-linking, between PDMS membranes used in different studies. Membrane structure and properties may well depend upon PDMS chain length and the nature of the cross-linking agent. It is very uncommon for chain length, cross-linking density and membrane physical properties to be reported and this may explain the sometimes substantial differences in performances reported between different studies for essentially the same separation.
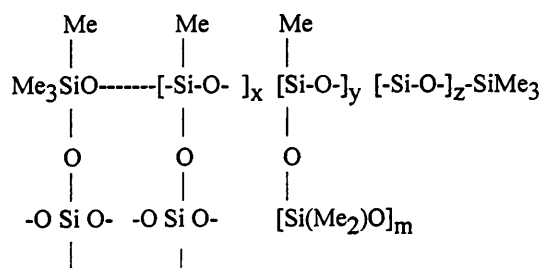
Fig 2.4 Cross Linked PDMS Membrane

PDMS belongs to a family of materials classified as silicone rubber. However, some researchers in reporting their pervaporation data, named their membrane as silicone rubber membrane. However, silicone rubber tubing or membrane might contain not only the repeating dimethylsiloxane units, but also contain different or additional units such as diethyl / dipropyl / etc. - methylsiloxane. Care should be taken when comparing the performance of this material with PDMS.

Pure PDMS membranes are fairly strong and it is relatively easy to form them into homogeneous films. In order to enhance mechanical rigidity and to allow the production of membranes with very thin active layers, it is common practice, throughout all areas of pervaporation, to form the dense layer on top of a strong microporous support material. The composite, asymmetric membrane so formed may exhibit significantly different performance to a homogeneous film. The support material itself may create a resistance to material transport through the membrane. Again it is uncommon to find data reporting the influence of the support material and variation between different studies could be partially explained by the use of different support materials.

2.5.2 Zeolite Filled and Modified PDMS

Numerous authors have studied the effect of incorporating zeolites into the PDMS membrane structure, in an attempt to enhance membrane performance. Zeolites are porous alumino-silicates and may be tailored to be either hydrophobic or hydrophilic by adjusting the ratio of aluminium to silicon (Hennepe et al, 1987). A decrease in aluminium content leads to increased hydrophobicity. A number of silicate rich zeolites have been investigated for this purpose and the most successful membranes contain either silicalite, of which commercially available membranes are available from GFT, or ZSM-5 (Vankelecom et al, 1995).

Hydrophobic zeolites enhance organic component permeability by increasing the sorption of the component into the membrane structure. At the same time water permeability is reduced as water is excluded from entering the zeolite particles. This leads to both decreased sorption of water and an increased path length for the water molecules, as they have to take a more tortuous path to travel through the membrane (Hennepe et al, 1991).

From the study of Goethaert et al (1992), selectivity towards chloroform can be significantly enhanced by the incorporation of zeolite. However, as described by Bennett (1996), the zeolite has very little effect upon selectivity towards pyridine. It has been found that the transport of small organic molecules is generally enhanced by the zeolite, but that voluminous molecules may be partly or totally excluded from entering the zeolite pores, due to the molecular sieving effect (Dotremont et al, 1995).

A few attempts have been made to modify PDMS in other ways, in order to enhance performance, particularly for the industrially important separation of ethanol from water. Segmented polyurethaneurea, containing PDMS as the soft segment and PDMS / polystyrene graft copolymers have been produced for this separation (Takegami et al, 1992). No great improvements in selectivity or permeability were realised. Fairly significant enhancements in selectivity, for the same separation, have been achieved by PDMS / PTMSP copolymer blends (Slater et al, 1990), although absolute selectivities are still not very high. The addition of a fluorinated, surface modifying copolymer was found to make the membrane more hydrophobic and led to an enhanced separation factor, towards ethanol, of 16.6 from 12.1 (Aoki et al, 1993).

Replacing the methyl groups with octyl groups has been found to enhance the selectivity of silicone rubber towards certain organics (Shanley et al 1994). It has also been shown that the permselectivities of PDMS membranes towards certain gas molecules can be improved significantly, without appreciable loss of flux, by introducing various organofunctional side chains (Ashworth et al, 1991)

$$\begin{array}{ccc} \text{Me} & \text{Me} & \text{Me} \\ | & | & | \\ \text{Me}_3\text{SiO-[-Si-O-]}_x & \text{[Si-O-]}_y\text{[-Si-O-]}_z\text{-SiMe}_3 \\ | & | & | \\ \text{O} & \text{[CH}_2\text{]}_n & \text{O} \\ | & | & | \\ \text{-O- Si O-} & \text{R} & \text{[Si(Me}_2\text{)O]}_m \\ | & & | \\ \text{O} & & \text{O} \\ | & & | \end{array}$$
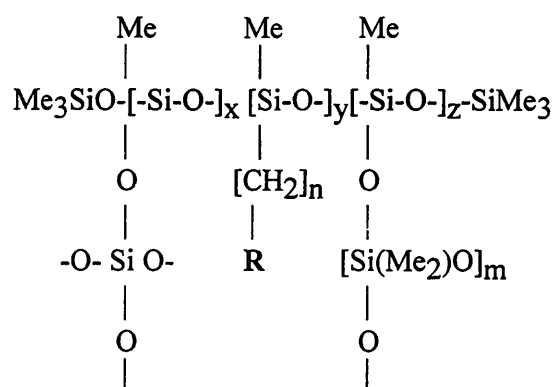
Fig 2.5. Cross Linked Organofunctional Siloxane Membrane

However, in the study on the pervaporation of organics especially pyridine and MIBK (Bennett, 1996), Bennett found that an increase of selectivity was compensated by a loss of permeability when a long chain or bigger functional group was introduced into PDMS. It was suggested that a thinner membrane might enhanced the flux without an appreciable loss of selectivity giving overall a lower membrane area requirement compared to normal PDMS whilst achieving the same task (Bennett, 1996).

2.5.3 Composite Membranes for Organophilic pervaporation

Dense homogeneous polymer films can achieve a high separation factor, but because of the relatively thick size (20-200μm) this has led to low permeation rates. In order to improve the permeation rates, the membrane are usually made thin enough ~10μm with a porous membrane as its support for sake of mechanical strength. Table 2.3 shows some commercialised PDMS and other organophilic pervaporation membranes

Table 2.3. Some commercialised organophilic pervaporation membrane (Ten, 1997)

Organization	Membrane	Composite (C) /Homogeneous (H)	Material of the active layer
GFT (Sulzer/	PDMS-1060	C	PDMS (30μm)
ChemTech)	PDMS-1070	C	PDMS + silicate (30μm)
Dow Corning	PDMS	C	PDMS
General Electric	PDMS	C	PDMS
	Vinyl-PDMS	C	Vinyl terminated PDMS
	PTMS-PDMS	C	Polytrimethylsiloxane blended with PDMS
Hoechst Celanese	PDMS-PT1100	C	PDMS
GKSS	POMS-PEI	C	Octyl- functionalised silicone
	POMS-PVDF	C	Octyl- functionalised silicone
	POMS-PVDF	C	Octyl- functionalised silicone
	PEBA	H	PEBA (70μm)

2.6 Organophilic pervaporation membrane module

The key to the successful application of pervaporation lies in the development of both the membrane and the module. The choice of membrane is critical, however, the hydrodynamic mass transfer on the feed side and on the permeate side can also affect the separation quality. Further, the choice of modules also influences the process economics. Generally, the cast membranes can be packaged into modules of several commercially available module geometries (Lipnizki et al, 1999) which are shown in Figure 2.6 - 2.9. Table 2.4 shows the cost and packing density of the current commercially available modules.

The plate-frame module requires the use of gasket materials that are resistant to corrosion. The hydrodynamic mass transfer resistance can become a limiting factor for separation in plate-frame modules, thus necessitating a high feed velocity to enhance feed side mass

transfer. For the separation of VOCs from water, a relatively inexpensive spiral wound modules made from plastics can also be used. To increase hydrodynamic mass transfer in the spiral wound modules, feed spacer design needs to be modified. For the hollow fibre module, a high packing density can be reached. The problems encountered with this module are longitudinal pressure build up on the permeate side (Fleming and Slater, 1992; Rautenbach and Albrecht, 1989; Hickey and Gooding, 1994). However, a novel design that gives good mass transfer on the feed side and low pressure drop at the permeate side is the pocket module of GKSS Research Centre Geesthacht GmbH, Germany (Sturken, 1994) which is shown in Fig. 2.9.

Table 2.4   **Module design characteristics** (Singh, 1998)

Module characteristics	Hollow fibre	Spiral wound	Plate-frame
Manufacturing cost[a], ($£/m^2$)	35-135	200-670	200-2000
Relative expense	Low	Low	High
Packing density	~1800-3600	~300	~150

[a] include the cost of membranes and modules
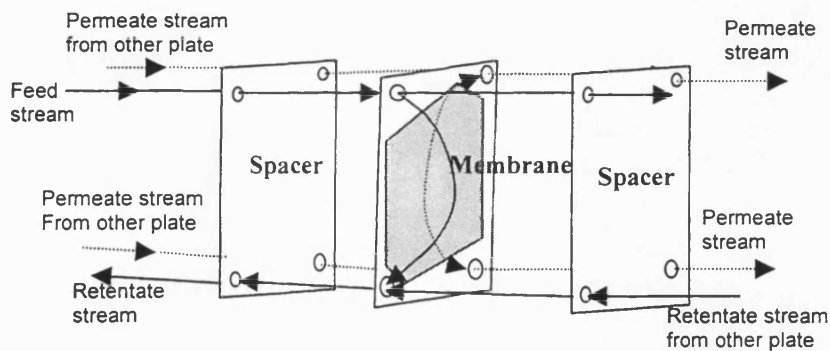
Fig. 2.6   Plate-frame modules (Adapted from Sander and Soukup, 1988)
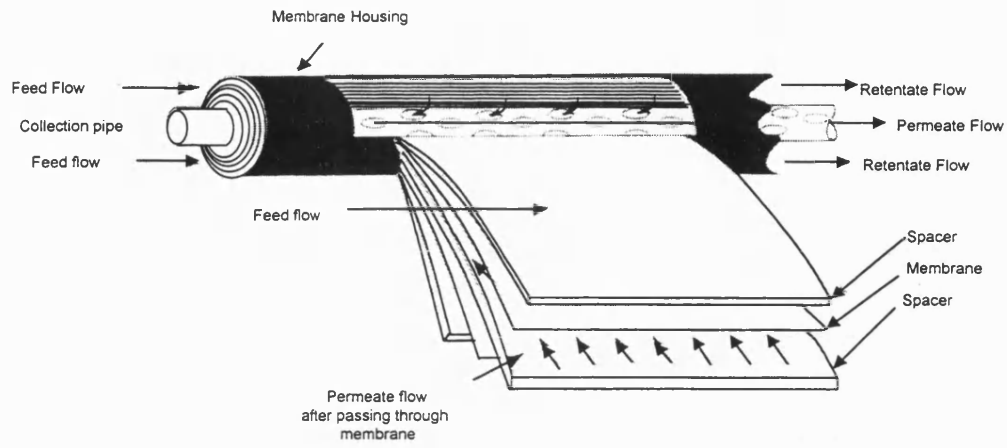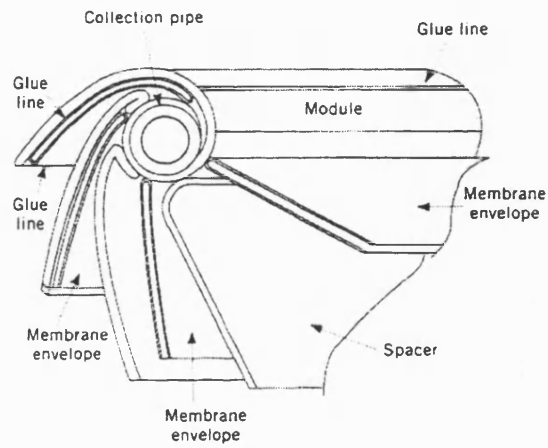
Fig. 2.7 (a) A cross-sectioned spiral-wound module; (b) An illustration on how the leaves in spiral-wound module are formed. (Adapted from Baker, 1996)
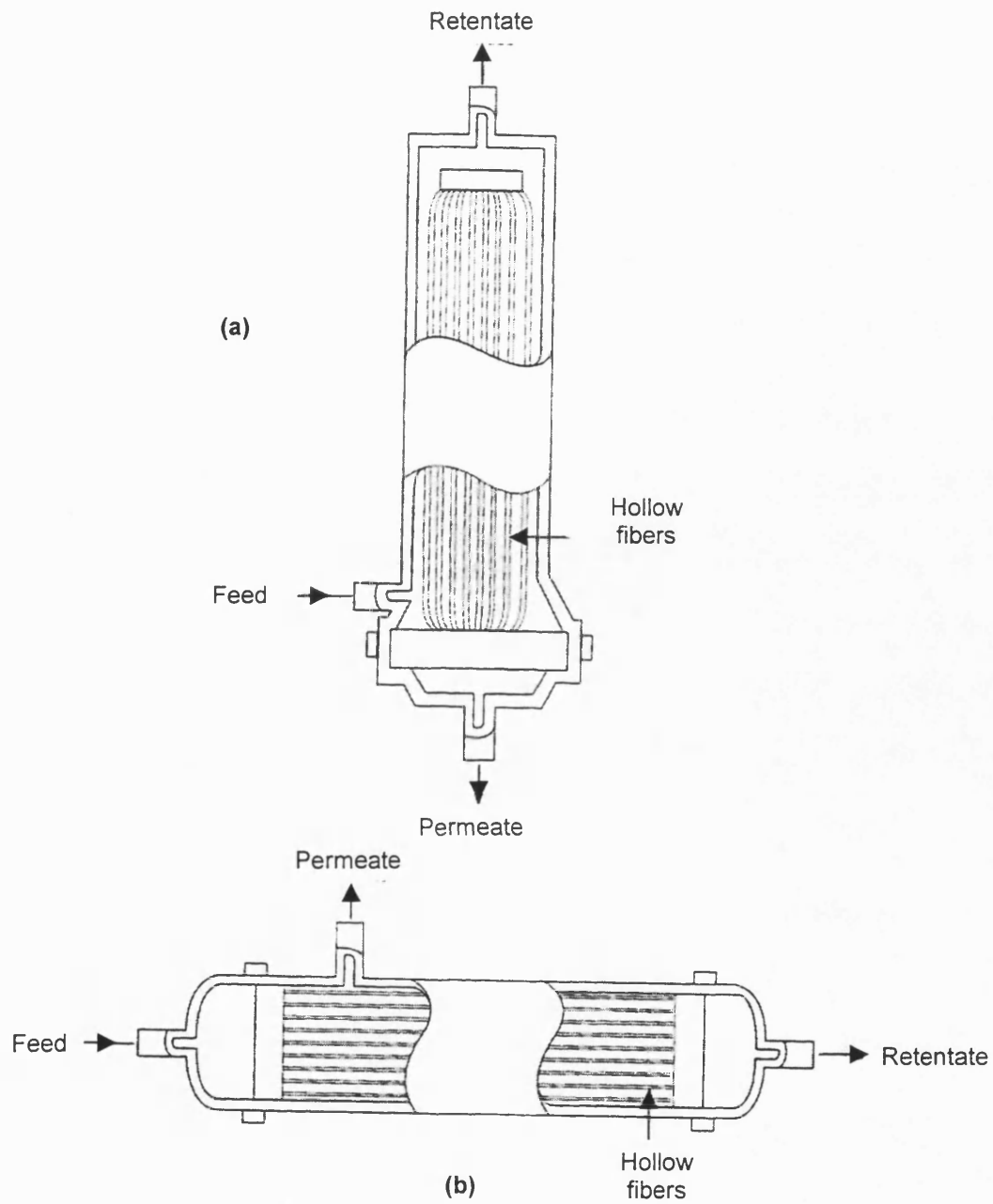
Fig. 2.8 Hollow-fibers / tubular module with two different mode of operations: (a) shell-side feed and tube-side permeate; (b) tube-side feed and shell-side permeate. (Adapted from Baker 1996)
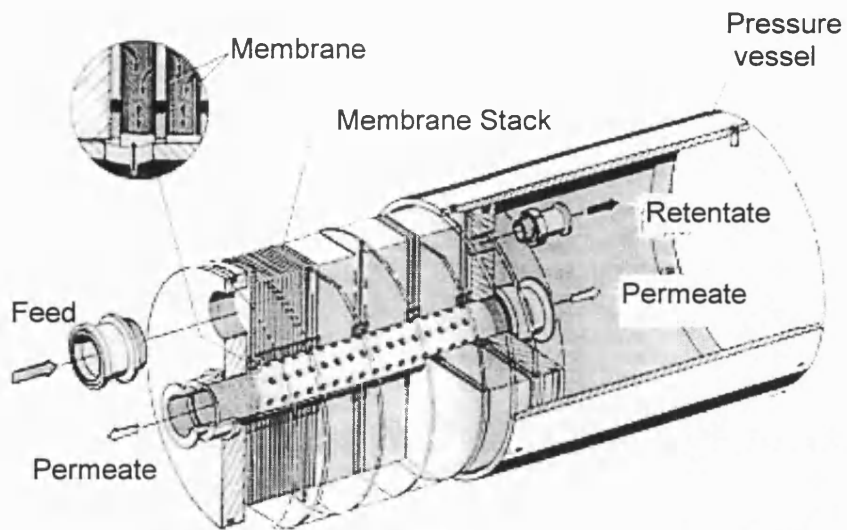
(a)
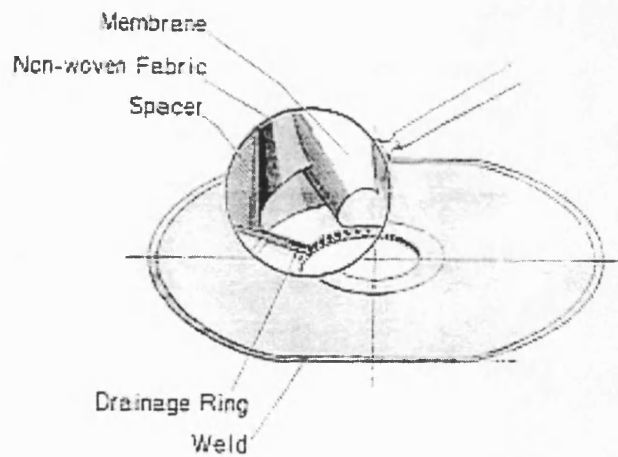
(b)

Fig 2.9 GKSS Gmbh's pocket module for pervaporation:
(a) module cross-section; (b) membrane disc cross-section.

(Adapted from Sturken, 1994)

2.7 The importance of permeate pressure

In pervaporation, a very important parameter is the permeate pressure in the module. With a variation in permeate pressure, the driving force for the process will vary and consequently the fluxes across the membrane. The vacuum provides the driving force but the cost of the vacuum system increases rapidly with the quality of the vacuum (Nguyen, 1987; Karlsson and Trägårdh, 1993). A perfect vacuum is a goal beyond reach but the limit is of great theoretical interest. There is a need to develop a simple model that can predict the variation in performance with respect to permeate pressure.

Several authors have tried to predict transport performance as a function of downstream pressure. Thompson and co-workers (Greenlaw *et al*, 1977a; Greenlaw *et al*, 1977b; Shelden and Thompson, 1978; Shelden and Thompson, 1984) developed a model that described how the separation factor and fluxes were affected by permeate pressure changes during pervaporation. Their model was one of Fickian diffusion with consideration being given to diffusion coupling. Nguyen (1987) developed a pervaporative transport model including the evaporation step of the permeants from the downstream interface that was considered as offering the rate limiting resistance. When explaining the deviation between experimental results for the pervaporation of water through PEBAX membranes and the behaviour predicted by the solution-diffusion model, Bode et al (1993) invoked a hypothesis concerning the downstream interface. Some back diffusion of vapour from the bulk of the permeate and their partial retrosorption into the membrane was envisaged. The mechanism for this is unclear. In the development below, the presentation is straightforward and it is simply assumed that the coefficient relating bulk activity to membrane concentration is not necessarily the same for the upstream and downstream faces of the membrane.

For composite membranes, Rautenbach et al (1989) estimated that the porous support could constitute an important resistance to the permeate transport and Liu et al (1996) modelled the effect of downstream pressure by the inclusion of molecular diffusion in the support layer. However, no experimental verification was demonstrated. The comprehensive approach developed by Ten and Field (2000) allows for both the contributions of the support and the

interaction between it and the active layer to the overall resistance. A detailed description can be found in Chapter 4.

Böddekker et al (1993) suggested that there is a desorption resistance for pervaporation of high boilers. Whether this is a real effect or simply an apparent effect due to the adverse influence of decreasing volatility upon the overall driving force is unclear. Ten and Field (2000) have clearly shown that for high boilers the performance is very pressure sensitive. Besides the possible resistance located near to the downstream side of the membrane, Beaumelle and Marin (1994) have pointed out that limitations to permeate transport can occur in the permeate circuit from the membrane to the condenser. This consideration is particularly important on the industrial scale.

In general, from the literature above, there are two approaches to predict the performance of pervaporation with respect to permeate pressure:

(1) Empirical/Numerical analysis: This is the most common approach that is used to analyse the performance of pervaporation with respect of permeate pressure. The approach requires many experimental data to form a general trend of change. Usually, if the errors in the experiments are significant, the analysis could give a misleading the interpretation. If a complex transport model is used, a time consuming numerical integration is needed and the interpretation usually is confined to a single system.

(2) Engineering science analysis: This approach usually involves a simplified theoretical transport model and by examining the limiting cases, a prediction of performance profile can be reached. The advantage of using such a method is the generality of the approach. Method of solving is simple and comparable. To date, only a few researchers (Gooding *et al*, 1991; Watson and Payne, 1990; Blume *et al*, 1990; Wijmans and Baker, 1993) have examined the limiting case or used dimensionless terms to predict pervaporation performance. In the present work allowance for all effects is made and dimensionless terms introduced into the field of pervaporation to describe performance. Table 2.5 shows the engineering science analysis carried out by various researchers and the comprehensiveness of their transport model. The work of Ten and Field (2000) is detailed in Chapter 4.

Table 2.5 Factors included in the analysis of organophilic pervaporation performance

Factors include / Authors	Effect of Activity Coeff.	Boundary layer	Active Layer		Support Layer	Performance Profile Prediction				Availability of Predictive Dimensionless Parameter
			$S_i^f = S_i^d$	$S_i^f \neq S_i^d$		y_i	α_{PV}	J_i	J_j	
Watson, 1990	✓	✗	✓	✗	✗	✗	✓	✗	✗	✗
Wijmans et al, 1993	✓	✓	✓	✗	✗	✗	✓	✗	✗	✓ α_{mem}, α_{VLE}
Gooding et al, 1991	✗	✓	✓	✗	✗	✗	D	✓	✓	✓ $\phi = \dfrac{\hat{K}_j P_j^{sat}}{\hat{K}_i P_i^{sat}}$
Ten and Field, 2000	✓	✓	✓	✓	✓	✓	✓	✓	✓	✓ $E = \dfrac{K_i \Theta_i}{K_j \Theta_j}$

✓ : factor considered   ✗ : factor ignored   D : merely presented in verbal discussion;

i : denotes organics j : denotes water; J : partial flux

K, $\hat{K}$: Mass transfer coefficient; P^{sat} : saturated vapour pressure; S^f : Sorption coefficient;

S_i^d : desorption coefficient y : permeate mole fraction; α_{PV}: separation factor;

α_{mem} : intrinsic membrane selectivity; α_{VLE} : vapour liquid selectivity; Θ : desorption factor

2.8 Chapter Conclusion

Organophilic pervaporation is an emerging technology that has a niche in the chemical industry. Due to its energy saving and moderate operating costs, it is able to compete with other existing organics recovery techniques. The most common membranes used for organophilic pervaporation are the rubbery PDMS membranes and modified PDMS. The key to success in organophilic pervaporation is to match the right membrane with the right modules and component systems. One of the essential parameters that affects the performance is permeate pressure. An engineering science analysis method will be introduced to predict the performance of organophilic pervaporation with respect to permeate pressure.

Part II Theory of Organophilic

Pervaporation Transport

Chapter 3

Mass Transport in Pervaporation

3.1 Chapter Objectives

- General introduction of mass transport in organophilic pervaporation .
- Overview of boundary layer transport and analysis.
- Overview of membrane transport mechanism.

    -Solution-diffusion model: - sorption, diffusion and desorption mechanism,

                           - introduction of coupling effect.

    -Pore flow model and its validity.

- Overview of support layer mass transport.
- Overview of two dimensional transport in a composite membrane

3.2 Introduction

To successfully design and implement organophilic pervaporation units requires a fundamental understanding of mass transport mechanisms in pervaporation. A knowledge of mass transport mechanisms in pervaporation will then enable engineers to design and improve membranes, membrane modules and associated process equipment. This includes, selection of appropriate material for separation and optimisation of process conditions and layouts.

Pervaporation differs from other membrane processes in that the membrane constitutes a dense barrier between a liquid feed and a permeate that is vapour. The driving force that is applied across the membrane creates a chemical potential gradient, and the selectivity of the membrane then determines the relative flow of different components. In contrast to reverse osmosis, the osmotic pressure is not limiting, because the permeate is kept under low pressure.

In pervaporation, transport across the non-porous membrane is generally considered to follow the well-known solution-diffusion model. A thorough discussion of the transport theory and models for pervaporation will be presented in the following section. In pervaporation, because of the relatively low permeability of dense membranes, the mass transfer resistance in the feed liquid is often neglected in the total resistance. However, the importance of boundary layer resistance will grow because membranes with improved permeability will be used. This is particularly true for the removal of VOCs from water via pervaporation processes. Thus, in the organophilic pervaporation process the overall mass transfer may not be solely controlled by the membrane itself but by the boundary layers that are developed on one side or both sides of the membrane (Gref et al., 1992). The mass transfer in this hypothetical, laminar boundary layer constitutes a resistance towards the material transport from bulk liquid to the surface of the membrane. Due to the composite nature of the membrane itself, the support layer and the selective/support layer interface might also contribute to the overall transport resistance (Gudernatsch et al, 1991). An illustration of material transport in organophilic pervaporation process is shown in Fig. 3.1.
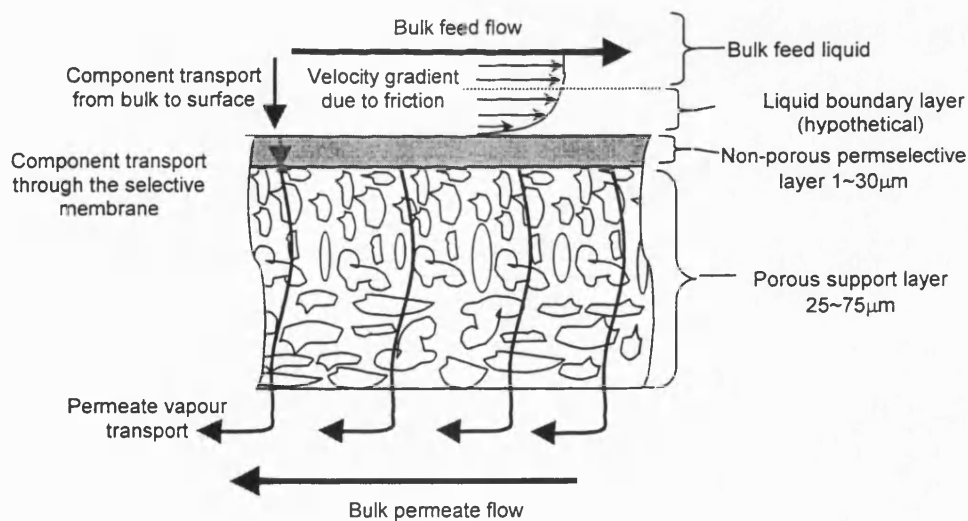
Fig. 3.1. Schematic of a multilayer composite membrane.

3.3 Boundary Layer Transport

It is widely accepted that the mass transfer resistance in the boundary layer was generated by the slow diffusion process which is not able to keep up with the possible rate of "material consumption" at the interface by permeation through the membrane phase (Gref et al, 1992). The first systematic investigation of the boundary layer transport in organophilic pervaporation was carried out by Psaume et al (1988) and following this, other researchers (Micheals, 1995; Feng and Huang, 1994; Wijmans et al, 1996; Baker et al, 1997; Bennett, 1996) have shown that the mass transport in this layer can be complicated by both diffusion and convective flow, and a high depletion in solute concentration at the surface of the membrane can result.

The cause of this phenomenon lies in the coupled convective and diffusive mass transfer between the bulk and the surface of the membrane. Due to the friction at the feed liquid/membrane surface interface, feed liquid velocity decreases as the distance from the membrane surface decreases and such a velocity gradient is illustrated in Fig. 3.2 (a). In order to facilitate the mass transfer analysis, a hypothetical boundary layer that is adjacent to the feed side of the membrane is assumed and all permeating components must pass through both the boundary layer and the membrane. According to film theory, it is assumed that no convective mixing occurs in the boundary layer adjacent to the membrane surface but a convective flow fluid occurs toward the membrane surface. The magnitude of this convective flow is determined by the total permeate molar flux, J_{tot}. The convective transport of the solute into the boundary layer from bulk solution is given by the product $J_{tot} \cdot x_{b,i}$, where $x_{b,i}$ is the mole fraction of solute in the well-mixed bulk feed solution. The rate at which the solute leaves the boundary layer and permeates through the membrane is given by another product $J_{tot} \cdot y_i$, where y_i is the mole fraction component i in the permeate.
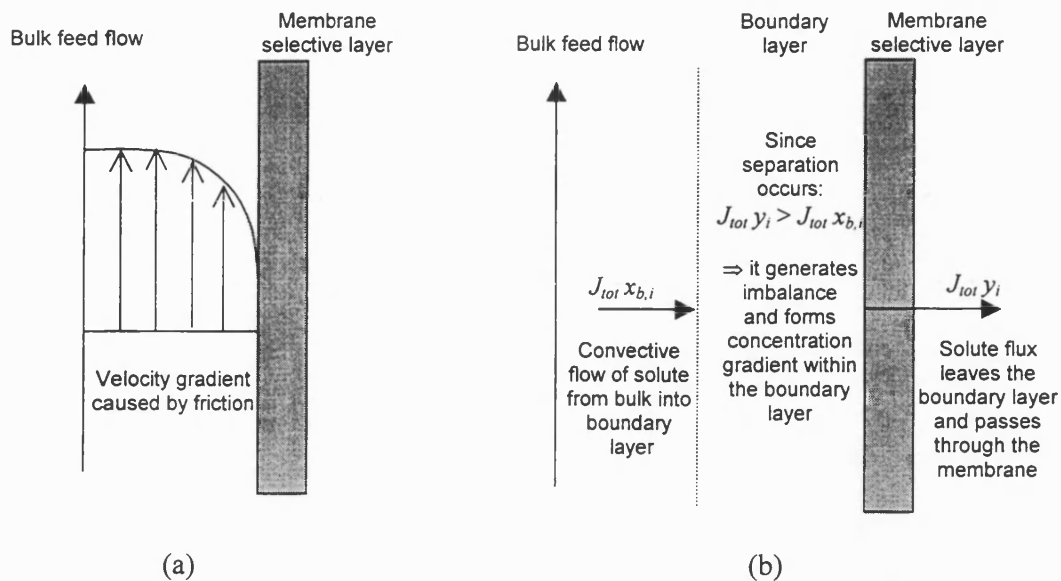
Fig. 3.2. Schematic of the boundary layer adjacent to the membrane surface: (a) the velocity profile along the surface of the membrane; (b) cause of concentration gradient in the boundary layer.

In general, if the enrichment of the solute is achieved, $J_{tot} \cdot y_i > J_{tot} \cdot x_{b,i}$, and this generates an imbalance which then forms a concentration gradient within the boundary layer as represented in Fig. 3.2(b). This concentration gradient of solute increases as the solute continues to deplete at the membrane surface until diffusion of the component down the concentration gradient is sufficient to restore the steady state. At steady state, the sum of the convective and diffusion transport in the boundary layer will equal to the amount permeated through the membrane. The phenomenon of the depletion of solute concentration adjacent to the membrane surface is sometimes called *concentration polarization*. This occurrence is illustrated in Fig. 3.3. where $C_{b,i}$ is the solute concentration in the bulk and $C_{mb,i}$ is the solute concentration adjacent to membrane surface. It should be noted in ultrafiltration where the minor component is rejected, that the term *concentration polarization* refers to the building up of the minor component concentration adjacent to the membrane. This differs from that found in pervaporation where the minor component is preferentially transmitted and the concentration of minor component adjacent to the membrane is depleted.
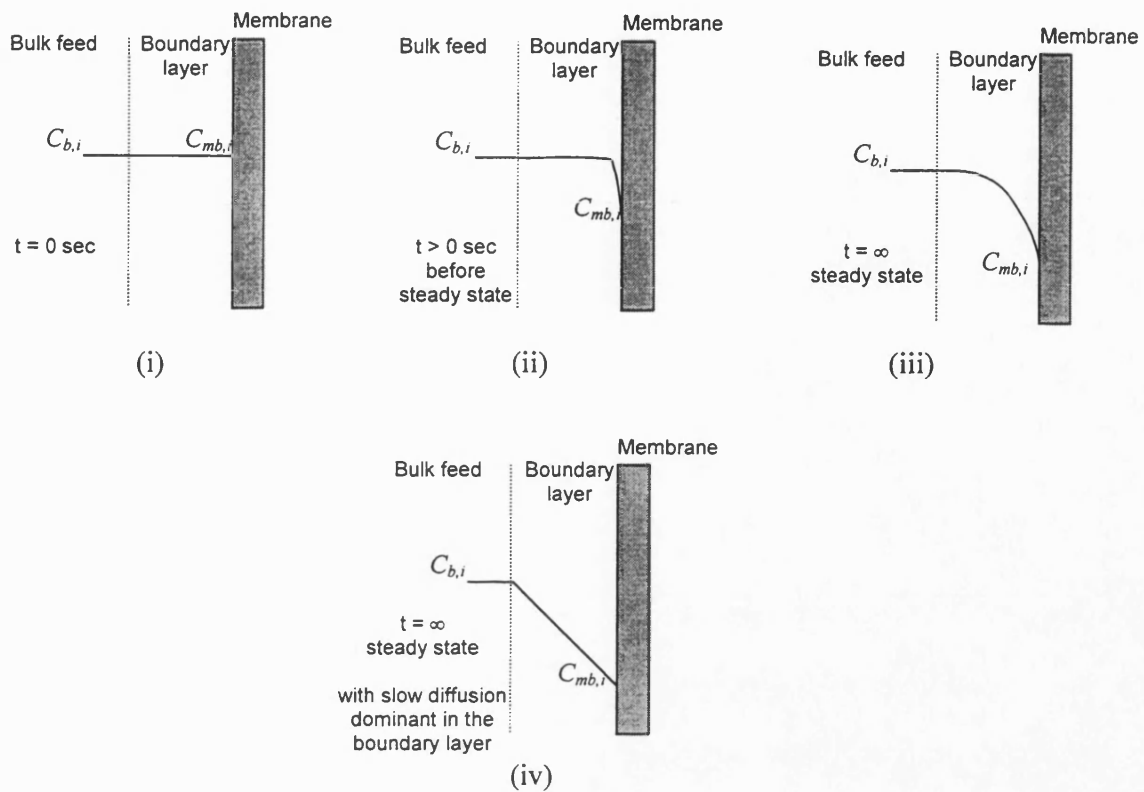
Fig. 3.3 Schematic of concentration profile in the boundary layer developed through time as a result of separation achieved by the membrane (i) Before separation started; (ii) profile before steady state achieved; (iii) profile at steady state (general); (iv) profile at steady state with slow diffusion dominant in the boundary layer.

From Fig. 3.3 (iii) and (iv), two possible concentration profiles can be developed in the boundary layer at steady state. It will be shown in the later section that when convective flow in the boundary layer is not negligible, an exponential decrease of concentration profile should be observed as shown in Fig 3.3 (iii) Otherwise a linear decrease of concentration profile as shown as Fig 3.3 (iv) is a realistic representation. The latter concentration profile implies that within the boundary layer the slow diffusion mechanism for solute dominanates over the convective flow of solute.

In the pervaporation of VOCs from water, the solute in the permeate is usually much more concentrate than it in the feed, i.e., the membrane selectively permeates VOCs. For these pervaporation applications, the solute concentration adjacent to the membrane surface, $C_{mb,i}$, is sometimes typically only 0.01 to 0.1 of the solute concentration of the bulk, $C_{b,i}$. As a result, the entire separation process can be dominated by boundary layer resistance (Psaume et al, 1988; Feng and Huang, 1994; Michaels, 1995; Wijmans et al, 1996; Baker et al, 1997).

3.3.1 Transport equation for boundary layer

According to Cussler (1984) the more general form of Fick's first law, at steady state, includes the migration of solute contributed by the concentration gradient and the bulk flow within the boundary layer. Hence, the steady state solute flux can be described, at any plane throughout the boundary layer, by:

$$J_i = -D_{l,i} \frac{dC_i}{dz} + \bar{u} C_i \tag{3.1}$$

Where: J = Molar flux, kmol/m^{2}s z = Distance, m

         D_l = Diffusion coefficient in liquid $\bar{u}$ = Convective velocity, m/s

         C = Molar concentration, kmol/m^3 i = denotes solute

3.3.1.1 Diffusion Coefficients, $D_{l,i}$

In a liquid system, $D_{l,i}$ is a function of concentration, however, it has been shown that $D_{l,i}$ remains effectively constant across a liquid boundary layer when either $\dfrac{dC_i}{dx}$ or $C_i \to 0$ (Brodkey and Hershey, 1988). In the case of removal of organic solutes from water $C_{b,i}$ is always low and hence it is safe to assume constant $D_{l,i}$. According to Feng and Huang (Feng and Huang, 1994), $D_{l,i}$ will rarely vary by more than 10% in organophilic pervaporation, hence in general, this assumption can be accepted unless pervaporation application operates at high solute feed concentrations.

Numerous correlations exist for predicting $D_{l,i}$ although most are only applicable to specific systems such as non-electrolyte or electrolyte solutions, dilute or concentrated solutions and aqueous or non aqueous solutions. Probably the most applicable to pervaporation processes is the Wilke-Chang correlation (Brodkey and Hershey, 1988), which is generally applicable to both aqueous and non aqueous, dilute, solutions of non-electrolytes:

$$D_{l,i} = 1.17 \times 10^{-16} \frac{T \sqrt{\phi M_j}}{\mu_j V_i^{0.6}} \qquad (3.2)$$

Where: T = Temperature, K ϕ = Association Parameter

M = Molecular Mass, kg/kmol μ = Viscosity, kg/ms

V = Molar Volume at Normal Boiling Point, m^3/kmol

j = denoted solvent

The term ϕ takes the value of 2.26 for water, 1.9 for methanol, 1.5 for ethanol and 1.0 for other unassociated solvents. $D_{l,i}$ values in liquids are generally low, being in the order of 10^{-9}m^2/s.

3.3.1.2 Convective velocity, $\bar{u}$

In general, the convective velocity can be related to total volume flux through the membrane:

$$\bar{u} = \frac{J_{tot} \overline{M}}{\overline{\rho}_l} \qquad (3.3)$$

Where: J_{tot} = Total molar flux, kmol/m^{2}s $\overline{M}$ = Average molar mass, kg/kmol

$\overline{\rho}_l$ = Average density of the liquid, kg/m^3

In a paper by Michaels (1995), it was argued that when solute concentration is very low, as in the case of the removal of trace organic solvent from water, convective velocity can be equated to the volume flux of the solvent:

$$\bar{u} = \frac{J_j M_j}{\rho_j} \qquad (3.4)$$

Where: ρ = Density, kg/m^3 j denotes solvent

M = Molar mass, kg/kmol

Although equation (3.4) offers a simplification of the convective velocity evaluation, the applicability of such an equation could only be applied to extremely low feed concentrations. According to Bennett (1996), a more general form of convective velocity approximation can be evaluated, without over complicating the subsequent analysis, by using the following:

$$\bar{u} = \frac{J_i M_i}{\rho_i} + \frac{J_j M_j}{\rho_j}$$ (3.5)

The assumption made in constructing equation (3.5) is that solute and solvent densities do not change upon mixing i.e.:-

$$\bar{\rho}_i = \phi_i \rho_i + (1 - \phi_i)\rho_j$$ (3.6)

Where: ϕ = Volume Fraction of Component

Typical values of $\bar{u}$ in pervaporation are less than 5×10^{-7} m/s (Feng and Huang, 1994)

3.3.1.3 Determination of boundary layer thickness, δ_l

Boundary layer thickness is a hypothetical thickness yet important in determining the resistance that resides in the boundary layer. In practice, the boundary layer thickness is indirectly determined from the Sherwood number that can be calculated by using appropriate Sherwood correlations. The Sherwood number is defined as the ratio of the characteristic hydraulic diameter (d_h) to the boundary layer thickness (δ_l). However in most chemical engineering text books the Sherwood number is defined as $k_l \cdot d_h / D_{l,i}$ where k_l is the mass transfer coefficient with the magnitude of $D_{l,i} / \delta_l$. Nevertheless, the application of such a correlation requires the knowledge of the specific range of conditions in the system otherwise there will be an erroneous estimation.

3.3.1.3.1 Sherwood Correlations

The Sherwood correlations are semi-empirical relationships between dimensionless parameters for varying flow conditions and geometries. In organophilic pervaporation, these correlations may take the following general forms (Cussler, 1984; Gekas and Hallstrom, 1987; Lipski and Cote, 1990; Nijhuis, 1990; Karlson and Tragargh, 1993; Gabelman and Hwang, 1999):

$$Sh = a\,Re^b\,Sc^c\left(\frac{d_h}{L}\right)^d \qquad (3.7)$$

or

$$Sh = a\,Re^b\,Sc^c \qquad (3.8)$$

or

$$Sh = aDe^b Sc^c \qquad (3.9)$$

Where:

$$Sh = \text{Sherwood number} = \frac{d_h}{\delta_l} = \frac{k_l d_h}{D_{l,i}} \qquad (3.10)$$

$$Re = \text{Reynolds number} = \frac{Vd_h}{v}\text{(Tubular or cross flow)or } \frac{\omega d_h^2}{v}\text{(Stirred cell)} \qquad (3.11)$$

$$Sc = \text{Schmidt number} = \frac{v}{D_{l,i}} \qquad (3.12)$$

$$De = \text{Dean number} = Re\left(\frac{d_h}{d_s'}\right)^{0.5} \qquad (3.13)$$

$$d_s' = d_{coil}\left[1 + (\lambda/\pi d_{coil})^2\right] \qquad (3.14)$$

L	= characteristic length, m	a,b,c,d	= coefficients
V	= feed velocity, m/s	v	= kinematic viscosity, m²/s
ω	= rotational velocity, rad/s		
d_h	= hydraulic diameter (Crossflow) or stirred cell radius (Stirred cell) or fibre internal diameter (Hollow fibre tube side flow), m		
d_{coil}	= coil diameter of a coiled hollow fibre, m		

λ = pitch of the coil in a coiled hollow fibre, m

The coefficients a, b, c and d are adjusted according to the feed side hydrodynamics, operation conditions and types of module used. A summary of the values taken under various regimes is given in Table 3.1 with reference to [1]Karlsson and Tragargh, 1993; [2]Gekas and Hallstrom, 1987; [3]Castello et al, 1993; [4] Wickramasinghe et al, 1993; [5]Schnabel et al, 1998; [6]Moulin et al, 1996).

Table 3.1 Sherwood Correlation

System	Equation	Flow Regime	*a*	*b*	*c*	*d*	*Ref.*
Crossflow	(3.1)	Laminar	1.62	0.33	0.33	0.33	[1]
Crossflow	(3.7)	$Re < 2000$	1.85	0.33	0.33	0.33	[1]
Crossflow	(3.7)	$10^4 < Re < 10^5$	0.34	0.75	0.33	0	[1]
Crossflow	(3.7)	$Re > 10^5$	0.023	0.8	0.33	0	[1]
Stirred Cell	(3.8)	Laminar	0.29	0.57	0.33	-	[1]
Stirred Cell	(3.8)	Turbulent	0.044	0.75	0.33	-	[1]
Hollow fibre (t,p)	(3.7)	Laminar	1.62	0.33	0.33	0.33	[2]
Hollow fibre (t,p)	(3.8)	$Re > 10^4$	0.0165	0.86	0.33	-	[2]
Hollow fibre (t,p)	(3.8)	$10^4 < Re < 10^5$	0.34	0.75	0.33	-	[2]
Hollow fibre (t,p)	(3.8)	$Re > 10^5$	0.023	0.8	0.33	-	[2]
Hollow fibre (t,h)	(3.9)	$150 < Re < 2000$	0.14	0.75	0.33	-	[6]
Hollow fibre (s,p)	(3.8)	$0 < Re < 324$ $0.32 < \phi < 0.76$	$0.53\text{-}0.58\phi$	0.53	0.33	-	[3]
Hollow fibre (s,h)	(3.8)	$Re < 2.5$	0.12	1.0	0.33	-	[4]
Hollow fibre (s,h)	(3.8)	$Re > 2.5$	0.15	0.8	0.33	-	[5]

(t,p) : tube side feed flow with parallel and straight hollow fibre configuration

(t,h) : tube side feed flow with coiled/helical hollow fibres configuration

(s,p) : shell side feed flow parallel to the straight hollow fibres configuration

(s,h): shell side feed flow with helical hollow fibres configuration.

ϕ : Packing density

Although there are many different Sherwood correlations available, many of them are only applied to a particular membrane module or component separation. If the slow diffusion mechanism is dominant over the convective flow in the boundary layer, the overall resistance can be assumed to be the sum of the resistance of the liquid boundary layer and the membrane. Under this condition, by considering equation (3.7) and (3.8), a Wilson plot can be established. From this plot, the following relationship between the overall mass transfer coefficient and either the crossflow velocity or the stirring speed for turbulent cross flow or a stirred cell module are respectively:

$$\frac{1}{k_{ov}} = a + b V^{0.75}$$
(3.15)

for turbulent cross flow

$$\frac{1}{k_{ov}} = a + b \omega^{0.75}$$
(3.16)

for stirred cell.

Where k_{ov} is the overall mass transfer coefficient of solute, m/s

The Wilson plot for cross flow/ stirred cell is graphically shown in Fig. 3.4
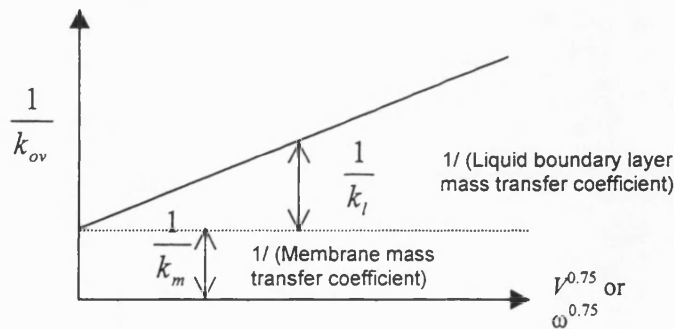
Fig. 3.4 Wilson plot for cross flow/ stirred cell

(Diffusive mass transfer dominant in boundary layer)

Such a method has been employed to determine k_l values for both crossflow and stirred cell configurations, using typical laboratory scale equipment and test conditions, employing flat sheet membranes (Ji et al, 1994; Raghunath and Hwang, 1992; Nijhuis et al, 1991; Burslem et al, 1992; Bennett, 1996). All k_l values fall in the range 7.4×10^{-6} - 3.3×10^{-5} m/s. It was

noted (Nijhuis et al, 1991) that a value of 2.5×10^{-5} m/s would be a high, but not unrealistic, value to be reached in practical applications. The highest reported k_l values have been found when hollow fibre membrane configurations are employed (Lipski and Cote, 1990; Borges et al, 1992; Gooding et al, 1991; Lipski et al, 1991). Transversal flow hollow fibre configurations of Zenon Environmental Inc are better than those with tube side feed flow and k_l values of 5.0×10^{-5} - 10^{-4} m/s are typically achieved (Lipski et al, 1991).

3.3.2 Boundary layer mass transport analysis

In order to understand the mass transport behaviour in the boundary layer, a mathematical analysis is carried out upon equation (3.1).

Integrating equation (3.1) over the thickness of the boundary layer δ_l, assuming $D_{l,i}$ to remain constant, yields:-

$$\int_{C_{b,i}}^{C_{mb,i}} \frac{dC_i}{C_i - \frac{J_i}{\bar{u}}} = \int_0^{\delta_l} \frac{\bar{u}}{D_{l,i}} dz \qquad (3.17)$$

$$\ln\left(\frac{C_{mb,i} - \frac{J_i}{\bar{u}}}{C_{b,i} - \frac{J_i}{\bar{u}}}\right) = \frac{\bar{u}\delta_l}{D_{l,i}} \qquad (3.18)$$

$$C_{mb,i} = \frac{J_i}{\bar{u}} - \left(\frac{J_i}{\bar{u}} - C_{b,i}\right)\exp\left(\frac{\bar{u}\delta_l}{D_{l,i}}\right) \qquad (3.19)$$

$$\frac{C_{mb,i}}{C_{b,i}} = \frac{J_i}{C_{b,i}\bar{u}} - \left(\frac{J_i}{C_{b,i}\bar{u}} - 1\right)\exp\left(\frac{\bar{u}\delta_l}{D_{l,i}}\right) \qquad (3.20)$$

Where: δ_l = Boundary layer thickness, m

  mb denotes upstream membrane surface

  b denotes bulk

The term $\dfrac{\overline{u}\delta_l}{D_{l,i}}$ is the Peclet number *(Pe)* and it is defined as the ratio of convective to diffusive velocity. From equation (3.18), the transport equation in the boundary layer can then be rewritten as:

$$J_i = \overline{u}\left[C_{b,i}\,\exp\!\left(\frac{\overline{u}\delta_l}{D_{l,i}}\right) - C_{mb,i} \right]$$

(3.21)

3.3.2.1 Concentration profile within the boundary layer

Solute concentration profile

The solute concentration profile in the boundary layer determines the degree of concentration polarization. In Fig. 3.3 (iii) and (iv), two distinct characteristic forms of the concentration profile across the boundary layer are shown. In the following section, mathematical analyses for these two cases are carried out.

From equation (3.19), the local concentration profile at position z can be written as below:

$$C_i(z) = \frac{J_i}{\overline{u}} - \left(\frac{J_i}{\overline{u}} - C_{b,i}\right)\exp(Pe_z)$$

(3.22)

where the local Peclet number is defined as:

$$Pe_z = \frac{\overline{u}}{D_{l,i}}\cdot z$$

(3.23)

By differentiating equation (3.22) with respect to distance z, the local concentration gradient can be obtained:

$$\frac{dC_i(z)}{dz} = -\frac{\overline{u}}{D_{l,i}}\left(\frac{J_i}{\overline{u}} - C_{b,i}\right)\exp(Pe_z)$$

(3.24)

At steady state, J_i, $\overline{u}$, $C_{b,i}$, $D_{l,i}$ are constant and $(J_i / \overline{u} - C_{b,i}) > 0$, the concentration gradient decreases in an exponential way with respect to distance along the boundary layer.

From equation (3.22), the concentration profile has the same characteristics of the function $f(x) = b - a \exp(cx)$ where a, b and c are arbitrary constants, hence a graphical illustration of equation (3.22) is obtained in Fig. 3.5.
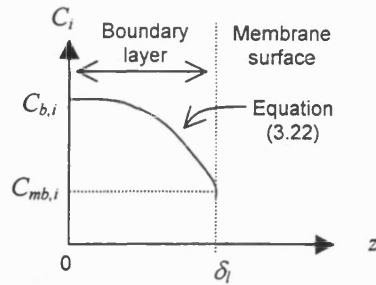
Fig. 3.5 Graphical illustration of solute concentration profile equation (3.22)

When the Peclet number is very small, the exponential term can be approximated as, $\exp(Pe_z) \approx 1 + Pe_z$. For this condition, equation (3.22) can be reduced to the following:-

$$C_i(z) = \frac{J_i}{\bar{u}} - \left(\frac{J_i}{\bar{u}} - C_{b,i}\right)(1 + Pe_z) \tag{3.25}$$

$$C_i(z) = C_{b,i}(1 + Pe_z) - \frac{J_i}{D_{l,i}} \cdot z \tag{3.26}$$

Since $Pe_z \ll 1$ therefore, equation (3.26) is reduced to a linear function:

$$C_i(z) = C_{b,i} - \frac{J_i}{D_{l,i}} \cdot z \tag{3.27}$$

A graphical illustration of equation (3.27) is shown in Fig. 3.6.

In most cases of organophilic pervaporation, particularly when the selectivity of the membrane is high, Pe has been found to be much smaller that unity (Karlsson and Tragargh, 1993), thus the concentration profile in the boundary layer can be assumed to be a linear function. When a high flux membrane is employed, the convective velocity is high and the assumption above may not hold. Therefore, equation (3.22) should be used to calculate the solute concentration profile. However, the actual value of the flux at which this is necessary depends upon the hydrodynamic conditions. For example, if $D_{l,i}/\delta_l \approx 2.5 \times 10^{-5}$ m/s and $Pe < 0.1$ then $\bar{u} < 2.5 \times 10^{-6}$ m/s, i.e. the mass flux has to be less than 9.0 kg/m²·h (calculated from equation (3.4)).
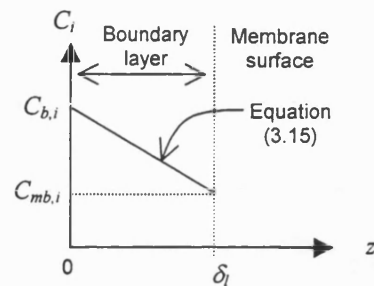
Fig. 3.6 Graphical illustration of solute concentration profile equation (3.27)

In summary, the characteristics of the solute concentration profile throughout the plane of boundary layer depends on the Peclet number, Pe. When $Pe \ll 1$, the slow diffusion mechanism dominants over convective flow in the boundary layer, thus a linear concentration profile over the plane of boundary layer is observed.

Solvent concentration profile

If separation is achieved with the permeate being relatively rich in the minor component, the solvent will be much slower in penetrating the membrane. This results in solvent being transported back to the bulk of the feed by a diffusion mechanism through the boundary layer. In relation to bulk composition, an increase of concentration of the slower permeant occurs near the membrane surface. In organophilic pervaporation, the solute concentration in the bulk is low compared to the solvent concentration. Thus, the *increase* of concentration of the solvent towards the membrane surface is insignificant compared to the actual concentration in the bulk. This implies that the transport resistance in the boundary layer for the highly concentrated solvent is negligible compared to the membrane resistance for transport of the solvent. Therefore, in practice, the concentration profile of solvent can be assumed constant throughout the boundary layer. A graphical illustration of the concentration of the solvent in the boundary layer is shown in Fig. 3.7.

39
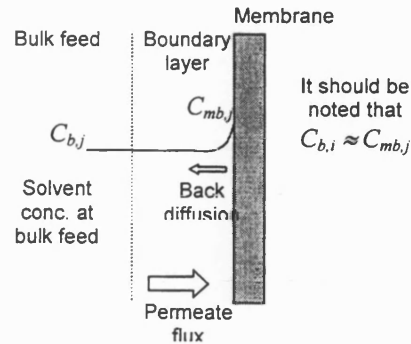
Fig. 3.7 Concentration profile of solvent throughout the boundary layer

3.3.2.2 Flux profile within boundary layer

From equation (3.1), the first term can be recognized as the flux due to diffusion while the second term is due to convective flow from the bulk. Thus, the local diffusion flux and convective fluxes at any plane throughout boundary layer can be defined as:

Diffusion flux: $\qquad J_{d,i}(z) = -D_{l,i}\dfrac{dC_i(z)}{dz}$ (3.28)

Convective flux: $\qquad J_{c,i}(z) = \bar{u}C_i(z)$ (3.29)

By substituting equation (3.24) into (3.28) and equation (3.22) into (3.29), the local fluxes for both diffusion and convective flow can be written as:

$$J_{d,i}(z) = (J_i - \bar{u}C_{b,i})\exp(Pe_z)$$ (3.30)

$$J_{c,i}(z) = J_i - (J_i - \bar{u}C_{b,i})\exp(Pe_z)$$ (3.31)

Thus under conditions where the convective flow is making a contribution, the contribution is not invariant with respect to z; $J_{c,i}(z)$ decreases as z increases whist $J_{d,i}(z)$ shows the opposite trend.

A graphical representation of the local components of the solutes flux throughout the boundary layer is shown as profiles in Fig.3.8. It should be noted that the magnitude of $J_{c,i}$ is lower than $J_{d,i}$.
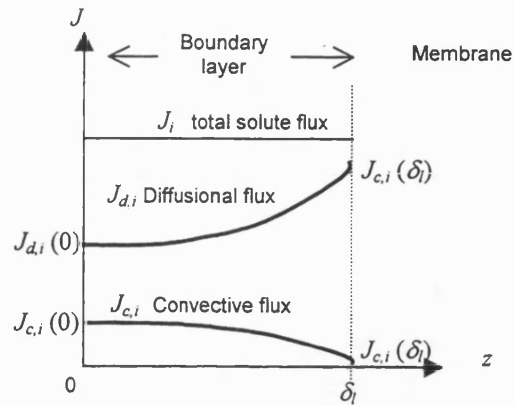
Fig. 3.8 Graphical illustration of local solute flux profile equations (3.30) and (3.31)

3.3.3   Factors that influence the degree of concentration polarization

The degree of concentration polarization is measured by an index I_{cp} as a percentage:

$$I_{cp} = \left(1 - \frac{C_{mb,i}}{C_{b,i}}\right) \times 100\% \tag{3.32}$$

In practice, this index should be as low as possible during the pervaporation process. If the convective flow is dominant over the diffusional flux, the degree of concentration polarization should attain a low value. This operating condition can be achieved by the combination of highly turbulent flow (plug flow) and novel design of the membrane feed channels (Michaels, 1995). Unfortunately, most of the currently available organophilic pervaporation units exhibit a high degree of concentration polarization as the slow diffusional flux is dominant over the convective flux throughout the boundary layer (Michaels, 1995; Wijmans et al, 1996; Baker et al, 1997). The understanding of the factors that influence the degree of concentration polarization becomes important for improving flux and separation performance.

By substituting equation (3.20) into (3.32), the degree of concentration polarization can be rewritten as:

$$I_{cp} = 100\left(\frac{J_i}{\overline{u}C_{b,i}} - 1\right)[\exp(Pe) - 1] \qquad (3.33)$$

Where $Pe = \dfrac{\overline{u}\delta_l}{D_{l,i}}$ or $\dfrac{\overline{u}}{k_l}$

In order to facilitate the analysis, the solute enrichment factor is defined as the ratio of molar composition of the permeate, y_i to the feed in the bulk, $x_{b,i}$:

$$\beta_i = \frac{y_i}{x_{b,i}} \qquad (3.34)$$

and the solute molar flux is the product of the total molar flux and the molar composition of solute in the permeate:

$$J_i = J_{tot}y_i \qquad (3.35)$$

Similarly, the solute molar concentration of the bulk feed can also be evaluated as follows:

$$C_{b,i} = C_{tot} \cdot x_{b,i} \qquad (3.36)$$

Knowing that the $\overline{u} = k_l \cdot Pe$, a new expression for equation (3.33) can be formed by combining equations (3.33) - (3.36):

$$I_{cp} = 100\left(\frac{J_{tot}\beta_i}{k_l C_{tot}} - Pe\right)\left(\frac{\exp(Pe) - 1}{Pe}\right) \qquad (3.37)$$

From equation (3.37), the degree of concentration polarization is affected by the total flux passing through the membrane, the solute enrichment factor, feed-side mass transfer coefficient and the Peclet number.

When the diffusional mechanism in the boundary layer prevails over convective flow, $Pe \ll 1$, and the degree of concentration polarization for this condition is defined as:

$$I_{cp}^d = 100\frac{J_{tot}\beta_i}{k_l C_{tot}} \qquad (3.38)$$

A controversial but beneficial idea proposed by Lipski and Cote (1992) in a patent argued that if a thick membrane ($\sim$ 50 – 200 μm) is employed, the effect of concentration polarization can be reduced. This effect corresponds to the influence of the total flux upon I_{cp}

in equation (3.37). If a thick membrane is employed, the total flux through the membrane will be reduced and this results in the reduction of I_{cp}. Another similar idea for total flux reduction was also proposed by others (Wijmans et al, 1996; Baker et al, 1997) and they argue that if a module is operated at a higher permeate pressure, this will lead to the reduction of total flux and hence of the concentration polarization effect.

It has been noted (Field and Burslem, 1992; Feng and Huang, 1994) that several authors have made the erroneous assumption that concentration polarization will only be significant at low feed concentrations. However, from equation (3.37) I_{cp} is also a function of C_{tot}. This shows that the concentration polarization effect should not be neglected even at a higher solute feed concentration.

In pervaporation, practical considerations always leads to the desirability of using the thinnest possible membranes consistent with a high observed solute selectivity. As the membrane becomes thin the overall resistance for solute transport tends to be dominated by the resistance at the feed side and concentration polarization effect can be detrimental to the separation process. This implies the need of putting a premium on the development of module designs, or novel fluid-flow management strategies, to minimize the feed side concentration polarization effect. Of commercially available membrane module designs, probably the best compromise for pervaporation is the hollow fiber module, operated such that the feed flow is turbulent. In summary, the factors that affect the degree of concentration polarization is shown in Table 3.2

Table 3.2 Various factors that influence the degree of concentration polarization

Index / Factors	Changes in factor	Changes in I_{cp}
β_i	↑	↑
	↓	↓
J_{tot}	↑	↑
	↓	↓
$1/k_l$	↑	↑
	↓	↓

3.4 Membrane Transport Mechanism

A proper understanding of the membrane transport mechanism would provide direct information to aid research and development of an appropriate membrane. Due to the complicated membrane-permeant interactions, it is difficult to formulate a single explanation for the complex transport process. Currently, there are principally two approaches to describe mass transfer through a pervaporation membrane. The first is the solution-diffusion model, in which permeants dissolve in the membrane material and then diffuse through the membrane down a concentration gradient. A separation is achieved between different permeants because of differences in their solubilities in the membrane and in the rate at which they diffuse through the membrane. The second approach is the pore flow model, in which permeants are separated by a pressure driven convective flow through tiny pores. A separation is achieved between different permeants because one of the permeants are excluded (filtered) from some pores in the membrane through which other permeants move. In pervaporation however, the solution-diffusion model is well accepted by the majority of membrane researchers (Kataoka et al., 1991a,b; Wijmans and Baker, 1995; Baker, 1996; Feng and Huang, 1997). In this chapter, the focus is on the solution-diffusion mechanism rather than the pore flow model.

3.4.1 Solution-diffusion model

The solution-diffusion model was first proposed by Graham (1866) to describe gas permeation through rubber septa. Later, Binning et al (1961) used this model to describe pervaporation performance. The underlying assumptions for this model for pervaporative transport are:

1. Sorption of liquid mixture on the feed side of the membrane;
2. Diffusion through the membrane;
3. Desorption on the permeate side of the membrane into the vapour phase.

A graphical illustration of the solution-diffusion steps and solute concentration profile of the pervaporation membrane is shown in Fig. 3.9.

(a)

(b)
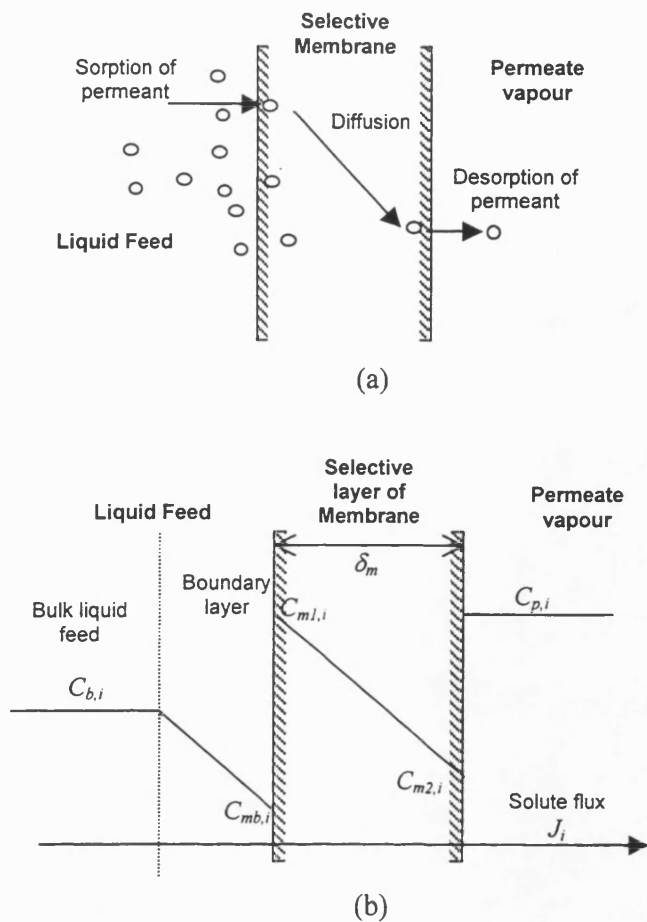
Fig 3.9. Schematic representation of solution-diffusion model in (a) explaining pervaporation transport mechanism and the (b) Concentration profile of the solute in the membrane and boundary layer.

Firstly, the solute is preferentially absorbed into the membrane. Let this concentration be $C_{m1,i}$. Since a low pressure exists at the permeate side, the permeate side is relatively dry compared to the feed side and so the solute concentration in the membrane adjacent to the permeate side, $C_{m2,i}$, is smaller than $C_{m1,i}$, giving a concentration gradient within the membrane. As the membrane is solute selective, the vapour permeate is rich in solute.

For theoretical interest, the driving force for transport across the pervaporation membrane is generally recognized as a chemical potential gradient across the membrane (Aptel and Neel, 1986; Wijmans and Baker, 1995). Thus the solute flux, J_i at steady state is described by the following equation:

45

$$J_i = -L_i \frac{d\mu_{m,i}}{dz} \qquad (3.38)$$

where $d\mu_{m,i}/dz$ is the gradient in chemical potential of component i and L_i, is a coefficient of proportionality linking the chemical potential driving force with flux. The general form of chemical potential can be described as a function of temperature, pressure and composition (Lee, 1975):

$$\mu_i = \mu_i^0 + RT \ln a_i + \int_{p_i^0}^{p} \hat{V}_i dp - \int_{T_i^0}^{T} \hat{S}_i dT \qquad (3.39)$$

Where μ_i = chemical potential within membrane, kJ   0 = Reference

a_i = activity of solute T = Thermodymanic temperature, K

$\hat{S}_i$ = molar entropy of the solute, kJ/kmol/K p = pressure, Pa

$\hat{V}_i$ = molar volume of solute, m³/kmol R = Universal gas constant, kJ/kmol/K

A number of assumptions must be made to define any model of permeation. Usually, the first assumption governing transport through membranes is that fluids on either side of the membrane are in equilibrium with the membrane material at the respective interface. It is implicit in this assumption that the rate of absorption and desorption at the membrane interface are much higher than the rate of diffusion through the membrane. This appears to be the case at the interfaces between fluid and the pervaporation membrane. This assumption is not applied to permeation which involves chemical reactions, such as facilitated transport, or in diffusion of gases through metals, where interfacial absorption can be slow. Another important assumption for the solution-diffusion model is that when a pressure is applied across a dense membrane, the pressure everywhere within the membrane is constant at the higher-pressure value. This assumes, in effect, that solution-diffusion membranes transmit pressure in the same way as liquids. Consequently, the pressure throughout the pervaporation membrane is uniform with the feed pressure. The consequence of these assumptions are illustrated in Fig. 3.10
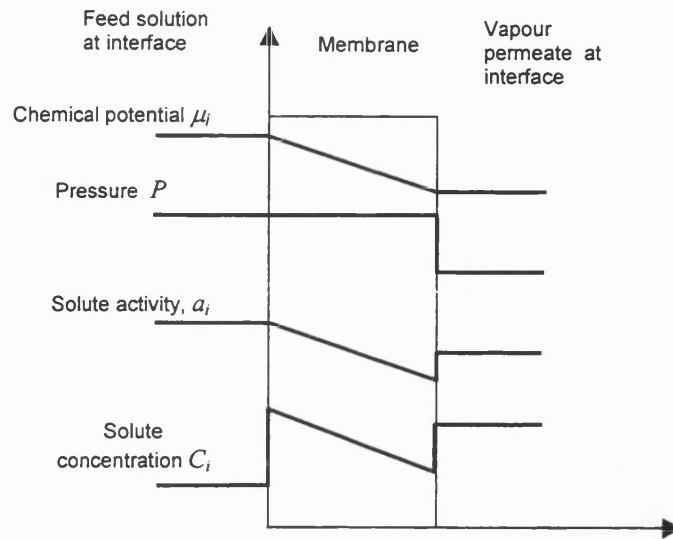
Fig. 3.10 Schematic of chemical potential, pressure, activity and solute concentration profiles in an organophilic pervaporation membrane that follows the solution-diffusion model assumptions (adapted from Wijmans and Baker, 1995).

From Figure 3.10, if the temperature gradient across the membrane is negligible and the molar volume of solute in the membrane is approximately the same as that in the liquid feed and vapour permeate, the solute activity in the membrane adjacent to the feed side, $a_{m1,i}$ and the one adjacent to the permeate side $a_{m2,i}$ can be related to the solute activity at liquid feed, $a_{mb,i}$ and the solute activity at vapour permeate, $a_{p,i}$ by the following expressions (Lee, 1975):

$$a_{m1,i} = a_{mb,i} \tag{3.40}$$

$$a_{m2,i} = a_{p,i} \cdot \exp\left[-\frac{\hat{V}_i}{RT}\left(p_f - p_p\right)\right] \tag{3.41}$$

Further, with the assumptions above, equation (3.38) can also be simplified to:

$$J_i = -L_i RT \frac{d\left(\ln a_{m,i}\right)}{dz} \tag{3.42}$$

or

$$J_i = -\frac{L_i RT}{a_{m,i}} \frac{da_{m,i}}{dz} \tag{3.43}$$

47

Knowing that the activity of the solute in the membrane $a_{m,i}$ can relate to the solute molar composition $x_{m,i}$ in the membrane by an activity coefficient $\gamma_{m,i}$ i.e. $a_{m,i} = \gamma_{m,i} \cdot x_{m,i}$, equation (3.43) is transformed to:

$$J_i = -L_i RT \left(1 + \frac{d \ln \gamma_{m,i}}{d \ln x_{m,i}} \right) \frac{dx_{m,i}}{dz} \tag{3.44}$$

It is interesting to note that if the solute concentration in the membrane $C_{m,i}$ can relate to the solute molar composition $x_{m,i}$ in the membrane by the average total concentration in the membrane C_m, i.e. $C_{m,i} = C_m \cdot x_{m,i}$, equation (3.44) will then be transformed to Fick's first law of diffusion:

$$J_i = -D_{m,i} \frac{dC_{m,i}}{dz} \tag{3.45}$$

Where $D_{m,i} = -C_m L_i RT \left(1 + \frac{d \ln \gamma_{m,i}}{d \ln x_{m,i}} \right) \tag{3.46}$

$D_{m,i}$ is the diffusivity of solute in the membrane according to Fick's first law. Since C_m and $\dfrac{d \ln \gamma_{m,i}}{d \ln x_{m,i}}$ are a function of $C_{m,i}$ or $x_{m,i}$, $D_{m,i}$ is therefore a function of solute composition in the membrane.

Integrating equation (3.45) over the thickness of membrane, δ_m, a simple form of the transport equation is obtained:

$$J_i = \frac{\overline{D}_{m,i}}{\delta_m} \left(C_{m1,i} - C_{m2,i} \right) \tag{3.47}$$

Where $\overline{D}_{m,i} = \dfrac{1}{\left(C_{m1,i} - C_{m2,i} \right)} \displaystyle\int_{C_{m2,i}}^{C_{m1,i}} D_{m,i} dC_{m,i}$ = mean diffusivity of solute. $\tag{3.48}$

From equation (3.48), the mean diffusivity is a function of solute concentration in the membrane. In organophilic pervaporation with low feed concentration, the mean diffusivity can be treated as constant and it can be determined experimentally via a sorption isotherm of the solute in the membrane which will be explained in a later section.

It is interesting to note that if $C_{m,i} = C_m \cdot x_{m,i}$ and $a_{m,i} = \gamma_{m,i} \cdot x_{m,i}$, the solute concentrations in the membrane adjacent to feed and to permeate can be related by the solute partial pressure in feed $(p_{mb,i})$ /permeate $(p_{p,i})$ by sorption (S_i^f) and desorption (S_i^p) coefficients respectively:

$$C_{m1,i} = S_i^f \cdot p_{mb,i} \tag{3.49}$$

$$C_{m2,i} = S_i^p \cdot p_{p,i} \tag{3.50}$$

Where:

$$S_i^f = \frac{C_m}{\gamma_{m1,i} \cdot P_i^{sat}} \tag{3.51}$$

$$S_i^p = \frac{C_m}{\gamma_{m2,i} \cdot P_i^{sat}} \cdot \exp\left[-\frac{\hat{V}_i}{RT}(P_f - P_p)\right] \tag{3.52}$$

Lee (1975), Rautenbach and Albrecht (1989) suggested that the exponential term in equation (3.41) can be assumed to be unity for pervaporation, hence equation (3.52) is reduced to:

$$S_i^p = \frac{C_m}{\gamma_{m2,i} \cdot P_i^{sat}} \tag{3.53}$$

By substituting equation (3.49) and (3.50) into (3.47) a new expression for the flux equation is obtained:

$$J_i = \frac{\hat{P}_i}{\delta_m}\left(p_{mb,i} - \Theta_i p_{p,i}\right) \tag{3.54}$$

Where $\hat{P}_i = \overline{D}_{m,i} S_i^f$ = Permeability.

$\Theta_i = \dfrac{S_i^p}{S_i^f} = \dfrac{\gamma_{m2,i}}{\gamma_{m1,i}}$. Herein this is termed the desorption factor.

In organophilic pervaporation with low feed concentration, $\hat{P}_i$ can be treated as constant. From the definition $\hat{P}_i = \overline{D}_{m,i} S_i^f$, one would expect the amount of solute permeating through the pervaporation membrane to be highly dependent on the preferential sorption and diffusion of the membrane. It is interesting to note that the driving force term in equation (3.54) can be affected by the desorption factor Θ_i. The importance of this factor in transport modelling was demonstrated by Ten and Field (1998) and will be discussed in Chapter 4 in detail. As a first approximation, Θ_i can usually be assumed as unity and equation (3.54) reduced to the flux equation that is similar to the one in gas permeation (Ten and Field, 2000).

49

3.4.1.1 Sorption in membranes

Usually, a solubility parameter is defined to measure the degree of sorption of a certain component in a membrane. Sorption into the polymeric membrane is preferential. This idea is the same as a solute being preferentially soluble into a liquid phase. In pervaporation, it is such preferential sorption coupled, in some case, with preferential diffusion that enable separation to be achieved. In rubbery membranes that are frequently employed for organophilic pervaporation, the permeability is mainly determined by preferential sorption rather than preferential diffusion. It is the opposite case for the glassy membranes that are usually used for hydrophilic pervaporation (Bell, 1988). This is because in a rubbery membrane, the flexibilty or available free volume in the membrane matrix is higher than in a glassy membrane, preferential diffusion is not as limiting as sorption. It is different for a glassy membrane because of the rigidity of the matrix, preferential diffusion becomes more limiting than sorption.

3.4.1.1.1 Solubility Parameter

Sorption is determined by the affinity of a feed component towards the membrane polymer. A semi-quantitative estimation of the interaction between component and polymer using the solubility parameter theory has been devised to measure the degree of preferential sorption (Barton, 1983). Thus, the solubility parameter of penetrant, δ_i, which contains contributions from dispersion $(\delta_{d,i})$, polar $(\delta_{p,i})$ and hydrogen bonding $(\delta_{h,i})$ can be estimated by:

$$\delta_i = \left(\delta_{d,i}^2 + \delta_{p,i}^2 + \delta_{h,i}^2 \right)^{1/2} \tag{3.55}$$

Where: δ = Solubility Parameter, $(J/cm^3)^{1/2}$

In a binary system (polymer and single penetrant) sorption is likely to be high if δ_i for the polymer and penetrant are similar. If the δ_i's are too similar, however, it has been demonstrated (Zhu et al, 1983) that penetrant molecules may become immobilised within the polymer, decreasing the effective size of the available transport corridor. For ternary systems the solubility parameter approach is less successful due to interactions between the components of the liquid feed, although in many cases a good correlation still exists between δ_i difference and preferential sorption. Nevertheless, the solubility parameter is a good guide

for appropriate selection of pervaporation membranes material (Nijhuis et al, 1993). In practice however, the experimentally determined sorption isotherm is frequently used to describe the solubility behaviour of a component in the membrane for a range of partial pressures (activity).

3.4.1.1.2 Sorption Isotherm

The sorption isotherm can be determined in various ways. The most common way is to immerse a membrane sample of known mass, into a solution of known initial concentration. When sorption equilibrium is reached the membrane sample is removed and weighed to determine the mass increase. The solution is analysed to determine equilibrium concentration. Sorption of each component, at this concentration, can be determined by mass balance. From the gas phase, the membrane is surrounded by a flowing gas consisting of a carrier, such as nitrogen and a component to be sorbed, of known partial pressure (activity). The mass increase of the membrane is monitored until equilibrium is reached (Heintz et al, 1991). It is important to note that if a sorption isotherm is used in pervaporation transport modelling, an assumption of thermodynamic equilibrium at the fluid/membrane interfaces is applied.

There are generally four possible kind of sorption isotherms behaviour found in dense membranes (Mulder, 1991) which are shown in Fig. 3.11. Henry's law and Flory-Huggins type isotherms are typical for rubbery and glassy membranes while Langmuir and dual sorption are commonly found for ceramic or glassy membranes.

(i) Henry's Law   (ii) Flory-Huggins   (iii) Langmuir   (iv) Dual-sorption
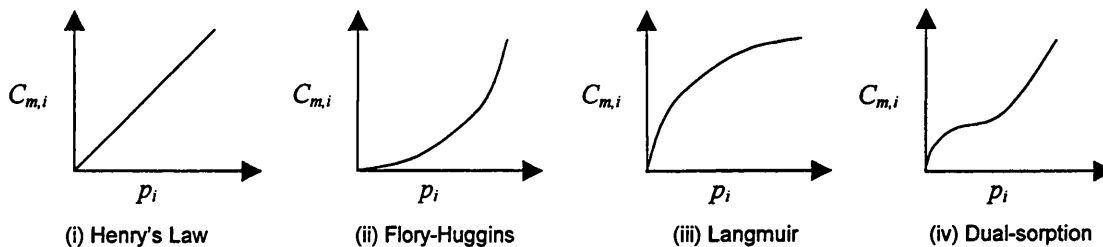
Fig 3.11. Various kind of sorption isotherm

Several researchers (Brun et al, 1985; Boddeker et al, 1990; Bell et al, 1988) have produced sorption isotherms for water and organics, from both liquid and gaseous phases. For typical organophilic pervaporation polymers (SBR, NBR, PDMS and PEBA), they found a linear sorption behaviour, i.e. the organic was sorbed in the membrane linearly for organic concentrations less than 8 mol %. This observation confirmed that for low feed solute concentrations, the interactions between individual components is less than the interaction between components and the membrane. Hence Henry's law generally applies to the sorption isotherm behaviour.

3.4.1.1.3 Flory-Huggins thermodynamics

In many cases, a linear relationship only exists at a very low concentration of the preferentially sorbed component. At higher concentrations the increase is non-linear. It is particularly true for benzene (linear up to 100ppm) and trichloroethylene (linear up to 200ppm) in NBR membrane (Brun et al, 1985; Nijhuis, 1990). The non-linearity of the sorption isotherm in the case above is due to the interaction between the components and the membrane. Thus, the Flory-Huggins thermodynamics which are based upon an expression for free enthalpy of mixing for the feed-membrane interface would be a useful tool to model the sorption between the membrane and the feed (Nijhuis, 1990; Huang and Rhim, 1991; Mulder, 1991; Favre et al, 1993, 1994).

According to Flory-Huggins thermodynamics, the volume fraction of liquid sorbed into the membrane for a binary system (a polymer and single liquid component system) can be related to liquid activity as follow (Flory, 1953):

$$\ln a_1 = \ln \phi_i + \left(1 - \frac{V_1}{V_3}\right)\phi_3 + \chi_{13}\phi_3^2 \qquad (3.56)$$

Where: a = Activity ϕ = Volume Fraction

V = Molar Volume, m³/mole χ = Interaction Parameter

1 denotes liquid   *3* denotes polymer

For a ternary system (e.g. organic(1)-water(2)-polymer(3)) the Flory Huggins equation can easily be extended:

$$\ln a_1 = \ln \phi_1 + (1 - \phi_1) - \phi_2 \frac{V_1}{V_2} - \phi_3 \frac{V_1}{V_3} + \left(\chi_{12}\phi_2 \frac{V_1}{V_2} + \chi_{13}\phi_3 \right)(\phi_2 + \phi_3) - \chi_{13} \frac{V_1}{V_2}\phi_2\phi_3 \qquad (3.57)$$

$$\ln a_2 = \ln \phi_2 + (1 - \phi_2) - \phi_1 \frac{V_2}{V_1} - \phi_3 \frac{V_2}{V_3} + \left(\chi_{12}\phi_1 \frac{V_2}{V_1} + \chi_{23}\phi_3 \right)(\phi_1 + \phi_3) - \chi_{13} \frac{V_2}{V_1}\phi_1\phi_3 \qquad (3.58)$$

In general the molar volume of the polymer is much larger than that of the penetrants and hence $\frac{V_1}{V_3}$ and $\frac{V_2}{V_3} \to 0$.

In organophilic pervaporation, water is less preferentially sorbed in the membrane and a low ϕ_2 in PDMS membrane has been reported to be of the order of 0.002 by various studies in the temperature range of 25-40°C (Watson and Payne, 1990; Mulder and Smolders, 1991; Favre et al, 1993; Favre et al, 1994). It is, therefore, normally appropriate to use the binary isotherm, equation (3.56), rather than the ternary isotherm, equation (3.58) to describe water sorption, outside of the region of Henry's law. Due to extreme clustering, it is not thought possible to accurately fit water sorption to existing isotherms (Favre et al, 1994).

To use Flory-Huggins thermodynamics to describe the sorption isotherm in glassy polymers, an additional term called the Flory-Rehner modification (Flory, 1953) has to be added to equation (3.56). This modification is to account for restrictions to chain segment mobility caused by adjacent crystallites in the glassy polymer. Hence, the modified Flory-Huggins sorption isotherm becomes:

$$\ln a_1 = \ln \phi_i + \left(1 - \frac{V_1}{V_3}\right)\phi_3 + \chi_{13}\phi_3^2 + \frac{\langle \alpha \rangle_o^2 (\upsilon / A)V_1\phi_3^2}{V_{3u}} \qquad (3.59)$$

Where: $\langle \alpha \rangle_o$ = ratio between the mean distance separating the junctions in the unswollen network and the mean end-to-end distance for the corresponding segment if this segment were unrestricted

υ = No. Effective Segments in Sample A = Avogadro Number

u denotes unswollen

In describing the energy change due to elastic strain in cross linked polymers, the Flory-Huggins expression for sorption isotherm can be modified as follow (Nijhuis, 1990):

$$\ln a_1 = \ln \phi_i + \left(1 - \frac{V_1}{V_3}\right)\phi_3 + \chi_{13}\phi_3^2 + \frac{V_1\rho_3}{M_c}\left(1 - \frac{2M_c}{M}\right)\left(\phi_3^{1/3} - \frac{1}{2}\phi_3\right)$$ (3.60)

Where: ρ = Density g/cm^3 $\qquad$ M_c = Molecular Mass per Cross Linked Unit

$\qquad$ M = Molecular Mass before crosslinking

The factor $(1 - 2M_c / M)$ expresses the correction for network imperfections resulting from chain ends. For a perfect network $M \rightarrow \infty$ and hence the factor reduces to unity. The same correction factors can also be added to equation (3.57) and (3.58) when describing a ternary system. For rubbery pervaporation membranes, in which swelling is low, the elastic strain term is small and can be neglected (Nijhuis, 1990). In addition if water sorption (i.e. ϕ_2) is very low, equation (3.60) reduces to the binary isotherm of equation (3.56).

Not all organic sorption isotherms fit well to the basic form of the Flory Huggins equation (3.57) and (3.58). This is because in the original Flory-Huggins theory the interaction parameters are considered a constant. On the contrary, experimental results indicate that the interaction parameters are quite concentration dependant, especially χ_{13}. For such poorly fitting systems, the basic Flory Huggins theory must be refined in order to produce an adequate fit. For sorption of alcohols it has been shown (Favre et al, 1993, 1994) that it is necessary to employ a variable interaction parameter, χ_{13}, as proposed by Koningsveld and Kleinjtens (1971):

$$\chi_{13} = \lambda + \frac{\Omega(1 - w)}{(1 - w\phi_3)^2}$$ (3.61)

Ω is an empirical correction term, λ is linked to mixing enthalpy and w to the coordination number of the network. Unfortunately λ, Ω and w can only be obtained experimentally, by a non-linear curve fit of sorption data and hence reduces the usefulness of the Flory-Huggins approach.

The basic Flory-Huggins theory assumes perfect mobility of polymer chains and no preferential sites in the lattice. It is thought that deviation results from the tendency for solvent to cluster within the polymer matrix. According to Zimm and Lundberg's analysis

(Favre et al, 1993, 1994) the average cluster size increases as solvent affinity for the membrane decreases. Nevertheless if the interaction χ_{13} is constant, it may be predicted using the solubility parameter approach (Zielinski and Duda, 1992):

$$\chi_{13} = \chi_1 + \frac{V_1}{RT}(\delta_1 - \delta_3)^2 \tag{3.62}$$

Where: R = Universal gas constant, kJ/kmol/K

T = temperature, K

From equations (3.56) and (3.62) sorption of organic increases as temperature increases. It has been shown that both phenol and water sorption in PEBA membranes, from aqueous solution, increase with temperature by almost an order of magnitude between 30 and 70°C, however, the shapes of the sorption isotherms remain similar over this temperature range (Kondo and Sato, 1994).

3.4.1.1.4 Sorption coefficient

In the range of low solvent activity (low feed solvent concentration in the case of ternary systems), and regardless of the overall form of the sorption isotherm, for first approximation the sorption isotherm can be assumed that of Henry's law. Hence, the volume fraction of liquid solute sorbed into the membrane can be related to liquid activity by an activity based sorption coefficient, S_i^a :

$$\phi_i = S_i^a \cdot a_i \tag{3.63}$$

Henry's law assumes that the sorption coefficient remains constant over the concentration range in which it applies. To account for non-linearity of the sorption isotherm, particularly at higher concentration, the sorption coefficient can be expressed as a function of solute activity in the liquid:

$$S_i^a = f(a_i) \tag{3.64}$$

If the density of the membrane throughout is relatively constant, the solute concentration sorbed into the membrane, $C_{m,i}$ (kmol/m^3) can be related to the volume fraction of liquid solute sorbed into the membrane, ϕ_i with the following approximation:

$$C_{m,i} = \frac{\rho_m}{M_i} \cdot \phi_i \qquad\qquad (3.65)$$

Where ρ_m = density of the membrane, kg/m^3. M_i = Molar mass of solute, kmol/kg.

By combining equation (3.63) and (3.65), the sorption isotherm can be expressed as:

$$C_{m,i} = \frac{\rho_m}{M_i} \cdot S_i^a \cdot a_i \qquad\qquad (3.66)$$

If the solvent activity coefficient is considered constant across a dilute concentration range, a concentration based sorption coefficient, S_i^c, can be defined to describe the sorption isotherm in terms of the liquid concentration of solute at membrane/feed interface, $C_{mb,i}$:

$$C_{m,i} = S_i^c \cdot C_{mb,i} \qquad\qquad (3.67)$$

The sorption relationship above was used by (Cote and Lipski, 1988) to model the pervaporation transport mechanism. Since the liquid concentration of solute adjacent to the membrane can be approximated as:

$$C_{mb,i} = \frac{\tilde{\rho}_l}{M_i} \cdot x_{mb,i} \qquad\qquad (3.68)$$

Where $\tilde{\rho}_l$ is the average density of the liquid feed and $x_{mb,i}$ is the solute mole fraction in the liquid adjacent to the membrane surface, S_i^c can be related to S_i^a by combining equations (3.66)-(3.68) and this yields:

$$S_i^c = \frac{\rho_m \gamma_{mb,i}}{\tilde{\rho}_l} \cdot S_i^a \qquad\qquad (3.69)$$

Where $\gamma_{mb,i}$ is the activity coefficient of solute in the liquid feed adjacent to the membrane.

It is obvious that if the solute in the feed liquid is low, the sorption coefficient is quasi constant which means Henry's law applies. For chloroform and alcohol in PDMS membrane, some researchers (Blume et al, 1991; Farve et al, 1993, 1994) found that S_i^a remains typically constant up to a component activity of about 0.4.

Temperature might affect the magnitude of S_i^c yet Henry's law still applies. This effect is shown by (Boddeker et al, 1990; Kondo and Sato, 1994) in which constant S_i^c has been

reported for phenol sorption in PEBA membranes up to 50 kg of phenol/m^3 at 30, 50 and 70°C.

For organophilic pervaporation, generally, the feed concentration of water is very high and the activity of water tends to unity. Although the organic feed concentration is very low in organophilic pervaporation, the water volume fraction in PDMS membranes is prevented from exceeding 0.3% due to the strong hydrophobicity of the membranes (Farve et al, 1993). In the case of phenol solution in PEBA membrane, Boddeker et al (1990), Kondo and Sato (1994) found that the water sorption was constant up to a phenol concentration of about 1.5wt%, after which it started to increase. The increase of water sorption was probably due to the interaction of between water and the organics sorbed in the membrane, i.e. χ_{23} in equation (3.48). A similar effect was reported by Mulder and Smolders (1991) for 5%wt. alcohol solutions, the volume fraction of water sorbed ϕ_j was found to increase from 0.0013 to 0.0022 as the alcohol was changed in the series from methanol to butanol, with a corresponding increase in alcohol sorption. In order to include this effect, S_j^a has to be defined as a function of organic solute activity, i.e. $S_j^a = f(a_i)$.

3.4.1.2 Diffusion in membranes

The diffusion of penetrants through non-porous pervaporation membranes can be described by free-volume theory (Fujita, 1961). According to free-volume theory, there are free volumes between the molecular chains or between polymer segments that are caused by continuous movement of the polymer. Rubbery polymers have a high degree of chain mobility and respond quickly to the presence of a permeant dissolved within them. In the pervaporation process, the feed liquid creates a concentration of penetrants at the feed side of the membrane. Drying on the permeate side (due to vacuum) creates an imbalance of free volume available across the membrane. By a hole-filling mechanism, the net movement is for molecules and penetrants to travel from feed side to the permeate side and the amount of molecular jump per unit time and area is the membrane diffusion flux of the permeant (Rhim and Huang, 1991; Atkins, 1996). It is possible to quantify the diffusion rate in polymeric membranes by Fick's first law as:

$$J_i = -D_{m,i} \frac{dC_{m,i}}{dz}$$
(3.45)

or in integrated form:

$$J_i = \frac{\overline{D}_{m,i}}{\delta_m} \left(C_{m1,i} - C_{m2,i} \right)$$
(3.47)

Where $\overline{D}_{m,i} = \dfrac{1}{\left(C_{m1,i} - C_{m2,i} \right)} \displaystyle\int_{C_{m2,i}}^{C_{m1,i}} D_{m,i} dC_{m,i}$, mean diffusivity, m^2/s
(3.48)

The solute diffusion coefficient or diffusivity $D_{m,i}$ is the measure of the mobility of the solute within membrane. The diffusivity is a function of membrane structure, physical properties of the permeating species and the process conditions. Since $C_{m1,i}$ and $C_{m2,i}$ can be calculated from sorption isotherms, and the thickness of membrane is known, the mean diffusivity can be determined. The magnitude of mean diffusivity changes with the membrane structure, physical properties of the permeating species and the process conditions. Hence, with the use of mean diffusivity, the mobility of different solutes can be compared quantitatively. The disadvantage of using the mean diffusivity is that the effect of interactions cannot be deduced.

The search for relationships between diffusion coefficient, $D_{m,i}$ and solute concentration in the membrane, $C_{m,i}$ has received much attention in the past. Early work by Fujita (1961), adapted by Fels and Huang (1971) which centered around the free-volume theory. This method is complex and found to be difficult to apply to pervaporation (Fleming and Slater, 1992). A phenomenological approach is generally used to estimate D_{mi} and appears to be of greater practical value (Rautenbach, Albrecht, 1985).

3.4.1.2.1 Diffusivity function

In order to fit pervaporation flux data, Long (1965) suggested that the diffusivity $(D_{m,i})$ can be expressed as an exponential function of the solute concentration in the membrane $(C_{m,i})$:

$$D_{m,i} = D_{m0,i} \exp(\tau_i C_{m,i}) \tag{3.70}$$

Where $D_{m0,i}$ is the diffusion coefficient at infinite dilution, and τ_i is a plasticization coefficient to account for the interaction of the particular permeant and polymer. Hence the mean diffusivity can be evaluated as follow:

$$\overline{D}_{m,i} = \frac{D_{m0,i}\left[\exp(\tau_i C_{m1,i}) - \exp(\tau_i C_{m2,i})\right]}{\tau_i\left(C_{m1,i} - C_{m2,i}\right)} \tag{3.71}$$

The function represents the magnitude of the effect of solute concentration on the solute mobility in the membrane. As $C_{m1,i}$ and $C_{m2,i}$ can be determined from a sorption isotherm, τ_i and $D_{m0,i}$ can then be obtained by a curve fitting method.

In modelling pervaporation of hexane through polyethylene membranes, Greenlaw et al (1977) proposed another form of relationship between diffusivity and concentration in pervaporation:

$$D_{m,i} = D_{m0,i}\left[1 + \tau_i\left(C_{m,i}\right)^n\right] \tag{3.72}$$

where n is an arbitrary constant, hence the mean diffusivity can be expressed as follows:

$$\overline{D}_{m,i} = D_{m0,i}\left\{1 + \frac{\tau_i\left[\left(C_{m1,i}\right)^{n+1} - \left(C_{m2,i}\right)^{n+1}\right]}{(n+1)\left(C_{m1,i} - C_{m2,i}\right)}\right\} \tag{3.73}$$

They found that the simplified expression:

$$D_{m,i} = \kappa_i C_{m,i} \tag{3.74}$$

followed the data obtained by Roger et al (1960) and its mean diffusivity reduced to:

$$\overline{D}_{m,i} = \frac{\kappa_i}{2}\left(C_{m1,i} + C_{m2,i}\right)$$ (3.75)

In their analysis of component transport in pervaporation, Rautenbach and Albrecht (1985a, 1985b) adapted a modified form of the diffusivity function used by Greenlaw et al (1977) that was sufficient for basic design calculations:

$$D_{m,i} = D_{m0,i}\left(1 + \tau_i C_{m,i}\right)$$ (3.76)

The corresponding mean diffusivity is:

$$\overline{D}_{m,i} = D_{m0,i}\left[1 + \frac{\tau_i}{2}\left(C_{m1,i} + C_{m2,i}\right)\right]$$ (3.77)

τ_i was used by Favre et al (1994) to explain the swelling effect by different individual organic solvents on PDMS membrane. Based on equation (3.70), the value of τ_i 's were found to be in the range of 150 to –2075. The negative τ_i were explained as the result of permeant molecules clustering within the membrane. In fact τ_i is simply a fitting parameter and cannot be measured independently, hence to deduce any physical significance from τ_i seems to be difficult. Also the value of τ_i depends on which diffusivity function is used.

It should be noted that all the diffusivity functions proposed above are established under the assumption of a negligible coupling effect for the transport. In organophilic pervaporation, with low feed concentration, the coupling effect is usually negligible. Also the plasticization effect of the rubbery membrane is small, thus $D_{m,i} \approx D_{m0,i}$ and therefore $\overline{D}_{m,i} \approx D_{m0,i}$.

Sorption measurements usually allow solubility and diffusion coefficients to be obtained. An alternative method based on Crank's work (Crank, 1975) for determining the membrane diffusivity at very low feed solute concentrations is described by Lamer (1994). Crank (1975) proposed a solution to Fick's law for the case when the variation of solute concentration in the membrane is solely due to the sorption of solute (solvent sorption is less than 0.1% of solute sorption) and $D_{m,i}$ remains constant with the concentration in the membrane. Assume that:

- The polymer is initially free from solute
- The solute diffuses through the membrane in the direction of thickness

- The rate at which solute leaves the solution is always equal to that at which it enters the membrane

- The concentration in the solution is always uniform and equal to the initial concentration

The sorption kinetics can be described by:

$$\frac{m(t)}{m(\infty)} = 1 - \sum_{n=1}^{\infty} \frac{8}{(2n+1)^2 \pi} \exp\left[-\frac{D_{m,i}(2n+1)^2 \pi^2 t}{\delta_m^2}\right]$$ (3.78)

Where $m(t)$ is the mass increase of solute in the membrane at time t, mg

$m(\infty)$ is the mass increase of solute in the membrane at equilibrium, mg

δ_m is the thickness of the membrane, m

$D_{m,i}$ is the constant diffusivity of solute in membrane, m^2/s

$\frac{m(t)}{m(\infty)}$ can be obtained by measuring the kinetics of sorption using a gravimetric technique to

monitor the mass increase of a membrane sample with time (Lamer et al, 1994). The diffusion coefficient can be calculated from the following expression:

$$D_{m,i} = 0.049 \frac{\delta_m^2}{t_{1/2}}$$ (3.79)

Where: $t_{1/2}$ is the half time when $\dfrac{m(t_{1/2})}{m(\infty)} = \dfrac{1}{2}$, s

It should be noted that such a method can only be used at low feed concentration ($< 2kg/m^3$) and the method is restricted for the determination of constant diffusivity (Lamer, 1994). Some researchers (Blume et al, 1991; Dotremont et al, 1995) use such a method to investigate the variation of diffusivity with feed activity even up to 0.7, hence, abnormal results were reported and in contradiction to normal theory.

3.4.1.2.2   The effect of temperature upon diffusivity

An increase in temperature results in increased flexibility of the polymer membrane structure, hence, the diffusivity is strongly dependent on the temperature. This phenomenon can be described with an Arrhenius type expression for the diffusion coefficient at infinite dilution (Karlsson and Tragrardh, 1993):

$$D_{m0,i} = D_i^* \exp(-E_D/RT)$$ (3.80)

Where D_i^* is the Arrhenius pre-exponential constant, m^2/s

E_D is the activation energy for diffusion, kJ/kmol

R is the universal gas constant, kJ/kmol/K

T is the thermodynamic temperature, K

As pervaporation involves evaporation, this probably results in a small temperature gradient across a membrane. This gradient is however, often considered to be negligible and the process is therefore usually modelled as locally isothermal (Karlsson and Tragrardh, 1993).

In organophilic pervaporation with low feed concentrations, $D_{m,i} \approx D_{m0,i}$ and are typically of the order of 10^{-11} to 10^{-10} m^2/s, at close to ambient temperatures. As the temperature is elevated to 80°C, the magnitude of $D_{m0,i}$ increased by up to two order of the magnitude (Watson and Payne, 1990; Lamer et al, 1994; Favre et al, 1994). Generally, the activation energy for diffusion is positive (Feng and Huang, 1996) and the typical value of E_D for organics in rubbery polymer are in the order of 10^4 kJ/kmol (Van Krevelen, 1976)

3.4.1.3 Desorption

Desorption is the transition of penetrants from the membrane matrix into the permeate side. The desorption step is not normally considered as the controlling resistance of the transport (Fleming and Slater, 1992). According to the assumptions that were laid down for the ideal solution-diffusion model, the chemical potentials at the membrane/permeate interface are in equilibrium with each other. The solute activity in the membrane adjacent to the permeate is related to the activity at the vapour permeate as equation (3.41):

$$a_{m2,i} = a_{p,i} \cdot \exp\left[-\frac{\hat{V}_i}{RT}\left(p_f - P_i^{sat}\right)\right]$$

(3.41)

The exponential term in equation (3.41) is usually very small and close to unity (Rautenbach and Albrecht, 1989), hence, $a_{m2,i} = a_{p,i}$ and the solute concentration in the membrane adjacent to the permeate side is defined as:

$$C_{m2,i} = \frac{C_m}{\gamma_{m2,i}} \cdot a_{p,i}$$

(3.81)

Where $\gamma_{m2,i}$ and C_m are the activity coefficient of solute in membrane and total molar density of membrane respectively. If a very high vacuum ($P_p \rightarrow 0$) is applied at the permeate side of the membrane, the maximum possible desorption rate might be higher than the absorption rate at the surface of the permeate side. There is however, the assumption of a close equilibrium condition at the surface. This holds because the diffusion rate is much slower than both the maximum absorption and maximum desorption rates. From equation (3.81), the desorption isotherm is a function of the $\gamma_{m2,i}$ and C_m which accounts for the penetrant/membrane interactions and the membrane structure. There is no direct experimental method or a semi-empirical relationship that can be used to determine $\gamma_{m2,i}$ unless a constant membrane density is assumed.

If the desorption isotherm can be described in a similar way as the sorption isotherm, Flory-Huggins thermodynamics can then be used to describe the relationship between the vapour activity and the volume fraction of penetrant on the downstream side. This gives:

$$\ln a_1 = \ln \phi_1 + \left(1 - \frac{V_1}{V_3}\right)\phi_3 + \chi_{13}\phi_3^2$$

(3.56)

Where: a = Activity ϕ = Volume Fraction

V = Molar Volume, m³/mole χ = Interaction Parameter

1 denotes solute   *3* denotes polymer

As the hysteric effect and the clustering or immobilization of some components in the membrane are significant, the desorption isotherm may not equal to the sorption isotherm. The desorption isotherm is a function of the volatility of the penetrant, component/membrane interactions and the structure of the membrane.

3.4.1.3.1 Desorption coefficient

No matter what the overall form of the isotherm is, the desorption isotherm can be first approximated as the form of Henry's Law since there is a relatively dry surface at the permeate side.

$$\phi_{m2,i} = S_i^d \cdot a_{p,i} \tag{3.82}$$

If the density of the membrane throughout is relatively constant, the solute concentration in the membrane adjacent to the permeate side can be described as:

$$C_{m2,i} = \frac{\rho_m}{M_i} \cdot S_i^d \cdot a_{p,i} \tag{3.83}$$

Where ρ_m = density of the membrane M_i = Molar mass of solute

In order to compare with the gas permeation studies, the desorption isotherm can be expressed in terms of partial pressure as in equation (3.50):

$$C_{m2,i} = S_i^p \cdot p_{p,i} \tag{3.50}$$

Where $S_i^p = \dfrac{\rho_m}{M_i P_i^{sat}} \cdot S_i^d$, partial pressure based desorption coefficient, kmol/m³·Pa

3.4.1.3.2 Desorption factor

In deriving the membrane mass transfer equation (3.54), a desorption factor is introduced to account for the difference between sorption and desorption coeficients.

$$J_i = \frac{\hat{P}_{m,i}}{\delta_m}\left(p_{mb,i} - \Theta_i p_{p,i}\right) \tag{3.54}$$

Where $\hat{P}_{m,i} = \overline{D}_{m,i}S_i^f$, permeability of solute in membrane, kmol/m·s·Pa

$$\Theta_i = \frac{S_i^f}{S_i^p} = \frac{S_i^d}{S_i^a} = \frac{\gamma_{m2,i}}{\gamma_{m1,i}} \text{, desorption factor}$$

From the literature, the desorption factor is usually assumed to be unity, i.e. sorption coefficient is same to the one for desorption (Wijmans and Baker, 1993). Thus equation (3.54) is reduced to the form similar to the one for gas permeation:

$$J_i = \frac{\hat{P}_{m,i}}{\delta_m}\left(p_{mb,i} - p_{p,i}\right) \tag{3.84}$$

However, Ten and Field (1998, 2000) has shown that for the mass transport of low volatility organics in organophilic pervaporation, the desorption factor was found to be important and not equal to unity. Mulder (1991), Karlsson and Tragrardh (1993) suggested that if the permeate pressure is low enough, the desorption factor would not be important and a similar conclusion was also drawn by Cote and Lipski (1988). In reality however, ultimate vacuum is beyond reach in industrial operation (Karlsson and Tragrardh, 1993) hence, the desorption factor should not be ignored. For first approximation, the desorption factor can be assumed to be unity for the ease of calculation. However, for more accurate calculations, such a factor should be included.

3.4.1.3.3 Desorption Resistance

The resistance at the membrane interface is usually considered negligible compared to the resistance of the membrane and of the boundary layer (for both feed and permeate side). If the flux through the membrane and boundary layer is high enough, the membrane interface resistance on the permeate side becomes significant. Bode et al (1993) suggested that if the temperature of the flux measurement is below or only moderately above the glass transition

temperature, T_g, the slow processes of rearrangement may occur in the polymer following a change in permeate concentration. In this case, if the flux is high enough, the interface resistance will be significant. Sturken (1994) and Yeom and Lee (1997) derived the desorption resistance by assuming chemical potential equilibrium at the interface, however, this is in contradiction to the solution-diffusion model derivation. It should be noted that whenever the membrane flux is comparable to the rates of absorption and desorption on the membrane surface adjacent to the permeate side, the system is no longer in near-equilibrium at the interface and some deviation from the solution-diffusion model is expected. In addition, if the membrane interface resistance at the permeate is due to the slow processes of rearrangement in the polymer, the concentration profiles in a membrane and hence also the fluxes will take a long time to become really stationary and comparable (Bode et al, 1993) and make the actual determination of desorption resistance difficult.

Separate studies of desorption resistance carried out by Sturken (1994), Yeom and Lee (1997) and Bode et al (1993) show that the desorption resistance is a function of permeate pressure, thickness of the membrane and the volatility of the solute. From their studies a mass transfer equation based on resistance-in-series is derived with the assumption of a desorption factor equal to unity as follow:

$$J_i = \frac{1}{\dfrac{\delta_m}{\hat{P}_{m,i}} + R_D}\left(p_{mb,i} - p_{p,i}\right)$$
(3.85)

Where R_D is the desorption resistance, Pa·s·m^2/kmol

They found that R_D increases as the permeate pressure increases. However it decreases as the thickness of the membrane and volatility of the solute increases. Although a semi-empirical adsorption-desorption model was devised by Bode et al (1993) to describe behaviour that implies a desorption resistance, the derived model is contradicts itself internally; there cannot be an additional resistance and near equilibrium.

3.4.1.4 Coupling Effect

The flux of pervaporation is determined not only by the driving force but the solubility and diffusivity of the solute in the membrane. However, the solubility of a solute in the membrane is not only determined by the solute itself but also by the solvent. In addition, the diffusivity of the solute is influenced by the diffusivity of the solvent. These two interactions are described as coupling effects, i.e. sorption coupling and diffusion coupling (Mulder and Smolder, 1991). These two phenomena are generally considered as two separate elements of coupling. The coupling effects are particularly important in high flux membranes and multicomponent pervaporation transport.

3.4.1.4.1 Sorption coupling

The phenomenon of sorption coupling may be explained as the result of free volume alteration in the membrane due to the existence of a second component or the change of membrane morphology due to competitive sorption of two components (Brun et al, 1985; Drioli et al, 1993). The degree of sorption coupling varies with different components and the membrane used. For instance, in polysulphone membranes no sorption of pure water can be detected, however in the presence of ethanol, water is both sorbed and transported preferentially (Mulder et al, 1985). For aqueous pyridine solutions, pyridine transport is facilitated at low pyridine concentrations and water transport facilitated at high pyridine concentrations, through PDMS membranes (Drioli et al, 1993). In some cases, the effect of sorption coupling can be adverse due to the sorption of another component, for instance in NBR (nitrile butadiene rubber) membranes, sorption of water from aqueous benzene solutions was found to fall dramatically as benzene activities exceeded 0.7 (Brun et al, 1985). In this case it was thought that the membrane was so swollen by hydrophobic benzene that water was almost totally excluded. A similar effect was also observed in a sorption study of zeolite filled PDMS membranes. It was found that the sorption of an organic, from dilute aqueous solution, into the membrane was always reduced by the presence of a second organic. On contrary, such an effect was not found in unfilled PDMS (Goethaert et al, 1993).

The sorption coupling phenomenon is difficult to measure quantitatively. It is also difficult to estimate beforehand the influence of this phenomenon on the separation properties. However,

it is possible to get indirect information from sorption and desorption experiments. In practice, sorption coupling effects on sorption behaviour can be described by the semi-empirical Flory-Huggins sorption isotherms.

Recall Flory-Huggins sorption isotherm for ternary system [solute(1)-solvent(2)-membrane(3)]:

$$\ln a_1 = \ln \phi_1 + (1 - \phi_1) - \phi_2 \frac{V_1}{V_2} - \phi_3 \frac{V_1}{V_3} + (\chi_{12}\phi_2 + \chi_{13}\phi_3)(\phi_2 + \phi_3) - \chi_{13}\frac{V_1}{V_2}\phi_2\phi_3 \qquad (3.57)$$

$$\ln a_2 = \ln \phi_2 + (1 - \phi_2) - \phi_1 \frac{V_2}{V_1} - \phi_3 \frac{V_2}{V_3} + \left(\chi_{12}\phi_1 \frac{V_2}{V_1} + \chi_{23}\phi_3\right)(\phi_1 + \phi_3) - \chi_{13}\frac{V_2}{V_1}\phi_1\phi_3 \qquad (3.58)$$

It can be seen that the interaction parameter χ_{12} can account for coupling between the sorption of components *1* & *2*. This interaction parameter is not concentration independent. However to facilitate the analysis, it is usually assumed as concentration independent (Mulder et al, 1985). The sorption coupling interaction parameter is also a function of temperature.

3.4.1.4.2   Diffusion coupling

Diffusion coupling may be explained as the result of interactions between components at a molecular level during the course of transport. In the solution-diffusion model, the flux coupling effect is described in terms of the themodynamics of irreversible processes. For a binary liquid mixture, the following equations are given (Mulder and Smolder, 1991):

$$J_i = -L_i \frac{d\mu_{m,i}}{dz} - L_{ij} \frac{d\mu_{m,j}}{dz} \qquad (3.86)$$

$$J_j = -L_j \frac{d\mu_{m,j}}{dz} - L_{ji} \frac{d\mu_{m,i}}{dz} \qquad (3.87)$$

L_i and L_j are the phenological coefficients to account for the mobility due to individual components and L_{ij} and L_{ji} are the phenological coefficients to account for the mutual drag or enhancement due to the facilitated interaction between components.

According to Onsager relations, the matrix of phenological coefficients is symmetric, hence $L_{ij} = L_{ji}$. If $L_{ij} < 0$, the two component flows enhance each other while for $L_{ij} > 0$ they hindered each other (Kedem, 1989).

$$J_i = -\frac{\left(L_i L_j - L_{ij}^2\right)}{L_j} \cdot \frac{d\mu_{m,i}}{dz} + \frac{L_{ij}}{L_j} \cdot J_j \qquad (3.88)$$

$$J_j = -\frac{\left(L_i L_j - L_{ij}^2\right)}{L_i} \cdot \frac{d\mu_{m,j}}{dz} + \frac{L_{ij}}{L_i} \cdot J_i \qquad (3.89)$$

According to thermodynamic principles the coefficients in equation (3.88) & (3.89) have to fulfill the three following conditions (Molina et al, 1997):

$$L_i > 0 \; ; \; L_j > 0 \, ; \, L_i \cdot L_j > L_{ij}^2$$

It should be noted that as the temperature increases, the total flux through the membrane increases exponentially. Hence, the coupling effect would be increased significantly. In the study of hexane and heptane separation with a polyethylene membrane, (Rautenbach and Albrecht, 1986) observed significant flux coupling effect at high temperature but a negligible coupling effect at low temperature.

When $L_{ij} \rightarrow 0$, the coupling effect would be negligible and equation (3.88) & (3.89) can be reduced to:

$$J_i = -L_i \frac{d\mu_{m,i}}{dz} \qquad (3.38)$$

$$J_j = -L_j \frac{d\mu_{m,j}}{dz} \qquad (3.90)$$

The diffusion coupling effect is also explained in terms of friction between components in the system (Kedem, 1989). If the flow interaction may be represented by friction coefficients, from the concept of irreversible thermodynamics, all the driving forces acting on a component moving through another medium are balanced by friction with that medium.

$-\Sigma$ (driving forces on i) = Σ (friction on i)

The above relationship is, in fact, the Maxwell-Stephan Equation. Hence for a ternary system two equations can be derived:

$$-\frac{1}{RT}\frac{d\mu_{m,i}}{dz} = \Omega_{ij}\left(v_i - v_j\right) + \Omega_{m,i}v_i \qquad (3.91)$$

$$-\frac{1}{RT}\frac{d\mu_{m,j}}{dz} = \Omega_{ji}\left(v_j - v_i\right) + \Omega_{m,j}v_j \qquad (3.92)$$

Where Ω_{ji} is the friction coefficients for the friction effect exerted by component j on i.

Ω_{ij} is the friction coefficients for the friction effect exerted by component i on j.

Ω_{mi} is the friction coefficients for the friction effect exerted by membrane on i

v_i and v_j are the local velocities of component i and j respectively.

According to Onsager relation, $\Omega_{ji} = \Omega_{ij}$. If the component fluxes can be related to its local velocity by the following relationship:

$$J_i = \frac{\rho_m}{M_i} \cdot v_i \qquad (3.93)$$

$$J_j = \frac{\rho_m}{M_j} \cdot v_j \qquad (3.94)$$

where ρ_m is the density of the membrane and M is the molar mass of the component, then the flux equation can be rewritten by combining equations (3.91)-(3.94) to yield:

$$J_i = \frac{\rho_m}{M_i\left(\Omega_{ij} + \Omega_{m,i}\right)}\left(-\frac{1}{RT}\frac{d\mu_{m,i}}{dz} + \frac{\Omega_{ij}M_j}{\rho_m} \cdot J_j\right) \qquad (3.95)$$

$$J_i = \frac{\rho_m}{M_j\left(\Omega_{ij} + \Omega_{m,i}\right)}\left(-\frac{1}{RT}\frac{d\mu_{m,j}}{dz} + \frac{\Omega_{ij}M_i}{\rho_m} \cdot J_i\right) \qquad (3.96)$$

If the friction between solute and solvent is much smaller than the friction caused by the membrane, equations (3.35) & (3.96) are reduced to:

$$J_i = -L_i\frac{d\mu_{m,i}}{dz} \qquad (3.38)$$

$$J_j = -L_j\frac{d\mu_{m,j}}{dz} \qquad (3.90)$$

Where $L_i = \dfrac{\rho_m}{M_i\Omega_{m,i}RT}$ and $L_j = \dfrac{\rho_m}{M_j\Omega_{m,j}RT}$

The flux equations (3.95) & (3.96) was used by Heintz and Stephan (1994) to model the pervaporation flux data of the water-ethanol-PVA system. It has been shown that the computational load increases significantly when the coupling effect was considered.

Apart from the flux equations derived from irreversible thermodynamics processes, Fick's first law can also be used to model the effect of diffusion coupling in pervaporation flux:

$$J_i = D_{m,i} \frac{dC_{m,i}}{dz}$$
(3.45)

The Fickian diffusivity has to be modified to account for the diffusion coupling. To do this, Brun et al (1985) and Mulder and Smolder (1984) modified the diffusivity in Fick's first law equation for a ternary system into a function containing both the sorbed concentration of solute and solvent as follow:

$$D_{m,i} = D_{m0,i} \exp(\tau_i C_{m,i} + \tau_{ij} C_{m,j})$$
(3.97)

τ_i accounts for swelling of the membrane, τ_{ij} accounts for diffusion coupling effect. However, there is no relation between τ_i and τ_{ij} since they are just curve fitting parameters. If sorption isotherms are available, assuming the sorption isotherms are equal to the desorption isotherm, from the equations above, six-parameters are required to fit the variation of flux measurement with permeate pressure (Brun et al, 1985).

An alternative approach to describe the transport of ethanol-water mixtures through silicone rubber was proposed by Radovanovic et al (1990). The coupling effect is considered to be due to dimerisation of ethanol and water. It is assumed that water clusters break down in the presence of ethanol to form ethanol-water dimers. A fraction of each species is transported both as monomer and dimer. The resulting transport equations are as follows:

$$J_i = -D_{m,i} \frac{dC_{m,i}}{dz} - D_{dim} \frac{dC_{dim}}{dz}$$
(3.98)

$$J_j = -D_{m,j} \frac{dC_{m,j}}{dz} - D_{dim} \frac{dC_{dim}}{dz}$$
(3.99)

Where D_{dim} and C_{dim} are the diffusivity and concentration of the dimer in the membrane.

71

3.4.1.4.3   Coupling effect in organophilic pervaporation

In organophilic pervaporation, with the use of hydrophobic membranes at low organic feed concentration, coupling effects are often much less important than other factors. This can be attributed to the low degree of swelling in crosslinked rubbery membranes, especially when feed organic concentrations tend to be low. Several studies have reported almost negligible coupling effects for good solvents, such as chlorinated organics, in rubbery membranes. Negligible coupling was observed, for either organic or water fluxes, for aqueous mixtures of toluene and/or various chlorinated hydrocarbons, for organic component concentrations up to 300ppm feed, in PDMS, PEBA and Polyurethane membranes (Ji et al, 1994). Similar conclusions were drawn from a study using silicone tubing for aqueous solutions of acetone, ethanol and halogenated hydrocarbons for feed concentrations up to 600 ppm (Nguyen and Nobe, 1987). It should be noted that the coupling effect in organophilic pervaporation could not be ignored when the feed concentration is high enough to swell the membrane and a high permeation flux is observed. Although a pervaporation plant may be designed for a higher organic feed concentration (e.g. 10,000ppm) at the inlet stream, during the sizing of membrane area, it is still reasonable to assume zero coupling effect as larger part of the area will be used for the "polishing".

3.4.2 Pore Flow Model

In order to improve the pervaporation flux through the membrane, some researchers suggested the use of integral asymmetric membranes as an alternative to dense membranes (Okada and Matsuura, 1991; Koops et al, 1992; Jian and Pintauro, 1996; 1997). These integral asymmetric membranes consist of a very thin skin with some very tiny pores on the surface and the number of pores and size increases from the top surface skin to the bottom surface. Such membrane morphology is obtained by the phase inversion method and is usually restricted to glassy polymers.

Although a high flux gain is achieved with such pervaporation membranes, a poor selectivity results. Indeed for any separation selectivity to be realised, the pores would have to be very small. The pore flow model was developed to describe the pervaporation flux through such membranes (Okada and Matsuura, 1991). It is assumed that there are bundles of straight cylindrical pores on the membrane surface. The mass transport by the pore flow mechanism consists of three steps: (i) Liquid transport from pore inlet to a liquid–vapour phase boundary, (ii) evaporation at the phase boundary, and (iii) vapour transport from boundary to pore outlet. A distinctive feature of this model is that the phase change occurs within the membrane and both liquid and vapour phases, separated by a clear boundary, are considered to exist within the membrane. The Fig. 3.12 illustrated the pore-flow mechanism for pervaporation transport.
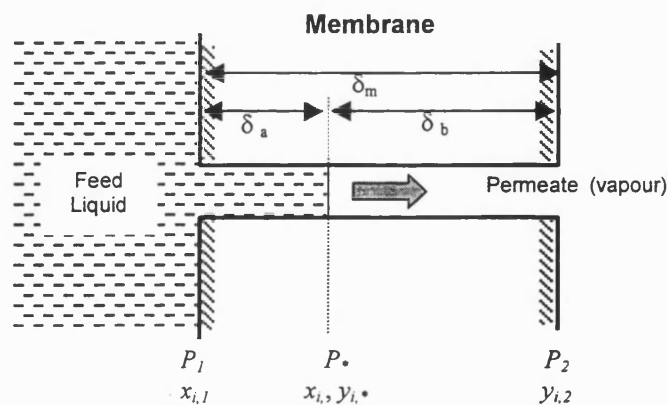
Fig. 3.12. Schematic representation of the pore-flow model applied to pervaporative transport

3.4.2.1 Liquid transport in the pores

The solution-diffusion and pore flow models differ in the way the chemical potential gradient in the membrane is expressed (Paul, 1974a; 1974b; Rosenbaum and Cotton, 1969; Mauro, 1960). The solution diffusion model assumes that the pressure within a membrane is uniform and that the chemical potential gradient across the membrane is expressed only as a concentration gradient. The pore flow model assumes that the concentrations of solvent and solute within a membrane are uniform and that the chemical potential gradient across the membrane is expressed only as a pressure gradient. In the pore flow model, the pressure difference produces a smooth gradient in pressure through the membrane, but the solvent activity remains constant within the membrane. It is worth noting that, in the pore flow model, the pressure gradient exists only in the fluid-filled pores and the vapour transport region. No pressure gradient exists within the membrane matrix material, which is at the feed pressure throughout.

According to Okada and Matsuura (1991), consider a single component transport system, assume that $P_2 < P_*$. the transport in the liquid filled portion of the cylindrical pore (See Fig. 3.12) can be expressed by Darcy's equation and can be written as :

$$J_{i,liq} = \frac{k_i}{\eta \delta_a}(P_1 - P_*)$$
(3.100)

Where k_i = the Darcy's permeation constant, m^2

η = the average viscosity of the liquid, Pa·s

δ_a = distance from inlet to the phase boundary, m

P_1 = the feed liquid pressure, Pa

P_* = the saturated vapour pressure at the phase boundary, Pa

3.4.2.2 Vapour Transport in the pores

For vapour transport in pores, the vapour pressure changes from P_* to P_2 as shown in Fig. 3.12. Okada and Matsuura (1991) assume that the pores are so small they are below the limit for Knudsen flow, a surface flow model is appropriate. The model of Gilliland (1958) is used to describe the vapour transport:

$$J_{i(vap)} = \frac{k_{s,i}}{\delta_b} \int_{P_2}^{P_*} \frac{x_i^2}{P} dP \tag{3.101}$$

Where x_i = amount of gas adsorbed in a given amount of membrane material, kmol/kg

$k_{s,i}$ = the proportionality constant, $m^5/mol \cdot s$

P_2 = the vapour pressure at the permeate side of membrane, Pa

δ_b = the pore cylindrical distance from the phase boundary to the outlet

If the vapour adsorption can be approximated by Henry's law, $x_i = k_H P$, equation (3.101) can be integrated to yield:

$$J_{i(vap)} = \frac{k_{s,i} k_H^2}{2\delta_b} \left(P_*^2 - P_2^2 \right) \tag{3.102}$$

where k_H = the Henry's law proportionality constant, kmol/kg·Pa

The proportionality constant $k_{s,i}$ can be calculated if monolayer adsorption occurs at the pore wall, this yields:

$$k_{s,i} = \frac{\pi \left(2rt - t^2 \right)^2 tN_t RT}{8r\mu_s} \tag{3.103}$$

Where t = thickness of adsorption monolayer, m $\quad$ r = pore radius, m

N_t = Total number of pores per effective membrane area, $/m^2$

μ_s = surface viscosity of the adsorption layer of vapour, Pa s

3.4.2.3 Flux equation based on pore flow model and arguments on its validity

An important and distinctive assumption made in pore flow model is that a clear and distinct phase change boundary exists within the membrane, i.e. the location of the phase boundary in a particular pore is the same as the other pores in the membrane. Since $\delta_m = \delta_a + \delta_b$ and in steady state $J_{i(liq)} = J_{i(vap)}$, the resulting flux equation can be written as:

$$J_i = \frac{A}{\delta_m}(P_1 - P_*) + \frac{B}{\delta_m}(P_*^2 - P_2^2)$$

(3.104)

Where $A = k_i / \eta$ and $B = k_{s,i} \cdot k_H^2 / 2$

Assuming that A, B and P_* are independent of permeate pressure, these parameters can be obtained by curve fitting of pervaporation flux data at various permeate pressures. If μ_s, N_t, t and k_H are known, the pore radii can be calculated from equation (3.103). In the study of the separation of ethyl alcohol/heptane mixtures through asymmetric cellulose membrane, the flux data was successfully modelled by using pore flow model and the estimated pore radii of these membranes were found to be more than 1.5 nm (Okada And Matsuura, 1991).

Several researchers (Okada and Matsuura, 1991, 1992; Okada et al, 1991; Zhang et al, 1992; Tyagi et al, 1995; Shieh and Huang, 1998) have extended the applicability of the pore flow model to pervaporation transport in dense membranes such as PDMS, Polyamide, Polyacylic acid membrane.

There are different views regarding the existence of pores in pervaporative dense membranes. An effective solution-diffusion membrane has no pores but relies on the thermally agitated motion to generate penetrant-scale transient gaps in the matrix, thereby allowing diffusion from upstream to downstream side of the membrane. The permeation is a net result of the random jumps of penetrant in the membrane. The pore flow modeller advocates that the pores in the pore flow model are defined as the space between unbound material entities in the polymer matrix through which mass transfer take place. The equivalent size of such a pore is expressed by any distance (however small) greater than zero (Sourirajan and Matsuura, 1985). The calculated pores in pervaporation and gas permeation membranes are

angstrom sized, and these pores are thus not directly observable, making it difficult to physically see whether pervaporative dense membranes have pores or not.

Fundamental problems appear in the pore flow approach when it is used to explain the experimental data that supports the solution-diffusion model. As P_2 approaches P_*, the first term in equation (3.104) dominates the transport process. From the studies of some researchers (Okada and Matsuura, 1991, 1992; Okada et al, 1991; Zhang et al, 1992; Tyagi et al, 1995), it appears that even when P_2 is very low, the first term is still significant. This suggests that as P_1 is increased J_i should increase significantly, which is in contradiction to the experimental evidence that support the solution-diffusion model in which the feed pressure has little effect on the permeation flux (Greenlaw et al, 1977; Rosenbaum and Cotton, 1969; Wijmans and Baker, 1995). As feed side activities are relatively unaffected by pressure, over a moderate pressure range, the solution diffusion model predicts that increasing feed side pressure has little effect upon sorption. Increasing pressure also has no direct effect upon the diffusion process. It is well known that in practice, feed side pressure has very little effect upon pervaporation performance using non porous membranes (Neel, 1991). From the pore flow model studies by Okada and Matsuura (1991, 1992); Okada et al (1991); Zhang et al (1992) and Tyagi et al (1995), it appears that equation (3.104) can describe the affect of changing permeate pressure, P_2 upon J_i reasonably well. No attempt was made, however, to fit the model to experimental data showing the variation of J_i with feed pressure, P_1, for non porous membranes. Recently, Shieh and Huang (1998) proposed a modified form of pore flow model to fit the pervaporation data from Greenlaw et al (1977) which supports the solution-diffusion model. In attempting to fit the variation of J_i with feed pressure, P_1, for the non porous membranes, their model over estimated the flux significantly. This shows that the discrepancy is due to the inherent problem in the pore flow model approach.

3.5 Support Layer Transport

Often, in laboratory development of pervaporation membranes, research has been focused upon the development of highly selective, highly permeable, tailor-made polymers which have been characterised using free, non-supported films. However, in commercial pervaporation membrane manufacturing, it is usual for a thin pervaporation dense membrane to have to be mechanically supported by a thicker porous membrane. Such membranes are called composite membranes.

According to the definition given by Henis and Tripodi (1980), a "porous" membrane is a membrane that has continuous channels, i.e. pores that give continuous channels between top and exit surfaces. In pervaporation, these continuous channels, if sufficiently large in number and in cross-section, can permit essentially all of the gaseous mixture that is desorbed from the selective layer, to flow through the porous membrane with little, if any, separation due to interaction with the porous membrane material.

The most commonly used porous supports for pervaporation composite membranes are the Loeb-Sourirajan phase inversion ultrafiltration membranes and the etched-stretched microfiltration membrane. According to Kesting (1985), an etched-stretched membrane, such as polypropylene microfiltration membranes is likely to be an isotropic porous membrane (e.g. Celgard PP microfiltration membrane) and the Loeb-Sourirajan phase inversion membranes are actually asymmetric membranes (e.g. Polysulfone, PVDF, PES). Such asymmetric membranes consists of an ultra-thin skin layer ($< 1\mu$m) with defects, i.e. very small pores (pore size ~ 10nm) and a highly porous substructure with lots of finger like pores that sometimes exceed the size of 5μm. An illustration of these two types of membranes with a perfect coating of selective layer are shown in Fig 3.13.
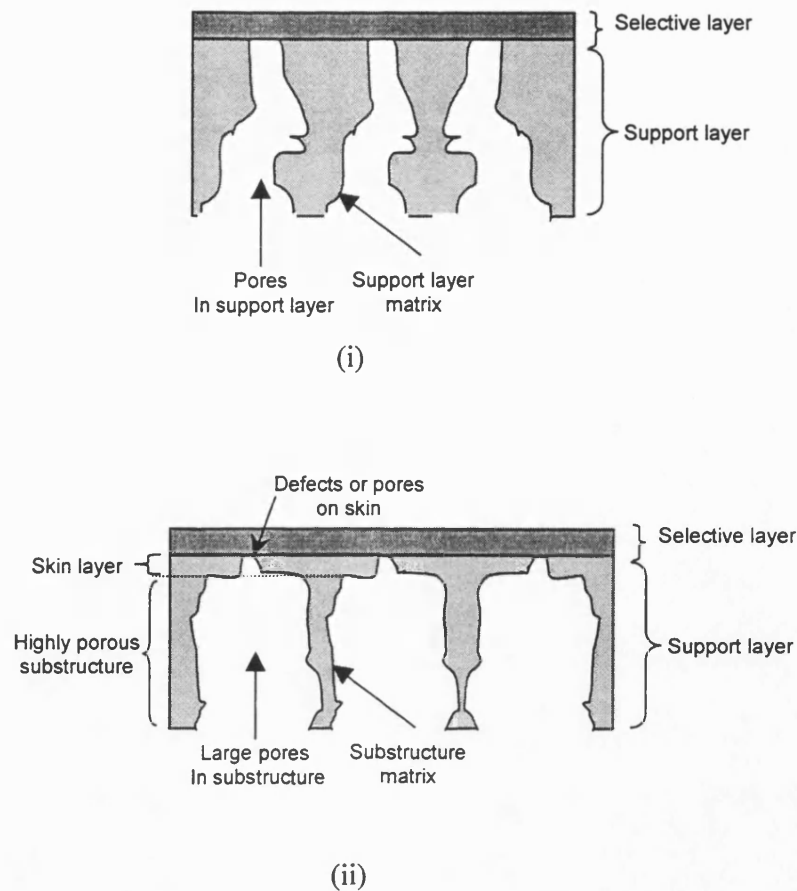
Fig. 3.13 An illustration of composite membranes with different porous support layer: (i) etched and stretched membrane, (ii) phase inversion membrane.

In an ideal composite membrane, negligible support resistance should be observed. In the study of organophilic pervaporation of toluene from aqueous solution, Nijhuis et al (1991) assessed the resistance of the polysulfone (ultrafiltration membrane) porous support layer and found it to be negligible compared to the top layer PDMS (3 - 50μm). However, in a study of pervaporation of ethanol from water, others (Gudernatsch et al, 1991; Gudernatsch and Kimmerle, 1991) found that for a composite membrane which consists of a top layer PDMS (0.61μm) and a polyethersulphone (PES) support layer (~75μm), the support layer consumed up to 50% of the driving force for mass transport. From these two studies, it is obvious to

79

note that the transport resistance due to a support layer is significant when the selective layer is very thin. In general, the porous support can affect pervaporation flux in five ways:

(a) Pressure loss in the support: Although the support is porous, pressure loss due to friction may result in the reduction of flux through the membrane. However, because the support layer is thin and highly porous, pressure loses have been found to have only a minor effect upon pervaporation flux unless a very thick support layer is employed (Kaka et al, 1992).

(b) Effect of support substrate geometry upon flow direction: Permeants in the selective layer have only a limited number of entry points into the support and so may have to travel on longer paths; two-dimensional diffusion in the selective layer occurs because of the spacing of pores. This effect is well known in composite gas separation membranes and becomes more critical as the thickness of top layer decreases (Barrer et al, 1962; Lopez et al, 1986; Strathmann et al, 1988; Bode and Hoempler, 1996).

(c) Resistance due to the penetration of selective layer material into the pores of support: The SEM evidence of such penetration has been shown by Kaka et al (1992). That penetrated material results in the significant reduction of pervaporation flux has been reported by others (Kaka et al, 1992; Field and Wu, 1998). Such penetration depends on the size of pores, porosity, nature of support matrix and the viscosity of the coating solution (Ebert, 1995). If the pores of the support are sufficiently small, penetration of coating solution can be prevented. According to He et al (1996), if the selective layer is relatively thin, the reduction of flux is mainly due to the penetrated material in the pores.

(d) Resistance due to skin layer of an asymmetric porous support: Most of the commercial pervaporation membrane manufacturers (e.g. GFT, GKSS, MTR, Bend Research etc.), have used asymmetric membranes (e.g. PVDF, Polysulfone, PES etc.) as the support. Although the membrane is highly porous *per se*, an ultra skin layer ($< 1 \mu m$) with defects exists on top of such membranes. A typical skin layer of an asymmetric membrane has a surface porosity of less than 1 % and a surface pore size of 10nm (Kesting, 1985). Such a skin layer may impose a resistance to mass transport if the thickness of this layer

compared to the selective layer is relatively high and the surface porosity is low enough. In most of the commercial pervaporation systems, the coated selective layer is usually more than 10 times thicker than the skin layer, hence the resistance due to the skin layer is not as much as the resistance due to the material penetration into the pores of the support.

(e) Resistance of vapour transport in the pores: In pervaporation, the permeate side is maintained at high vacuum and the transport resistance of permeate vapour through the porous region depends on the size of the pores. The average pore size $(2r_{pore})$ for a microfiltration membrane is typically ~ 50nm and for an ultrafiltration membrane, the typical surface pores have an average size of ~10nm. According to Liu et al (1997), at a permeate pressure less than 10 cmHg (~133mbar), where the mean free path of vapour molecules, λ is in the order of a micrometer, the Knudsen number, $Kn = \lambda / 2r_{pore}$, may be much more than 1. If the vapour transport is in the Knudsen region ($Kn \gg 1$), then the vapour flow in the pores of a microfiltration membrane and in the surface pores of an ultrafiltration membrane is likely to follow the Knudsen flow mechanism (Feng and Huang, 1997).

3.5.1 Transport equation in support layer

The vapour mass transport in the support layer can be distinguished into mass transport in the pores and in the support matrix. Due to the different membrane structure between a microfiltration membrane and an ultrafiltration membrane, the transport equations in the support will be derived separately according to structure.

3.5.1.1 Symmetric porous support

To facilitate the derivation of a mass transport equation in a symmetric porous support, the following assumptions need to be made:

- Symmetric porous support has identical cylindrical pores that connect the feed side of support with the permeate side.

- Some of the selective material has partially penetrated the pores with identical depths.

- The transport in the support matrix and the filled portion of the pores follows the solution-diffusion model.

- Since the pore size of a symmetric membrane is about ~ 50nm, the Knudsen number is >> 1 when the permeate pressure is less than 10cmHg (~133mbar). The vapour phase transport mechanism in the unfilled section of the cylindrical pore can then be assumed to be Knudsen diffusion.

- The diffusion process is one dimensional in the support.

A symmetric membrane can be schematically illustrated as a membrane with identical cylindrical pores (see Fig. 3.14):
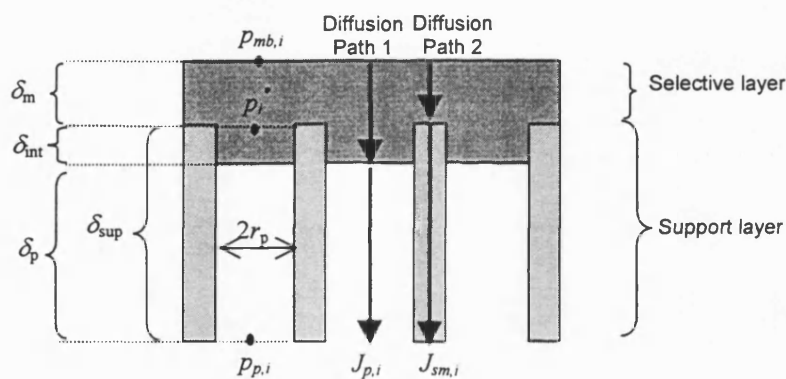
Fig. 3.14 Schematic diagram for the composite membrane with symmetric membrane as porous support

Where:

$J_{p,i}$ = molar flux of the component through the pores

$J_{sm,i}$ = molar flux of the component through the support matrix

$p_{mb,i}$ = partial pressure at feed side of membrane

p_i^* = equivalent partial pressure in the membrane at position shown in Fig. 3.14

$p_{p,,i}$ = partial pressure at permeate side of porous support

r_p = average radius of the pore

δ_m = thickness of the selective layer δ_{sup} = thickness of the support layer

δ_{int} = average filled distance in the pore δ_p = average unfilled distance in the pore

If the porous support has a surface porosity of ε_s, the average component flux through the support can be written as:

$$J_i = \varepsilon_s J_{p,i} + (1 - \varepsilon_s) J_{sm,i} \qquad (3.105)$$

Normally in symmetric membranes (e.g. PP and PTFE porous membrane), the surface porosity is quite high compared to asymmetric membranes and has a range of 35 – 70%. Also the flux in the pores is much higher than that through the support matrix ($J_{p,i} >> J_{sm,i}$). Hence, the average flux through the support layer can be approximated as the flux through the pores, i.e. $J_i \approx \varepsilon_s J_{p,i}$.

The transport in the cylindrical pores can be categorized by solution-diffusion for transport through the selective material that penetrated the pores, and Knudsen diffusion in the unfilled section of pores. If the filling fraction (ψ) is defined as the ratio of the average filled distance in the pore (δ_{int}) to the thickness of the support layer (δ_{sup}), the flux equation through the cylindrical pores can be written as:

$$J_{p,i} = \frac{\overline{P}_{pore}}{\delta_{sup}} \left(p_i^{\bullet} - \Theta_i p_{p,i} \right) \qquad (3.106)$$

where $\overline{P}_{pore} = \dfrac{1}{\dfrac{\psi}{\hat{P}_{m,i}} + \dfrac{(1-\psi)\Theta_i}{\hat{P}_{knud,i}}}$, Mean permeability of the pores $\qquad (3.107)$

$\hat{P}_{knud,i} = \dfrac{D_{K,i}}{RT}$, Permeability of the unfilled pores $\qquad (3.108)$

$\hat{P}_{m,i} = D_{m,i} S_i^f$, Permeability of the selective layer material in filled pores $\qquad (3.109)$

$D_{K,i} = 97 r_p \sqrt{T/M_i}$ Knudsen diffusivity, m^2/s $\qquad (3.110)$

From equation (3.110), r_p is measured in metre and T (temperature) is measured in Kelvin and M_i (molecular mass) is measured in kg/kmol.

Knowing that $J_i \approx \varepsilon_s J_{p,i}$ and using equation (3.106), an overall transport equation for a composite membrane, with a symmetric porous membrane as its support, can be obtained:

$$J_i = \frac{1}{\dfrac{\delta_m}{\hat{P}_{m,i}} + \dfrac{\delta_{sup}}{\varepsilon_s \overline{P}_{pore,i}}} \left(p_{mb,i} - \Theta_i p_{p,i} \right) \tag{3.111}$$

If the resistance due to penetration is much greater than that of the unfilled pores, i.e. $\overline{P}_{pore,i} \approx \hat{P}_{m,i}/\psi$, the equation reduces further to:

$$J_i \approx \frac{\hat{P}_{m,i}}{\delta_m + \psi \delta_{sup}/\varepsilon_s} \left(p_{mb,i} - \Theta_i p_{p,i} \right) \tag{3.112a}$$

If the selective layer resistance, $\delta_m/\hat{P}_{m,i}$, is sufficiently greater than the support layer resistance, $\delta_{sup}/\left(\varepsilon_s \overline{P}_{pore,i} \right)$, the mass transport equation reduces further to:

$$J_i \approx \frac{\hat{P}_{m,i}}{\delta_m} \left(p_{mb,i} - \Theta_i p_{p,i} \right) \tag{3.112b}$$

3.5.1.2   Asymmetric porous support

To facilitate the derivation of the mass transport equation in the asymmetric porous support, the following assumptions need to be made:

- Asymmetric membrane consists of two layers, i.e. skin layer and porous substrate layer.

- Although the pore size in the asymmetric membrane varies from feed to permeate side, it is assumed that only two distinct pore sizes and porosities exist in the skin layer and porous substructure.

- It is assumed that the pores in both skin layer and porous substructure are in cylindrical form and are channels that connect the feed side of support with the permeate side.

- Some of the selective material has partially penetrated the pores in the skin layer with identical depths.

- Transport in the support matrix and in the filled cylindrical pores region follows solution-diffusion model.

- Since the pore size on the skin layer of an asymmetric membrane is about $\sim$ 10nm, the Knudsen number is $>>$ 1 when the permeate pressure is less than 10cmHg. The vapour

phase transport mechanism in the unfilled section of the skin layer cylindrical pore can then be assumed to follow the Knudsen diffusion mechanism.

- In the porous substructure, the pore size is much larger than the pores of the skin layer. Typical size reached ~ 5μm, thus the vapour transport in this region follows viscous flow mechanism. According to (He et al, 1996; Field and Wu, 1998), the transport resistance in this region is negligible compared to the resistance in the skin layer itself and the penetrated pores of the skin. Hence, the transport resistance in this region can be assumed to be negligible.

- For the skin layer, a parallel resistance layer is assumed. The overall flux can be assumed to be the sum of the flow through the skin layer material itself and the flow through the pores therein.

- Assume ideal gas behaviour for the vapour in the pores.

- The diffusion process is one dimensional in the support.

A symmetric membrane can be schematically illustrated as a membrane with identical cylindrical pores (see Fig. 3.15):
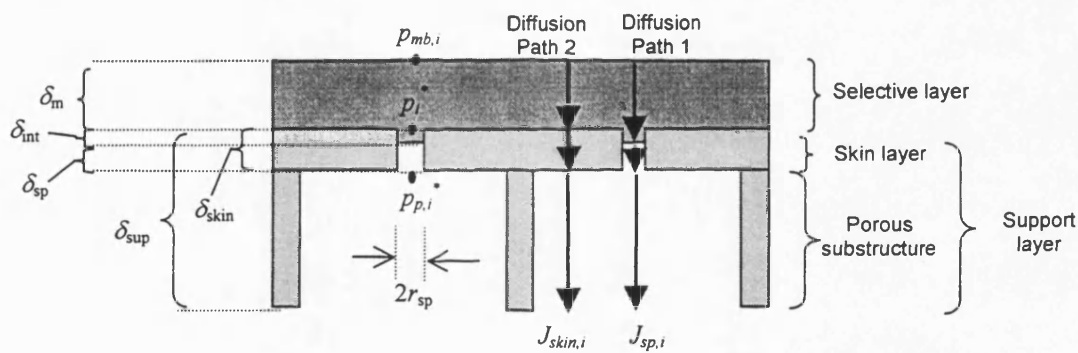
Fig. 3.15 Schematic diagram for composite membrane with
asymmetric membrane as porous support

Where:

$J_{sp,i}$ = molar flux of the component through the pores of skin layer

$J_{skin,i}$ = molar flux of the component through the skin layer

$p_{mb,i}$ = partial pressure at feed side of membrane

p_i^* = equivalent partial pressure in the membrane at position shown in Fig. 3.15

$p_{p,i}$ = partial pressure at permeate side of skin layer

r_{sp} = average radius of the cylindrical pore of skin layer

r_{subs} = average radius of the cylindrical pore of skin layer

δ_m = thickness of the selective layer

δ_{sup} = thickness of the support layer

δ_{skin} = thickness of the skin layer

δ_{int} = average filled distance in the cylindrical pore of skin layer

δ_{sp} = average unfilled distance in the cylindrical pore of skin layer

If the porosity of skin layer and the porous substructure of the support are ε_s and ε_{subs} respectively, the average component flux through the support can be written as:

$$J_i = \varepsilon_s J_{sp,i} + \left(\varepsilon_{subs} - \varepsilon_s\right) J_{skin,i} \qquad (3.113)$$

3.5.1.2.1 Transport in the cylindrical pores of the skin layer

The transport in the cylindrical pore of the skin layer can be categorized into two mechanisms, namely, solution-diffusion model for transport through the selective material in the pores of the skin layer and Knudsen diffusion in the unfilled section of pores. By applying Fick's first law and resistance in series model, the flux equation through the cylindrical pores can be written as:

$$J_{sp,i} = \frac{\overline{P}_{sp,i}}{\delta_{skin}}\left(p_i^* - \Theta_i p_{p,i}\right) \qquad (3.114)$$

where $\overline{P}_{sp,i} = \dfrac{1}{\dfrac{\psi}{\hat{P}_{m,i}} + \dfrac{(1-\psi)\Theta_i}{\hat{P}_{knud,i}}}$, average permeability through pores. $\qquad (3.115)$

$\hat{P}_{knud,i} = \dfrac{D_{K,i}}{RT}$, permeability of the unfilled pores of skin layer $\qquad (3.116)$

$\hat{P}_{m,i} = D_{m,i} S_i^f$, Permeability of selective layer material in filled pores of skin layer

$\psi = \dfrac{\delta_{int}}{\delta_{skin}}$, filling fraction in the cylindrical pores of the skin $\qquad (3.117)$

$D_{K,i} = 97 r_{sp} \sqrt{T/M_i}$, Knudsen diffusivity $\qquad (3.118)$

Θ_i = desorption factor of the selective layer material in the filled region of the pores

3.5.1.2.2 Transport in the skin layer matrix

The mass transport through the skin layer matrix follows solution-diffusion mechanism hence the transport equation can be written as:

$$J_{skin,i} = \frac{\hat{P}_{skin,i}}{\delta_{skin}} \left(p_i^* - \Theta_{skin,i} p_{p,i} \right) \tag{3.119}$$

Where $\hat{P}_{skin,i} = D_{skin,i} S_{skin,i}^f$, Permeability of the porous substructure matrix $\qquad$ (3.120)

3.5.1.2.3 Overall transport equation for a composite membrane with an asymmetric porous support

Knowing that the average component flux through the support is $J_i = \varepsilon_s J_{sp,i} + (\varepsilon_{subs} - \varepsilon_s) J_{skin,i}$ and by combining equations (3.113) – (3.120), the flux equation for asymmetric support can be expressed as follow:

$$J_i = \frac{\hat{P}_{sup,i}}{\delta_{skin}} \left(p_i^* - \Theta_i p_{p,i} \right) \tag{3.121}$$

Where: $\hat{P}_{sup,i} = \varepsilon_s \overline{P}_{sp,i} + (\varepsilon_{sub} - \varepsilon_s) \hat{P}_{skin,i} \dfrac{\left(p_i^* - \Theta_{skin,i} p_{p,i} \right)}{\left(p_i^* - \Theta_i p_{p,i} \right)}$ $\qquad$ (3.122)

When the flow in pores of skin layer is dominant:

$$\hat{P}_{sup,i} \approx \varepsilon_s \overline{P}_{sp,i} \tag{3.123}$$

and the overall mass transport equation for such a composite membrane can be expressed as :

$$J_i = \frac{1}{\dfrac{\delta_m}{\hat{P}_{m,i}} + \dfrac{\delta_{skin}}{\varepsilon_s \overline{P}_{sp,i}}} \left(p_{mb,i} - \Theta_i p_{p,i} \right) \tag{3.124}$$

3.5.2 Selective material penetration and the argument for the use of "thick" film membranes.

The support layer of a composite membrane has often been assumed to have negligible resistance and act solely as a mechanical support, hence making the selective layer of the composite membrane the rate-controlling step. So in order to produce a high flux and highly selective membrane, much work was devoted to producing a "thin" film on the support layer. Commercial techniques like dip coating (Riley and Grabowski, 1981), interfacial polymerisation (Blume and Pinnau, 1990) and plasma polymerisation (van der Scheer, 1986) are employed to produce ultra thin selective layers on a support. The typical thickness is that produced by these methods ranges from 0.25 - 20 μm.

Due to non-ideal coating, some selective material will be intruded into the pores during the coating process (Henis and Tripodi, 1981; He et al, 1996). Such penetration causes the overall membrane resistance to increase significantly. The extent of the increase will depend on the penetration distance and is a function of surface pore size and porosity (Field and Wu, 1998). Apart from using a support with suitable pore size, Ebert (1995) and Burslem (1996) found that the degree of penetration could be significantly reduced by coating a water impregnated porous support membrane. For flat sheet supports, the impregnation of the porous support is achieved by injection of water into the support. For hollow fibres supports, the impregnation of the porous support is achieved by suction of water through the bore side of the support fibres via a vacuum pump.

If the penetration of the selective layer material into the pores of the support is prevented, the support layer resistance is significantly reduced. Further, if the composite membrane has an ultra-thin selective layer, higher fluxes should be expected. However, this in turn will make the boundary layer resistance at the feed side the rate controlling step instead of the membrane itself. This is particularly so for the removal of highly volatile substances, e.g. Chloroform (Wijmans and Baker, 1996). In this case, modification of a pervaporation module design is needed so as to enhance feed side mass transfer.

Instead of preventing the penetration of coating material into the pores of support, (Lipski and Cote, 1992) invented a controversial pervaporation membrane that comprises a porous support (microfiltration membrane) will completely filled pores containing a solid, non-removable organophilic polymer which exhibits permselectivity (see Fig 3.16). The typical thickness of this "thick film" membrane ranges from $20 - 200\mu m$. If the filled support is of thickness δ_{sup} and of porosity ε_s, then its resistance is proportional to $\delta_{sup}/\varepsilon_s$.

(i)   (ii)
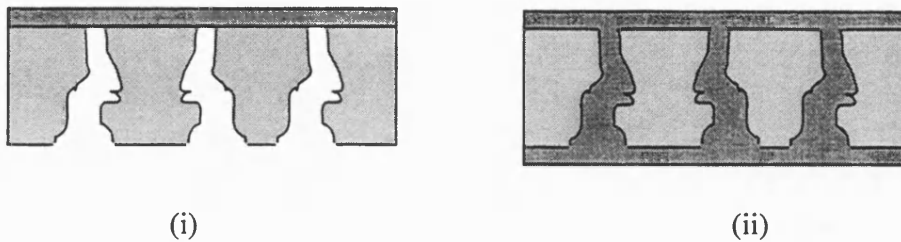
Fig. 3.16 Graphic illustration of (i) conventional "thin film" membrane and (ii) novel "thick film" membrane

The inventors claimed that in organophilic pervaporation, the pervaporation module with their "thick film" pervaporation membranes would provide a separation factor at least double that of a conventional model with "thin film" membranes coated upon a porous support and not filling its pores. This thick film membrane is a low flux membrane due to its high transport resistance. In organophilic pervaporation with significant feed side boundary layer resistance, a *relatively* high membrane resistance is desirable to prevent the domination of boundary layer resistance in separation. In this case, the inventors achieve this purpose by filling the pores in the support layer with selective material and creating a membrane whose resistance is high *absolutely*.

3.6 Two-dimension diffusion in selective layer of a composite membrane

In the derivation of the above membrane transport equation, a unidirectional diffusion within the selective layer was assumed. Thus, by using Kirchhoff's law of resistance, an overall resistance for a composite membrane is obtained as shown in equation (3.124). However, if the support layer matrix is impermeable and low in surface porosity, with an ultra thin selective layer, a unidirectional flow within the selective layer will no longer be a good approximation. The resultant two-dimensional flow within the selective layer could be significant.

3.6.1 Two-dimensional diffusion models

Several researchers (Barrer et al, 1962; Lopez et al, 1986; Strathmann et al, 1988) have investigated the possibility of two dimensional flow patterns. In Fig. 3.17, different postulated two-dimensional flow patterns (Model B, C and D) in comparison with unidirectional flow pattern (Model A) are shown.
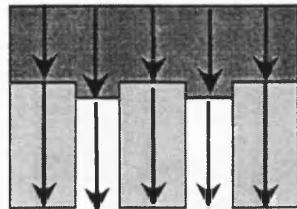
Model A
(Henis and Tripodi, 1980)
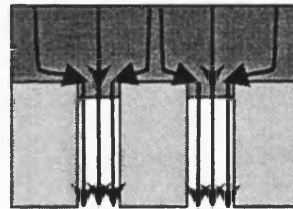
Model B
(Barrer et al, 1962)
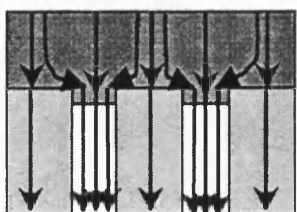
Model C
(Lopez et al, 1986)
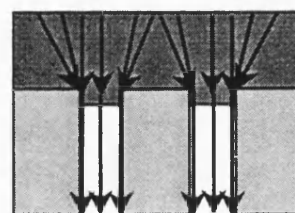
Model D
(Strathmann et al, 1988)

Fig. 3.17 Various postulated flow patterns that found in literature for diffusion in a composite membrane

The pores in the composite membrane in postulated models are approximated as a repeating pattern of circular cylindrical unit cells as shown in Fig. 3.18. Such a unit cell will be used to derive the mass transfer equations for model B, C and D. From Fig. 3.18, surface porosity can be approximated as:

$$\varepsilon_s = \frac{\text{Surface area covered by pores}}{\text{Total surface area}} = \frac{\pi}{4}\left(\frac{r_{\text{pore}}}{r_{\text{core}}}\right)^2 \cong 0.79\varepsilon_r^{\,2}$$

where ε_r is the radial porosity = (r_{pore} / r_{core}).

In order to facilitate the analysis, the surface area contribution of the gaps in between the unit cells was assumed to be negligible and hence the surface porosity can be approximated as the square of radial porosity ($\varepsilon_s \cong \varepsilon_r^{\,2}$). Such assumptions were used in models B, C and D.
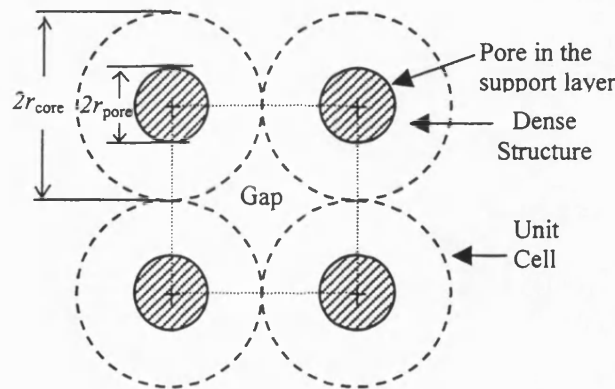
Fig. 3.18 Surface view of the idealized cylindrical unit cells in composite membrane

In the following sections, the equations for model B, C and D will be derived and then a comparison between them will be given.

3.6.1.1 Model A

In model A, Henis and Tripodi (1980) suggested that the flow pattern in a composite membrane could be approximated as unidirectional. However, the flux will be overestimated. Whether overestimation is significant will be determined in section 3.6.1.5.

3.6.1.2 Model B

In Model B, Barrer et al (1962) suggested that if the support matrix and skin layer are considered to be impermeable, the flux that is obstructed by the support matrix would change its direction towards the pores as shown in Fig. 3.19. Thus, steady state flux equation for the selective layer has to be derived from the two-dimensional diffusion process.
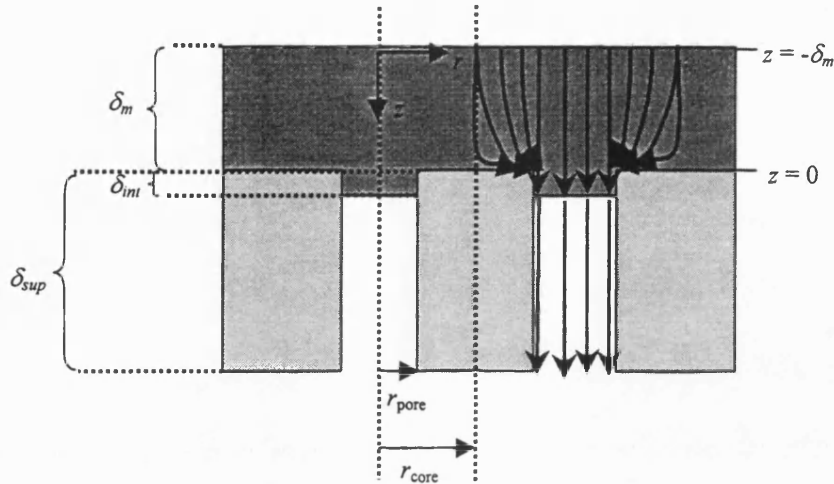
Fig. 3.19 Flow pattern of component flux based on Barrer (1962)

Considered a cylindrical co-ordinate system (z, r) with a co-ordinate normal to the membrane surface. For constant diffusion coefficient the steady state diffusion equation becomes:

$$\frac{\partial^2 C_{m,i}}{\partial r^2} + \frac{1}{r}\frac{\partial C_{m,i}}{\partial r} + \frac{\partial^2 C_{m,i}}{\partial z^2} = 0 \qquad (3.125)$$

with the following boundary conditions,

(a) $\quad C_{m,i} = C_{m1,i}$, $\qquad 0 < r < r_{core}$, $\qquad z = -\delta_m$;

(b) $\quad C_{m,i} = C^*_{m2,i}$, $\qquad 0 < r < r_{pore}$, $\qquad z = 0$;

(c) $\quad \partial C_{m,i}/\partial z = 0$, $\qquad r = r_{core}$, $\qquad z = 0$, ;

(d) $\quad \partial C_{m,i}/\partial r = 0$, $\qquad 0 < r < r_{pore}$, $\qquad -\delta_m < z < 0$;

If l_{eff} is defined as the effective diffusion path length, by solving the differential equation above, an analytical solution for component flux equation for selective layer can be expressed

as: $J_i = \dfrac{D_{m,i}}{l_{eff}}\left(C_{m1,i} - C^*_{m2,i}\right)$ $\qquad (3.126)$

where $\quad l_{eff} = \delta_m \left(1 + \dfrac{16}{\pi^2} Q_n \right)$ (3.127)

$$Q_n = \sum_{n=1}^{\infty} \dfrac{1}{n^2} \dfrac{B_0(n\omega)}{B_0(n\xi)} \left[B_0(n\xi)B_1(n\omega) - B_1(n\xi)B_0(n\omega) \right]$$ (3.128)

$\xi = \pi r_{core} / \delta_m$;

$\omega = \pi r_{pore} / \delta_m$;

B_0 = Modified Bessel function of the first kind and order 0

B_1 = Modified Bessel function of the first kind and order 1

$C^{\bullet}_{m2,i}$ = average solute concentration in the selective membrane at the pore mouth.

3.6.1.3 Model C (Lopez et al, 1986)

In Model C, Lopez et al (1986) suggested a cylindrical pore cell model that is similar to Barrer et al (1962). However, instead of assuming the support dense layer to be impermeable, Model C is generalised for a composite membrane with either permeable or impermeable skin layer.
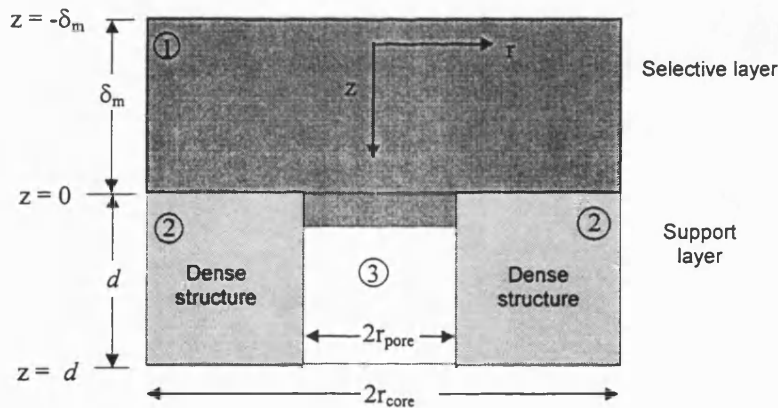
Fig. 3.20 A schematic diagram of a cylindrical pore cell

From Fig. 3.20, the cell was subdivided into three regions, with each region characterised by its own diffusion coefficient and permeability. Region 1 represents the selective layer which contains the selective material while region 2 is the dense structure of the support and region 3 is the pore region which includes the intruded material from region 1. The cell is applicable to composite membranes either with a microfiltration or an asymmetric membrane as

support. For a composite membrane, with an asymmetric membrane as its support, the pore in the cell would be the defects and the thickness beneath the selective layer would be the thickness of the skin layer of the asymmetric membrane.

Consider a cylindrical co-ordinate system (z, r) with a co-ordinate normal to the membrane surface. For constant diffusion coefficient the steady state diffusion equation becomes:

$$\frac{\partial^2 C_{m,i}}{\partial r^2} + \frac{1}{r}\frac{\partial C_{m,i}}{\partial r} + \frac{\partial^2 C_{m,i}}{\partial z^2} = 0 \tag{3.129}$$

In the regions of the support matrix and the pores region (includes filled and unfilled pore region), the diffusion transport is one-dimensional and hence the equation above becomes

$$\frac{\partial^2 C_{m,i}}{\partial z^2} = 0.$$

In the regions of the selective layer, the following boundary conditions are established:

(a) $C_{m,i} = C_{m1,i}$, $\qquad 0 < r < r_{core}$, $\qquad z = -\delta_m$;

(b) $\partial C_{m,i}/\partial r = 0$, $\qquad r = 0$ $\qquad -\delta_m < z < 0$;

(c) $\partial C_{m,i}/\partial r = 0$, $\qquad r = r_{pore}$, $\qquad -\delta_m < z < 0$;

(d) $-D_{m,i}\,\partial C_{m,i}/\partial z = q_p$, $\qquad 0 < r < r_{pore}$, $\qquad z = 0$, ;

(e) $-D_{m,i}\,\partial C_{m,i}/\partial z = q_s$, $\qquad r_{pore} < r < r_{core}$, $\qquad z = 0$, ;

The quantities q_p and q_s are defined as the component flux into the pores and support matrix respectively. Since the concentration at $z = 0$ is dependent on radial position, it follows that q_p and q_s are also a function of r. However, for mathematical simplicity q_p and q_s are taken to be constant. To simplify the derivation, the desorption factor is assumed to be unity. By solving the differential equation above and applying Fick's first law, the total resistance of the composite membrane is expressed as:

$$R_i = \frac{\left(p_{mb,i} - \Theta_i P_{p,i}\right)}{J_i} = \frac{\delta_m(1+G)}{\hat{P}_{m,i}} + \frac{d}{\hat{P}_{sm,i}\left(1-\varepsilon_s\right) + \overline{P}_{pore,i}\varepsilon_s} \tag{3.130}$$

where:

$$G = \frac{d}{\delta_m}\left\{\frac{1+F[\gamma_3 + \gamma_2\varepsilon_s/(1-\varepsilon_s)]}{\gamma_2(1-\varepsilon_s)+\gamma_3\varepsilon_s + \gamma_2\gamma_3 F/(1-\varepsilon_s)} - \frac{1}{\gamma_2(1-\varepsilon_s)+\gamma_3\varepsilon_s}\right\}$$ (3.131)

$$F = \frac{4\beta}{\upsilon}\sum_{n=1}^{\infty}\frac{B_1^2(q_n/\beta)\tanh(q_n\lambda/\beta)}{q_n^3 B_0^2(q_n)}$$ (3.132)

$\beta = r_{core}/r_{pore} = 1/\varepsilon_r$; $\qquad \lambda = \delta_m/r_{pore}$; $\qquad \upsilon = d/r_{pore}$;

$\gamma_2 = \hat{P}_{sm,i}/\hat{P}_{m,i}$; $\qquad\qquad \gamma_3 = \overline{P}_{pore,i}/\hat{P}_{m,i}$;

q_n = the roots of the $B_1(q) = 0$

$\hat{P}_{m,i}$ = permeability of the selective layer

$\hat{P}_{sm,i}$ = permeability of the dense structure in support layer

$\overline{P}_{pore,i}$ = average permeability of the pores (include the penetrated materials)

ψ = filling fraction of the pore

ε_s = surface porosity $\cong \varepsilon_r^2 = (r_{pore}/r_{pore})^2$

When $F = 0$, $G = 0$ and hence equation (3.132) above collapse to a one dimensional transport:

$$R_i(F = 0) = \frac{(p_{mb,i} - \Theta_i p_{p,i})}{J_i} = \frac{\delta_m}{\hat{P}_{m,i}} + \frac{d}{\hat{P}_{sm,i}(1-\varepsilon_s)+\overline{P}_{pore,i}\varepsilon_s}$$ (3.133)

Wakeham and Mason (1979) have developed an expression that can approximate the value of F:

$$F = \frac{0.8(1-1/\beta)}{\upsilon(1+2/\beta^3)}$$ (3.134)

This relatively simple expression gives an accurate representation of F (within 5%) for all values of β whenever $\lambda > 8$. Keller and Stein (1967) gives another limiting range with the following equation

$$F = \frac{0.8(1.033\lambda)}{\upsilon(0.564 + \lambda)}$$ (3.135)

for $1 < \lambda < 1000$ and $100 < \beta < 1000$ with largest error of 2.6%

3.6.1.4 Model D

In model D, Strathmann et al (1988) assumed that if the flux only goes through the surface pores of the support and that the flux direction in the selective layer could be approximated by a funnel shown in the Fig. 3.21. The average diffusion path length for the component diffusing through the selective layer increases as shown. The minimum diffusion path length, $l_{\min}$ is equal to the selective layer thickness, δ_m.
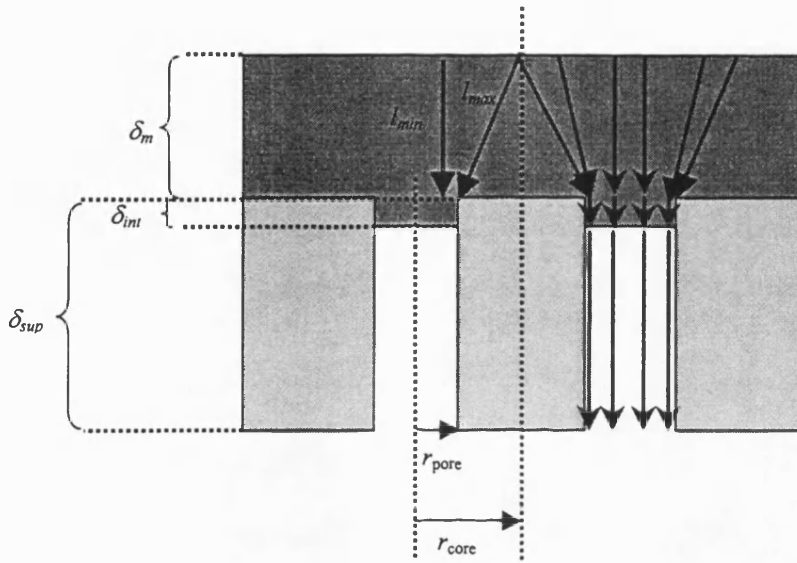
Fig. 3.21 Flow pattern of component flux based on Strathmann (1988).

If the r_{pore} and r_{core} are defined as the radius of the pore and the distance between the core axis of pore and support matrix respectively, the maximum diffusion path for the component obstructed by the support layer matrix can be calculated by using Pythagoras' theorem and yields:

$$l_{\max} = \sqrt{\left(r_{\text{core}} - r_{\text{pore}}\right)^2 + l_{\min}^2} \tag{3.136}$$

From equation above, the average of $l_{\max}$ and $l_{\min}$ is :

$$l_{avg} = \frac{1}{2}\left(l_{\min} + \sqrt{\left(r_{core} - r_{pore}\right)^2 + l_{\min}^2}\right) \tag{3.137}$$

Consider that the effective diffusion path is the mean of all the obstructed and unobstructed paths. It can then be written as:

$$l_{eff} = \varepsilon_r l_{\min} + \left(1 - \varepsilon_r\right)l_{avg} \tag{3.138}$$

or

$$l_{eff} = \varepsilon_r l_{min} + \frac{(1-\varepsilon_r)}{2}\left(l_{min} + \sqrt{r_{pore}^2 \left(\frac{1-\varepsilon_r}{\varepsilon_r}\right)^2 + l_{min}^2} \right) \qquad (3.139)$$

where: $\varepsilon_r = \dfrac{r_{pore}}{r_{core}}$ \qquad (3.140)

In order to facilitate the comparisons between models, equation (3.139) that was developed by Strathmann et al (1988) can be expressed in terms of surface porosity (ε_s) instead of radial porosity (ε_r). Let $\lambda = \delta_m / r_{pore}$ and since $\varepsilon_r \cong \sqrt{\varepsilon_s}$, the ratio of the effective diffusion path to the minimum path (χ) can be expressed as:

$$\frac{l_{eff}}{l_{min}} = \chi = \sqrt{\varepsilon_s} + \frac{(1-\sqrt{\varepsilon_s})}{2}\left[1 + \sqrt{\frac{1}{\lambda^2}\left(\frac{1-\sqrt{\varepsilon_s}}{\sqrt{\varepsilon_s}}\right)^2 + 1} \right] \qquad (3.141)$$

By applying Fick's first law, the component flux through the selective layer can be written as:

$$J_i = \frac{D_{m,i}}{\delta_m \chi}\left(C_{m1,i} - C_{m2,i}^* \right) \qquad (3.142)$$

the ratio of the effective diffusion path to the minimum path (χ) is visualized in Fig 3.22.
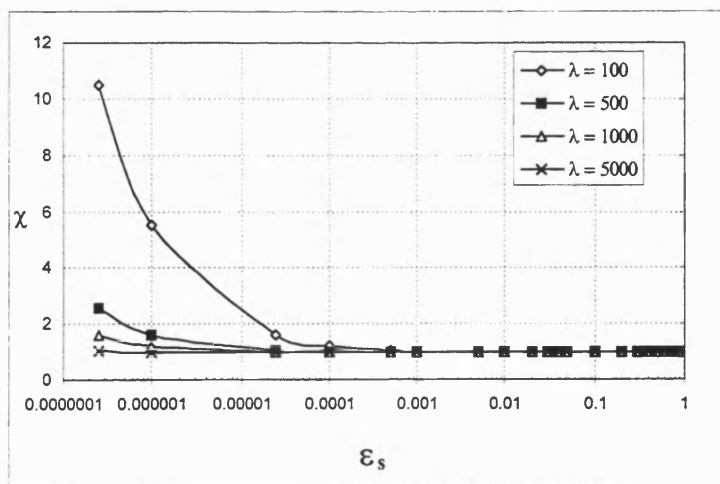
Fig. 3.22 Variation of χ according to Model D based on equation (3.141)

3.6.1.5 Model E - an alternative to model B, C and D

From investigating the two-dimensional diffusion models given in the literature (model B, C and D), the solutions for the ratio of effective diffusion path to the thickness of selective layer are either complex or require pre-knowledge of the membrane permeabilities. Although model D offers a simplistic solution, the flux pattern and derivation of model D is found to be oversimplified. Thus, an alternative two-dimensional diffusion model is proposed and it does not require pre-knowledge of membrane permeabilities. Nevertheless it is adequate to describe the variation of the ratio of the effective diffusion path to the thickness of selective layer. To derive the equation for model E, the following assumptions are made based on a cylindrical unit cell:

- There is no radial concentration gradient within the membrane.
- The porosity and pore size of the support layer only affect the imaginary surface area for diffusion within the selective layer matrix.
- The imaginary surface area is only a function of thickness of the selective layer, porosity and pore size of the support layer.

A three-dimensional diagram for model E is visualised in Fig. 3.23
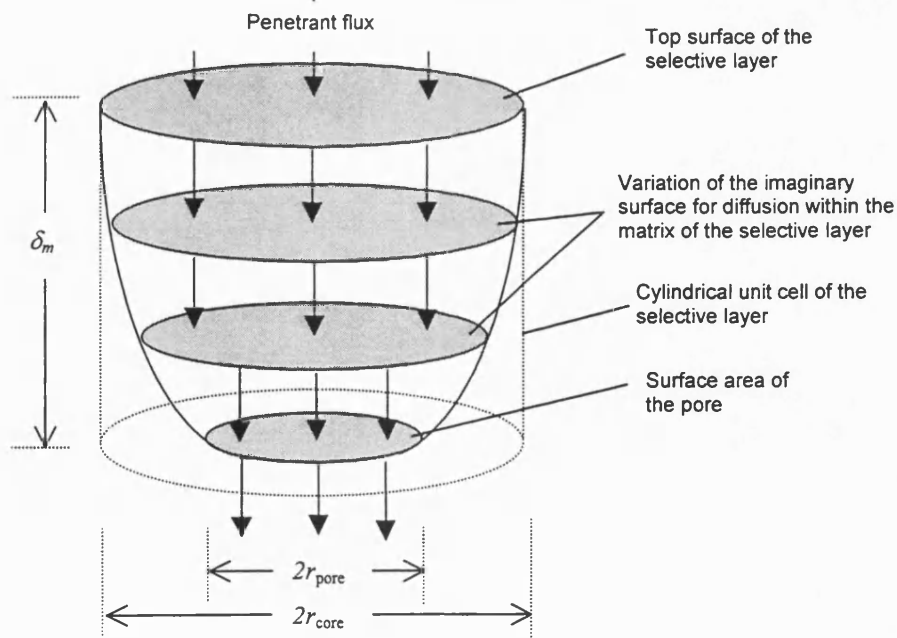
Fig. 3.23 A 3-dimensonal view of the flux through the selective layer based on model E

98

Mathematically, the variation of the radius of the imaginary circular surface can be translated as in Fig. 2.34. Dimensionless variables are defined, i.e. $r^* = (r - r_{pore}) / (r_{core} - r_{pore})$ and $z^* = z/\delta_m$. The top surface of the selective layer (i.e. $z = 0$, $r = r_{core}$), $z^* = 0$ and $r^* = 1$ while at the exit surface of the selective layer (i.e. $z = \delta_m$, $r = r_{pore}$), $z^* = 1$ and $r^* = 0$.
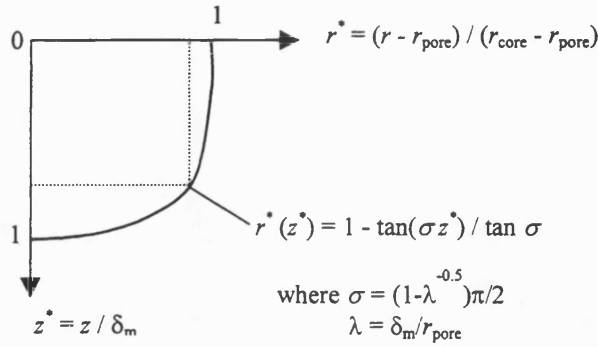
Fig. 3.24 A mathematical description of the relationship between the thickness and radial variation of the surface.

It is assumed that radial variation of the imaginary surface in the selective layer matrix has the following relationship:

$$r^* (z^*) = 1 - \tan(\sigma z^*) / \tan \sigma \qquad \text{for } 0 \leq z^* \leq 1 \qquad (3.143)$$

where: $\sigma = (1 - \lambda^{-0.5})\pi/2 \qquad \lambda = \delta_m/r_{pore}$.

As the thickness to pore size ratio λ increases (provided $\lambda > 1$), curvature of equation (3.143) starts linear and the curvature increases dramatically near the pores. From equation above, the ratio of the imaginary surface area, $A(z^*)$, to the top surface area, $A(0)$, can determined as follows:

$$\frac{A(z^*)}{A(0)} = \left(\frac{r}{r_{core}}\right)^2 = \left(1 - \kappa \tan(\sigma z^*)\right)^2 \qquad (3.144)$$

where $\kappa = (1 - \sqrt{\varepsilon_s}) / \tan\sigma$ and $\varepsilon_s = (r_{pore} / r_{core})^2$ = surface porosity

According to First Fick's law, the solute flux through the imaginary surface within the selective layer matrix can be determined by the following:

$$J_i = -\frac{A(z^*)}{A(0)} \frac{D_{m,i}}{\delta_m} \frac{dC_{m,i}}{dz^*}$$

(3.145)

or integrated over the length of thickness, δ_m, yield:

$$J_i = \frac{D_{m,i}}{\delta_m \chi} \left(C_{m1,i} - C_{m2,i} \right)$$

(3.142)

where χ is the ratio of the effective diffusion path to the thickness of the selective layer, i.e.

$$\chi = \int_0^1 \frac{dz^*}{\left[1 - \kappa \tan\left(\sigma z^* \right) \right]^2}$$

(3.146)

The analytical solution for the above integral is found to be:

$$\chi = \omega_1 \ln\left(\varepsilon_s^{-0.5} \sec \sigma \right) + \omega_2 \varepsilon_s^{-0.5} + \omega_3$$

(3.147)

where: $\omega_1 = \dfrac{2\kappa}{\left(1 + \kappa^2\right)^2}$ $\omega_2 = \dfrac{\kappa^2 \tan \sigma}{\left(1 + \kappa^2\right) \sigma}$ $\omega_1 = \dfrac{1 - \kappa^2}{\left(1 + \kappa^2\right)^2}$

A graphical representation for the analytical solution of χ is shown in Fig. 3.25
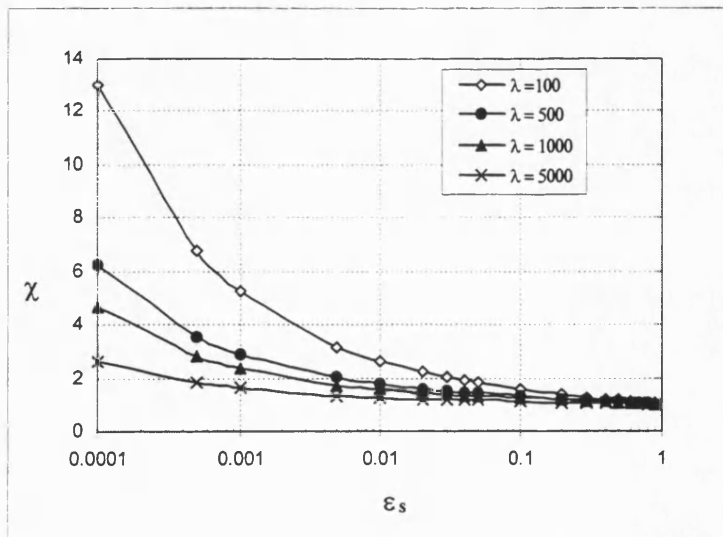
Fig 3.25 Variation of χ according to Model E based on equation (3.147)

3.6.2 Numerical examples and models comparisons

In order to test the effect of two-dimensional diffusion upon diffusion path length, two types of composite membrane are selected. Their relevant properties are shown in Table 3.3. The diffusion path lengths for various membranes are then computed and tabulated in Table 3.4 according to the different diffusion models derived previously.

Table 3.3 Properties of the composite membrane for organophilic pervaporation

Composite Membrane		Case I GKSS membrane	Case II Bath's membrane
Selective Layer	Material	PDMS	PDMS
	Thickness δ_m, (μm)	10	50
Support Layer	Material	Polysulfone[1]	Polypropylene[2]
	Thickness d, (μm)	1*	25
	Pore radius, r_{pore} (μm)	0.005*	0.0357
	Surface porosity, ε_s	0.01*	0.4

Note: [1] Asymmetric membrane   [2] Symmetric membrane   * skin layer properties

Table 3.4 Effective diffusion path lengths according to various models

Models	Effective diffusion path length (μm)		Increase in diffusion path length (%)	
	Case I	Case II	Case I	Case II
A	10.00000	50.00000	0.00	0.00
B	10.35928	50.01743	3.59	3.40×10^{-2}
C*	10.35928	50.01743	3.59	3.40×10^{-2}
D	10.00009	50.00000	9.10×10^{-4}	0.00
E	14.12319	53.90657	42.19	7.81313

* The skin layer is assumed to be impermeable

From Table 3.4, the effective diffusion path length that is predicted by Model B and C are numerically the same when the support matrix/ skin layer is assumed to be impermeable. This was also confirmed by Bode and Hoempler (1996). However, these models predict a relatively longer diffusion path length compared to model D. It is also noted that model E

101

predicts a relatively longer diffusion path length compared to the other model. When the selective layer thickness is relatively thick and for porosities sufficiently large (in Case II for instance), models B, C, D and E virtually collapse to Model A. The sensitivity of the effective diffusion path length towards the surface porosity is presented in Fig. 3.26 according to different models ($\lambda = \delta_m/r_{pore} = 2000$ accords with case I)
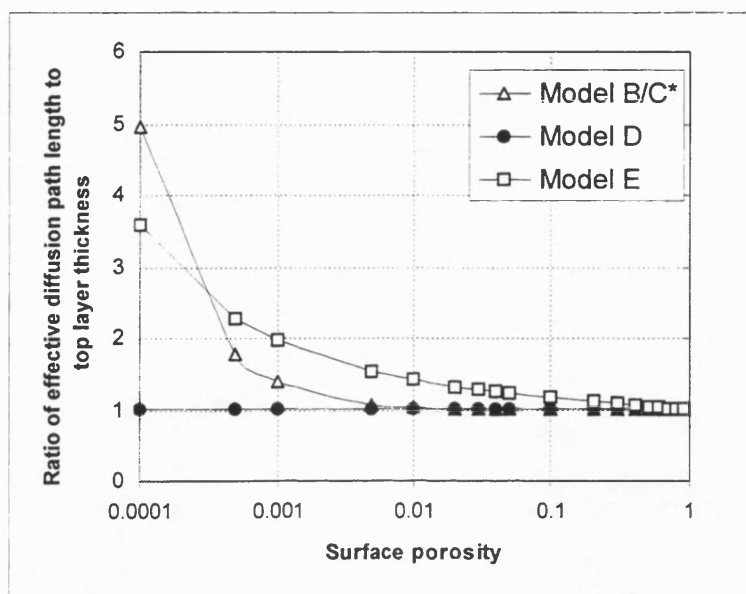
Fig. 3.26 Sensitivity of effective diffusion path lengths towards surface porosity

($\lambda = 2000$, *the support matrix/skin layer is assumed to be impermeable)

From Fig. 3.26, model B, C and E are more sensitive towards porosity compared to model D. If the support matrix/ skin layer is assumed to be permeable, model C would give a less sensitive curve towards porosity compared to model B because of the smaller curvature of the diffusion path length. From Fig. 3.21 and other researchers (Bode and Hoempler, 1996; He et al, 1996; Lopez et al, 1986), model A (Henis and Tripodi, 1980) can give a good approximation for effective diffusion path unless an ultra thin selective layer (<0.5μm) and very low surface porosity (<10^{-4}) support layer are employed.

3.6.2 Observations on the importance of support layer resistance

It has just been shown that the effective increase in path length of the selective layer above the support layer will rarely be significant. This accounts for the effect of support geometry

upon flow direction and the resistance due to the penetration of selective layer material into the pores of support. In the study of support layer influence, Bennett et al (1997) have readily shown that the penetrated material with intruded depths of δ_{int} has a resistance proportional to $\delta_{int}/\varepsilon_s$ (Bennett et al, 1997). If the vapour transport resistance is negligible, the effective thickness of membrane, $\delta_{m,eff}$ could have been taken to be $(\delta_m-\delta_{int})+ \delta_{int}/\varepsilon_s$. Unlike the effective path length in the top layer, this can be significant in pervaporation (Field and Wu, 1998). For instance, if a composite membrane has a top selective layer thickness (δ_m) of 10μm, intruded depths (δ_{int}) of 0.025μm and a support with surface porosity (ε_s) of 0.01 μm, the effective membrane thickness $(\delta_{m,eff}$) would be 12.5μm. However, the degree of penetration is influenced by the nature of the support and the resistance due to the penetration has been included in the support resistance as observed in equation (3.107) and (3.115).

3.7 Derivation of Overall Mass Transport Equation for Organophilic Pervaporation Process

In deriving an overall mass transport equation for pervaporation process, it is important to consider the various aspects of mass transfer steps that has been discussed in sections 3.2-3.3 of this chapter. In general, the steady state concentration profile in each mass transfer step can be illustrated in Fig.3.27. The curvature of the concentration profile is due to the non-ideal condition in each mass transfer step. These factors are (i) convective flow contribution in the boundary layer; (ii) swelling and coupling effects within the membrane and (iii) complication due to the support layer; and (iv) possible complications regarding vapour side flow.
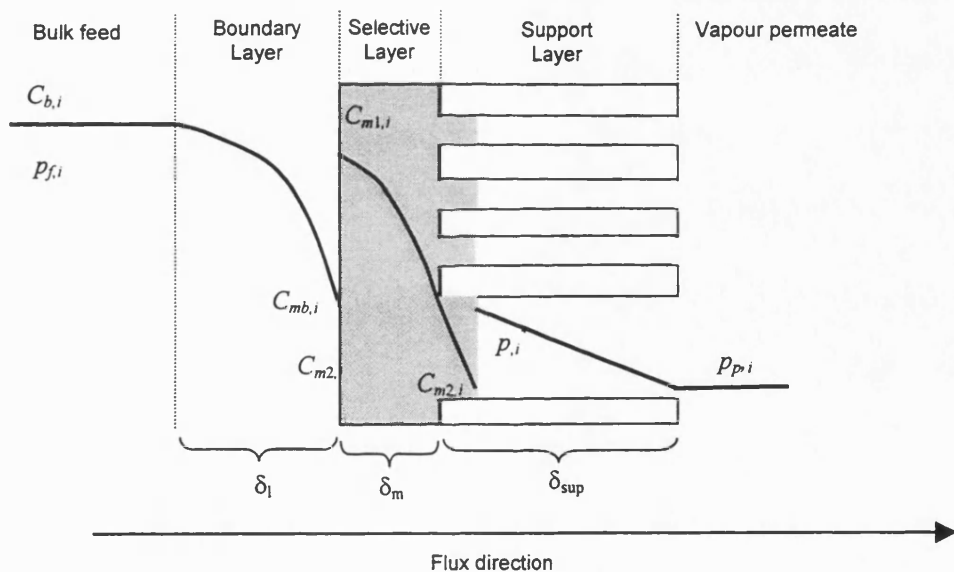
Fig 3.27 Steady-state solute concentration profile of pervaporation process in non-ideal condition

However, in the removal of trace organic contaminants from an aqueous stream, using organophilic composite membranes, convective flow terms are usually negligible, owing to

the low organic component feed concentration and low water sorption within the membrane. Membrane swelling and flux coupling are also generally very low. Often organic component sorption may be successfully described by Henry's law and membrane diffusion coefficient treated as being quasi constant. In addition, the effect of two dimensional diffusion in the selective layer caused by the impermeable support matrix can be assumed to be negligible for most of the commercial membranes. Hence, one-dimensional diffusion is an appropriate approximation for the selective layer. Therefore, the concentration profiles generated in each step for organophilic pervaporation can be approximated as a linear decrease of concentration as shown as Fig. 3.28
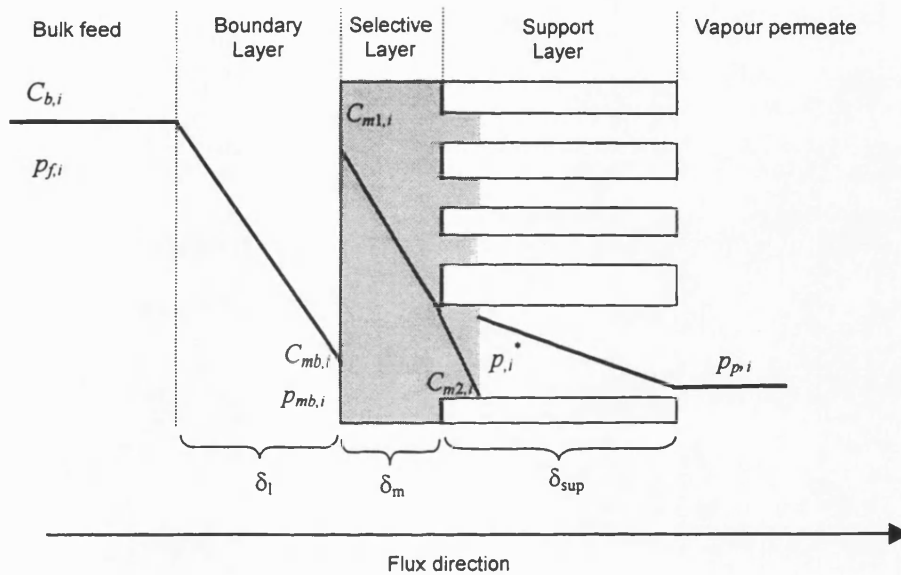
Fig 3.28 Steady-state solute concentration profile of organophilic pervaporation process

These greatly simplify the mathematical treatment of mass transport and if the partial pressure based sorption and desorption coefficients are defined as $S_i^f = C_{m1}/p_{mb,i}$ and $S_i^d = C_{m2}/p_i^*$ respectively, the overall mass transport equation for organophilic pervaporation can be written as:

$$J_i = K_i\left(p_{f,i} - \Theta_i\, p_{p,i}\right) \tag{3.148}$$

Where: $K_i = \dfrac{1}{R_{bl} + R_{top,i} + R_{sup,i}}$, overall mass transfer coefficient of solute. (3.149)

$$R_{bl} = \frac{P_i^{sat} \gamma_i}{k_i \widetilde{\rho}_l}, \text{ liquid boundary layer resistance at the feed side.} \quad (3.150)$$

$$R_{top,i} = \frac{\delta_m}{\hat{P}_{m,i}}, \text{ selective layer resistance.} \quad (3.151)$$

$$R_{sup,i} = \frac{\delta_{sup}}{\overline{P}_{pore,i} \varepsilon_s}, \text{ resistance of the support layer} \quad (3.152)$$

3.7.1 Liquid Boundary Layer Resistance

The liquid boundary layer resistance in equation (3.150) is inversely proportional to the feed liquid mass transfer coefficient, $k_l, = D_{l,i} / \delta_l$, which can be determined for various modules from Sherwood correlations given in Table 3.1. Further, it is also proportional to the volatility of the target component in the solvent, $P_i^{sat} \gamma_i$, hence, for highly volatile components, the liquid boundary layer resistance must be significant. For very dilute feed solute concentration, the mean molar density of feed liquid, $\widetilde{\rho}_l$ can be approximated as the molar density of the solvent ($\approx \rho_j / M_j$).

It should be noted that due to the high concentration of solvent in the bulk solution and its rejection at the surface of membrane, the solvent concentration gradient in the boundary layer is relatively small. Hence, the boundary layer term for the solvent flux can be ignored in the formulation of the overall mass transfer coefficient of this component.
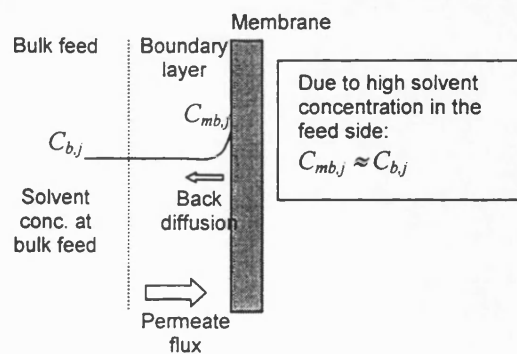
Fig. 3.24 Concentration profile of solvent throughout the boundary layer

3.7.2 Selective layer resistance

For a composite membrane, the selective layer resistance is determined by the permeability of the selective layer material, $\hat{P}_{m,i} = D_{m,i} S_i^f$, which is the product of the membrane diffusivity and the sorption coefficient. However, the magnitude of the selective layer resistance is also determined by its thickness. From the experience of gas permeation. it might be suggested that flux would be improved without the loss of the separation efficiency, by employing an ultra-thin selective layer. However, this is not the case for organophilic pervaporation and in turn, the reduction of top layer thickness would lead to feed side mass transfer control instead of membrane control. This is because diffusion coefficients in liquid are much smaller than those in gas.

3.7.3 Support layer resistance

The ideal, support layer would act solely as a mechanical support. However the support layer resistance is significant if there is significant penetration of selective layer material into the pores. The degree of penetration is dependent on the pore diameters and surface porosity of the support layer, ε_s. In addition, the resistance of support layer is inversely proportional to

the mean permeability of the support , $\overline{P}_{pore,i} = \dfrac{1}{\dfrac{\psi}{\hat{P}_{m,i}} + \dfrac{(1-\psi)\Theta_i}{\hat{P}_{knud,i}}}$, where ψ is the filled

fraction within the support layer, the permeability of the unfilled pores is $\hat{P}_{knud,i} = \dfrac{D_{K,i}}{RT}$ and

the desorption factor $\Theta_i = S_i^f / S_i^d$.

3.7.4 Further simplification of the overall mass transport equation

For a homogeneous membrane with permeate pressure close to zero, the overall mass transport equation can be simplified to absolute flux, J_i^*:

$$J_i^* = K_i p_{f,i} \qquad (3.153)$$

Several researchers (Cote and Lipski, 1988; Nijhuis et al, 1991;Gref et al, 1992; Raghunath and Hwang, 1992; Ji et al, 1994) have derived a similar overall mass transfer equation. With this assumption, one can avoid the evaluation of the desorption factor. However when permeate pressure is not low enough, using equation (3.153) for flux prediction would lead to significant error. Hence, it is recommended that the more general form of overall mass transport equation (3.148), as derived in the present study, be used.

3.8 Chapter Conclusion

In general, the mass transport mechanism for the removal of trace organic contaminants from aqueous streams, using organophilic composite membranes, can be considered as a series of mass transfer steps, i.e. boundary layer transport, selective layer transport and the support layer transport. The concentration profiles generated in each step can be approximated as a linear decrease of concentration. Due to the low feed concentration of the organic component and low water sorption within the membrane, the convective flow term is usually negligible. Furthermore, owning to the low feed concentration, membrane swelling and flux coupling are generally very low. It is evident that the solution-diffusion model can describe the mass transport in the dense selective layer of the membrane more successfully than the pore flow model. Organic component sorption may be successfully described by Henry's law and membrane diffusion coefficient treated as being quasi constant. The effect of two dimensional diffusion in the selective layer caused by the impermeable support matrix can be assumed to be negligible for most of the commercial membranes, so justifying use of one dimensional diffusion equations. This greatly simplifies the mathematical treatment of mass transport and allows for the use of the resistances in series model.

In the present study, a comprehensive transport model is derived based on the above assumption that could account for the resistances in the boundary layer, the selective layer and the support layer. In addition it could also account for the effect of permeate pressure and the adverse effect caused by the desorption factor. It should be noted that the transport model cannot be applied in other areas of pervaporation, particularly when feed concentrations are high and especially for the dehydration of organic solvents using hydrophilic membranes. In these cases, significant departure from ideality may occur at every stage during mass transport. The models presented within this chapter should provide the basis for describing transport in organophilic pervaporation membranes. These models are more comprehensive and soundly based than those used by most other groups (Cote and Lipski, 1988; Nijhuis et al, 1991; Watson and Payne, 1991; Gref et al, 1992; Raghunath and Hwang, 1992; Wijmans and Baker, 1993; Ji et al, 1994; Liu et al, 1996)

Part III   Engineering Science Analysis

Chapter 4

Engineering Science Analysis of Component Transport and the Classification of Behaviour with Reference to Permeate Pressure

4.1 Chapter Objectives

- A review of the importance of permeate pressure effect upon separation performance.
- Develop an improved mathematical description for pervaporation separation .
- Develop a comprehensive transport model for organophilic pervaporation.
- Derive analytical solutions for performance parameters.
- Compare the description and analytical solutions with those for gas permeation.
- Perform engineering science analysis upon the performance of orgnaophilic pervaporation and classification of performance behaviour with respect to permeate pressure.

4.2 Introduction

In the design and operation stage of an organophilic pervaporation unit, it is important for the chemical and environmental engineers to understand the essential aspects of the process. Apart from the mass transport through the membrane, as discussed in Chapter 3, the other aspects like separation factor and permeate concentration are determined by the process parameters and module design. One of the key process parameters is the permeate pressure in the module. In pervaporation, the lowering of permeate pressure increases the driving force for the permeation through the membrane. Theoretically, maximum driving force, which leads to maximum flux throughput, can be achieved by applying an ultimate vacuum at the permeate surface of the membrane. In pervaporation, however, an ultimate vacuum on the permeate side is impractical since the cost of the vacuum system increase rapidly with the quality of the vacuum.

In providing the driving forces for the component fluxes, the permeate pressure is also a critical parameter that influences the separation performance of an organophilic pervaporation process. For instance, in the pervaporation of phenol from water, Boddeker and Bengston (1990) found that a slight increase of permeate pressure would lead to a drastic decline in the separation performance. However, in the case of the pervaporation of trichloroethylene (TCE) from water, Baker et al (1997) found that the separation performance can be enhanced with an increase of permeate pressure. The contradictary separation performance behaviour with respect to an increase of permeate pressure has made the design of a multi-component organophilic pervaporation unit difficult.

Although the dependence of separation performance on permeate pressure is an important consideration in the overall pervaporation separation process, a review of basic principles of pervaporation by Aptel and Neel (1986) offers no explanation of this dependence, and very little discussion. A review by Neel (1989) provides considerably more discussion on this aspect but is largely concerned with aspects of a particular case. On the other hand, extracting a simple quantitative description of the phenomenon from the very comprehensive work of others for example Sheldon and Thompson (1978), Brun et al (1986), or of Nyugen (1987), is rather a laborious task.

More recently Watson and Payne (1990), Blume et al (1990), Wijmans and Baker (1993) have developed a simplified transport model that can describe the separation in terms of the contribution of each driving force. Owning to the oversimplification of their transport model, an overestimation of performance occurs.

An ingenious engineering approach proposed by Gooding et al (1991), showed that a dimensionless group can be derived which indicates whether the water permeation rate increases or decreases relative to the VOC permeation rate with increasing permeate pressure. Due to the oversimplification of their transport model, this application is limited to highly volatile hydrocarbons. Also the dimensionless group can not account for the effect of the support layer or of the desorption factor.

In view of above considerations, there is a need to set out a broader framework for the understanding of the pervaporation process. An engineering approach will be used to analyze

the separation performance behaviour of organophilic pervaporation. The developed framework will be used to analyze the separation performance in different component and membrane systems.

4.3 Simple description of pervaporation separation

In order to improve understanding, an improved format to express the separation factor will be derived. The format will be able to distinguish between the effect of vapour-liquid equilibrium separation, module effectiveness, membrane properties, support layer effect and the influence of the driving forces. A comparison with the gas permeation process will be made.

4.3.1 Separation factor due to vapour-liquid equilibrium

In the organophilic pervaporation process, the volatility of the organics play an important role in the separation process (Wijmans and Baker, 1993; Baudot and Marin, 1997), hence it is important to distinguish the contribution of this effect to the overall separation performance.

The separation of two volatile liquids by means of a single stage distillation is determined by the difference in their volatility (Fig. 4.1). The separation factor due to vapour-liquid equilibrium expressed as the relative volatility is shown below:

Relative volatility:
$$\alpha_{VLE} = \frac{y_i^{VLE} / y_j^{VLE}}{x_i / x_j} = \frac{P_i^{sat} \gamma_i}{P_j^{sat} \gamma_j} \tag{4.1}$$
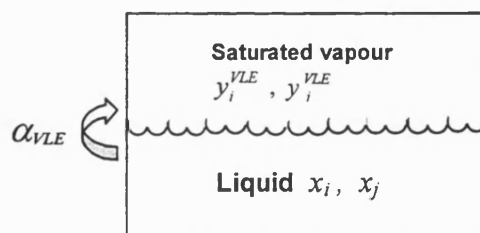
Fig. 4.1: Vapour liquid equilibrium separation

4.3.2 Separation factor due to pervaporation process and the enhancement factor

In contrast to the previous separation, the two phases in pervaporation are separated by a semi-permeable barrier (membrane), in which the liquid solution is in contact with the feed side of the membrane and a low pressure vapour is withdrawn on the permeate side as shown in Fig 4.2. The separation achieved by a pervaporation process is defined as follows:

Separation factor (Selectivity): $\alpha_{PV} = \dfrac{y_i/y_j}{x_i/x_j}$ (4.2)
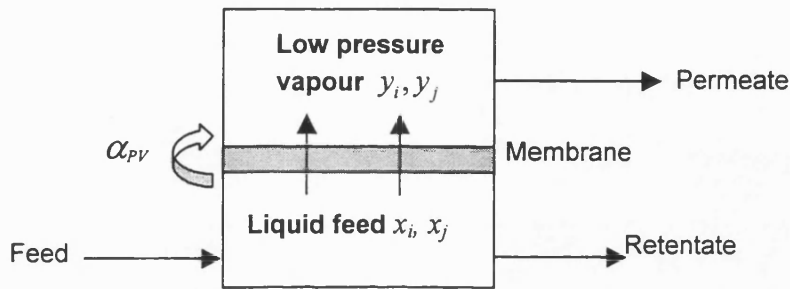
Fig. 4.2 Separation by pervaporation

Mathematically, however, the separation factor for pervaporation can be rearranged as follows:

$$\alpha_{PV} = \frac{y_i/y_j}{y_i^{VLE}/y_j^{VLE}} \cdot \frac{y_i^{VLE}/y_j^{VLE}}{x_i/x_j}$$

(4.3)

An enhancement factor due to pervaporation, E', is defined as:

$$E' = \frac{y_i/y_j}{y_i^{VLE}/y_j^{VLE}}$$ (4.4)

Thus, an expression is obtained: $\alpha_{PV} = E'\alpha_{VLE}$ (4.5)

The enhancement factor is similar to the one Wijmans and Baker (1993) proposed, β_{mem}. In addition to the superficial change of β_{PV} and β_{evap} to α_{PV} and α_{VLE} respectively, there is an important difference. According to Wijmans and Baker (1993), β_{mem} refers solely to the membrane itself whilst as shown below E' is a function of all transport coefficients including

113

that of the membrane and that of the boundary layer. Thus, it is referred to simply as an enhancement factor in order to avoid any confusion about whether it is solely due to membrane characteristics or not.

According to the relationship in equation (4.5), the pervaporation process can be hypothetically visualised as shown in Fig 4.3 Firstly, the feed liquid is hypothetically vaporised to a saturated vapour, which then permeates through the membrane. As discussed by Wijmans and Baker (1993), the above hypothetical process is thermodynamically identical to the one in Fig. 4.2.
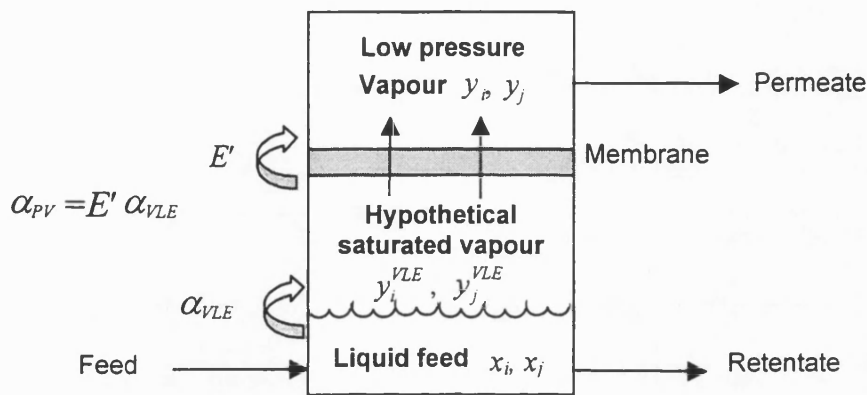
Fig. 4.3 A hypothetical permeation process for pervaporation

Since the relationship between the permeate concentration and the feed concentration for a binary system can be expressed as follows:

y-x relationship:
$$y_i = \frac{\alpha_{PV} x_i}{(\alpha_{PV} - 1)x_i + 1} \tag{4.6}$$

By substitution of equation (4.5) into (4.6) a transformed y -x relationship can be formed in below:

$$y_i = \frac{E' \alpha_{VLE} x_i}{(E' \alpha_{VLE} - 1)x_i + 1} \tag{4.7}$$

Equation (4.7) can then be visualised as shown as Fig. 4.4.
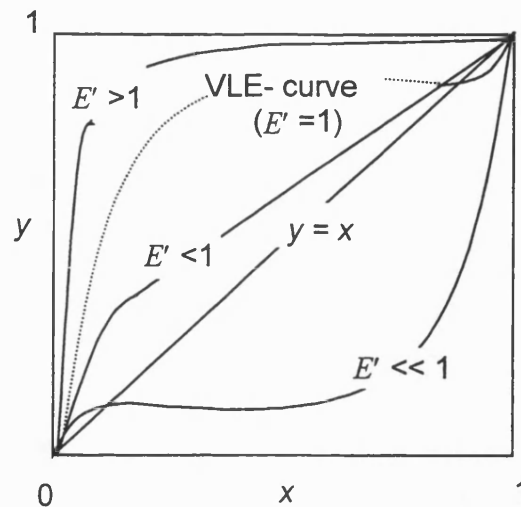
Fig. 4.4 The effect of E' upon y-x relationship in pervaporation as shown. E', x and y are all with respect to the more volatile component.

From Fig. 4.4, for $E' > 1$, the process of pervaporation has enhanced the separation achieved by vapour-liquid equilibrium. When $E' < 1$, the process of pervaporation gives a permeate less rich in the more volatile component. If E' is sufficiently low, then the $y-x$ relationship line is lower than $y = x$ line. In this case the separation is more beneficial for removing the less volatile component. Such a condition is achieved for the industrial dehydration of volatile organic solvents. An azeotropic mixture, where α_{VLE} is equal to unity, can be broken by pervaporation.

If the enhancement factor is relatively constant, according to equation (4.5), one should expect an increase in the pervaporation separation factor as the volatility of the target organic increases. To test out the theory, some measured pervaporation separation factors (α_{PV}) for various dilute aqueous VOC solutions obtained by Athayde et al (1997) were used. The separation data was obtained with a module containing a PDMS membrane. The separation data is then plotted against the vapour-liquid separation factor (α_{VLE}), obtained from Henry's law data, which is shown in Fig. 4.5. By using the data from Fig. 4.5, the enhancement factor (E') was evaluated and plotted against the vapour-liquid separation factor of VOC solutions which is shown in Fig. 4.6.

115
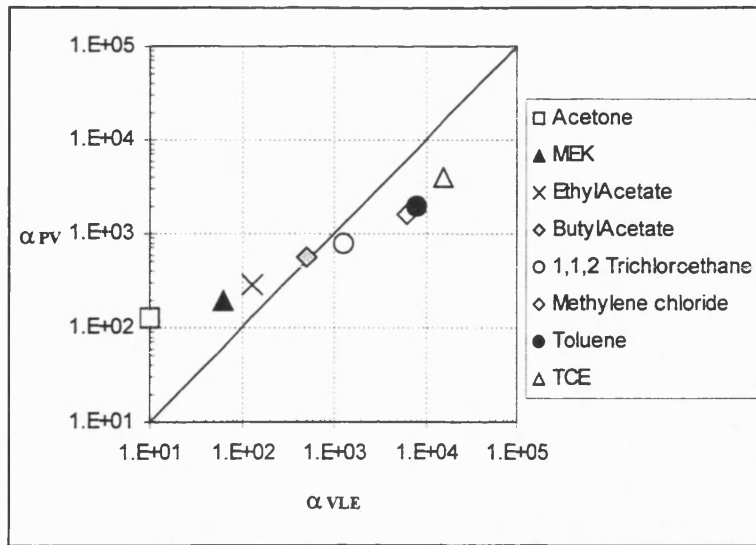
Fig 4.5 Separation factor (α_{PV}) obtained from lab scale membrane modules with PDMS
membrane and the vapour-liquid equilibrium selectivity of various dilute VOCs
solutions (Athayde et al, 1997)
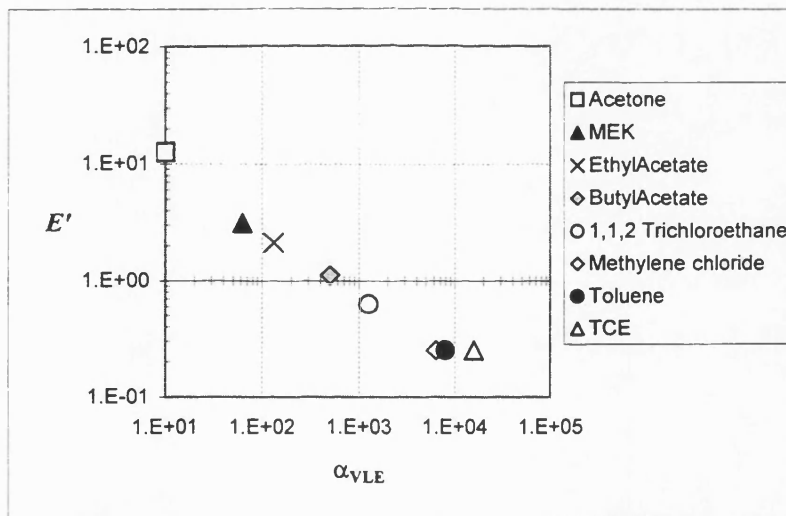
Fig 4.6 Enhancement factor (E') of VOCs system that computed from the
separation factor data obtained from Fig. 4.5

Consider acetone, which has α_{PV} of approximately 150 using a PDMS membrane. In this case, the α_{VLE} is 10; therefore, E' is evaluated and found to be 15. Hence, the separation factor has enhanced 15 fold over that achievable with a single stage vapour-liquid separation of the dilute acetone solution. Although the separation factor due to pervaporation increases with the volatility of the VOCs, the enhancement factor of the separation process decreases. For instance, the enhancement factor for butyl acetate is close to unity and this implies that the separation of the pervaporation process can be attributed to the vapour-liquid separation. The pervaporation separation factor for tri-chloroethylene is an impressive 4000, but it is entirely attributable to the vapour-liquid separation in which the enhancement factor is found only to be 0.3.

In order to improve a pervaporation process, it is important to improve the enhancement factor rather than reporting impressive separation factors. In addition, it should be noted that the enhancement factor is not only affected by the membrane material itself but also the permeation driving force, the operating condition and geometry of the membrane modules. Hence, to investigate how the driving force affects E' and the performance of pervaporation, a comprehensive transport model that can describe the whole process should be used. In Chapter 3, section 3.5, an overall mass transport equation for organophilic pervaporation was derived. It is shown below:

$$J_i = K_i \left(p_{f,i} - \Theta_i p_{p,i} \right) \tag{3.148}$$

Where: $K_i = \dfrac{1}{R_{bl} + R_{top,i} + R_{sup,i}}$, overall mass transfer coefficient of solute. $\qquad$ (3.149)

$R_{bl} = \dfrac{P_i^{sat} \gamma_i}{k_i \tilde{\rho}_l}$, liquid boundary layer resistance at the feed side. $\qquad$ (3.150)

$R_{top,i} = \dfrac{\delta_m}{\hat{P}_{m,i}}$, top selective layer resistance. $\qquad$ (3.151)

$R_{sup,i} = \dfrac{\delta_{sup}}{\overline{P}_{pore,i} \varepsilon_s}$, resistance of the support layer $\qquad$ (3.152)

4.4 Relationship between Separation Factor and Driving Force

Although equation (4.5) offers a simple description of the pervaporation process, the relationship between separation performance and driving force is not known. However, through the use of the comprehensive transport model for organophilic pervaporation, the relationship between separation factor and the driving force can be derived in the format that is consistent with equation (4.5).

From the model equation (3.148), the partial fluxes for solute i and solvent j are defined as follow:

Solute partial flux: $\quad J_i = K_i \left(p_{f,i} - \Theta_i p_{p,i} \right)$ $\hspace{4cm}$ (3.148)

Solvent partial flux: $\quad J_j = K_j \left(p_{f,j} - \Theta_j p_{p,j} \right)$ $\hspace{4cm}$ (4.6)

Since the ratio of the partial molar fluxes for a particular component is the ratio of the permeate mole fraction of components, one obtains:

$$\frac{J_i}{J_j} = \frac{y_i}{y_j} = \frac{K_i}{K_j} \frac{\left(p_{f,i} - \Theta_i p_{p,i} \right)}{\left(p_{f,j} - \Theta_j p_{p,j} \right)} \hspace{3cm} (4.7)$$

Knowing that the separation factor due to vapour liquid equilibrium can also be expressed as:

$$\alpha_{VLE} = \frac{P_i^{sat} \gamma_i}{P_j^{sat} \gamma_j} = \frac{p_{f,i}}{p_{f,j}} \bigg/ \frac{x_{b,i}}{x_{b,j}} \hspace{3cm} (4.8)$$

by combining equation (4.2), (4.7) and (4.8), a relationship that links the pervaporation separation factor to the driving force is established as follows:

$$\alpha_{PV} = \alpha_{VLE} \cdot \frac{K_i}{K_j} \cdot \frac{1 - \Theta_i p_{p,i} / p_{f,i}}{1 - \Theta_j p_{p,j} / p_{f,j}} \hspace{3cm} (4.9)$$

Further, from the relationship $\alpha_{PV} = E'\alpha_{VLE}$, the enhancement factor E' can be related with driving force by the following expression:

$$E' = \frac{\alpha_{PV}}{\alpha_{VLE}} = \frac{K_i}{K_j} \cdot \frac{1 - \Theta_i p_{p,i}/p_{f,i}}{1 - \Theta_j p_{p,j}/p_{f,j}} \tag{4.10}$$

From equation (4.10), it is immediately recognised that the enhancement factor is influenced by the ratio of mass transfer coefficients and also the driving forces term.

4.4.1 Ultimate enhancement factor, intrinsic enhancement factor and module effectiveness

In order to isolate the effect upon separation due to the driving force from the membrane itself, it is necessary to identify other factors that could influence the separation factor. When the permeate pressure tends to ultimate vacuum (i.e. $p_{p,i} \to 0$ and $p_{p,j} \to 0$), the enhancement factor is solely dependent on the ratio of mass transfer coefficients. Hence, for the purpose of analysis, an ultimate enhancement factor E^* is defined as the enhancement factor that is independent of downstream pressure:

$$E^* = \frac{K_i}{K_j} \tag{4.11}$$

Although independent of downstream pressure, E^* is still a function of the boundary layer resistance; as equation (3.149), shows K_i includes R_{bl} and so it does not represent the intrinsic characteristics of the membrane alone. In order to distinguish the enhancement factor due to intrinsic characteristics of the membrane, an intrinsic enhancement factor, E^*_{mem}, that applies at ultimate vacuum *and* in the absence of a boundary layer is defined as:

$$E^*_{mem} = \frac{R_{top,j} + R_{sup,j}}{R_{top,i} + R_{sup,i}} \tag{4.12}$$

Hence, an effectiveness factor reflecting the relative influence of the boundary layer, ε_{bl}, can be defined as:

$$\varepsilon_{bl} = \frac{E^*}{E_{mem}^*} = \frac{1}{1 + \left(\dfrac{R_{bl}}{R_{top,i} + R_{sup,i}}\right)}$$

(4.13)

The term, ε_{bl}, is labelled the module effectiveness factor and has a range of $0 < \varepsilon_{bl} \le 1$. A value of less than 0.9 indicates that boundary layer resistance is over 10% of the total resistance. If ε_{bl} has a value less than 0.5, the whole pervaporation process is essentially controlled by liquid feed mass transfer. Hence, the separation performance is no longer represented by the intrinsic membrane separation performance and this is usually the case in the removal of highly volatile organics from aqueous streams. In such cases, modification of membrane module in order to achieve high liquid feed mass transfer is more important than enhancing the selectivity of the membrane material.

4.4.2 Overall expression of separation factor in relation to driving forces, volatility, module effectiveness and the intrinsic membrane characteristics

In organophilic pervaporation, it is important to have a simple quantitative expression that can distinguish the various parameters that influence the separation performance. By combining equations (4.9), (4.12) & (4.13), a well differentiated expression for the separation factor is obtained:

$$\alpha_{PV} = \alpha_{VLE} \cdot \varepsilon_{bl} \cdot E_{mem}^* \cdot \frac{1 - \Theta_i p_{p,i}/p_{f,i}}{1 - \Theta_j p_{p,j}/p_{f,j}}$$

(4.14)

It is the first time in pervaporation literature that one can identify the four distinct terms that determine the separation performance of a pervaporation system, i.e. vapour-liquid equilibrium separation factor (α_{VLE}), intrinsic enhancement factor due to membrane material (E_{mem}^*), module effectiveness factor (ε_{bl}) and a function reflecting the influence of the permeate on the driving force term.

4.5 Comparison between pervaporation and vapour/ gas permeation

It is widely recognised that there are similarities between pervaporation and vapour/gas permeation process. Wijmans and Baker (1993), in particular attempted to take advantage of the well-established gas permeation field by expressing the mass transport equation of pervaporation in the format of gas permeation. In the present study, the contrast between pervaporation and gas permeation will be addressed as well as the similarities.

In gas permeation, the feed is in gaseous form and is pressurised in order to provide a driving force for the permeation. A simplified diagram for the process is illustrated in Fig. 4.7.
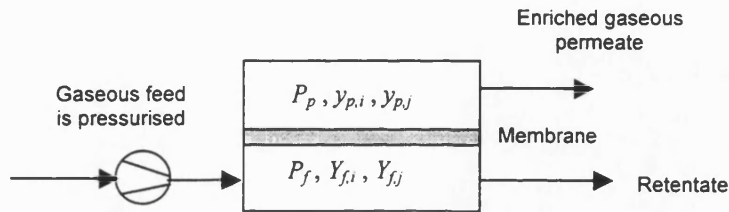
Fig. 4.7 A simplified schematics of gas permeation process

The separation factor for gas permeation is defined as:

$$\alpha_{GS} = \frac{y_i}{y_j} \Big/ \frac{Y_{f,i}}{Y_{f,j}} \tag{4.15}$$

and the component molar permeate flux, Q is usually expressed as:

$$Q_i = \frac{\hat{P}^G_{m,i}}{\delta_m}\left(p_{f,i} - p_{p,i}\right) \tag{4.16}$$

where $\hat{P}^G_{m,i}$ is the gas permeability of the membrane. It should be noted that the feed partial pressure in gas permeation is feed pressure dependent, i.e. $p_{f,i} = P_f Y_{f,i}$ whereas in pervaporation it is saturated vapour pressure dependent, i.e. $p_{f,i} = P_i^{sat}\gamma_i x_{b,i}$. It is also well known that the separation factor of gas permeation can be related to its driving force by the following equation as in Wijmans and Baker (1993):

$$\alpha_{GS} = \alpha^{\bullet}_{mem} \cdot \frac{1 - p_{p,i}/p_{f,i}}{1 - p_{p,j}/p_{f,j}} \qquad (4.17)$$

Where $\alpha^{\bullet}_{mem}$ is the intrinsic membrane selectivity $= \hat{P}^G_{m,i} / \hat{P}^G_{m,j}$

Another process similar to pervaporation is vapour permeation, the liquid is first vaporised and then the driving force is realised by lowering the permeate pressure.
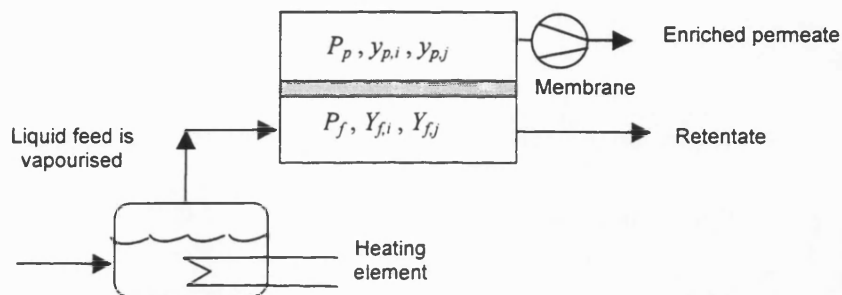
Fig. 4.8 A simplified schematics of vapour permeation process

Again, the mathematical expressions for the mass transport equation and separation factor are essentially the same.

In the limiting case of permeate pressure tending to ultimate vacuum, the separation factor of gas / vapour permeation tends to the intrinsic membrane selectivity, i.e. $\alpha_{GS} = \alpha^{\bullet}_{mem}$.

A summary of the parallelism and a comparison between the model for pervaporation and the conventional model for gas permeation is shown Table 4.1. Whilst there is a clear parallel, the greater complexity of pervaporation is clear.

Table 4.1: Comparison between pervaporation and gas /vapour permeation

	Pervaporation	*Gas / vapour permeation*
Mass Transport Equation	$$J_i = K_i \left(p_{f,i} - \Theta_i P y_i \right)$$ • Simple mass transfer equation but complicated by compound nature of K_i and activity coefficient. • $p_{f,i} = P_i^{sat} \gamma_i x_{b,i}$ • The feed partial pressure is dependent on the saturated vapour pressure instead of feed side pressure. • Mass transfer dependent on the desorption factor, Θ_i. If $\Theta_i = 1$, the driving force is the difference of vapour pressure.	$$Q_i = \frac{\hat{P}_{m,i}^G}{\delta_m} \left(p_{f,i} - p_{p,i} \right)$$ • Simple mass transport equation • $p_{f,i} = P_f Y_{f,i}$ • The feed partial pressure is dependent on the feed side pressure for gas permeation. • Simple mass transfer coefficient • Partition coefficient for sorption and desorption are equal
Separation Factor	$$\alpha_{PV} = \alpha_{VLE} \cdot \varepsilon_{bl} \cdot E_{mem}^* \cdot \frac{1 - \Theta_i p_{p,i}/p_{f,i}}{1 - \Theta_j p_{p,j}/p_{f,j}}$$ • Affected by vapour-liquid equilibrium • Affected by intrinsic selectivity of membrane material, E_{mem}^* • Affected by boundary layer effect, ε_{bl} • Affected by ratio of vapour pressure at the feed to the one at the permeate if $\Theta_i = 1$, otherwise ratio of pseudo-vapour pressures have to be used (see section 4.6). • When $P = 0$, $\alpha_{PV} = \alpha_{VLE} \cdot \varepsilon_{bl} \cdot E_{mem}^*$	$$\alpha_{GS} = \alpha_{mem}^* \cdot \frac{1 - p_{p,i}/p_{f,i}}{1 - p_{p,j}/p_{f,j}}$$ • Affected by intrinsic selectivity membrane material, α_{mem}^* • Affected by the ratio of partial pressure at the feed to the one at the permeate • Negligible boundary layer effect. • When $P = 0$, $\alpha_{GS} = \alpha_{mem}^*$

4.6 Determination of pervaporation performance parameters

In order to examine the effect of permeate pressure, the performance parameters, i.e. permeate composition, partial flux and separation factor have to be expressed in terms permeate pressure. However, the performance parameters equation shown in equations (3.143), (4.7) & (4.14) are implicit functions, and so explicit functions for performance parameters have to be derived.

4.6.1 Permeate composition

In order to determine the permeate composition explicitly, the system has to be restricted to a binary mixture. Knowing that the permeate vapour pressure can be expressed as the product of permeate pressure, P_p, and the permeate composition, y_i, $(p_{p,i} = P_p \, y_i)$, equation (4.7) is rewritten for a binary mixture in a form suitable for mathematical manipulation, i.e.

$$\frac{y_i}{1-y_i} = E\frac{f_i - P_p y_i}{f_j - P_p(1-y_i)} \tag{4.18}$$

$$\text{Where } E = \frac{K_i \Theta_i}{K_j \Theta_j} \tag{4.19}$$

$$\text{and } f_i = \frac{p_{f,i}}{\Theta_i} \text{ and } f_j = \frac{p_{f,j}}{\Theta_j}, \text{ pseudo-feed partial pressures.} \tag{4.20a) \& (4.20b}$$

Rearranging equation (4.18), a quadratic equation can be formed:

$$(E-1)P_p y_i^2 - [(E-1)P_p + f_i E + f_j] \cdot y_i + f_i = 0 \tag{4.21}$$

In order to solve for the permeate composition, y_i, with the use of equation (4.21), three possible cases are identified, i.e. (i) when $P_p = 0$, (ii) $P_p > 0$ & $E = 1$, (iii) $P_p > 0$ & $E \neq 1$.

4.6.1.1 Solution for permeate composition in the case of $P_p = 0$

When the permeate pressure is so low and tends to zero, equation (4.21) is simplified and thus the permeate composition at ultimate vacuum, y_i^* can be evaluated as follow:

$$y_i^* = \frac{Ef_i}{f_j + Ef_i} = \frac{1}{1 + p_{f,j}/\left(p_{f,i}\varepsilon_{bl}E_{mem}^*\right)} \tag{4.22}$$

Although permeate composition is now permeate pressure independent, it is influenced by the effectiveness of the module (the boundary layer resistance), intrinsic enhancement factor and the feedside partial pressure ratio. It is interesting to note that the permeate composition for a pervaporation system with $E > 1$ and small f_i is smaller than the one with $E < 1$ and larger f_i. In a later section the significance of these parameters will be discussed.

4.6.1.2 Solution for permeate composition in the case of $P_p > 0$ & $E = 1$

The limiting case is not only restricted to $P_p = 0$. Another limiting case is $E = 1$ for any P_p. In this case, the permeate composition, y_i^E, can be evaluated as:

$$y_i^E = \frac{1}{1 + f_j/f_i} \tag{4.23}$$

Although the permeate pressure is not fixed, the permeate composition is found to be independent of permeate pressure.

4.6.1.3 Solution for permeate composition for $P_p > 0$ & $E \neq 1$

In general, the pervaporation system usually operates with $P_p > 0$ and $E \neq 1$. It is of great utility to note that the permeate concentration can be solved through a simple quadratic equation. Rearranging equation (4.21) and to yield:

$$y_i^2 - \left(1 + AB/P_p\right)y_i + A/P_p = 0 \tag{4.24}$$

Where: $A = \dfrac{f_i E}{(E-1)}$ $\tag{4.25}$

125

And
$$B = 1 + \frac{1}{E}\left(\frac{f_j}{f_i}\right) = \frac{1}{y_i^*} \qquad (4.26)$$

As the permeate concentration is constrained to be in the range of $0 \leq y_i \leq 1$, it is restricted to one solution for each of the two regions, i.e. $E < 1$ and $E > 1$:

When $E < 1$:

$$y_i = \frac{1}{2}\left[\left(1 + AB/P_p\right) + \sqrt{\left(1 + AB/P_p\right)^2 - 4A/P_p}\right] \qquad (4.27a)$$

When $E > 1$:

$$y_i = \frac{1}{2}\left[\left(1 + AB/P_p\right) - \sqrt{\left(1 + AB/P_p\right)^2 - 4A/P_p}\right] \qquad (4.27b)$$

4.6.2 Determination of partial flux

To determine the partial flux for solute i, for a binary system, the permeate composition equations are coupled with the overall mass transfer equation.

4.6.2.1 Solution for partial flux in the case of $P_p = 0$

When driving force is at maximum ($P_p = 0$), the partial flux is simplified into $J_i^* = K_i p_{f,i}$. In the next section, all the partial fluxes will be normalised with J_i^* and will be referred to as "absolute fluxes". Thus, changes in partial flux at elevated downstream pressure can be observed.

4.6.2.2 Solution for partial flux in the case of $P_p > 0$ & $E = 1$

For pervaporation system with $E = 1$ and $P_p > 0$, the partial flux equation is immediately recognised as:

$$J_i^E = K_i\left(p_{f,i} - \Theta_i P_p y_i^E\right)$$

(4.28)

However, when it is rearranged, an interesting relationship between J_i^E and J_i^* is established as shown as below:

$$J_i^E = J_i^*\left(1 - P_p / f_{total}\right)$$

(4.29)

Where $f_{total} = f_i + f_j$, total pseudo-partial vapour pressure at the feed-side.

It is interesting to note that for pervaporation system with $E = 1$, partial flux linearly decreases with an increase of permeate pressure.

4.6.2.3 Solution for partial flux for $P_p > 0$ & $E \neq 1$

For pervaporation system with $E \neq 1$ and $P_p > 0$, the partial flux equations can be obtained by combining equation (3.130), (4.27a) and (4.27b) to yield:

$$J_i = J_i^*\left\{1 - \frac{1}{2f_i}\left[\left(P_p + AB\right) + \sqrt{\left(P_p + AB\right)^2 - 4AP_p}\right]\right\} \quad \text{when } E < 1$$

(4.30a)

$$J_i = J_i^*\left\{1 - \frac{1}{2f_i}\left[\left(P_p + AB\right) - \sqrt{\left(P_p + AB\right)^2 - 4AP_p}\right]\right\} \quad \text{when } E > 1$$

(4.30b)

It should be noted that both equations (4.30a) & (4.30b) are also applicable in limiting cases. The first case is that when $P_p \rightarrow 0$, the flux equations reduced to: $J_i^* = K_i \gamma_i x_i$ or $J_i^* = K_i \Theta_i f_i$ which is defined as an absolute flux. The second case is that when $P_p \rightarrow f_{total}$

$(= f_i + f_j)$, i.e. $Py_i \rightarrow f_i$ and $Py_j \rightarrow f_j$, equation (4.30a) & (4.30b) will be reduced to zero. Hence, the explicit solution above is applicable for permeate pressures which fall in the range of $0 \leq P_p \leq f_i + f_j$.

4.6.3 Determination of separation factor

Although a relationship of separation factor with driving force was derived, i.e. equation (4.14), it could not be determined explicitly. Knowing that $\alpha_{PV}^* = \alpha_{VLE} \varepsilon_{bl} E_{mem}^*$ and

$$f_i = \frac{p_{f,i}}{\Theta_i} \quad \& \quad f_j = \frac{p_{f,j}}{\Theta_j},$$ for a binary mixture, equation (4.14) can be rewritten as:

$$\alpha_{PV} = \alpha_{PV}^* \frac{1 - P_p y_i / f_i}{1 - P_p (1 - y_i) / f_j} \tag{4.31}$$

Recalling equation (4.6), for a binary mixture; the permeate composition can be expressed in terms of α_{PV} and $x_{b,i}$ as follow:

$$y_i = \frac{\alpha_{PV} x_{b,i}}{(\alpha_{PV} - 1) x_{b,i} + 1} \tag{4.6}$$

By combining equation (4.3) and (4.6), y_i can be eliminated and a quadratic equation is formed (a detail derivation is shown in appendix A1):

$$\alpha_{PV}^2 - \left\{ \alpha_{PV}^* + \left[(1 - E) \cdot (P_p / f_j) - 1 \right] \cdot (1/\pi_f) \right\} \cdot \alpha_{PV} - \alpha_{PV}^* / \pi_f = 0 \tag{4.32}$$

Where $\pi_f = \dfrac{x_{b,i}}{1 - x_{b,i}}$

Since there is only one unique solution for $\alpha_{PV} > 0$, separation factor for a pervaporation system with $E > 0$ can be obtained explicitly as follow:

128

$$\alpha_{PV} = \frac{\alpha_{PV}^*}{2} \left\langle 1 + \frac{1}{\pi_f \alpha_{PV}^*} \left[(1-E) \cdot \frac{P_p}{f_j} - 1 \right] \right.$$

$$\left. + \left\{ \left\{ 1 + \frac{1}{\pi_f \alpha_{PV}^*} \left[(1-E) \cdot \frac{P_p}{f_j} - 1 \right] \right\}^2 + \frac{4}{\pi_f \alpha_{PV}^*} \right\}^{0.5} \right\rangle \qquad (4.33)$$

It is interesting to note that in both limiting cases, i.e. (i) $P_p = 0$ and (ii) $E=1$, the separation factor for both cases are independent of permeate pressure and both equal to α_{PV}^*. However,

for system with $E=1$, the separation factor has a value of $\alpha_{PV}^* = \alpha_{VLE} \dfrac{\Theta_j}{\Theta_i}$.

4.6.4 Significance of dimensionless group, E, and pseudo-feed partial pressures, f_i & f_j

It has found that the dimensionless number E and the pseudo-feed partial pressures, f_i & f_j, are significant in determining separation performance, particularly the range of E. In mathematical terms, E is defined as the product of the enhancement factor at ultimate vacuum ($E^* = K_i/K_j$) and the ratio of partition coefficient ratios, Θ_i/Θ_j, or expressed in terms of module effectiveness and intrinsic enhancement factor as follow:

$$E = \frac{K_i \Theta_i}{K_j \Theta_j} = \varepsilon_{bl} E_{mem}^* \frac{\Theta_i}{\Theta_j} \qquad (4.34)$$

It should be noted that there is an indirect influence of feed composition upon E due to the influence of the feed concentration has upon the membrane properties. However, in organophilic pervaporation, such an influence is a second order effect.

The partition coefficient ratios in equation (4.34) can also be identified as:

$$\Theta_i/\Theta_j = \frac{\left(S_i^d / S_i^f \right)}{\left(S_j^d / S_j^f \right)} = \frac{\left(S_i^d / S_j^d \right)}{\left(S_i^f / S_j^f \right)}$$

$$= \frac{\text{Ratio of partition coefficients on the downstrean side}}{\text{Ratio of partition coefficients on the upstream side}} \qquad (4.35)$$

To a first approximation only, the Θ terms can be taken to be unity. The terms f_i and f_j are considered to be pseudo feed-side vapour pressures and are dependent on feed composition, temperature and the ratio of the partition coefficients. If the partition coefficient ratios Θ_i/Θ_j = 1, E can then be equated to E^* (= K_i / K_j). In this case, E can be expressed in terms of transport resistances:

$$E = \frac{R_{top,j} + R_{sup,j}}{R_{bl} + R_{top,i} + R_{sup,i}}, \text{ for } \Theta_i/\Theta_j = 1. \qquad (4.36)$$

For pervaporation systems with Θ_i/Θ_j = 1 and $E < 1$, this equation implies that the total transport resistance for the solute is much larger than the transport resistance for solvent. This is because of the significantly high liquid boundary layer resistance. If the selective layer of the membrane is very thin, the overall transport will be controlled by feed side resistance and such dominance may well give a larger resistance for solute transport than the transport resistance of the solvent despite the membrane being solute selective. This is usually the case in the removal of highly volatile organics from an aqueous stream.

For $E > 1$ with Θ_i/Θ_j = 1, the overall transport resistance for solute is less than the resistance for solvent. If $E \gg 1$, the membrane has a very high resistance towards solvent.

If $\Theta_i/\Theta_j \neq 1$, a new expression for E can be obtained by combination of the absolute fluxes and the pseudo feed-side vapour pressures:

$$E = \frac{J_i^*}{f_i} \bigg/ \frac{J_j^*}{f_j} \qquad (4.37)$$

If a relative flux of a component i is defined as the absolute flux of a component i per unit of pseudo-partial pressure driving force at $P_p = 0$, i.e. J_i^*/f_i , E can then be seen as the ratio of

the relative flux of solute to the solvent. Hence, $E < 1$ can be interpreted as $\dfrac{J_i^\bullet}{f_i} < \dfrac{J_j^\bullet}{f_j}$, i.e. the

relative flux of the solute is less than the one of solvent, and vice versa for $E > 1$.

4.7 Performance Behaviour in Response to Elevated Permeate Pressure

Having obtained the equations that enables one to determine performance parameters for known feed conditions, module effectiveness and membrane properties, the response of these performance parameters towards permeate pressure can now be investigated. In order to obtain a more generalised analysis, no specific feed conditions, test components or membrane or module are used to initialise the analysis. However, the framework that is used in the present study will be restricted to organophilic pervaporation with dilute feed concentration. A set of dimensionless numbers will be derived to determine the response profile of the performance towards permeate pressure. By performing calculus analysis upon the performance parameters, i.e. y_i, α_{PV}, J_i and J_j, the effect of permeate pressure can be investigated and an useful dimensionless number derived.

4.7.1 Calculus analysis upon performance behaviour in response to elevated permeate pressure
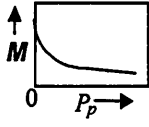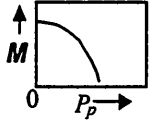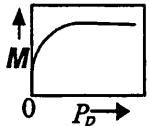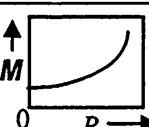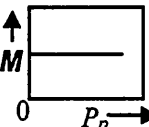
Before calculus analysis is performed upon the performance functions, several assumptions need to be made:

- Organophilic pervaporation of binary mixture with low feed concentration.

- The mass transport can be predicted by equation (3.143): $J_i = K_i \left(p_{f,i} - \Theta_i p_{p,i} \right)$

- Feed conditions like feed concentration and temperature are assumed to be constant throughout the elevation of permeate pressure. Hence, the overall mass transfer coefficients, feed side partial pressure and module effectiveness are considered constant.

- The desorption coefficient is independent of permeate pressure. Thus the desorption factor, Θ_i, can be considered to be constant.

With the above assumptions, the performance parameter equations (4.21), (4.29), (4.30a,b) & (4.33) are reduced to single variable functions. In this case, all the performance parameters are solely a function of permeate pressure, i.e. $y_i = y_i(P_p)$, $J_i = J_i$ (P_p) and $\alpha_{PV} = \alpha_{PV} (P_p)$. Hence, first and second order ordinary differential equations can be derived for the determination of function behaviour. If that performance parameter

function can be represented by $M = M\left(P_p\right)$, the first order derivatives of the performance parameter, i.e. $\dfrac{dM}{dP_p} = M'\left(P_p\right)$, gives information about its gradient. If $M'\left(P_p\right) > 0$, it indicates that the function is increasing as P_p increases while $M'\left(P_p\right) < 0$ indicates a decreasing function. For a function that has a positive second derivative, i.e. $M''\left(P_p\right) > 0$, a concave shape of profile is observed. A summary of the calculus analysis is shown in Table 4.2.

Table 4.2 Summary of calculus analysis upon function M.

$M'\left(P_p\right)$	$M''\left(P_p\right)$	Type of function	Shape of profile function
< 0	> 0	Decreasing	
	< 0		
> 0	> 0	Increasing	
	< 0		
= 0	= 0	Independent of P_p	

Details of the derivation of the performance derivatives are shown appendix A1. In order to derive useful dimensionless numbers, the first and second order derivatives of performance parameters at $P_p = 0$ are evaluated. The advantage is that the dimensionless numbers that are derived would be permeate pressure independent and the result of analysis would be the same as the one in Table 4.2. The calculus analysis upon performance parameters have been obtained and are shown in appendix A1. Such results are translated graphically as shown in Table 4.3 and discussed in the next section.

Table 4.3: System Classification and the performance profiles as a function of permeate pressure

$E=\dfrac{K_i\Theta_i}{K_j\Theta_j}$	y_i^*	Type of system	Performance profiles with evolution of downstream pressure, P_p.		
			y_i	J_i & J_j	α_{PV}
$E>1$	<0.5	**Type A** $\dfrac{J_i^*}{f_i} > \dfrac{J_j^*}{f_j}$ $J_i^* < J_j^*$	y_i vs P_p (decreasing)	J_i vs P_p (decreasing)	α_{PV} vs P_p (decreasing)
	>0.5	**Type B** $\dfrac{J_i^*}{f_i} > \dfrac{J_j^*}{f_j}$ $J_i^* > J_j^*$	y_i vs P_p (decreasing)	J_j vs P_p (decreasing)	
$E<1$	<0.5	**Type C** $\dfrac{J_i^*}{f_i} < \dfrac{J_j^*}{f_j}$ $J_i^* < J_j^*$	y_i vs P_p (increasing)	J_i vs P_p (decreasing)	α_{PV} vs P_p (increasing)
	>0.5	**Type D** $\dfrac{J_i^*}{f_i} < \dfrac{J_j^*}{f_j}$ $J_i^* > J_j^*$	y_i vs P_p (increasing)	J_j vs P_p (decreasing)	

4.7.2 Classification of performance behaviour in response to elevated permeate pressure

It can be seen that there are four types of behaviour. For the sake of classification and interpretation of physical significance, a useful distinction between normalised partial fluxes and absolute flux is made.

Absolute flux i with $P_p = 0$:

an absolute flux of a component i was defined as the partial flux of i at $P_p = 0$, i.e. $J_i^* = K_i p_{f,i}$

Relative flux i :

a normalised flux of a component i was defined as the absolute flux for i per unit of pseudo-partial pressure driving force at $P_p = 0$, i.e. J_i^* / f_i.

Type A: The normalised flux of component i at $P_p = 0$ is greater than the normalised flux of component j but the absolute flux of component i is less than that of component j. The system exhibits a sharp decrease in permeate concentration as permeate pressure increases from absolute vacuum.
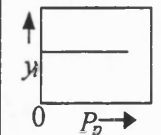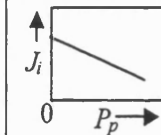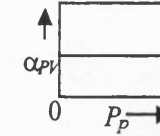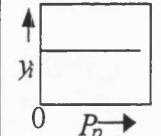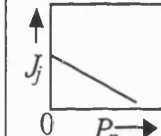
Type B: The normalised flux of component i at $P_p = 0$ is greater than the normalised flux of component j. Also, the absolute flux of i is greater than that of component j. The system exhibits an increasingly steeper slope of decrease in permeate concentration as permeate pressure increases from absolute vacuum.

Type C: The normalised flux of component i at $P_p = 0$ is smaller than the normalised flux of component j and at the same time, the absolute flux of i is less than that of component j. Such a pervaporative system is unattractive for recovery of i from j.

Type D: The normalised flux of component i at $P_p = 0$ is smaller than the normalised flux of component j but the absolute flux of i is greater than that of component j. The system exhibits increases in permeate concentration as permeate pressure increases.

It is interesting to note that for pervaporation systems with $E = 1$, all the performance parameters are independent of permeate pressure except that the partial flux linearly decreases as the permeate pressure increases. A graphical illustration of performance with respect to permeate pressure is shown in Table 4.4.

Table 4.4 Performance Behaviour of Pervaporation System with $E = 1$

Thus, from the results of the calculus analysis, a performance behaviour classification plane can be formed as shown as Fig. 4.9. By determining E and y_i^*, the type of behaviour can be known. In powder technology, the Geldart classification plane provides information on powder behaviour in response to gas velocity. However, in the present study, the classification plane is simple and provides information of the performance behaviour in response to permeate pressure.
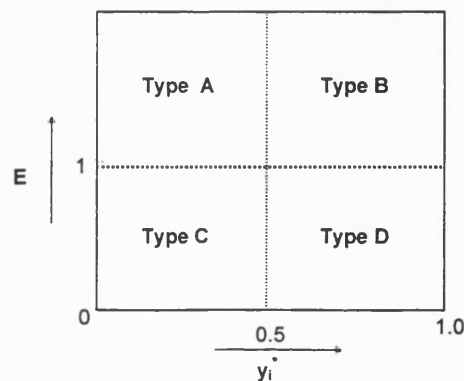
Fig. 4.9. E and y_i^* classification diagram

4.8 The Effect of E upon the Separation Factor Gradient $\dfrac{d\alpha_{PV}}{dP_p}$

In the earlier section of analysis, an overall picture of the effect of permeate pressure upon separation factor was analysed by its gradient. From the derivative function of separation factor in appendix A1, it is possible to analyse the sensitivity of this gradient function by performing calculus analysis upon this gradient with respect to E. Hence, the first and second order derivative function of the gradient $\dfrac{d\alpha_{PV}}{dP_p}$ and $\left(\dfrac{d\alpha_{PV}}{dP_p}\right)_{P_p=0}$ with respect to E can be obtained. From the derivation of gradient function shown in appendix A1:

$$\frac{d}{dE}\left[\left(\frac{d\alpha_{PV}}{dP_p}\right)_{P_p=0}\right] = -\left[\frac{x_{b,j}\,y_i^{\bullet}}{x_{b,i}f_j}\cdot\frac{\left(f_i/f_j+1\right)}{\left(E+f_i/f_j\right)^2}\right] \tag{4.38}$$

$$\frac{d^2}{dE^2}\left[\left(\frac{d\alpha_{PV}}{dP_p}\right)_{P_p=0}\right] = \frac{2x_{b,j}\,y_i^{\bullet}}{x_{b,i}f_j}\cdot\frac{\left(f_i/f_j+1\right)}{\left(E+f_i/f_j\right)^3} \tag{4.39}$$

Hence the profile of the gradient function of separation factor with respect to E can be translated graphically as shown in Fig. 4.10. As noted earlier in Table 4.4 and in Fig 4.10, if $E = 1$, the selectivity will be independent of pressure change. This situation is convenient from a control point view. The separation factor **gradient** decreases as the magnitude of E increases and vice versa. From Fig. 4.10, as E get larger, separation factor **gradient** will tends to a stable value. As seen below a large magnitude of E corresponds to conditions that generate a large separation due to a large membrane enhancement factor.
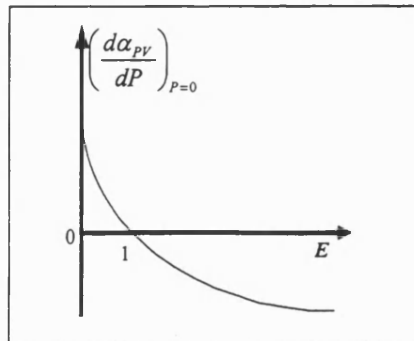
Fig. 4.10 The effect of E upon separation factor gradient

4.9 Estimating the Optimum Range of Operating Permeate Pressure

It is of industrial interest to estimate the optimum range of operating permeate pressure. From the performance behaviour analysis, $E > 1$, the separation factor increases as permeate pressure increases while for $E < 1$, an opposite behaviour is observed.

Whether $E < 1$ or >1, provided $E \neq 1$, one can link a given ξ fraction loss of organic flux against the maximum organic flux with the separation factor. By arranging equation (4.30a) & (4.30b), ξ fraction loss of organic flux can be evaluated as follow:

$$\xi = 1 - \frac{J_i}{J_i^*} = \frac{1}{2f_i}\left[(P_p + AB) \pm \sqrt{(P_p + AB)^2 - 4AP_p}\right] \quad \text{for } E < 1 \text{ and } E > 1 \quad (4.40a)$$

where:

Where: $A = \dfrac{f_i E}{(E-1)}$ $\qquad\qquad\qquad\qquad\qquad\qquad$ (4.25)

$$B = 1 + \frac{1}{E}\left(\frac{f_j}{f_i}\right) = \frac{1}{y_i^*} \qquad\qquad\qquad\qquad (4.26)$$

$$E = \frac{K_i \Theta_i}{K_j \Theta_j} \qquad\qquad\qquad\qquad\qquad\qquad (4.19)$$

and $f_i = \dfrac{p_{f,i}}{\Theta_i}$ and $f_j = \dfrac{p_{f,j}}{\Theta_j}$, pseudo-feed partial pressures. $\qquad$ (4.20a) & (4.20b)

Hence, if an allowance of ξ fraction loss of organic flux is known, the solution for the lower bound of the optimum permeate pressure operating range $P_{p,1}$ can be solved from equation (4.40a) and yields:

$$P_{p,1} = \frac{f_i \xi (f_i \xi - AB)}{f_i \xi - A} \qquad \text{for} \qquad E < 1 \text{ and } E > 1 \qquad (4.40b)$$

If the allowance of ξ fraction loss of organic flux is not known, a crude approximation is necessary. However, in the present study, a simple and useful approximation of the optimum permeate pressure range will be developed for organophilic pervaporation system with $E < 1$ and $E > 1$.

4.9.1 Approximation of optimum operating permeate pressure range for pervaporation system with $E < 1$

The performance behaviour for organophilic pervaporation system with $E < 1$ is shown in Table 4.3. For to the analysis obtain in the previous section, for system with $E < 1$, the separation factor increases as permeate pressure increases. However, the organic flux is relatively constant over the a range of permeate pressure while the water flux decreases relatively quicker than the organic flux. Assume that the ratio $\alpha_{PV}/\alpha_{PV}^{*}$ and J_i/J_i^{*} versus $P_p/(f_i + f_j)$ can be approximated as a quartile circular curve with radius R as shown in Fig. 4.10. It is interesting to note that in a pervaporation system with $E < 1$, the loss of organic flux is compensated by the gain in separation factor as the permeate pressure increases. Assume that the loss of flux and gain in separation performance is fully compensated at the curve evolution equal to $\pi/4$ radian or $45°$ from the y-axis. Hence, the optimum permeate pressure range can be estimated.
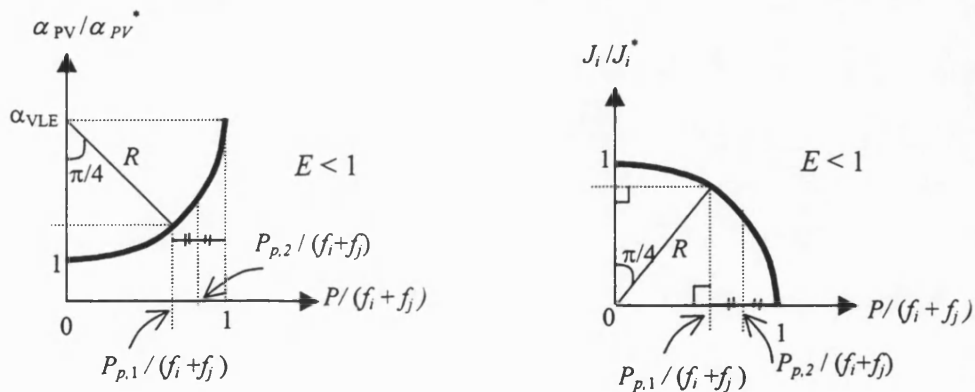
Fig. 4.11 Optimum Permeate Pressure Range Determination for System with $E < 1$

From Fig. 4.11, with the use of simple geometry, the optimum permeate pressure range can be approximated as follow for pervaporation with $E < 1$:

Lower bound: $P_{p,1} = (f_i + f_j)\dfrac{\sqrt{2}}{2}$ $\qquad\qquad$ (4.41)

Upper bound: $P_{p,2} = P_{p,1} + 0.5(f_i + f_j - P_{p,1}) = \dfrac{2+\sqrt{2}}{4}(f_i + f_j)$ $\qquad$ (4.42)

For first approximation, $\Theta_i = \Theta_j = 1$, hence, $f_i = p_{f,i}$ and $f_j = p_{f,j}$. It is interesting to note that the approximation is solely dependent on the feed-side partial pressures and in the range of $0.71(f_i + f_j)$ to $0.85(f_i + f_j)$.

4.9.2 Approximation of optimum operating permeate pressure range for pervaporation system with $E > 1$

For pervaporation system with $E > 1$, separation factor decreases as permeate pressure increases and partial fluxes decrease sharply as permeate pressure decreases from $P_p = 0$. Unlike the system with $E < 1$, the decrease of organic flux is accompanied by the sharp decrease of separation factor as the permeate pressure increases. Hence, the best separation performance and flux for this kind of system is when the permeate pressure is at ultimate vaccum, $P_p = 0$. According to the engineering analysis for system with $E > 1$, particularly high boilers system, its separation performance and organic flux are very sensitive to permeate pressure. A dramatic deterioration of performance may occur as permeate pressure exceeds the organic partial vapour pressure (Boddekker and Bengston, 1990; Bennett, 1994). Since flux of i, is proportional to $f_i - P_p y_i$, the upper limit for P_p will be around f_i. Thus, the optimum permeate pressure range can be approximated as follow for pervaporation with $E > 1$:

Lower bound: $P_{p,1} = 0$ for $E > 1$ (4.43)

Upper bound: $P_{p,2} = f_i$ for $E > 1$ (4.44)

Despite P_p close to zero is desirable, the optimum within the range of $0 - f_i$ will depend upon the cost of the vacuum system.

4.9.3 Optimum operating permeate pressure estimation based on literature data

In order to show the applicability of the optimum permeate pressure range approximation, literature data from Baker et al (1997) and Bennett (1994) were used to test out the validity of equation (4.41) to (4.44).

TCE/water separation (Baker et al, 1997)

From the study of organophilic pervaporation of TCE/water separation by Baker et al (1997), the flux and separation performance through the 10μm silicone rubber membrane modules at 50°C with respect to permeate pressure was investigated. For their experimental conditions, a 100ppm TCE feed solution has a total vapour pressure of 111mmHg (92mmHg water, 19mmHg TCE), hence, the permeate pressure is a significant fraction of the feed pressure. According to their study, α_{PV} was found to be less than α_{VLE}

(i.e. $E' < 1$). It implies the pervaporation system has the characteristic of class C or D (i.e. $E < 1$). Assume that Θ_i and Θ_j are unity and thus the optimum operating permeate pressure range is estimated by using equation (4.41) to (4.42) as follow:

Upper bound: $P_{p,1} = (111mmHg) \times \dfrac{\sqrt{2}}{2} = \underline{78.5mmHg}$

Lower bound: $P_{p,2} = 78.5mmHg + 0.5 \times (111mmHg - 78.5\ mmHg) = \underline{94.8mmHg}$
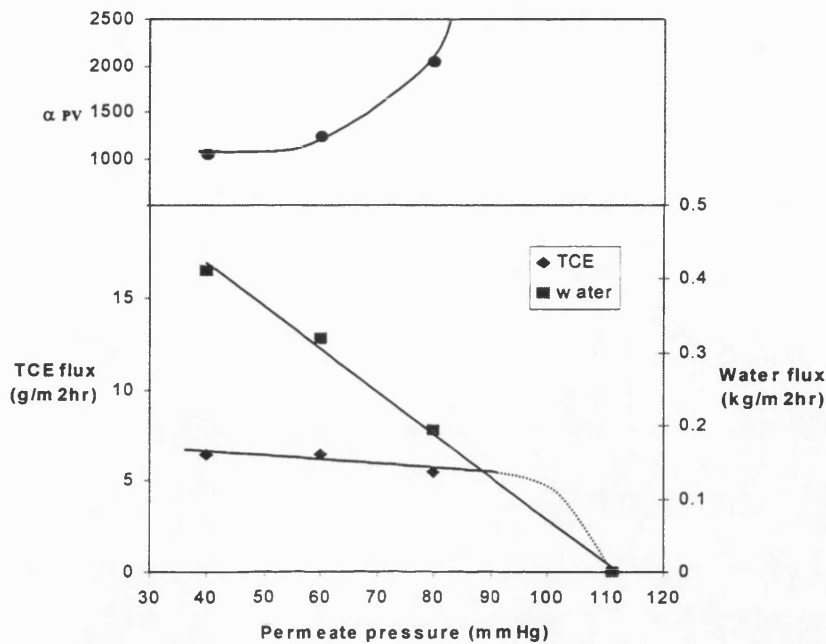
Fig. 4.12 TCE/water separation performance in various permeate pressure
(100ppm TCE feed solution at 50°C) based on Baker et al (1997)

From the experiments data shown in Fig 4.12, Baker et al (1997) had actually found that the optimum permeate pressure range for this pervaporation system fell in the range of 80mmHg < P_p < 100mmHg. This is within the predicted result.

Phenol/water separation (Bennett, 1994)

From the study of Bennett (1994) on phenol/water separation via pervaporation, an acetate functionalised PDMS was used. A 5wt% of phenol feed solution was used at 70°C and separation performance was studied. The partial vapour pressure of phenol in the feed was about 2.24mbar and the enhancement factor was found to be greater than 1. Hence, the system behaviour is likely to be that of class A or B and from equation (4.43) to (4.44), the optimum operating permeate pressure range can now be determined as follows:

Upper bound: $P_{p,1} = \underline{0 \text{ mbar}}$

Lower bound: $P_{p,2} = \underline{2.24\text{mbar}}$
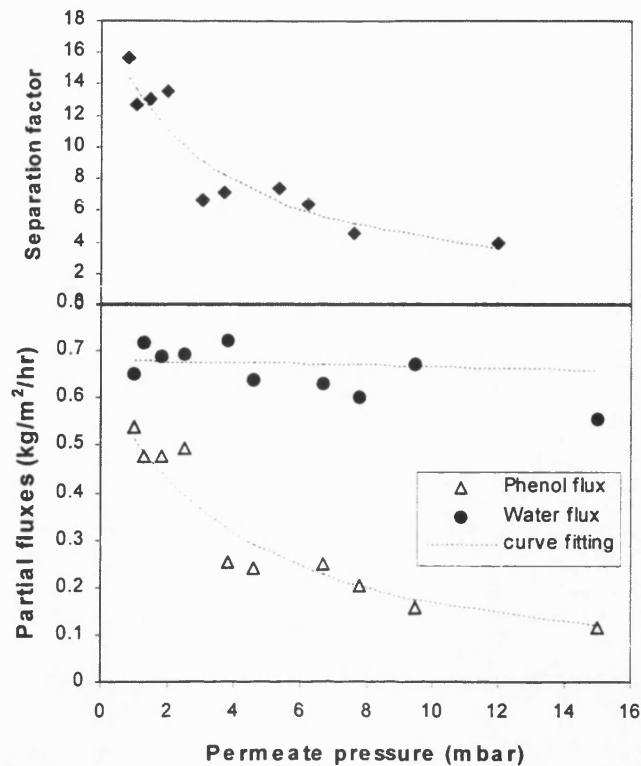
Fig. 4.13 Phenol/water separation performance in various permeate pressure (5wt% phenol feed solution at 70°C) based on Bennett (1994)

From Fig. 4.13, Bennett (1994) actually confirmed that the optimum operating range is actually within the range that is predicted by equation (4.43) to (4.44).

4.11 Chapter Conclusions

A useful transport model has been presented, model analysis has been done and a classification of pervaporation has been given. A mathematical treatment definition was introduced, namely, the enhancement factor, E', to account for the effect of the operating conditions, module design, membrane material and the composite nature of the membrane that are used in a pervaporation process. The enhancement factor, E', enables one to account for the enhancement achieved by the chosen pervaporation modules and operating conditions separate from the contribution of ordinary vapour-liquid equilibrium. For $E' > 1$, separation achieved by organophilic pervaporation is better than that by

vapour liquid equilibrium separation. For $E' < 1$, the separation achieved by organophilic pervaporation is less effective than that achieved by vapour-liquid equilibrium.

In order to model the effect of permeate pressure upon performance, a comprehensive permeation model that includes the mass transfer in (1) boundary layer, (2) membrane and (3) support layer was introduced. The model derived also accounts for the non-linearity of the partition coefficient by introducing a partition coefficient ratio Θ_i which is the ratio of the partition coefficient for the upstream interface to the one for the downstream side of the membrane.

With the derived transport model, a distinction can be made between intrinsic membrane properties (E_{mem}^*), effectiveness of the module (ε_{bl}) and the operating conditions. A comparison between pervaporation and gas permeation was presented. An explicit solution linking parameters that include permeate pressure, feed composition, feed side mass transfer and membrane permeability was obtained. This will enable engineers to use literature pervaporation data to calculate performance at different operating conditions.

By calculus analysis upon the derived transport model with respect to permeate pressure, its influence upon permeate composition, partial fluxes and the separation factor profile was investigated. This analysis has led to the classification of pervaporation system behaviour that is similar to Geldart's classification of powder behaviour in a fluidisation system. A classification plane with y_i^* (permeate concentration obtained at ultimate vacuum) as its x-axis and E (the product of the ratio of overall mass transfer coefficients and the ratio of partition coefficient ratios) as its y-axis was presented.

According to the earlier analysis, A, B, C and D type of pervaporation system was derived. Type A is the pervaporation system in which its separation performance is very pressure sensitive while type D is less pressure sensitive. For types C & D the separation factor increases as permeate pressure increases. It has been found that the most favorable system is type B which is not only less pressure sensitive than type A but has $E > 1$. A special case is a pervaporation system with $E = 1$, the separation performance parameter are found to be permeate pressure independent whist its partial fluxes decrease linearly with an increase of the permeate pressure. In order to estimate the optimum operating permeate pressure range, simple approximations were introduced for both systems with E <1 and $E >1$ solely based on partial vapour pressure of the components.

143

Chapter 5

Application of the Engineering Analysis:
Experimentation and Model Validation

5.1 Chapter Objectives

- Describe apparatus and experimentation for organophilic pervaporation.
- Develop methods to determine mass transfer coefficients and desorption ratio.
- Transport model validation and comparison with conventional model.
- Comparison of the experimental results and the predicted results using the engineering analysis developed in Chapter 4.
- Investigate the influence of membrane properties, module effectiveness, feed concentration and temperature upon the $E - y_i^*$ classification diagram.
- Develop general rules for displacement in the $E - y_i^*$ classification diagram caused by the above influences.

5.2 Introduction

In order to test out the applicability of the transport model and engineering analysis in Chapter 4, an experimental study of pervaporation performance for varied permeate pressure will be demonstrated in this chapter. It is the object of the present study to include as much literature data as possible to test out the applicability of the analysis and to show the advantage of comparing data with different conditions. Hence, literature data will also be used to confirm the predictability of the model and to investigate the effect of membrane properties, module effectiveness, feed concentration and temperature upon the $E - y_i^*$ behaviour classification plane.

144

5.3 Experimentation

In the present study, aqueous pyridine and aqueous methyl-isobutyl-ketone (MIBK) solutions were pervaporated through a commercial PDMS composite membrane. Both pyridine and MIBK are the target components to be recovered during the pervaporation process. These compounds are among the pollutants that are of concern to the environmental regulators.

5.3.1   Membrane

The commercial composite membrane used for organophilic pervaporation was supplied by GKSS Research Centre of Germany. The composite membrane consists of a 10μm selective layer made of PDMS, a 75μm of polysulfone porous support and as backing material a 200μm non-woven polyester. See Fig. 5.1.

Selective layer:
PDMS (10μm)

Porous support layer:
Polysulfone (75μm)

Non-woven
polyester (200μm)
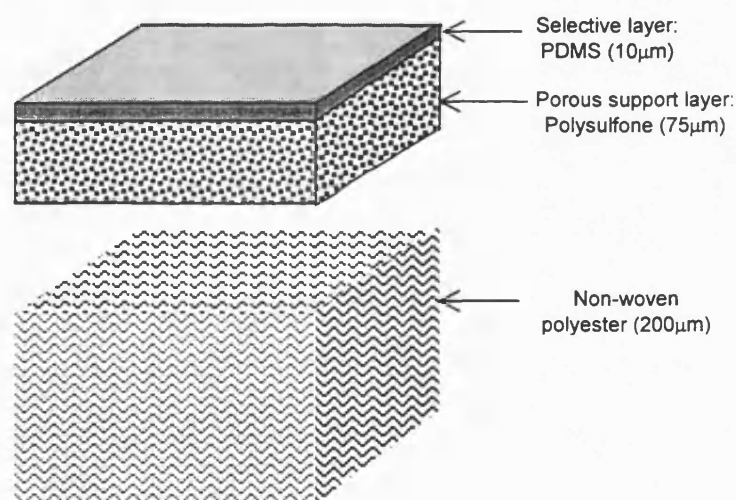
Fig 5.1 Schematic compositions of GKSS membrane

The pictures obtained from scanning electron microscope (SEM) as shown in Fig. 5.2 confirmed the physical dimensions given by GKSS.

(a) Horizontal cross section view

(b) Vertical cross section view

(c) Feed side of the membrane

(d) Permeate side of the membrane
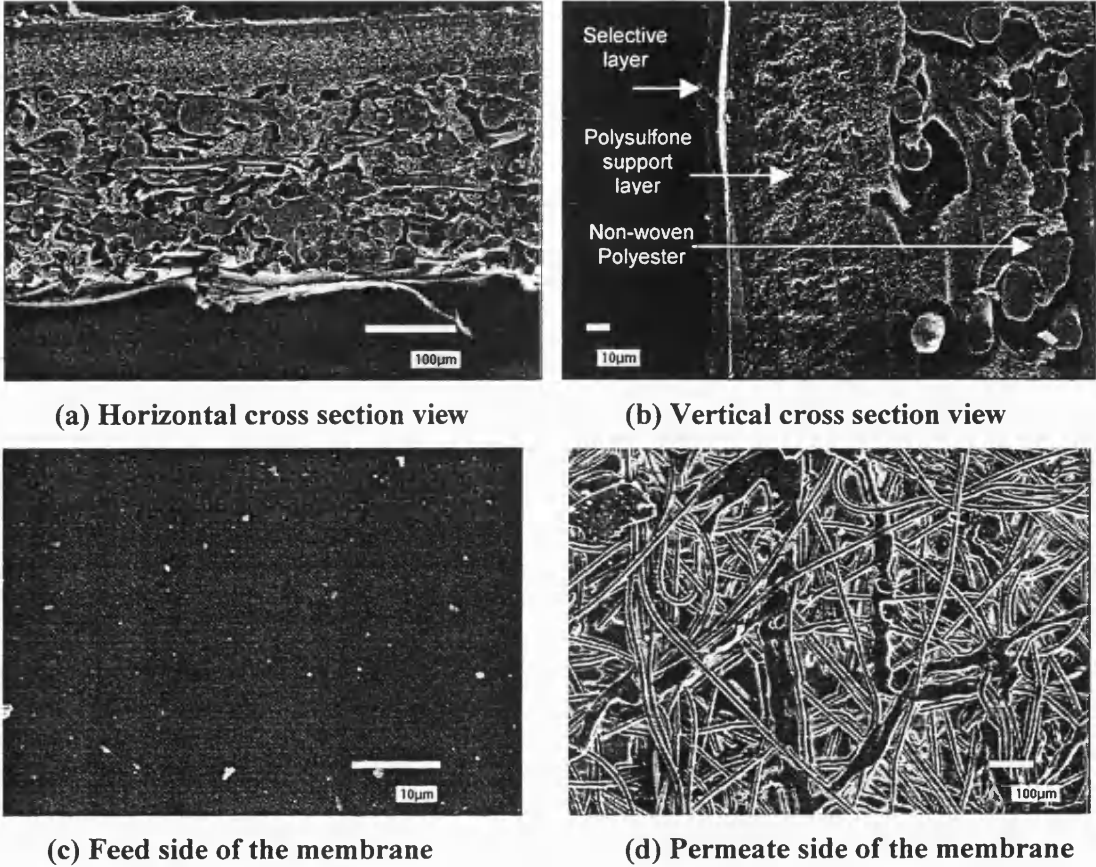
Fig. 5.2 Scanning electron microscope (SEM) pictures of GKSS membrane

5.3.2 Experimental Procedure

The pervaporation experiments were carried out within a standard, batch pervaporation test rig as shown in Fig 5.3. Details are given elsewhere (Ten et al, 1998).
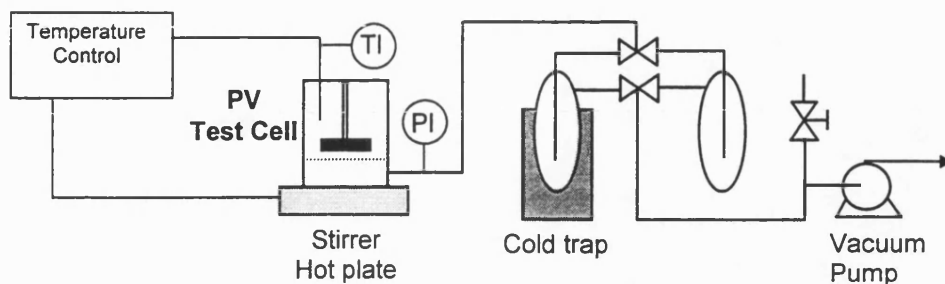
Fig 5.3 Schematic diagram for pervaporation test rig

A circular piece of membrane was cut and clamped into a sealed stainless steel test cell above a porous sintered metal support with a viton "o" ring arrangement forming a leak free seal. The cell was filled with the feed solution and placed upon a stirrer/hotplate, the solution being stirred by a magnetic follower at about 1000 rpm. A more detailed schematic diagram of the test cell is displayed in Fig. 5.4.

The cell temperature measured with a thermocouple, was controlled at 70°C by electronic temperature control system. A vacuum was pulled, by means of a vacuum pump, from the downstream side and the downstream pressure measured between the cell and cold traps. In order to carry out pervaporation tests at various downstream pressures, a sensitive manual controlled leak valve is used. It has been noted that the change of permeate pressure during the course of the experiment is negligible.

The permeate was condensed and frozen within one of the cold traps, which was cooled with liquid nitrogen.

147
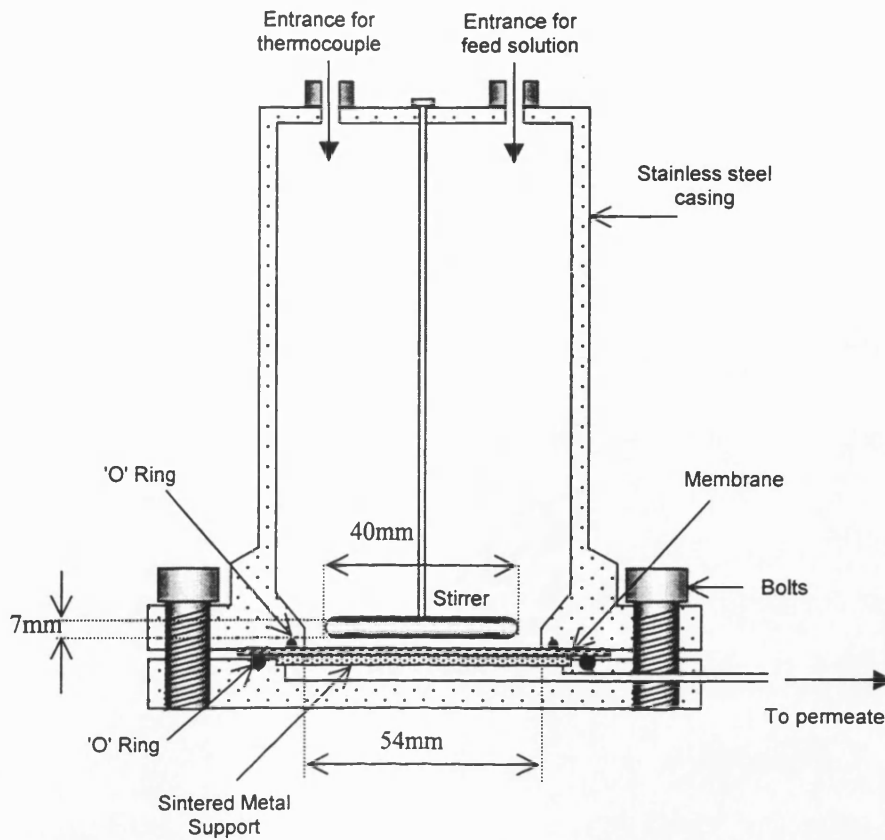
Fig. 5.4 Pervaporation Test Cell

Permeate was collected for a measured length of time, after which it was weighed and analysed for composition, in order to determine flux and separation factor as follows:

Partial flux:
$$J_i = \frac{W \times w_{p,i}}{A \times t_b \times M_i}, \text{kmol/m}^2 \cdot \text{h} \tag{5.1}$$

Separation factor:
$$\alpha_{PV} = \frac{w_{p,i}}{\left(1 - w_{p,i}\right)} \times \frac{\left(1 - w_{f,i}\right)}{w_{f,i}} \tag{5.2}$$

Where A is the effective contact area of the membrane (= 0.0029m^2)

M_i is the molar mass of the component, kmol/kg.

t_b is the batch time of the experiment, s

W is the total mass of the permeate, kg.

$w_{f,i}$ is the average mass fraction of target organic in the feed

$w_{p,i}$ is the mass fraction of the target organic in the permeate.

As experiments were carried out within a batch test rig, feed concentration was constantly changing throughout the duration of the experiment. For pyridine separation, the final concentration was found to be 95 - 98 % of its initial concentration. In the case of MIBK separation, the feed concentration dropped to 85 - 90 % of its initial concentration. Hence, the average mass fraction of target organic in the feed, $w_{f,i}$, can be taken as a simple average of initial and final feed mass fraction.

It should be noted that whenever a new piece of membrane disc is employed in the test rig, membrane conditioning is necessary before any reliable results can be taken. Usually, the first two experiments for each new membrane disc were disregarded. Subsequent experiments were repeated until consecutive sets of results were closely similar. Only very rarely did the results of the third and forth experiments differ by greater than 5 %.

Although many of the joints of the downstream circuit and cold trap are sealed with sealant, a minute air leak into the downstream system is inevitable. As downstream pressure is increased, more air will leak directly into the downstream system. Hence, some of the water vapour in the controlled air leak together will condense in the cold trap with the permeate from the test cell. The amount of the ingress of water vapour can be minimised by putting silica gel in the fume cupboard and stoppers on the entrances in the test cell. Leak test runs were also conducted for an empty test cell and water vapour leaks into the cold trap was found to be 0.1 - 0.95g/h in the range of 7mbar - 75mbar. In addition, the water vapour leak into the cold trap was found to be in linear relationship with the downstream pressure. So, in each experiment, the actual mass of water in the permeate due to pervaporation was obtained by the subtraction of the amount due to the water vapour leak for the corresponding permeate pressure from the measured mass of water in the cold trap.

5.3.3 Analytical procedure

The minor component of the permeate was always water. Maximum accuracy was obtained by analysing for water as opposed to the organic component. If the analysis is for the major component, a small percentage error in the determination of its concentration can lead to a large percentage error in the minor component concentration.

In the experiment, the permeate sample was taken and analysed for water concentration, using a Mettler D18 Karl Fischer Titrator and standard solvents. At room temperature, pyridine is totally miscible with water for all concentrations. Hence, the permeate was allowed to slowly warm to room temperature before a sample was injected directly into the Karl Fischer Titrator. The permeate typically consisted of nearly 50% w/w water. However, for MIBK separation from water, due to the low solubility of it in water, the permeate invariably contained two phases, a water saturated organic and organic saturated water phase. A measured quantity of 2-propanol, which is an excellent solvent for both water and organic components, was added to the permeate in order to form a single homogeneous liquid phase. Approximately 9 g of 2-propanol was added to a typical permeate mass of the order of 2 g. A sample was then taken and analysed for water concentration, using a Mettler D18 Karl Fischer Titrator and standard solvents. Each batch of 2-propanol was itself periodically analysed for water content, which was found to be of the order of 0.05% w/w. This was subtracted from the total mass of water calculated within the permeate / 2-propanol solution to give the total water content of the permeate. As MIBK is volatile, stoppers were placed at either ends of the permeate collection tubes immediately at the end of each experiment, in order to prevent mass loss.

5.4 Experimental Results and Model Validation

One of the objectives of the present study is to make a comparison between present results and the data found in literature. As most of the data from other laboratories and on gas separation have been presented with cmHg as the measuring unit for the vacuum, all data in the figures of this chapter are presented on this basis. Both saturated pressure of pure components and the activity coefficient were generated by using the Antoine equation and modified UNIFAC (Reid et al, 1987) respectively in order to obtain the feed partial pressure, $p_{f,i}$, and vapour-liquid equilibrium data that is required for calculation.

In addition, it is also the object of the present study to demonstrate the use of engineering analysis to predict the performance of pervaporation in respect of permeate pressure with a minimal amount of pervaporation experimental data and information. This is demonstrated in the following examples with minimum information for pyridine/water and MIBK/water pervaporation data. Relevant information is tabulated in Table 5.1

Table 5.1 Minimal pervaporation experimental data for pyridine/water and MIBK/water system at various feed concentration.

Pervaporation system Experimental Data and Information	Pyridine/water		MIBK/water	
Solute concentration in the feed (wt%)	5%	2.5%	0.50%	0.25%
Relative volatility, α_{VLE}	5.6	6.3	145.0	147.3
Feed solute partial pressure, $p_{f,i}$ (cmHg)	1.556	0.847	3.056	1.549
Feed solvent partial pressure, $p_{f,j}$ (cmHg)	23.062	23.203	23.318	23.328
Permeate pressure, P_p (cmHg)	0.375	0.526	0.375	0.375
Solute partial flux, $J_i \times 10^3$ (kmol/m^2/h)	7.456	3.404	0.460	0.233
Solvent partial flux, $J_j \times 10^3$ (kmol/m^2/h)	24.927	14.853	17.730	17.785
Separation factor, α_{PV}	25	39	29	29

Knowing that $y_i = J_i /(J_i + J_j)$, with the assumption of desorption factors being unity in value, i.e. $\Theta_i = \Theta_j = 1$, the mass transfer coefficient of solute and solvent can be approximated as:

Solute:
$$K_i = \frac{J_i}{p_{f,i} - P_p y_i} \qquad (5.3)$$

Solvent:
$$K_j = \frac{J_j}{p_{f,j} - P_p(1 - y_i)} \qquad (5.4)$$

With this knowledge of the mass transfer coefficients, the E-y_i^* co-ordinates, the types of performance behaviour and the optimum operating permeate pressure range can be determined via the application of engineering analysis of Chapter 4. The results are tabulated in Table 5.2

Table 5.2: Application of engineering analysis with minimal experimental data and information from Table 5.1

Pervaporation system	Pyridine/water		MIBK/water	
Solute concentration in the feed (wt%)	5%	2.5%	0.50%	0.25%
Approximated mass transfer coefficients				
$K_i \times 10^3$ (kmol/m^2/h/cmHg)	5.073	4.542	0.1509	0.151
$K_j \times 10^3$ (kmol/m^2/h/cmHg)	1.095	0.652	0.7725	0.775
Classification of performance behaviour with respect to permeate pressure on E-y_i^* plane				
E	4.63	6.96	0.20	0.19
y_i^*	0.238	0.203	0.025	0.013
Type of performance profile: (See Table 4.3 in Chapter 4)	A	A	C	C
Approximated optimum operating permeate pressure range				
Lower bound: $P_{p,1}$ (cmHg)	0	0	18.6	17.6
Upper bound: $P_{p,2}$ (cmHg)	1.566	0.847	22.5	21.2

From table 5.2, the performance profiles that are predicted are type A and type C for pervaporation of pyridine/water and MIBK/water system respectively. The expected performance profiles were shown in Table 4.3 in Chapter 4. These will be compared with experimental results shortly.

5.4.1 Method to evaluate mass transfer coefficient (K_i) and desorption factor (Θ_i) from the comprehensive transport model

The evaluation method used for the mass transfer coefficients of the above model i.e. equations (5.3) and (5.4) is potentially inadequate due to the assumption of unity for the value of the desorption factor. This crude assumption might lead to an over or under estimate of the performance with respect to permeate pressure.

In order to evaluate K_i and Θ_i from the comprehensive transport model derived from Chapter 4, it is necessary to plot the partial flux of component i, J_i, against the partial pressure of the component, Py_i. Thus, the overall mass transfer coefficient of component i, K_i is the ratio of the intercept to the partial pressure at the feed side. For the partition coefficient ratio, Θ_i, one takes the product of the feed side component partial pressure and the ratio of the slope to the intercept. The method to evaluate K_i and Θ_i is demonstrated in Fig. 5.5 and table 5.3 for 5wt% of aqueous pyridine feed. The quality of the linear regression is also shown.
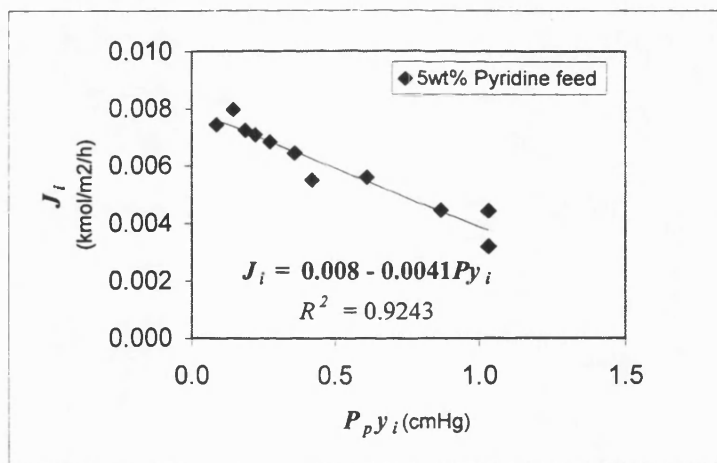
Fig 5.5 Linear regression plot of J_i vs. $P_p y_i$

Table 5.3 Results from linear regression on Fig. 5.4 and the determined parameters, i.e. mass transfer coefficient, K_i and desorption factor, Θ_i.

Gradient	Intercept	$p_{i,f}$ (cmHg)	$K_i \times 10^3$ kmol/m²/h/cmHg	Θ_i
-0.0041	0.008	1.5563	5.139	0.8

5.4.2 Experimental results and model validation

In the following section, the pervaporation experimental results of pyridine/water and MIBK/water separation will be presented. The calculated lines in the graphs are the performance predicted by the transport model using the value of K_i, K_j and Θ_i that were evaluated from the plots similar to Fig. 5.5.

5.4.2.1 Pyridine/water separation

For pyridine/water separation, 2.5wt% and 5wt% pyridine solutions were used in the pervaporation test cell. The pervaporation performance and its transport properties are shown in Fig 5.6 - 5.11.
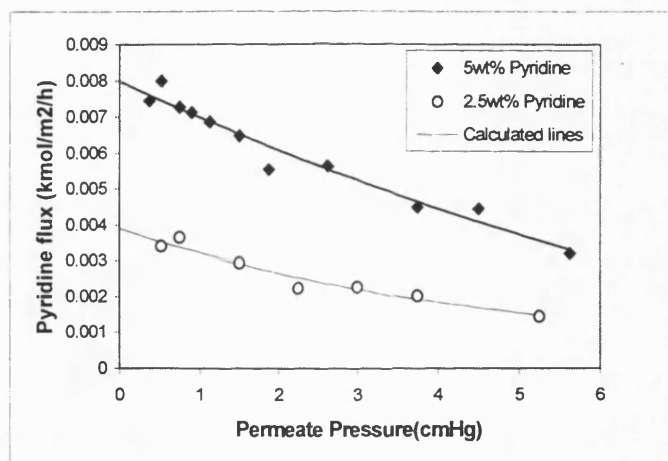
Fig 5.6 The effect of permeate pressure upon pyridine partial flux
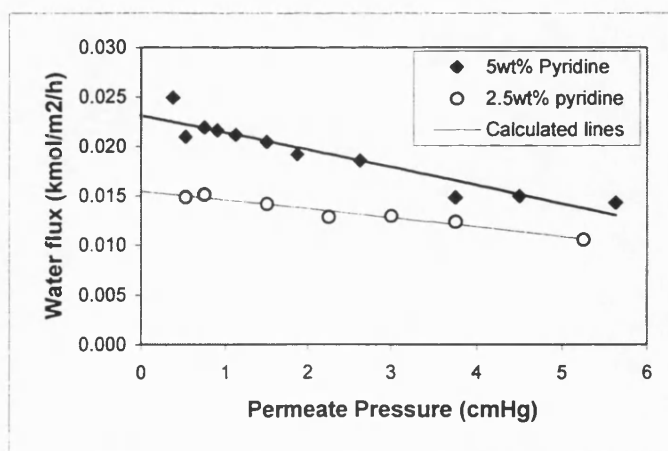
Fig 5.7 The effect of permeate pressure upon water flux
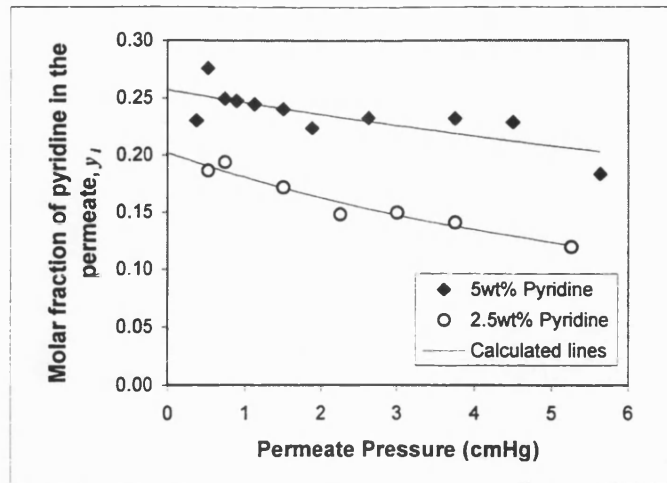
Fig 5.8 The effect of permeate pressure upon pyridine composition in the permeate
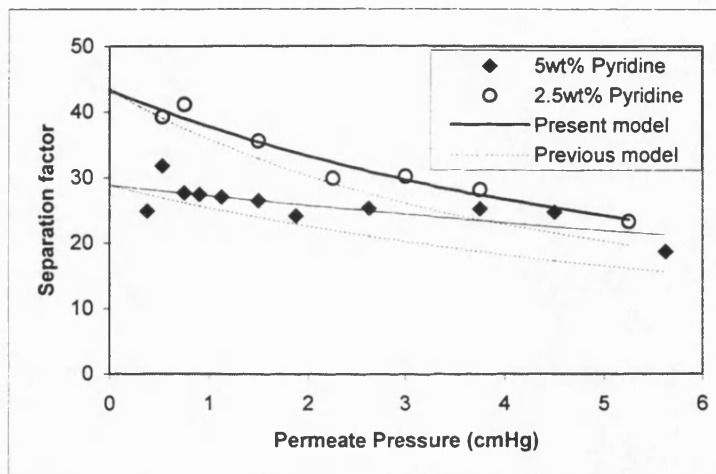
Fig.5.9 The effect of permeate pressure upon separation factor

From Fig. 5.6- 5.9, the performance profiles were found to correspond to the descriptions of type A as predicted in Table 5.2. As observed in Fig. 5.6 - 5.9, the suggestion that the optimum operating permeate pressure range is under 1.0cmHg is also found to be reasonable. The lines calculated using the transport model from the present study were found to be in agreement with the experimental results. In modeling the separation factor, the previous model suggested by Wijmans and Baker (1993) has underestimated the separation performance. This is shown in Fig. 5.9. The deviation is due to their implicit assumption that the desorption factor is equal to unity ($\Theta_i = \Theta_j = 1$). A comparison is shown in Fig 5.10.

155
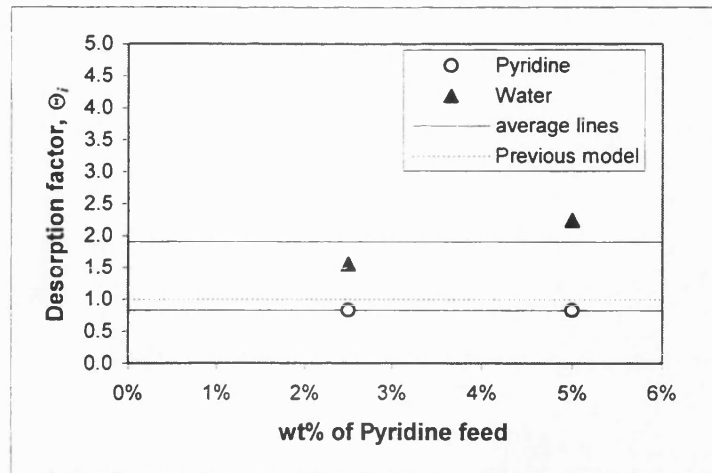
Fig. 5.10 Desorption factor vs. pyridine feed concentration at 70°C
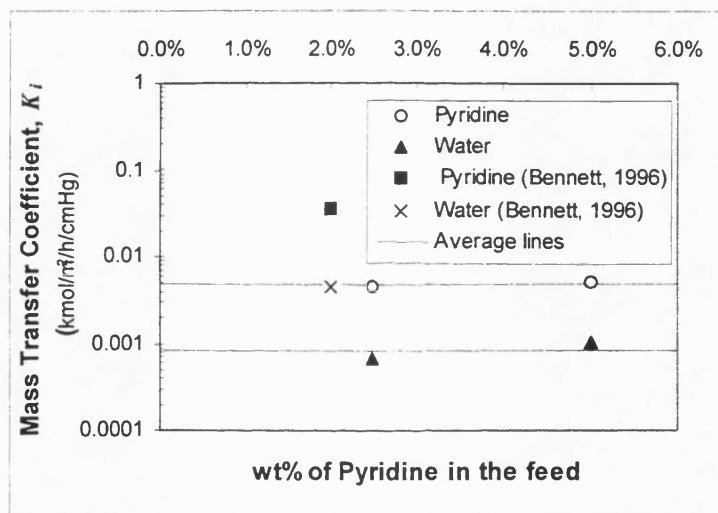
Fig. 5.11 Mass transfer coefficient vs. pyridine feed concentration at 70°C

The mass transfer coefficients determined shown in Fig. 5.11. The average mass transfer coefficients for pyridine (K_i) and water (K_j) were found to be 4.88×10^{-3} and 8.34×10^{-4} kmol/m^2/h/cmHg respectively. It is interesting to note that the values of K_i and K_j obtained from the present study via a PDMS-Polysulfone composite membrane are 5 to 7 times smaller than the one obtained with a homogeneous PDMS membrane (Bennett, 1996) which the thickness was normalized to 10μm. With the use of the Wilke-Chang correlation equation (3.2), the Sherwood correlation equation (3.8) and the resistance in series model in Chapter 3, the proportion of mass transfer resistance contributed by various layers in the composite

156

membrane was determined. Assuming that the permeability of the selective layer is the same as that of the PDMS used by Bennett (1996), the results are as shown in Fig.5.12. From Fig. 5.12, the boundary layer resistance under 1000rpm of turbulent agitation was found to be negligible compared to the resistance due to the membrane itself and particularly the resistance of the support layer which contribute 85% of the total resistance. Such a dominance of the support layer resistance is probably due to the fact that it has a thickness of 7.5 times that of the selective layer *and* the intrusion of selective material into pores. Although the support structure is hydrophilic in nature (Polysulfone), the mass transfer resistance in the support layer for pyridine was found to be smaller than the one for water. Due to the complex nature of the support layer, the reason behind this result has not been fully determined in the present study.
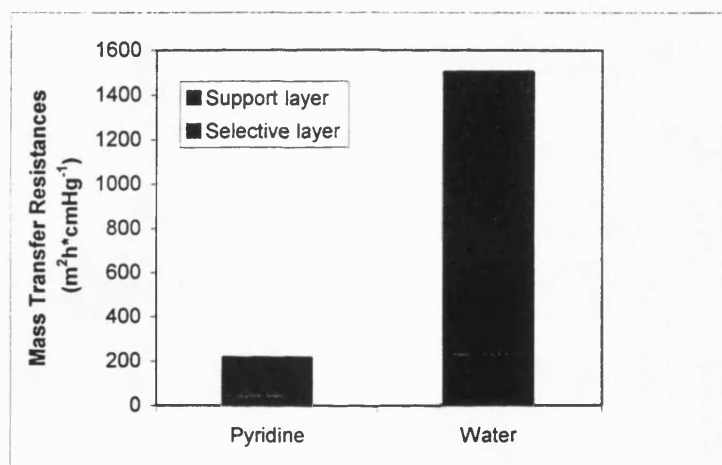
Fig. 5.12 Estimated mass transfer resistance of a composite membrane for pyridine/water separation at 70°C. (Boundary layer resistance is negligibly small)

In the present study, the ultimate enhancement factor of pyridine/water separation was found to be greater than unity and the separation factor achieved via pervaporation is 5 to 7 times higher than the one achieved by simple vapour-liquid equilibrium. From Fig. 5.13, the value of E^* evaluated from mass transfer coefficient data of Bennett (1996) was relatively higher than the one achieved by the commercial membrane used in the present study. This is probably due to the high contribution of the support layer resistance as shown in Fig. 5.12.
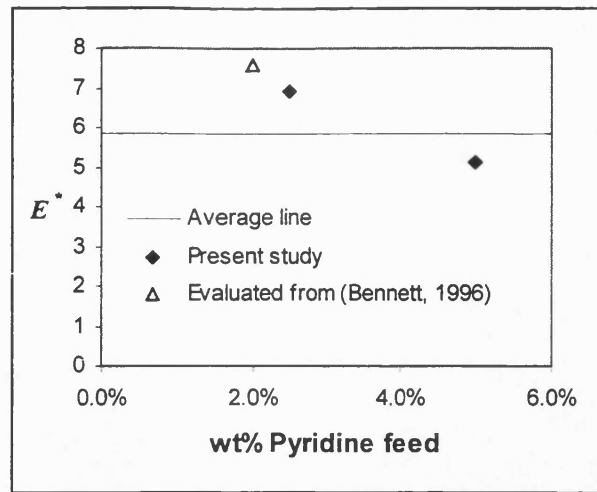
Fig. 5.13 Ultimate enhancement factor, E^*, vs. pyridine feed concentration at 70°C

According to the engineering analysis performed in Chapter 4, the dimensionless numbers, E and y_i^* can be used to predict the profile of the separation behaviour in response to permeate pressure. Even with one experimental data, with the assumption of desorption factor equal to unity, one could evaluate the ideal mass transfer coefficients as in equations (5.3)-(5.4) and subsequently E and y_i^* can be estimated. By using the mass transfer coefficients provided by Bennett (1996) for a homogeneous membrane which was normalized to 10μm, the performance behaviour in response to permeate pressure for a pyridine-water-PDMS system was determined and found to be a type A system(see Fig. 5.14). A more precise determination of co-ordinates of $E-y_i^*$ plane with the inclusion of desoprtion factor again confirmed the system as type A. The performance behaviour in response to the changes in permeate pressure is less than that obtained with a homogeneous PDMS membrane. It is interesting to note that the co-ordinates on the plane are shifted as the feed concentration increases as shown in Fig. 5.14.
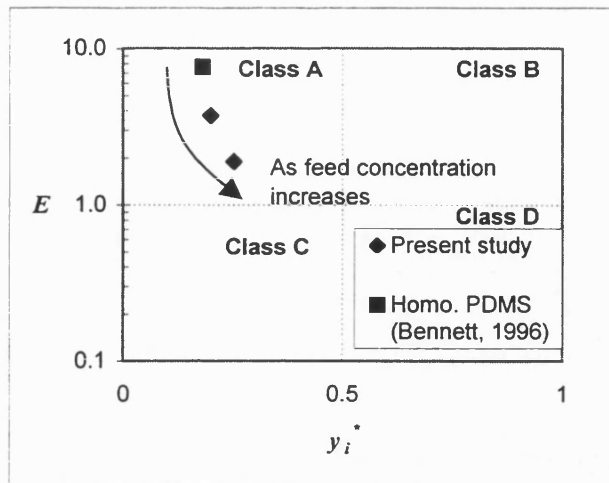
Fig. 5.14 Classification of performance behaviour in response to permeate pressure on E - y_i^* plane

5.4.2.2 MIBK/water separation

For MIBK/water separation, 0.25wt% and 0.5wt% MIBK solutions were fed into the test cell and pervaporation performance in response to permeate pressure are shown in Fig. 5.15 - 18. From Fig. 5.15 - 5.18, the lines calculated from the transport model were found to be in agreement with the experimental data. The performance profile in response to permeate pressure from Fig. 5.15 - 5.18 were found to correspond to type C, which was the prediction made in Table 5.2.

From Fig. 5.15 - 5.16, the MIBK partial flux is seem to be quasi constant when the permeate pressure is less than 5 cmHg while a linear decrease of water flux with an increase of permeate pressure is shown. Thus an increase of MIBK permeate composition and separation factor results, as observed in Fig. 5.17- 5.18. The dramatic increase of separation factor predicted by the transport model occurs in the range of permeate pressure 15 - 20 cmHg. The vapour-liquid equilibrium separation factor for 0.25wt% and 0.5wt% MIBK aqueous solutions were found to be 147 and 145 respectively. Hence, the enhancement factor is less than unity and the increase in pervaporation separation factor as observed in Fig. 5.18 is much less than the separation factor achieved in vapour liquid equilibrium. As the permeate

159

pressure increases, the pervaporation separation factor for MIBK/water would tends to increase until it reaches its equilibrium, i.e. $\alpha_{PV} \rightarrow \alpha_{VLE}$.
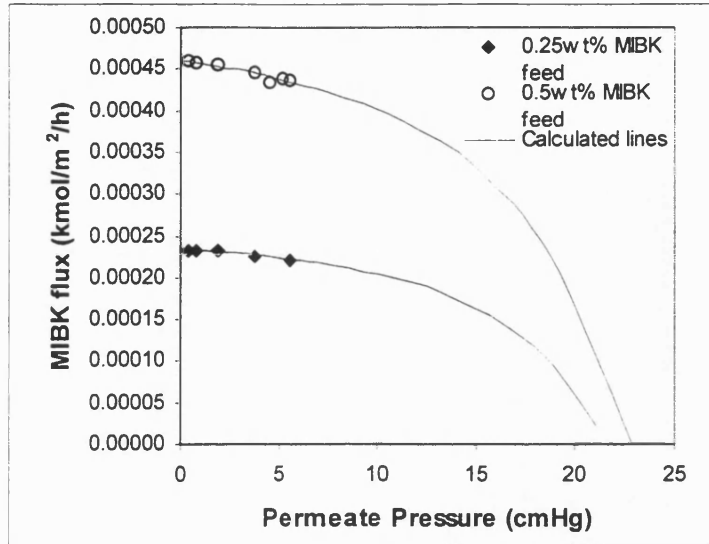
Fig. 5.15 The effect of permeate pressure upon MIBK
permeate flux at 70°C
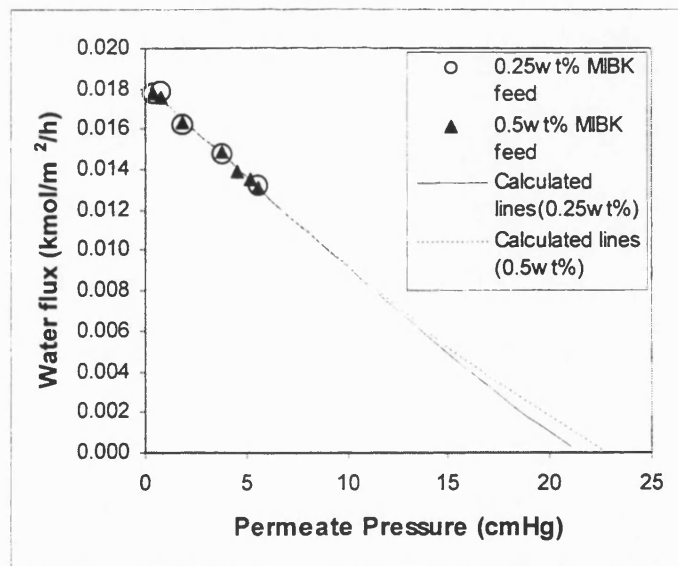
Fig. 5.16 The effect of permeate pressure upon water
permeate flux at 70°C
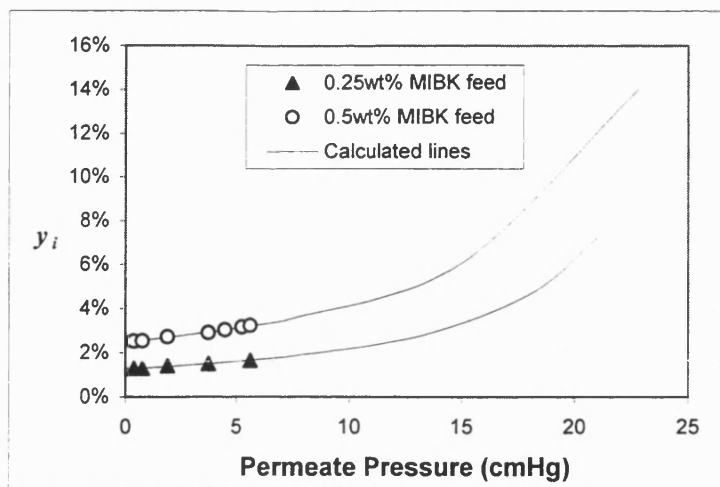
Fig. 5.17 The effect of permeate pressure upon permeate
molar composition of MIBK at 70°C
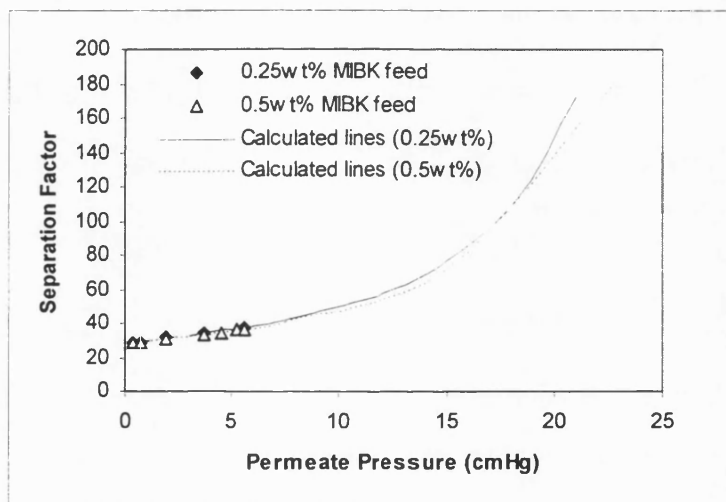
Fig. 5.18 The effect of permeate pressure upon separation factor at 70°C
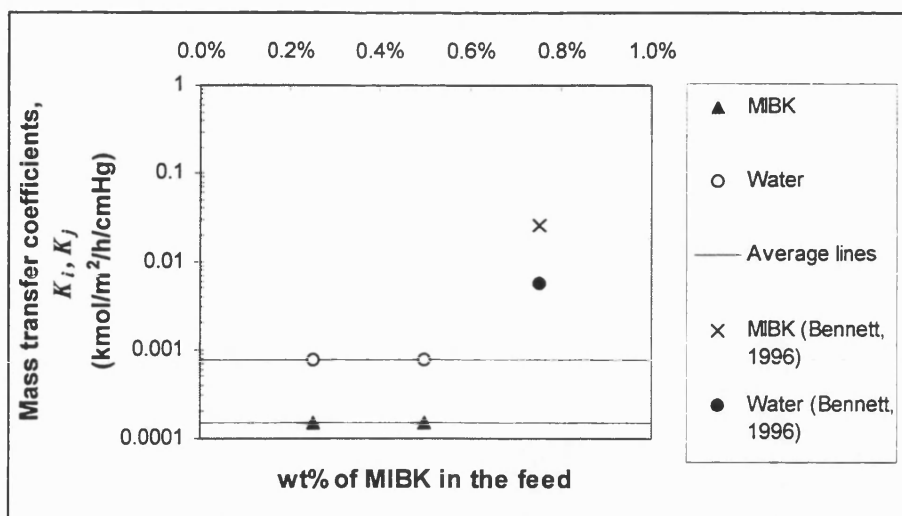
Fig. 5.19 Mass transfer coefficients vs. MIBK feed concentration at 70°C

The mass transfer coefficients determined from Fig. 5.15 - 5.16 for MIBK and water are shown in Fig. 5.19. In the present study, the average K_i and K_j were found to be 1.51×10^{-4} and 7.78×10^{-4} kmol/m²/h/cmHg. However, the K_i and K_j obtained by Bennett (1996) with homogeneous PDMS (normalized to 10μm thickness) and in the absence of a boundary layer resistance were found to be 2.61×10^{-2} and 5.48×10^{-3} kmol/m²/h/cmHg resepctively..

From the permeation experiments of Bennett (1996), the liquid mass transfer velocity, k_{bl}, for MIBK at 70°C at 1000rpm in a stirred cell (same dimensions as the one use in the present study) was found to be 6.344×10^{-5} m/s. Hence, with the use of resistance in series model, the mass transfer resistance contributions of various layers of a composite membrane were determined and are shown in Fig. 5.20. From Fig. 5.20, it is clear that the relatively low mass transfer coefficient of solute in the present study is probably due to the presence of boundary layer resistance and relatively thick support layer (75μm) compared to the selective layer (10μm). Hence, it is vital for the industrial membrane manufacturer to use or design a membrane module with high module effectiveness, ε_{bl}, and appropriate selection of support layer in order to achieve a high separation quality.
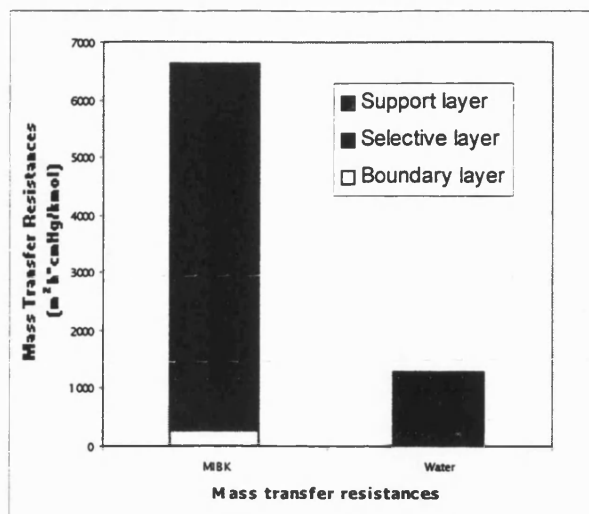
5.20 Mass transfer resistances of a composite membrane for
MIBK/water separation at 70°C

The desorption factors determined from the Fig. 5.15 - 5.16 for MIBK and water are shown in Fig. 5.21. The average desorption factors for both MIBK and water were found to be 0.94 and 1.18 respectively. Since their desorption factors values were close to unity, the transport model used by Wijmans and Baker (1993) can reasonably predict the pervaporation performance.
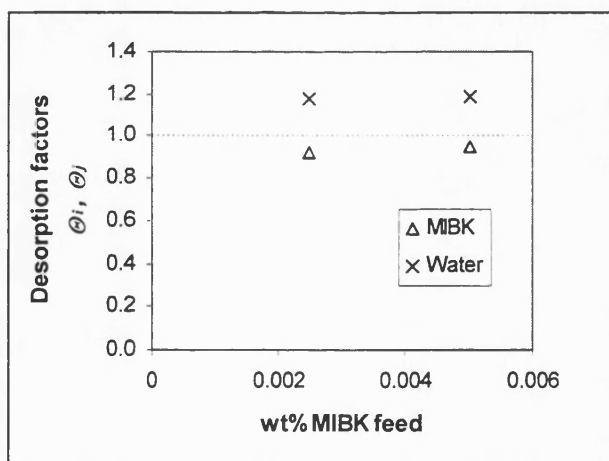
Fig. 5.21 Desorption factors vs. MIBK feed concentration at 70°C

By evaluating the dimensionless term, E and y_i^* , one can locate the type of performance behaviour in respect to permeate pressure. The (E, y_i^*) coordinates for the present study was shown in Fig. 5.22 and was identified with class C as predicted in Chapter 4.
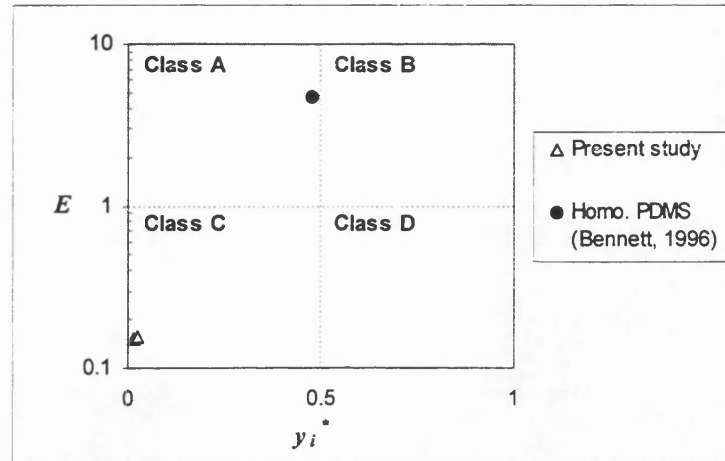
Fig. 5.22 Classification of performance behaviour in response to permeate pressure on $E - y_i^*$ plane

It is interesting to note that the (E, y_i^*) coordinates produced from homogeneous PDMS membranes in the absence of boundary layer resistance (Bennett, 1996) are located in the class A zone. With the membrane produced by himself, Bennett (1996) obtained α^*_{PV} =680 whereas in this work, α^*_{PV} =29. However, MIBK has a α_{VLE} = 149 which mean the thick homogeneous membrane is actually enhancing the separation while the commercial composite membrane selectivity was compromised by its support layer and boundary layer resistance. Such a compromise has meant that the pervaporation system is switched from class A to C. To date, no published work on MIBK/water separation is published other than by Bennett (1996), hence no further comparison is possible.

5.5 Applications of Engineering Analysis on Literature Data

Apart from using the experimental data produced from the present study, literature data were also extracted from Bennett *et al* (1997), Bennett (1994) and from others (Blume *et al*, 1990; Wijmans and Baker, 1993) for validation of the transport model and the engineering analysis presented in Chapter 4.

5.5.1 Separation of phenol/water solution

In order to show the applicability of the present model to the separation of high boiling point organics from water, the data of Bennett (1994) was analysed. According to (Bennett, 1994), a 5wt% aqueous phenol was fed into the pervaporation test at 70°C. The test cell has the same dimensions as the present study and a 20% acetate functionalised PDMS membrane was employed for permeation experiments. Using the same method of evaluation for Θ_i and K_i shown in the previous section, all necessary parameters were evaluated. These are shown in Table 5.4.

Table 5.4. A summary of evaluated parameters

Θ_i	Θ_j	$K_i \times 10^3$ kmolm^{-2} h^{-1}cmHg^{-1}	$K_j \times 10^3$ kmolm^{-2} h^{-1}cmHg^{-1}	$E^*=K_i/K_j$	α_{VLE}	Θ_i/Θ_j	y^*_i	E
5.0	1.0	2.827	0.164	17.24	1.04	5.0	0.153	86.2

From table 5.4, Θ_i was found to be 5 instead of unity. This shows that all previous models cannot be applied for the permeation of high boilers such as phenol through PDMS unless the vacuum is below 0.1cmHg. The deviation of the previous model from the new comprehensive model is shown in Fig. 5.22 - 5.25. The water flux data is less sensitive to permeate pressure because of its higher saturated vapour pressure and a value of Θ_j =1 was found to be applicable. The ultimate enhancement factor E^* was about 17 times the vapour-liquid separation, this implies recovery by pervaporation of a high boiler like phenol is significantly improved by high vacuum. From table 5.4, the co-ordinates of E and y^*_i show that the phenol-water-20% functionalised PDMS system can be classified as class A. The performance profile shown in Fig. 5.23 - 5.26 are in agreement with the illustrations in Table 5.4
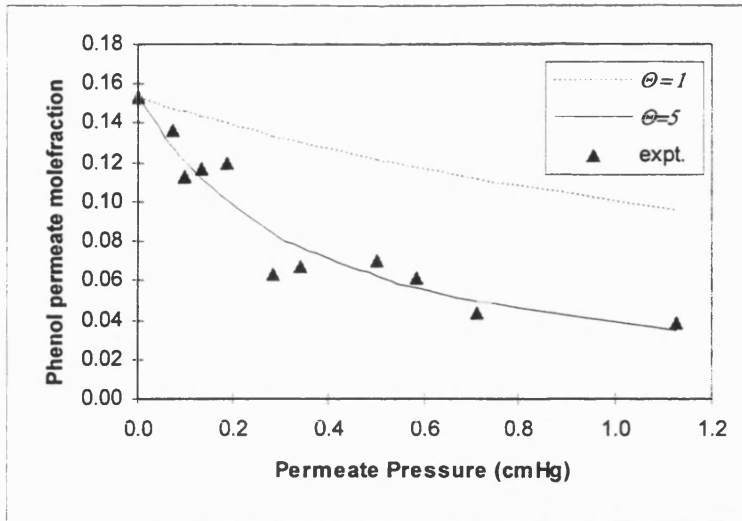
Fig. 5.23 Phenol permeate concentration for various permeate pressures
(5wt% feed conc. with 20% acetate functionalised PDMS membrane at 70°C)
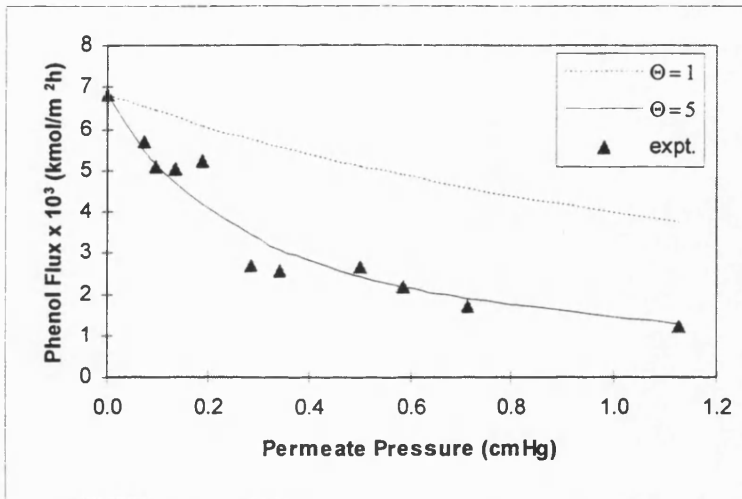
Fig. 5.24 Phenol partial flux for various permeate pressures
(5wt% feed conc. with 20% acetate functionalised PDMS membrane at 70°C)
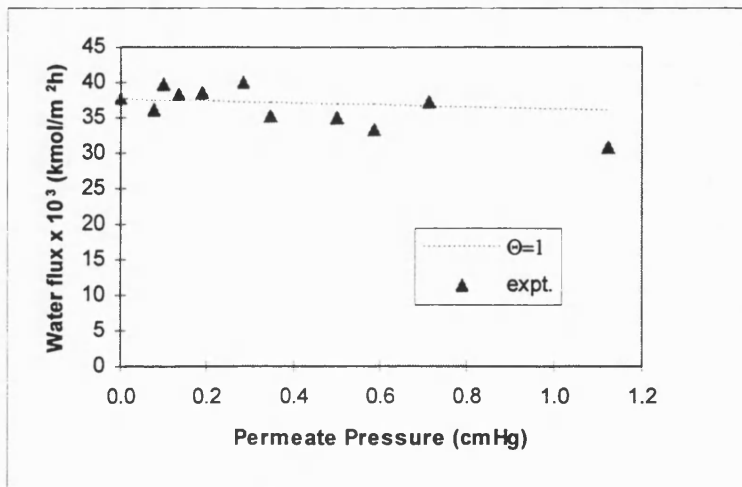
Fig. 5.25 Water partial flux for various permeate pressures
(5wt% feed conc. with 20% acetate functionalised PDMS membrane at 70°C)
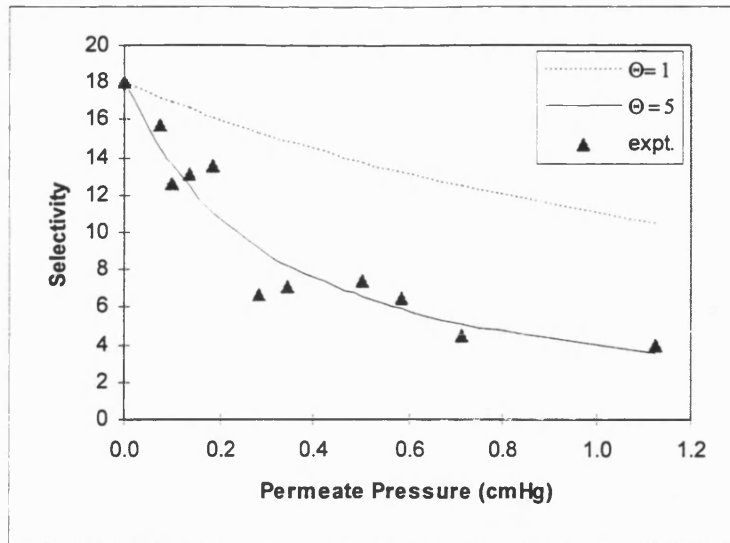
**Fig. 5.26 Selectivity (separation factor) for various permeate pressures
(5wt% feed conc. with 20% acetate functionalised PDMS membrane at 70°C)**

5.5.2 Separation of ethanol/water

In order to show the applicability of the present model, the evaluation was extended to the separation of a volatile organic aqueous solution: ethanol-water. The literature pervaporation data was used (Blume *et al*, 1990; Wijmans and Baker, 1993) and are shown in Fig. 5.27 - 5.28. The evaluated parameters were shown in Fig. 5.29-5.32.
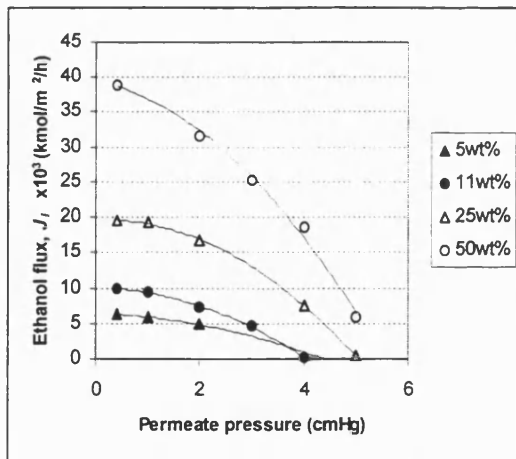
**Fig. 5.27 Ethanol partial flux through
PDMS at 30°C (Blume *et al*, 1990;
Wijmans and Baker, 1993)**
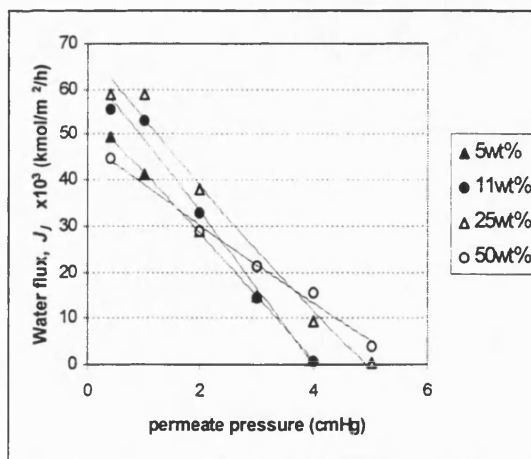
**Fig. 5.28 Water partial flux through
PDMS at 30°C (Blume *et al*, 1990;
Wijmans and Baker, 1993)**
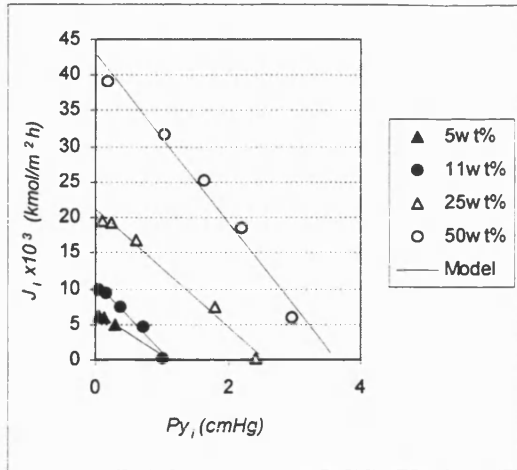
Fig. 5.29 Evaluation of K_i and Θ_i by plotting J_i against Py_i for ethanol
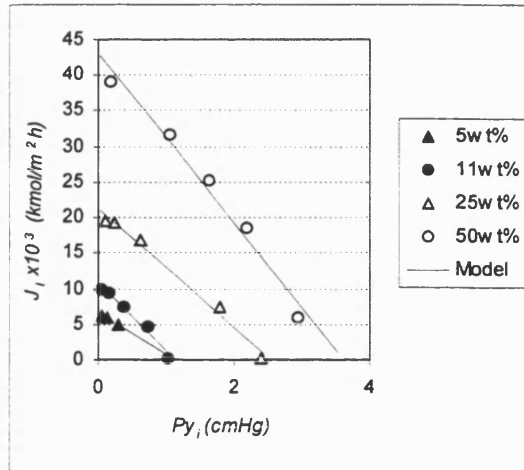
Fig. 5.30 Evaluation of K_j and Θ_j by plotting J_j against Py_j for water

The overall mass transfer coefficient of ethanol, K_i was found to be smaller than the one for water, K_j (Fig. 5.31). Hence, the ultimate enhancement factor, E^*, (Fig. 5.34) is smaller than unity and implies that the separation is not as large as that achievable using vapour-liquid equilibrium separation. This analysis is in agreement with that of (Kaschemekat *et al*, 1991). Thus distillation alone is the process of choice, provided that an appropriate temperature can be guaranteed if biomass is present.
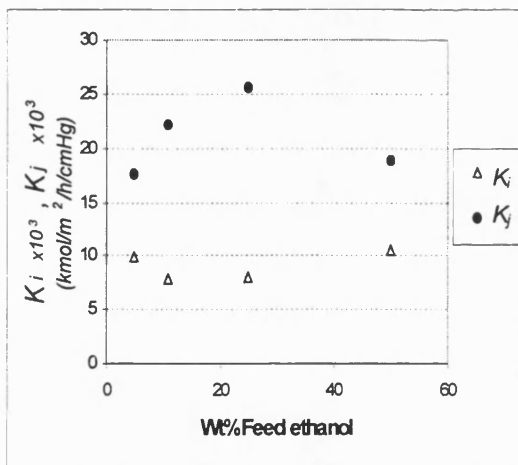
Fig. 5.31 Mass transfer coefficients of ethanol (K_i) and water (K_j) in ethanol-water-PDMS system
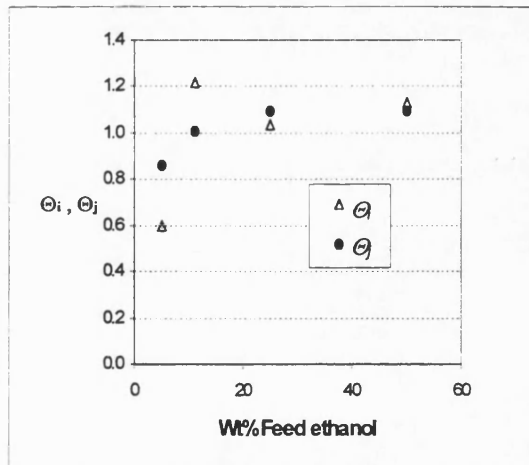
Fig. 5.32 Partition coefficients ratio for ethanol (Θ_i) and water (Θ_j) in ethanol-water-PDMS system

168
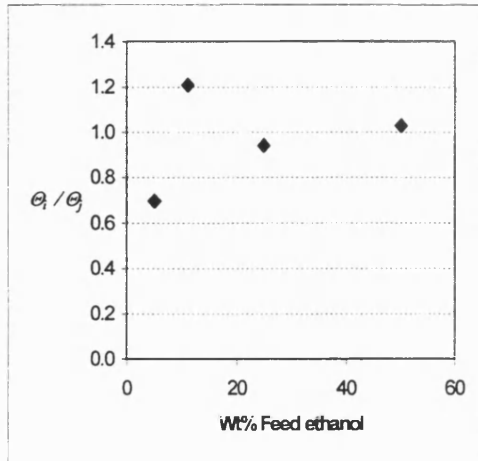
Fig. 5.33 Ratio of partition coefficients (Θ_i / Θ_j) for various concentration of ethanol in ethanol-water-PDMS system
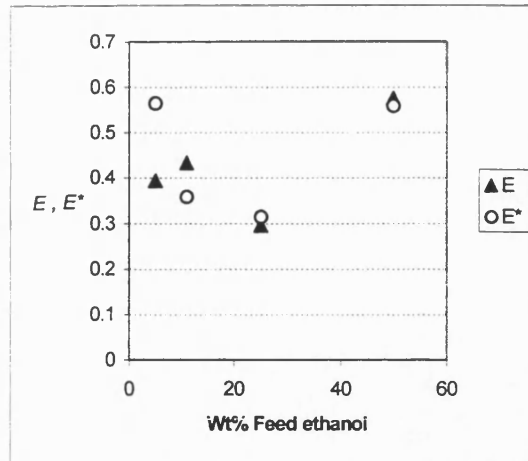
Fig. 5.34 Ultimate enhancement factor (E^*) and dimensionless E number for ethanol-water-PDMS system

Fig. 5.31 shows that over the wide range of concentration used, the overall transfer coefficient can change by nearly 50%. The change in boundary layer mass transfer coefficient k_{bl} with concentration will be small and so the change in K_i and K_j reflects changes in membrane permeability. The ratio of partition coefficients was found to be less than unity at low feed concentrations but it tended to unity at higher feed concentrations. This implies changes in the sorption coefficient. A comparison between the present and previous model presented of Wijmans and Baker (1993) and the data is shown in Fig. 5.35. The present model has been found to give good agreement with the experimental performance profiles (see Fig. 5.35 - 5.36). From the values of E and y_i^* in Fig. 5.34 and Fig. 5.36, it is seen that the system is predominately in class C.
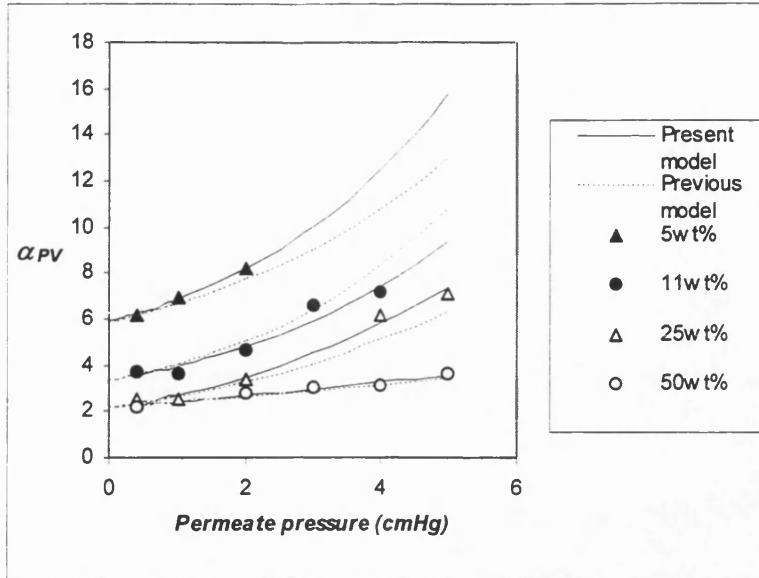
Fig. 5.35 Separation factor at various permeate pressures for
ethanol-water-PDMS system and the comparison between
previous and present models.
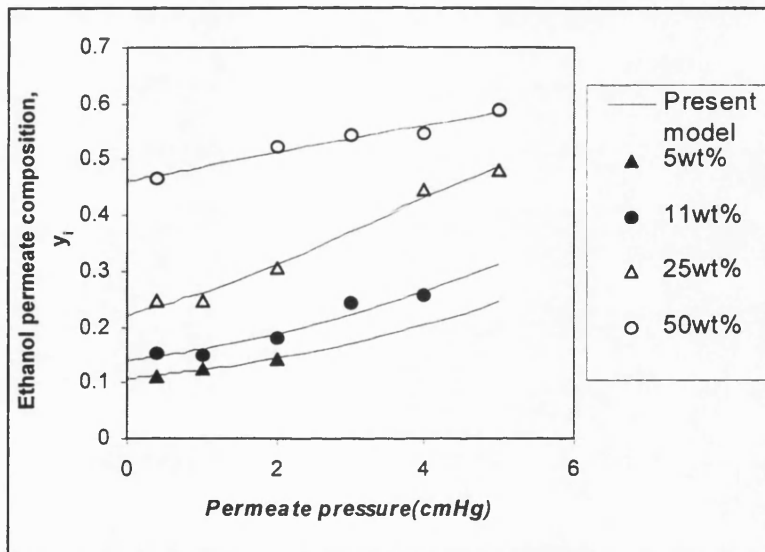
Fig. 5.36 Ethanol permeate concentration at various permeate pressures for
ethanol-water-PDMS system and the trends predicted by the present model.

170

5.6 Factors that influence the shifting of the coordinates $(E,\ y_i^*)$ on the performance behaviour classification plane

It has been shown that the pervaporation perfomance profile in response to permeate pressure changes can be predicted with minimal experimental information through the evaluation of dimensionless coordinates $(E,\ y_i^*)$. However, the dimensionless coordinates $(E,\ y_i^*)$ vary with the operating conditions such as temperature, feed concentration and boundary layer resistance as well as with membrane material.

In order to show the applicability of the engineering analysis upon literature data, the work of (Bennett, 1996; Bennett et al, 1997) were used to investigate the shifting of coordinates $(E,\ y_i^*)$ on the behaviour classification plane that caused by different membrane materials and operating conditions.

Recall equation (4.34) in Chapter 4, E is dependent upon the mass transfer coefficients and the ratio of partition coefficients.

$$E = \frac{K_i \Theta_i}{K_j \Theta_j} = E^* \frac{\Theta_i}{\Theta_j} = \varepsilon_{bl} E_{mem}^* \frac{\Theta_i}{\Theta_j} \tag{4.34}$$

Due to the inadequate information of the effect of permeate pressure on the partial fluxes, it had to be assumed that the ratio, $\Theta_i / \Theta_j = 1$. The mass transfer coefficients are derived from the work of (Bennett, 1996; Bennett et al, 1997), hence the estimation of E^*, E_{mem}^* and y_i^* are made possible.

5.6.1 The influence of the mass transfer in boundary layer

The effect of boundary layer resistance will be illustrated by data for the chloroform-water-PDMS system obtained from experiments that operate with different stirring speeds. This is shown in Fig. 5.37. The feed solution used contained 0.3 wt% of chloroform and the operating temperature was 25°C. The PDMS membrane used has a thickness of 106 μm.

From Fig. 5.37, concentration polarization was greatly reduced by the degree of turbulence that was generated by the stirring.
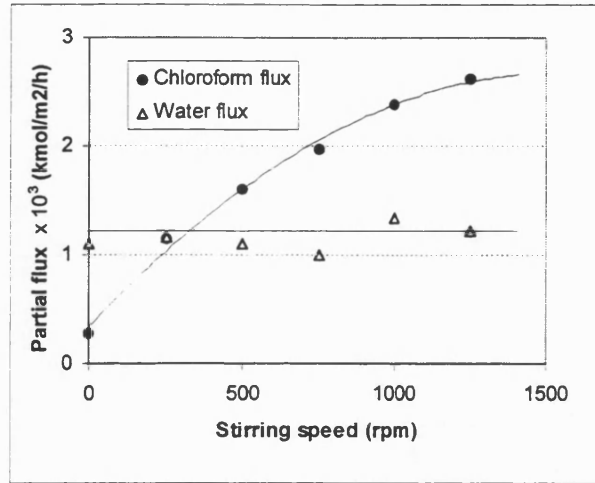
Fig. 5.37 The influence of stirring speed upon partial fluxes for chloroform-water-PDMS membrane system (Bennett, 1996).
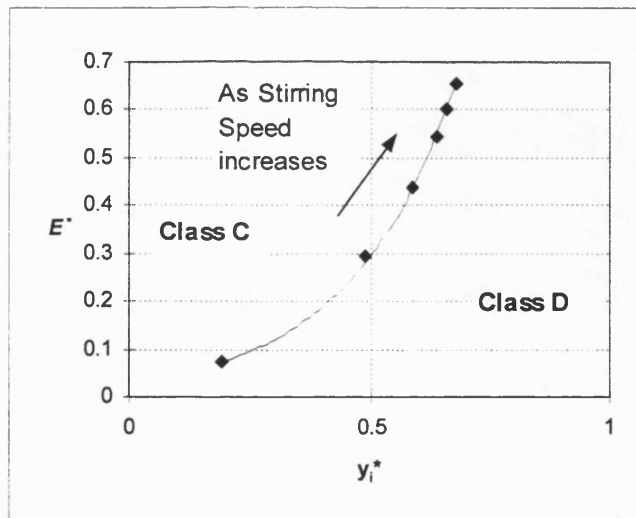
Fig. 5.38 The effect of stirring speed upon the location of chloroform-water-PDMS system on the E^* - y^*_i classification plane

From the partial flux data from Fig. 5.37, the values of E^* and y_i^* were obtained. The only change in process conditions was stirring speed that gave different boundary layer resistances. One trend is shown in Fig. 5.38. As the stirring speed increases, y_i^* increases dramatically from 0.2 to 0.68. This is due to the reduction of boundary layer thickness and

consequently a reduction in the overall resistance towards chloroform transport. The change of system behavior on the E^* - y_i^* plane due to stirring speed is noted Fig. 5.38. Initially, it starts at the bottom left of class C and crosses over to class D with an increasing ultimate enhancement factor. Thus the increase in stirrer speed has shifted the overall behaviour into a class where the absolute flux of the organic is greater than that of water, and because E^* has moved closer to unity, the effect of pressure upon performance has been reduced.

5.6.2 The influence of feed concentration

Various pervaporation experiments were carried out with different concentrations of pyridine using a pure PDMS membrane with a thickness of 161 µm under 70 °C. The stirring rate of the experiment was 1000rpm and the permeate pressure were operated under 2mbar. The partial fluxes of these experiments are shown in Fig. 5.39.
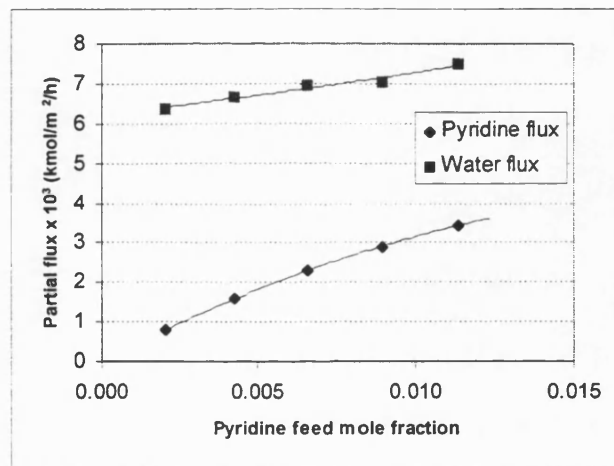
Fig. 5.39 The influence of feed concentration upon partial fluxes in pyridine-water-PDMS membrane system (Bennett, 1996).

The influence of feed concentration upon E^* and y_i^* are shown in Fig. 5.40. As feed concentration increases there is a modest increase in E^*, and as expected, a significant increase in y_i^* . Fig. 5.40 showed the effect of the concentration of pyridine upon the pyridine-water-PDMS system in the E^* - y_i^* classification plane. As feed concentration increase the class A system is displaced in the direction of class B. Thus the system becomes somewhat less sensitive to permeate pressure effects as feed concentration increases. The

corollary is that for the batch recovery of pyridine from water (and other systems with an E^* value of more than unity) the process performance becomes more pressure sensitive as batch time increases.
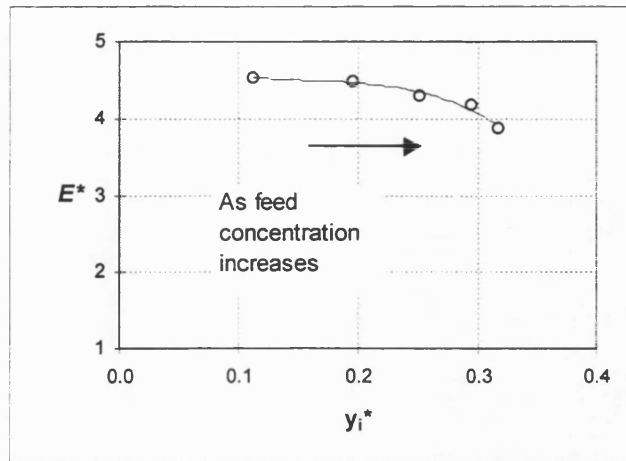
Fig. 5.40 The effect of pyridine feed concentration upon location of pyridine-water-PDMS system on $E^* - y^*_i$ classification plane

5.6.3 The influence of feed temperature

Various pervaporation experiments were carried out with different feed temperatures for pyridine/water separation. A pure PDMS membrane with a thickness of 151µm and feed solution concentration of 0.75wt% are used. The stirring rate and permeate pressure of the experiments were 1000 rpm and less than 2mbar respectively. The partial fluxes for various feed concentration are shown in Fig. 5.41. It was found that the partial flux increases exponentially with the feed temperature.
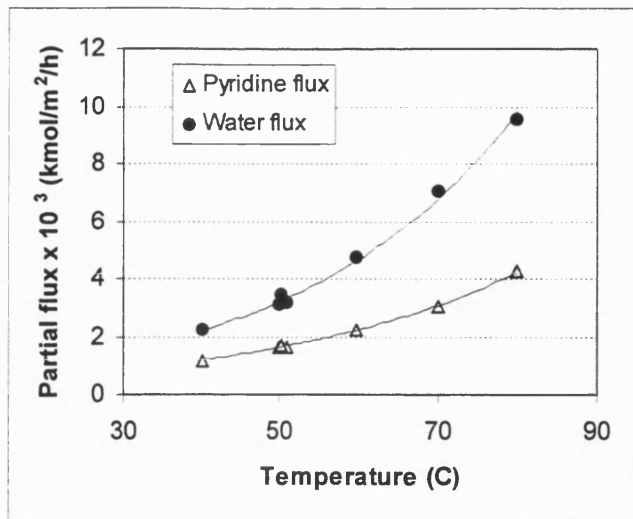
Fig. 5.41 The effect of feed temperature upon the partial fluxes in pyridine-water-
PDMS system (Bennett, 1996).
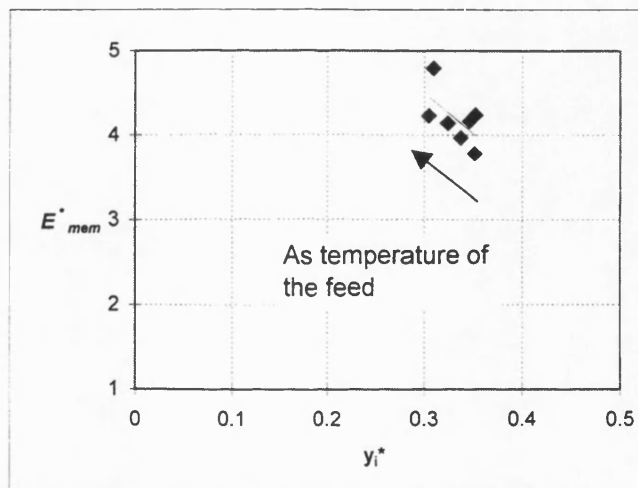
Fig. 5.42 The effect of feed temperature on the location of
the pyridine-water-PDMS system on E^* - y^*_i classification plane.

From the partial flux data obtained in Fig. 5.41, E^* and y_i^* values are obtained and the
influence of feed temperature on E^* and y_i^* value of the pyridine-water-PDMS system are
shown in Fig. 5.42. Modest changes in E and y_i^* were observed, but are of little significance
in themselves. In the E^* - y_i^* classification plane (Fig. 5.42) there is a move in the direction
away from class B. The magnitude of the change is small and insignificant compared to the
benefits of increased flux that would occur over the same temperature range.

5.6.4 The influence of the membrane properties

In order to investigate the influence of membrane properties due to functionalisation of a PDMS membrane, E^*_{mem} and y_i^* values were derived from the permeabilities of various functionalised PDMS membranes. Data were obtained from the work of Bennett *et al* (1997). In his work, the permeability of each type of functionalised membrane were obtained with a correction for the resistance due to the boundary layer. Hence, the calculated values of E^*_{mem} are those that would be obtained when the resistance is that due to the membrane only. This enables one to examine the effect of changes in intrinsic permeability of various membrane materials. (In practice the effect of the feed-side boundary layer would be of major significance for the chloroform systems, insignificant for phenol systems and of modest significance for other systems. Fig. 5.43 shows the effect of a change in membrane properties for each organic system (i.e. changes in $\hat{P}_{m,i}$ and $\hat{P}_{m,j}$). Functionalisation creates a locus of points in the $E^*_{mem} - y_i^*$ classification plane. Improved membrane properties (higher organic flux and larger y_i^*) tends to move an aqueous organic-membrane system towards class B.
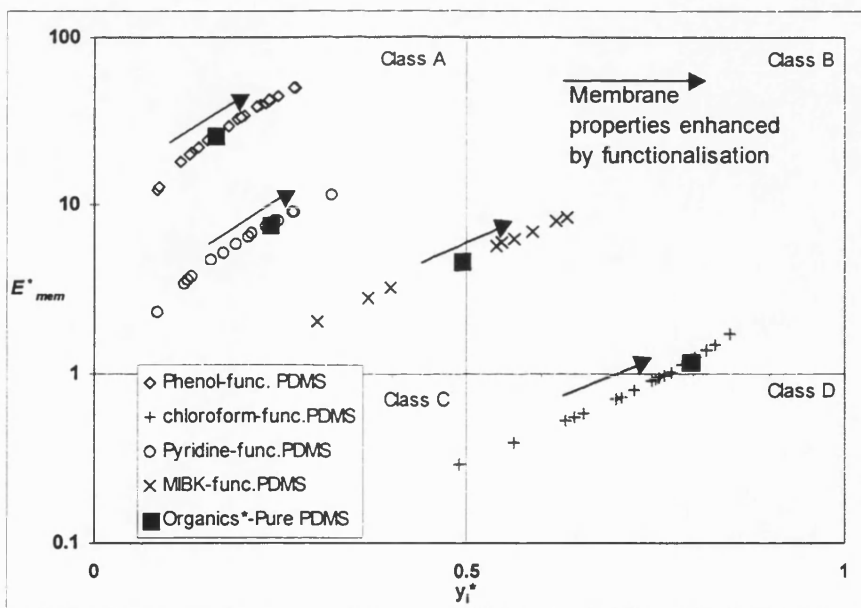
Fig. 5.43 The effect of functionalisation of PDMS upon location of chloroform, phenol, MIBK, pyridine-water-membrane systems within the $E^*_{mem} - y_i^*$ classification plane.

Table 5.5 E^*_{mem} and y^*_i for various functionalised PDMS membranes

Functional Group	Load %	Phenol y_i^*	Phenol E^*_{mem}	Type	Chloroform y_i^*	Chloroform E^*_{mem}	Type	Pyridine y_i^*	Pyridine E^*_{mem}	Type	MIBK y_i^*	MIBK E^*_{mem}	Type
Pure PDMS	0	0.16	25.91	A	0.79	1.18	B	0.23	7.66	A	0.49	4.73	A
Acetate-	10	0.13	20.11	A	0.64	0.55	D	0.12	3.38	A			
	20	0.13	19.92	A	0.63	0.52	D	0.13	3.72	A			
Di-Acetate-	10	0.19	32.27	A	0.72	0.80	D						
	20	0.15	24.15	A									
	30	0.08	12.30	A									
Hexanoate-	10	0.20	34.39	A	0.83	1.49	B	0.24	7.93	A			
	20	0.22	39.29	A	0.70	0.73	D	0.16	4.63	A	0.30	2.06	A
Cyano-	10	0.22	38.09	A	0.75	0.92	D	0.20	6.44	A			
	20	0.19	32.17	A	0.49	0.29	C	0.08	2.27	A			
Octyl-	10	0.23	40.46	A	0.85	1.70	B	0.32	11.67	A	0.59	6.92	B
Benzyl-	10	0.19	32.56	A	0.82	1.37	B	0.27	9.09	A			
PentaFluroBenzyl-	10	0.14	21.98	A	0.80	1.24	B	0.26	9.04	A	0.54	5.72	B
	20				0.66	0.58	D	0.23	7.44	A			
Phenyl Ether-	10	0.14	22.15	A	0.76	0.95	D	0.24	8.11	A			
Ethyl Ether-	10	0.23	41.73	A	0.79	1.14	B	0.21	6.68	A			
	20	0.24	44.48	A	0.77	1.03	B	0.17	5.15	A	0.37	2.83	A
Alkenyl-	10	0.16	25.75	A	0.79	1.12	B	0.23	7.44	A	0.40	3.21	A
	20	0.09	12.79	A	0.76	0.98	D	0.19	5.82	A			
Amino-	10	0.23	41.94	A									
	20	0.27	50.35	A	0.56	0.40	D						
Amido-	10	0.20	33.29	A									
Pyridyl-	10	0.27	49.85	A				0.12	3.55	A			
Cyano-*	10	0.18	29.72	A	0.75	0.90	D						
	20	0.12	17.89	A	0.70	0.71	D						
Tridecyl-	6.67										0.62	7.94	B
	10										0.63	8.43	B
Branch Heptyl-	10										0.57	6.33	B
	12.5										0.55	5.92	B

*See appendix A2

5.6.5 General rules for displacement

From the previous section, general rules for displacement on the E^*_{mem} - y_i^*, classification plane can be deduced and these are shown in Fig. 5.44. The improvement in membrane selectivity could, for example, be functionalisation. The relative effect of turbulence is small if membrane permeability is low, but more important in certain cases than the membrane material itself. Thus, the lengths of arrows in Fig. 5.44 represent a generalisation.
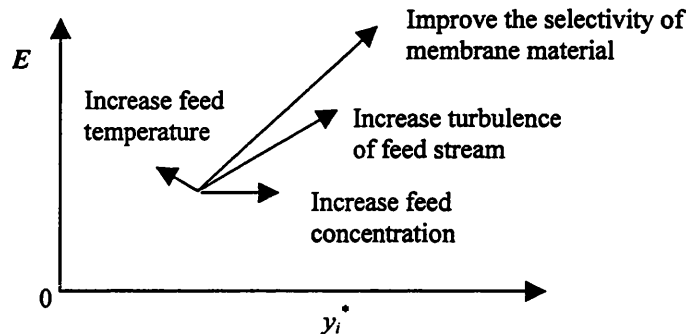
Fig. 5.44 Illustration of the effect of various factor upon position in the classification plane. The lengths of the arrows represent a generalisation.

Table 5.5 gives a classification for aqueous-organic mixtures and a number of membranes using the permeability data of (Bennett 1996). As the values of Θ_i and Θ_j are not available in most cases, the class is well defined, only when values of E^*_{mem} and y_i^* are not close to 1 and 0.5 respectively. MIBK-water- pure PDMS system the value of E^*_{mem} is sufficiently high for one to conclude that the system is of class A and B. The actual classification (whether it is A or B) is concentration- and membrane-dependent. However, for MIBK-water-GKSS PDMS system, its behaviour is lied in class C. For chloroform most of the data is close to the border between B and D, thus further work to determine the desorption factor Θ_i is required.

5.7 Chapter Conclusions

In this chapter, transport model and engineering analysis verification were carried out with pervaporation experimental data from the present study and literature. In general, the transport model prediction was in agreement with the experimental data. The usefulness of evaluating the dimensionless term E and y_i^* using only a small amount of data was tested and found to be in agreement with the experimental results on performance profile classification. In addition, the optimum operating permeate pressure range determined by the approximation method described in Chapter 4 was also found to be reasonable when it is compared to experimental results.

178

A method to determine the mass transfer coefficient and desorption factor was demonstrated and for high boilers like phenol was found to be important. In evaluating the mass transfer coefficient of the commercial composite membrane, the support layer was found to be the dominant resistance in both pyridine and MIBK pervaporation experiments due to the thin selective layer. The performance of the commercial membrane with aqueous MIBK was significantly different from that obtained previously by Bennett (1996).

Classification for aqueous -organic-PDMS system has been given above. A summary of the present study and literature cases is shown in Table 5.6.

Table 5.6 Classification for aqueous-organic-PDMS systems

Feed	Class
Aqueous-pyridine	Class A
Aqueous-MIBK	Class A or B or C; depends on membrane type and concentration.
Aqueous-phenol	Class A
Aqueous-ethanol	Class C up to at least 50 wt% ethanol feed
Aqueous-chloroform	Mainly class D, but in class B if ε_{bl} tends to 1

For a given feed-membrane combination one can identify a point in the $E\text{-}y_i^*$ classification plane. The effect of changing feed composition, temperature, feed side hydrodynamic conditions or improved membrane properties upon location has been identified and typical loci given.

Part IV   Design Tool Development

Chapter 6

Analytical Design Tools Development

6.1 Chapter Objectives

- To discuss the scale up and optimization problems of membrane and module design

- To introduce for organophilic pervaporation the transfer units design concept that is an analogue to both packed bed absorption and distillation.

- To develop an analytical solution for membrane area determination and to use it to examine the various factors that influence scale-up and design.

- To devise and discuss a flexible way to improve pervaporation process schemes

6.2 Introduction

In Chapter 4, a comprehensive transport model for organophilic pervaporation was developed and it was verified in Chapter 5 by laboratory data from various sources. In addition, the engineering analysis tool, i.e. E and y_i^*, was also proven useful for predicting the performance profile in response to permeate pressure changes. A method to approximate the optimum operating permeate pressure range was developed and its prediction was found to be reasonable when compared to experimental data.

In the field of membrane gas permeation, scale-up studies have been investigated extensively as early as 1950 (Weller and Steiner, 1950a; 1950b). By contrast, in the field of pervaporation and despite many new pervaporative membranes having been reported in recent years the scaling up of pervaporation membrane from lab data has rarely been reported. Some of the scale up procedures used by some researchers e.g. Jordt et al (1997) still rely on the scale up method that was offered by Weller and Steiner (1950a; 1950b). More recently some researchers (Aptel and Neel, 1986; Gooding, 1991; Feng and Huang,1992; Rautenbach et al, 1989) have outlined procedures for membrane area determination and investigated the engineering aspect of pervaporation modules. None of their investigations, however, has involved other literature sources, being solely confined

to their own investigated membrane systems. Since most of these scale up investigations are analyzed either empirically or numerically, the studies become less comparable one to the other and are condition specific. It is the object of the present study to investigate the feasibility of scaling a pervaporation plant analytically with the use of the transport model developed in Chapter 4. In addition, a design tool that adopts conventional chemical engineering unit scale up analysis will be developed for systematic membrane screening and module design optimization.

In the literature, the first systematic scale up studies for membrane gas separation based on conventional chemical engineering unit operations, were carried by Hwang and Thorman (1980). **HMU** (Height of Membrane Units) and **NMU** (Number of Membrane Units) were introduced which are analogous to conventional **HTU** (Height of Transfer units) and **NTU** (Number of Transfer Units) used in a packed bed distillation column design. According to a review by Mason et al (1983), the HMU and NMU are not that useful for conceptual design. Most importantly, unlike the HTU in packed bed distillation column, the definition of HMU was found to be driving force dependent. Thus, it makes HMU and NMU meaningless as a design tool compared to the HTU and NTU concept used in packed bed distillation column design. In addition, unlike the HTU and NTU for packed bed absorption tower, the lack of analytical solution for membrane area calculation, has led to limited usage of HMU and NMU.

Although the solution for membrane area calculation can be obtained via digital computer or spreadsheet software, an analytical solution for membrane area requirement should shed more light on design and optimization than numerical solutions.

After nearly a decade of neglect of such analysis, Meckl (1994) first introduced the ATU (Area per Transfer Unit) and NTU (Number of Transfer Unit) concept for the scale-up study of pervaporative removal of aniline from water. The ATU and NTU design concept studies carried out by Meckl (1994), however, have been over simplified and empirically derived. Thus it inherited the same difficulty as Hwang and Thorman (1980).

Firstly in this chapter, the scale-up of pervaporation units will be discussed in the light of conventional chemical engineering scale up principles. Secondly, based on the transport model developed in Chapter 4, the analytical solutions for ATU and NTU will be derived.

Then a comparison between gas/vapour permeation and pervaporation will be given and the influence of process conditions and membrane selection upon ATU and NTU will be investigated.

6.3 Stage Process and Differential Process

When one tries to model a pervaporation unit, one should be clear that a pervaporation unit is unlike, say, a bubble cap distillation column which can be modeled as a *stage process*. Although some researchers e.g. Naylor *et al* (1955) have treated a membrane process such as gas separation as an *equilibrium stage proceesses*, according to Bennedict (1947), all membrane processes such as gas separation should be treated as *differential processes*. The accepted approach is based upon mass-exchange processes. In the present study, two mode of operations, i.e. continuous and batch mode, will be modeled separately.

6.4 Continuous Pervaporation Unit

In a continuous pervaporation unit as shown in Fig. 6.1, the feed water which is contaminated with VOC is continuously supplied into a pervaporation unit. Treated water is then withdrawn from the module in an exit stream that is normally called a retentate or residue stream. The removed VOC is concentrated in the permeate stream and recovered via a condenser. The driving force of the permeation is maintained by a vacuum at the downstream. In reality the pervaporation unit could be a series of modules but for the sake of simplicity, modeling of the unit will be treated as a whole.
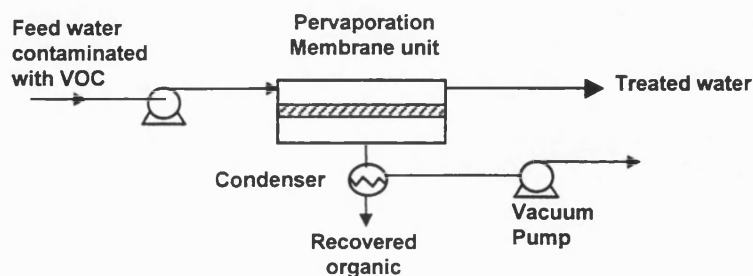
Fig 6.1 A continuous pervaporation unit

6.4.1 The material balance and design equations

The design equations for a continuous pervaporation unit can be derived from the differential mass balance across a single stage membrane. There are many operational modes for a continuous pervaporation unit can be made, for instance, cross- flow, co-current flow and countercurrent flow. These various operation modes have been extensively studied by others for gas separation (Stern and Walawender, 1969; 1972; Pan and Habgood, 1978; Pan, 1983) which as discussed in Chapter 4 is a related process. In analyzing the effect of different operational modes upon performance, Stern and Walawender (1972) found that the flow pattern has *relatively* little effect on the membrane area requirement. However, for a membrane with very high separation factor, this effect can become significant. Hence, in the present study, cross-flow pervaporation unit was chosen for study for it is the simplest case and most applicable especially for the cheap and easy constructed spiral-wound module. In studying a cross-flow gas permeator, Pan and Habgood (1978) found that it is possible to assume that there is no mixing of permeate fluxes due to the porous supporting layer and permeate spacer. Hence, the permeate composition *at any point* near the membrane is then determined by the relative rates of permeation of the feed components at that point.
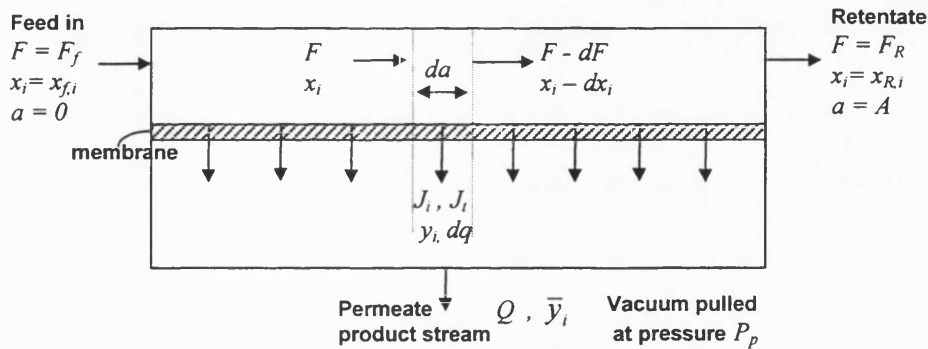
Fig 6.2 Differential mass balance in a continuous pervaporation unit

F_f	Feed molar flow rate, kmol h^{-1}	Q	Permeate product rate, kmol h^{-1}
F_R	Retentate mass flow rate, kg h^{-1}	J_t	Local total molar flux, kmol h^{-1} m^{-2}
$x_{f,i}$	target mole fraction at the feed	J_i	Local component molar flux, kmol h^{-1} m^{-2}
$x_{R,i}$	target mole fraction at the retentate	y_i	Local component mole fraction in permeate
A	Total membrane area, m^2	$\overline{y}_i$	Mean component mole fraction in the final permeate

From Fig. 6.2, it possible to outline the differential mass balance for a cross-flow pervaporation module in steady state as follows:

Overall material balance: $-\dfrac{dF}{da} = J_t$ (6.1)

Component material balance: $-\dfrac{d(Fx_i)}{da} = -\left(F\dfrac{dx_i}{da} + x_i\dfrac{dF}{da}\right) = J_i$ (6.2)

Mass transfer equation :

Component i (organic): $y_i\dfrac{dq}{da} = J_t y_i = K_i\left(P_i^{sat}\gamma_i x_i - \Theta_i P_p y_i\right)$ (6.3)

Component j (water): $y_j\dfrac{dq}{da} = J_t y_j = K_j\left(P_j^{sat}\gamma_j x_j - \Theta_j P_p y_j\right)$ (6.4)

Knowing that $\dfrac{dx_i}{da} = \dfrac{dx_i}{dF}\times\dfrac{dF}{da}$ and $J_i = J_t y_i$, by substituting equation (6.1) into (6.2), the

following relationship is obtained:

$$F\dfrac{dx_i}{dF} = y_i - x_i$$ (6.5a)

or integrating the above equation over the boundary conditions and yield:

$$\int_{F_f}^{F_R}\dfrac{dF}{F} = \int_{x_{f,i}}^{x_{R,i}}\dfrac{dx_i}{y_i - x_i}$$ (6.5b)

or

$$\ln\left(\dfrac{F_R}{F_f}\right) = \ln(1-\phi) = \ln\left(1-\dfrac{Q}{F_f}\right) = \int_{x_{f,i}}^{x_{R,i}}\dfrac{dx_i}{y_i - x_i}$$ (6.5c)

ϕ, is the ratio of product rate to the feed rate ($=Q/F_f$) and is known as *stage-cut*.

The experimental results of the pervaporation separation gives the relationship between y_i and x_i. The integration of Eq. (6.5c) can be done graphically by plotting $1/(y_i - x_i)$ versus x_i and getting the area under the curve between $x_{f,i}$ and $x_{R,i}$ as shown in Fig. 6.3. Equation (6.5c) is in the form of the *Rayleigh equation* which is frequently used for batch distillation design.
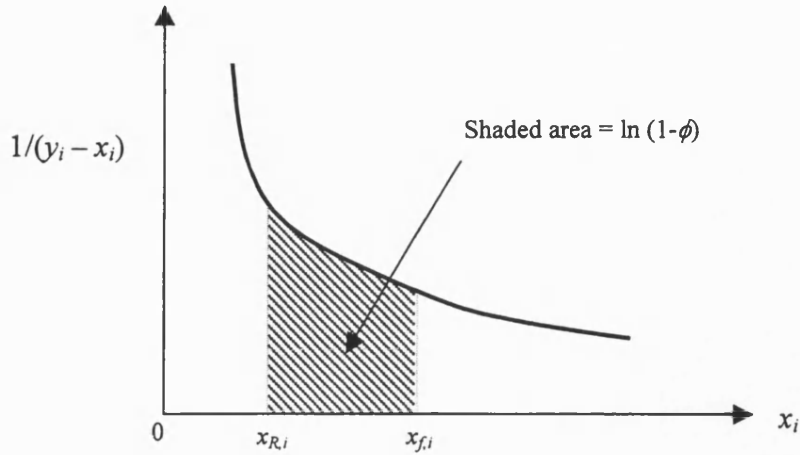
Fig. 6.3 Determination of cut-stage, ϕ.

If a required stage-cut is given, it is possible to obtain the retentate composition, $x_{R,i}$ by iterating the *Rayleigh equation* to give a required shaded area under the curve.

When the component mass balance is performed over the whole pervaporation unit instead of the differential element, the following relationship is obtained:

$$F_f x_{f,i} = Q \cdot \overline{y}_i + F_R x_{R,i} \tag{6.6}$$

In practice, Q and $\overline{y}_i$ are measurable quantities and are the indicators of the performance and efficiency of a pervaporation unit. Equation (6.6) can also be obtained by integrating equation (6.1) over the boundary conditions where Q and $\overline{y}_i$ are the integrals stated below:

$$Q = \int_0^A J_i da = \int_0^Q dq \tag{6.7} \quad \text{and} \quad \overline{y}_i = \frac{1}{Q} \int_0^A J_i da = \frac{1}{Q} \int_0^Q y_i dq \tag{6.8}$$

For a given cut stage, $\phi = Q / F_f$, the average or mean composition of solute can be expressed in terms of the stage cut and the solute compositions of the feed and retentate:

$$\overline{y}_i = \frac{x_{i,f} - (1-\phi)x_{R,i}}{\phi} \tag{6.9}$$

185

The membrane area requirement for a continuous pervaporation unit can be derived by solving equation (6.1) - (6.9).

6.4.2 An analytical solution for area requirement of a continuous pervaporation unit

Although it has been proposed by others (Neel, 1991; Wijmans and Baker,1992) that equations (6.1)-(6.7) can be solved numerically by using digital computer or even a spreadsheet software, it is always an advantage if one can solve the equations analytically.

From the analytical solution, one can spot or capsulate the critical parameters within the analytical solution. It is also true that, if an analytical solution is provided, one can develop useful design tool to optimize the membrane manufacture and module design together. However, in order to ease the derivation, the following assumptions have been made:

- temperature within the module was assumed constant throughout, i.e. negligible temperature drop within the system. Since interstage heating will be provided, as a whole, the above assumption is applicable.

- the permeate pressure within the module was assumed constant, i.e. negligible pressure drop on the permeate side. This is not totally true for some modules like hollow-fibre modules which have a pressure build up in the lumen but as long as the hollow fibres are short enough, the constant permeate pressure assumption is reasonable.

- no interaction between component fluxes. For feed side low concentration (<10wt%) especially for organophilic pervaporation, coupling effects are negligible.

- binary component system.

- permeability of the membrane assumed independent of concentration. This assumption can be made for a low feed concentration and is especially true for organophilic pervaporation

6.4.2.1 Analytical solution for stage-cut, ϕ.

In order to solve the *Rayleigh equation*, the relationship between y_i and x_i has to be established. Recall equation (4.18) in Chapter 4 for pervaporation of a binary mixture, the relationship between y_i and x_i can be expressed as:

$$\frac{y_i}{1-y_i} = E \frac{P_i^{sat}\gamma_i x_i/\Theta_i - P_p y_i}{P_j^{sat}\gamma_j(1-x_i)/\Theta_j - P_p(1-y_i)} \qquad (4.18)$$

Where $E = \dfrac{K_i\Theta_i}{K_j\Theta_j}$ \qquad (4.19)

In order to avoid the integration of the square root term that is caused by the introduction of equations (4.27a) & (4.27b) from Chapter 4, x_i was chosen to be eliminated instead of y_i from the *Rayleigh equation*. Hence, equation (4.18) is rearranged to form $x_i = f(y_i)$ as follows:

$$x_i = \frac{1-E}{D_j - ED_i} \cdot y_i \cdot \frac{y_i + (D_i + E - 1)/(1-E)}{y_i + ED_i/(D_j - ED_i)} \qquad (6.10)$$

where: $D_i = \dfrac{P_i^{sat}\gamma_i}{\Theta_i P_p}$ \qquad (6.11) \qquad $D_j = \dfrac{P_j^{sat}\gamma_j}{\Theta_j P_p}$ \qquad (6.12)

Since the feed concentration is low in organophilic pervaporation, it is possible to assume that the activity coefficient of the solute is close to the activity coefficient at infinite dilution while for the solvent it is close to unity ($\gamma_i \rightarrow \gamma_i^\infty; \gamma_j \rightarrow 1$). Hence, equations (6.11) & (6.12) can be treated as constant. Hence, differentiate equation (6.10) with respect to y_i to form $dx_i = f'(y_i)dy_i$. By substituting $x_i = f(y_i)$ and $dx_i = f'(y_i)\,dy_i$ into *Rayleigh equation*, the following integral can be obtained:

$$\ln(1-\phi) = \int_{y_{i,f}}^{y_{i,R}} \frac{f'(y_i)}{y_i - f(y_i)}dy_i \qquad (6.13)$$

Where the boundary conditions $y_{f,i}$ and $y_{R,i}$ are the permeate concentration corresponding to $x_{f,i}$ and $x_{R,i}$ respectively. Both $y_{f,i}$ and $y_{R,i}$ can be determined via equations (4.27a) &

(4.27b) found in Chapter 4. By separation of variables, equation (6.13) can be solved analytically. A detailed derivation of the analytical solutions can be found in Appendix A4 and the solution for stage-cut was found to be as follows:

$$\phi = \frac{Q}{F_f} = 1 - \frac{F_R}{F_f} = 1 - \left(\frac{y_{R,i}}{y_{f,i}}\right)^{\hat{a}} \left(\frac{1-y_{R,i}}{1-y_{f,i}}\right)^{\hat{b}} \left(\frac{\beta - y_{R,i}}{\beta - y_{f,i}}\right) \tag{6.14}$$

Where:

$$\hat{a} = \frac{\beta}{1 - \lambda/D_j} - 1 \tag{6.15}$$

$$\hat{b} = \frac{1-\beta}{1 - \lambda/D_j} - 1 \tag{6.16}$$

$$\beta = \frac{\alpha_{PV}^{*}}{\alpha_{PV}^{*} - 1} \tag{6.17}$$

$$\lambda = \frac{E-1}{\alpha_{PV}^{*} - 1} \tag{6.18}$$

It should be noted that $\alpha_{PV}^{*} = \dfrac{K_i P_i^{sat} \gamma_i}{K_j P_j^{sat} \gamma_j}$ and is the intrinsic separation factor at ultimate vacuum.

Hence, with the knowledge of the cut-stage, ϕ, the total permeate flow, Q, and mean permeate composition of the solute, $\bar{y}_i$, can be evaluated via equations (6.5c) and (6.9) respectively. In addition, the overall organic removal efficiency can also be obtained via the following relationship:

$$\text{Removal Efficiency } \% = \frac{F_f x_{f,i} - F_R x_{R,i}}{F_f x_{f,i}} \times 100\% = \phi\left(\frac{\bar{y}_i}{x_{f,i}}\right) \times 100\% \tag{6.19}$$

6.4.2.2 Analytical solution for membrane area requirement

From equation (6.3), the solute flux at any point of the membrane is expressed:

$$y_i \frac{dq}{da} = K_i \left(P_i^{sat} \gamma_i x_i - \Theta_i P_p y_i\right) \tag{6.3}$$

188

By substituting equation (6.10) into (6.3) to eliminate variable x_i and integration of both sides of the equation, the following relationship is obtained:

$$\int_0^Q D_i \left(y_i + \frac{ED_i}{D_j - ED_i} \right) dq = \int_0^A K_i P_i^{sat} \gamma_i \left[\left(\frac{D_i(1-E)}{D_j - ED_i} - 1 \right) y_i + \frac{D_i(D_j - 1)}{D_j - ED_i} \right] da \quad (6.20a)$$

or

$$D_i \left[\int_0^Q y_i dq + \left(\frac{ED_i}{D_j - ED_i} \right) Q \right] = K_i P_i^{sat} \gamma_i \left[\left(\frac{D_i(1-E)}{D_j - ED_i} - 1 \right) \int_0^A y_i da + \left(\frac{D_i(D_j - 1)}{D_j - ED_i} \right) A \right]$$

$$(6.20b)$$

In order to evaluate the membrane area, integrals in equation (6.20b) need to be known. From equation (6.8), it is known that $\int_0^Q y_i dq = Q \cdot \bar{y}_i$. However, the integral $\int_0^A y_i da$ can not be evaluated directly. It can be expressed as the area averaged solute concentration of the permeate stream:

$$\frac{1}{A} \int_0^A y_i da = \frac{\int_0^A \left(\frac{J_i}{J_t} \right) da}{\int_0^A da} \quad (6.20c)$$

In organophilic pervaporation, very high solvent concentration of the feed is normally found. Thus, it is reasonable to assume that the total flux, J_t, at any point of the membrane is quasi constant due to the high concentration of solvent in the feed. The approximation of this integral can then be evaluated as follow:

$$\frac{1}{A} \int_0^A y_i da \cong \frac{\int_0^A J_i da}{\int_0^A J_t da} = \frac{\int_0^Q y_i dq}{\int_0^Q dq} = \bar{y}_i \quad (6.20d)$$

The difference between the values of integral $\frac{1}{Q} \int_0^Q y_i dq$ and $\frac{1}{A} \int_0^A y_i da$ is relatively small and a qualitative discussion is detailed in Appendix 4. By using equation (6.20d) the membrane area requirement for a continuous organophilic pervaporation unit can be solved analytically. A detailed derivation can also be obtained in the Appendix A4 and the solution is as follows:

Membrane area requirement:

$$A = \frac{F_f \phi \beta (\beta - \bar{y}_i)}{K_i P_i^{sat} \gamma_i (\beta - 1)(1 - \pi / D_i)} \qquad (6.21)$$

where :
$$\pi = \frac{\beta - \left[\frac{\overset{\bullet}{\alpha_{PV}}}{E} \lambda (1 - \bar{y}_i) + \bar{y}_i \right]}{\beta - 1} \qquad (6.22)$$

and β, λ are defined in equations (6.17) & (6.18).

The analytical solutions have provided a way for us to investigate the design and optimization of a pervaporation unit. Clearly, the area requirement would be reduced as the mass transfer coefficient for organic, K_i, increases. In addition, the organic component that has a high Henry constant (i.e. $P_i^{sat} \gamma_i^\infty$) at the feed may have a lower membrane area requirement. Due to the low concentration of organic at the feed, the mass transfer coefficient of water flux cannot be ignored in obtaining a low membrane area requirement and a high removal efficiency. It is interesting to note that by manipulating β in equation (6.21), the membrane area requirement solution can be transformed to:

$$A = \frac{F_f \phi (\beta - \bar{y}_i)}{K_j P_j^{sat} \gamma_j \beta (1 - \pi / D_i)} \qquad (6.23)$$

From equation (6.23), some might note that the membrane area will also increase if a high water resistant membrane was used. If a low-flux-high-selectivity membrane like PEBA is employed, one might expect a higher membrane area requirement to result. However, this is not the case in the findings of Meckl (1994) for their system, i.e. aqueous aniline separation by PEBA membrane. This is because the membrane area requirement does not solely depend on either the organic mass transfer coefficient nor water mass transfer coefficient of the membrane, but highly depends on both mass transfer coefficients. This can be observed from the integral form of equation (6.1) as shown below:

$$A = \int_{F_f}^{F_R} \frac{dF}{J_t} = \int_0^Q \frac{1}{J_t} dq \qquad (6.24a)$$

From equation (6.24), the area requirement is inversely proportional to the total flux through the membrane. Hence, a high-flux-high-selectivity membrane would significantly reduce the membrane area requirement and have a high quality permeate. In hydrophilic pervaporation, the invention of high-flux-high-selectivity PVA-PAN composite membrane by GFT (*Sulzer ChemTech*) indeed has led to the commercialization of these pervaporation units for organic dehydration. However, for organophilic pervaporation, according to Meckl (1994) and Baker et al (1997), in most cases, commercialized PDMS, EDPM composite membrane or PEBA homogeneous membrane were employed. These are either a high-flux-low-selectivity or low-flux-high-selectivity membranes. In either case, membrane area increases compared to the ideal of high-flux-high-selectivity membrane.

6.4.2.3 A simplified approach of membrane area approximation

Apart from the rigorous solutions like equations (6.21) and (6.23), for preliminary consideration, it is useful to have a simplified method to determine the membrane area within ±20% by a value averaging means. Since water flux in organophilic pervaporation is relatively constant, the membrane area can then be determined by the ratio of water flowrate in the permeate (Q_j) to the mean water flux ($\bar{J}_j$) through the membrane.

Assume that the mean water flux ($\bar{J}_j$) through the membrane can be determined by the following relationship:

$$\bar{J}_j = \frac{1}{A} \int_0^A J_j \, da = \frac{Q_j}{A} \cong K_j \left(P_j^{sat} \gamma_j \bar{x}_j - \Theta_j P_p \bar{y}_j \right) \qquad (6.24b)$$

where $\bar{x}_j$ and $\bar{y}_j$ are the mean mole fraction of water at the feed and permeate respectively. Knowing that $\bar{x}_j \cong 1$ and $Q_j = F_f \phi(1 - \bar{y}_i)$, the area can be approximated as follows:

191

$$A = \frac{Q_j}{J_j} \cong \frac{F_f}{K_i P_i^{sat} \gamma_i} \cdot \alpha_{PV}^* \cdot \frac{\phi}{\left(1 - (1 - \bar{y}_i)/D_j\right)} \qquad (6.24c)$$

Where $\alpha_{PV}^* = \frac{K_i P_i^{sat} \gamma_i}{K_j P_j^{sat} \gamma_j}$ and the parameters ϕ, $\bar{y}_i$ and D_j can be determined from equations (6.14), (6.9) and (6.12) respectively. Comparison between the rigorous method and simplified approximation will be carried out in a later section.

6.5 A Batch Mode Pervaporation Unit

In a batch mode pervaporation unit as shown in Fig. 6.4, VOC contaminated water is circulated through a pervaporation unit and the retentate stream is recycled back to the feed tank. The targeted organics are selectively permeated through the pervaporative membrane due to a vacuum at the permeate side and collected via condensation. The concentration in the feed tank will fall to the required level over time.
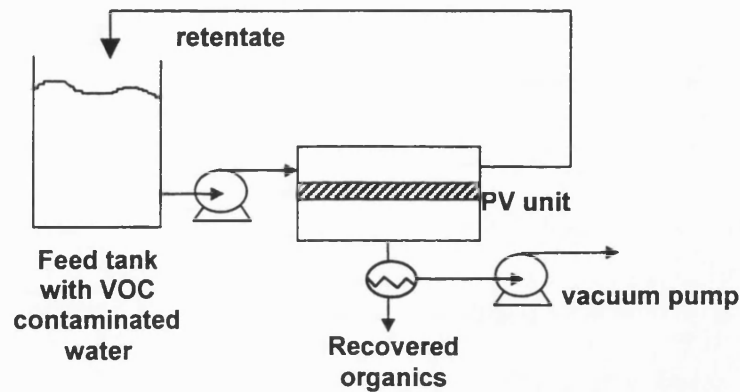
Fig. 6.4 Batch mode pervaporation unit

6.5.1 The material balance and the design equations

The material balance of a batch pervaporation unit has been considered as a non-steady state system. To model the system, a differential rate of change was used. Initially the feed tank has a total moles of m_1 and has a composition of organic $x_{1,i}$. After a period of operation, t_b (batch time), the total moles in the feed tank are reduced to m_2 and the composition of organic depleted to $x_{2,i}$. Since the application of a batch system usually implies a smaller pervaporation unit, the feed composition within the pervaporation unit can be assumed to be a well-mixed system as illustrated in Fig.6.5.
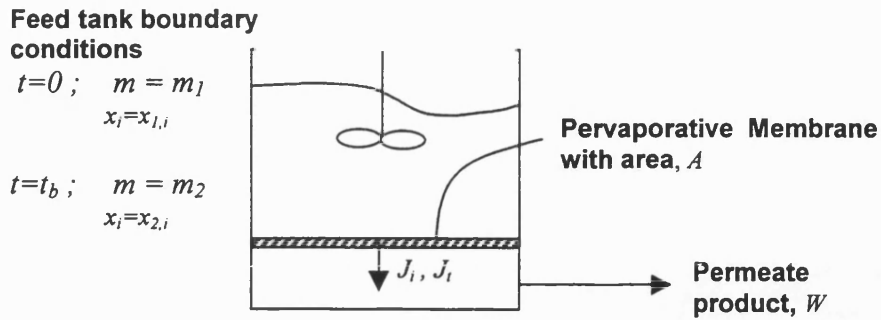
Fig. 6.5 A simplified well-mixed batch mode pervaporation unit

If the membrane area used is A, the material balance and design equations can be evaluated as followed:

Overall material balance:
$$-\frac{1}{A}\frac{dm}{dt} = J_t \tag{6.25}$$

Component material balance:
$$-\frac{1}{A}\frac{d(m \cdot x_i)}{dt} = -\frac{1}{A}\left(m\frac{dx_i}{dt} + x_i\frac{dm}{dt}\right) = J_t y_i \tag{6.26}$$

Mass transfer equation:

Component i (organic):
$$\frac{y_i}{A}\frac{dW}{dt} = J_t y_i = K_i\left(P_i^{sat}\gamma_i x_i - \Theta_i P_p y_i\right) \tag{6.27}$$

Component j (water):
$$\frac{y_j}{A}\frac{dW}{dt} = J_t y_j = K_j\left(P_j^{sat}\gamma_j x_j - \Theta_j P_p y_j\right) \tag{6.28}$$

where W is the product from the permeate side, kmol.

By dividing equation (6.26) by equation (6.25), the following relationship is established:

$$\ln\left(1 - \phi_{batch}\right) = \ln\left(1 - \frac{W}{m_1}\right) = \ln\left(\frac{m_2}{m_1}\right) = \int_{x_{1,i}}^{x_{2,i}}\frac{dx_i}{y_i - x_i} \tag{6.29}$$

Where the stage-cut for batch mode , $\phi_{batch} = W / m_1$, is defined as the ratio of permeate product to the total moles in the feed tank at $t = 0$. If a required stage-cut is given, it is possible to obtain the final composition, $x_{2,i}$ by iterating the *Rayleigh equation* to give a required area under the curve as performed in Fig. 6.3. When the batch time is reached (process completed, i.e. $t = t_b$), the following material balance is established:

$$m_1 x_{1,i} = W \cdot \bar{y}_i + m_2 x_{2,i} \qquad (6.30)$$

In practice, $\bar{y}_i$ and W are measurable quantities and are the indicators of the performance and efficiency of a pervaporation unit. Equation (6.30) can also be obtained by integrating equation (6.25) over the boundary conditions where W and $\bar{y}_i$ are the integrals stated below:

$$W = A \int_0^{t_b} J_i dt \qquad (6.31) \quad \text{and} \quad \bar{y}_i = \frac{A}{W} \int_0^{t_b} J_i dt = \frac{1}{W} \int_0^{W} y_i dW \qquad (6.32)$$

Knowing that the cut stage, $\phi_{batch} = W / m_1$, from equation (6.30), the average or mean composition of organic can be expressed in terms of stage cut and the composition of organic before and after the batch process:

$$\bar{y}_i = \frac{m_1 x_{1,i} - m_2 x_{2,i}}{W} = \frac{x_{1,i} - (1 - \phi_{batch}) x_{2,i}}{\phi_{batch}} \qquad (6.31)$$

The membrane area requirement for a batch mode pervaporation unit can be derived by solving equation (6.25) - (6.31).

6.5.2 An analytical solution for area requirement of a batch mode pervaporation unit

As in scaling up a continuous pervaporation unit, the analytical solution for membrane area requirement for the batch mode pervaporation unit is obtained through the evaluation of the stage cut, ϕ_{batch}. In deriving the membrane area requirement, the same assumptions as made to continuous pervaporation unit are equally applied to the batch mode. By substituting equation (6.10) into equation (6.29), the *Rayleigh equation* can be expressed as equation (6.13). Thus the analytical solution for ϕ_{batch} can be obtained as follow:

$$\text{Stage-cut}: \quad \phi_{batch} = \frac{W}{m_1} = 1 - \frac{m_2}{m_1} = 1 - \left(\frac{y_{2,i}}{y_{1,i}} \right)^{\hat{a}} \left(\frac{1 - y_{2,i}}{1 - y_{1,i}} \right)^{b} \left(\frac{\beta - y_{2,i}}{\beta - y_{1,i}} \right) \qquad (6.32)$$

Where the boundary conditions $y_{i,1}$ and $y_{i,2}$ are the permeate concentration correspond to $x_{i,1}$ and $x_{i,2}$ respectively. Both $y_{i,1}$ and $y_{i,2}$ can be determined via equations (4.27a) & (4.27b) found in Chapter 4. The constants $\hat{a}$, $\hat{b}$ and β are determined from equation (6.15)-(6.18).

From equation (6.27), the solute flux at any point of the membrane is expressed:

$$\frac{y_i}{A}\frac{dW}{dt} = K_i\left(P_i^{sat}\gamma_i x_i - \Theta_i P_p y_i\right)$$ (6.27)

By substituting equation (6.10) into (6.27) to eliminate variable x_i and integrate both side of the equation, the following relationship is obtained:

$$\int_0^W D_i\left(y_i + \frac{ED_i}{D_j - ED_i}\right)dW = A\int_0^{t_b} K_i P_i^{sat}\gamma_i\left[\left(\frac{D_i(1-E)}{D_j - ED_i}\right)y_i + \frac{D_i(D_j-1)}{D_j - ED_i}\right]dt$$ (6.33a)

or

$$D_i\int_0^W y_i dW + \left(\frac{ED_i}{D_j - ED_i}\right)W = AK_i P_i^{sat}\gamma_i\left[\left(\frac{D_i(1-E)}{D_j - ED_i}\right)\int_0^{t_b} y_i dt + \left(\frac{D_i(D_j-1)}{D_j - ED_i}\right)t_b\right]$$

(6.33b)

In order to evaluate the membrane area, integrals in equation (6.33b) need to be known. From equation (6.32), it is known that $\int_0^W y_i dW = W \cdot \bar{y}_i$. However, the integral $\int_0^{t_b} y_i dt$ can not be evaluated directly and it can expressed as time average solute concentration at permeate stream:

$$\frac{1}{t_b}\int_0^{t_b} y_i dt = \frac{\int_0^{t_b}\left(\frac{J_i}{J_t}\right)dt}{\int_0^{t_b}dt}$$ (6.33c)

In organophilic pervaporation, very low feed concentration is often found. Thus, for batch mode organophilic pervaporation, it is reasonable to assume that the total flux, J_t, at any batch time of the membrane is quasi constant due to the high concentration of solvent in the feed. The approximation of this integral can then be evaluated as follow:

196

$$\frac{1}{t_b}\int_0^{t_b} y_i \, da \cong \frac{\int_0^{t_b} J_i \, dt}{\int_0^{t_b} J_i \, dt} = \frac{\int_0^{W} y_i \, dW}{\int_0^{W} dW} = \overline{y}_i \qquad (6.33d)$$

Hence, the membrane area requirement for an organophilic pervaporation in a batch mode unit can be determined analytically as follows:

Area requirement:
$$A = \frac{m_1 \phi_{batch} \beta (\beta - \overline{y}_i)}{t_b K_i P_i^{sat} \gamma_i (\beta - 1)(1 - \pi / D_i)} \qquad (6.34)$$

It should be noted that the constant π can be evaluated from equation (6.22) and β, λ are defined in equations (6.17) & (6.18) respectively.

A simplified approach to estimate the membrane area can also be obtained by using the averaging means. Assume that the mean solvent flux $(\overline{J}_j)$ through the membrane can be determined as follows:

$$\overline{J}_j = \frac{W_j}{t_b A} \cong K_j \left(P_j^{sat} \gamma_j \overline{x}_j - \Theta_j P_p \overline{y}_j \right) \qquad (6.35a)$$

where $\overline{x}_j$ and $\overline{y}_j$ are the mean mole fractions of water at the feed and permeate respectively. Knowing that $\overline{x}_j \cong 1$ and $W_j = m_1 \phi(1 - \overline{y}_i)$, the area can be approximated as follow:

$$A = \frac{W_j}{t_b \overline{J}_j} \cong \frac{m_1}{t_b K_i P_i^{sat} \gamma_i} \cdot \alpha_{PV}^* \cdot \frac{\phi}{\left(1 - (1 - \overline{y}_i)/D_j\right)} \qquad (6.35b)$$

Where $\alpha_{PV}^* = \dfrac{K_i P_i^{sat} \gamma_i}{K_j P_j^{sat} \gamma_j}$ and the parameters ϕ, $\overline{y}_i$ and D_j can be determined from equation (6.14), (6.9) and (6.12) respectively.

From equation (6.34) & (6.35b), the membrane area requirement for a batch mode unit seems to be similar to the area equation (6.21) & (6.24c) for continuous mode except the feed flow rate in the continuous mode equation has been replaced by the ratio of initial total moles in the feed tank, m_l to the batch time, t_b . Hence, a relationship between continuous mode and batch pervaporation unit can be derived provided the operating conditions are the same.

$$\frac{A_{continuous}}{A_{batch}} = \frac{F_f t_b}{m_1} \qquad (6.35c)$$

This relationship permits one to design batch mode units using results from programmes designed for units with a continuous feed.

6.6 Design Concept of Transfer Units – An analogy to gas stripping

The design concept of transfer units was originally proposed by Chilton and Colburn (1935) and been used extensively for design and scale-up purposes for gas absorption (and stripping). A similar design approach for organophilic pervaporation unit should be feasible and has been used by Meckl (1994).

6.6.1 Performance characterization of a gas stripper

In the gas stripping process, the differential mass balance can be formulated as follows if the component to be stripped is dilute:

$$-\dot{m}_G \frac{dy}{dz} = K_G a \left(y - y^* \right)$$ (6.36)

where $\dot{m}_G$ is the molar feed flow rate of the gas stream to be stripped, z is the differential height of the column, $K_G a$ is the overall mass transfer coefficient in the gas, y is the gas phase composition of the component to be stripped and y^* is the gas phase compositions which would be in equilibrium with the liquid.

If $y \gg y^*$, equation (6.36) can be easily integrated over the inlet and outlet compositions boundary conditions. Thus, the height of the column, H can be evaluated easily as follows:

$$H = \frac{\dot{m}_G}{K_G a} \ln \frac{y_{in}}{y_{out}}$$ (6.37)

More complex relationships exist when y^* is significant. According to the transfer unit design concept, the theoretical height of the gas stripper is the product of HTU (Height per Transfer Units) and NTU (Number of Transfer Units) where their definitions are as follows:

$$H = HTU \times NTU$$ (6.38)

where   HTU (Heigth of Transfer Units) $= \dfrac{\dot{m}_G}{K_G a}$ (6.39)

NTU (Number of Transfer Units) $= \ln \dfrac{y_{in}}{y_{out}}$ (6.40)

It should be noted that the NTU definition can be complicated by vapour-liquid equilibrium relationship and the assumptions made for the design. However, the HTU definition can stay the same. In order to improve the design of a gas stripper, one could reduce HTU by improving the mass transfer coefficient or area of contact through the use of a different packing. NTU represents the difficulty of stripping conditions. Through such analysis, correlations can be established and optimization for column design is made possible.

6.6.2 Performance characterization in pervaporation unit

Firstly, consider organophilic pervaporation with a very dilute VOC in the aqueous feed that is to be removed from the feed. Assume that both the cut stage and the permeate pressure are very low ($\phi \to 0$ or $F_f \to F_R$, $P_p \to 0$). For this limiting case, the differential mass balance can be simplified as follow:

$$-F_f \frac{dx_i}{da} = J_i = K_i P_i^{sat} \gamma_i x_i$$ (6.41)

Thus, by integrating equation (6.41) over the inlet and outlet boundary conditions, the area requirement of a pervaporation unit is found to be:

$$A = \frac{F_f}{K_i P_i^{sat} \gamma_i} \ln \frac{x_{f,i}}{x_{R,i}}$$ (6.42)

By analogy to the gas stripper, the membrane area requirement is the product of ATU (Area per Transfer Units) and NTU (Number of Transfer Units) where their definitions are formulated as:

$$A = ATU \times NTU$$ (6.43)

where   ATU (Area of Transfer Unit) $= \dfrac{F_f}{K_i P_i^{sat} \gamma_i}$ (6.44)

NTU (Number of Transfer Unit) $= \ln \dfrac{x_{f,i}}{x_{R,i}}$ (simple form)   (6.45)

As in gas stripping, the NTU definition of a pervaporation unit can be complicated by the permeate pressure and the selectivity of the membrane, however, the ATU definition can remain the same. In order to improve the design of a pervaporation unit, one can reduce ATU by using a highly permeable composite membrane that retains an acceptable selectivity towards target component or raise the temperature of the feed or redesign the module for better feed side mass transfer.

Secondly, for analysis purposes, it is not essential to make simplifying assumptions. ATU and NTU of both continuous and batch pervaporation unit based on equation (6.21) & (6.34) were obtained and tabulated as below.

Table 6.1: ATU and NTU definitions for pervaporation unit

Mode of operation	Continuous	Batch	Both continuous and batch	
			NTU	
	ATU	ATU	Rigorous method Eq. (6.21) & (6.34)	Simplified Approach Eq. (6.24c) & (6.35b)
Vacuum pressure $P_p > 0$	$\dfrac{F_f}{K_i P_i^{sat} \gamma_i}$	$\dfrac{m_1}{t_b K_i P_i^{sat} \gamma_i}$	$\dfrac{\phi \beta (\beta - \bar{y}_i)}{(\beta - 1)(1 - \pi / D_i)}$	$\alpha_{PV}^{*} \cdot \dfrac{\phi}{\left(1 - (1 - \bar{y}_i)/D_j\right)}$
Vacuum Pressure $P_p \to 0$			$\dfrac{\phi^{*} \beta (\beta - \bar{y}_i^{*})}{\beta - 1}$	$\alpha_{PV}^{*} \cdot \phi^{*}$

Where ϕ^{*} and $\bar{y}_i^{*}$ are determined by using equations (6.14) & (6.9) at $P_p = 0$.

It is interesting to find that the NTU based on the rigorous analytical solutions and the simplified solutions are solely a function of E, α^{*}_{PV}, permeate pressure and the difficulty of

separation. For ATU, is a function of feed flow rate, membrane permeability and the Henry's law constant of the organic to be removed from the aqueous feed.

Based on the rigorous analytical solution obtained, its applicability was extended to gas/vapour permeation through a membrane. Compared to gas permeation, the solutions were found similar to the one derived by Saltonstall (1987):

$$\text{Area requirement for gas permeation} = \frac{F_f}{K_i^G p_f} \times \frac{\phi_G \beta_G (\beta_G - \bar{y}_i)}{(\beta_G - 1)(1 - 1/D)} \tag{6.46a}$$

$$\text{Stage-cut } (\phi_G) \text{ for gas permeation} = = 1 - \left(\frac{y_{R,i}}{y_{f,i}}\right)^{\hat{a}_G} \left(\frac{1 - y_{R,i}}{1 - y_{f,i}}\right)^{\hat{b}_G} \left(\frac{\beta - y_{R,i}}{\beta - y_{f,i}}\right) \tag{6.46b}$$

$$\text{where } K_i^G = \frac{\hat{P}_{m,i}^G}{\delta_m} \quad (6.47a), \qquad \beta_G = \frac{\alpha_{GS}^*}{\alpha_{GS}^* - 1} \quad (6.47b), \qquad \alpha_G^* = \frac{\hat{P}_{m,i}^G}{\hat{P}_{m,j}^G} \tag{6.47c}$$

$$\hat{a}_G = \frac{\beta}{1 - 1/D} - 1 \quad (6.47d) \qquad \hat{b}_G = \frac{1 - \beta}{1 - 1/D} - 1 \quad (6.47e), \qquad D = \frac{p_f}{P_p} \tag{6.47f}$$

The stage-cut (ϕ_G) in Saltonstall's solution also resembles to the one derived in equation (6.14) except in gas permeation the value of E is actually equal to the ideal separation factor α_{GS}^*, hence, the value of $\lambda = 1$ in gas permeation. it should be noted that in Saltonstall's derivation, the membrane resistance is assumed to be dominated by the top selective layer, hence, the permeability of the selective layer determine the ideal separation factor. In gas permeation, the membrane area is dependent on the ratio of feed side pressure (p_f) to the permeate pressure (P_p) whilst in pervaporation it is dependent on the ratio of pseudo-partial pressure (f_i) to the permeate pressure (P_p).

By using the rigorous analytical solutions obtained in pervaporation and gas permeation, ATU and NTU definitions can be tabulated as shown in Table 6.2. In order to take advantage of the similarity between pervaporation and gas/vapour permeation, a comparison of the parameters are also shown in Table 6.3. Unlike HMU definition proposed by Hwang and Thorman (1980), the ATU definition in the present study is well defined and able to be

partitioned from the driving force. In addition, HMU is restricted to a continuous membrane unit only but the ATU definition developed here is applicable to different mode of operation.

Table 6.2: Comparison between pervaporation and gas/vapour permeation

Membrane separation		Pervaporation	Gas / vapour permeation [Based on Eq. (6.46a) in Saltonstall (1987) solution]
ATU	$P_p \geq 0$	$\dfrac{F_f}{K_i P_i^{sat} \gamma_i}$	$\dfrac{F_f}{K_i^G p_f}$
NTU	$P_p > 0$	$\dfrac{\phi \beta (\beta - \bar{y}_i)}{(\beta - 1)(1 - \pi / D_i)}$	$\dfrac{\phi_G \beta_G (\beta_G - \bar{y}_i)}{(\beta_G - 1)(1 - 1/D)}$
	$P_p \rightarrow 0$	$\dfrac{\phi \beta (\beta - \bar{y}_i)}{\beta - 1}$	$\dfrac{\phi_G \beta_G (\beta_G - \bar{y}_i)}{(\beta_G - 1)}$

Table 6.3: Parameters comparison between pervaporation and gas/vapour

Parameters	Pervaporation	Gas/vapor permeation
Ideal separation factor	$\alpha^*_{PV} = (K_i/K_j) * \alpha_{VLE}$	$\alpha^*_{GS} = \hat{P}_{m,i} / \hat{P}_{m,j}$
Pressure ratio	$D_i = (P_i^{sat} \gamma_i x_i) / (P_p \Theta_i)$	$D = p_f / P_p$
E	$(K_i/K_j) * (\Theta_i / \Theta_i)$	$\alpha^*_{GS} = \hat{P}_{m,i} / \hat{P}_{m,j}$

Where $\hat{P}_{m,i}$ and $\hat{P}_{m,j}$ are the gas permeability of the membrane, p_f is the feed pressure.

6.6.3 Validation of approach and sample calculation

The derivation of the analytical solution for the membrane area of a continuous pervaporation unit is based on three assumptions: i.e. constant operating temperature and permeate pressure and concentration independent mass transfer coefficients. In the present study, the result of membrane area calculation will be demonstrated and compared to the results obtained from Bennett (1996) via numerical solution based on Euler techniques. Due to the energy required for permeate to evaporate from the membrane, particularly water which possesses a high latent heat of vaporisation, feed temperature will drop rapidly. In order to maintain satisfactory fluxes, interstage reheating is necessary. In solving the mass and energy balance equations, Bennett (1996) allows the feed temperature to drop not more than 15°C and it is then reheated back to the original feed temperature. The commercially available pervaporation sizing computer program, PVDESIGN 3.1 (supplied by Institut fur verfrahren technik, RWTH Aachen) is similar using a Runge-Kutta numerical solution technique. According to Bennett (1996), agreement was found to be extremely close (±2-3%) between his solutions and those obtained from PVDESIGN 3.1.

In the following calculation of membrane area requirement, the difference between analytical solution will be compared with Bennett (1996) solutions. In addition, the simplified approach will also be shown.

Example 6.1 Pyridine/water separation

A continuous organophilic pervaporation unit is modeled for the removal of pyridine from an effluent stream (1000kg/h). The required target pyridine concentration reduction is from 1 wt% to 300ppm, before the subsequent biological treatment process. A pure PDMS membrane with a thickness of 25μm was used to evaluate the membrane area requirement at 70°C feed temperature. The following are the parameters for the calculations:

Henry's law constant at 70°C for pyridine in water, $P_i^{sat}\gamma_i^{\infty}$ = 146 cmHg kmol/kmol

Pyridine feed side mass transfer coefficient (70°C), k_l = 0.09 m/h (=2.5 × 10^{-5} m/s)

Pyridine permeability in PDMS membrane (70°C), $\hat{P}_{m,i} = 3.53 \times 10^{-6}$ kmol/m²/h/cmHg/m

Water permeability in PDMS membrane (70°C), $\hat{P}_{m,j} = 4.65 \times 10^{-8}$ kmol/m²/h/cmHg/m

Operating permeate pressure, P_p = 0.566 cmHg (=7.54 mbar)

Saturated vapour pressure of pure water (P_j^{sat}) at 70°C = 23.34 cmHg

Density of water at 70°C   = 978 kg/m³

Molecular weight of water   = 18.02 kg/kmol

Calculation of overall mass transfer coefficients, K_i and K_j using equations (3.149)-(3.151):

$$K_i \cong \frac{1}{\dfrac{146 \times 18.02}{0.09 \times 978} + \dfrac{25 \times 10^{-6}}{3.53 \times 10^{-6}}} = \underline{9.935 \times 10^{-3}} \text{ kmol/m}^2\text{/h/cmHg}$$

$$K_j = \frac{4.65 \times 10^{-8}}{25 \times 10^{-6}} = \underline{1.86 \times 10^{-3}} \text{ kmol/m}^2\text{/h/cmHg}$$

Assuming that the desorption factors equal unity, E, D_i, D_j, λ and α^*_{PV} can be evaluated:

$E = (9.935 \times 10^{-3})/(1.86 \times 10^{-3}) = \underline{5.34}$

$D_i = 146/0.566 = \underline{257.92}$, $D_j = 23.34/0.566 = \underline{41.23}$

$\alpha^*_{PV} \cong (9.935 \times 10^{-3} \times 146)/(1.86 \times 10^{-3} \times 23.34) = \underline{33.42}$

$\lambda = (5.34-1)/(33.42-1) = \underline{0.1339}$

With the use of equation (4.27), the corresponding permeate composition at the feed and retentate were found to be $y_{f,i} = \underline{6.524 \times 10^{-2}}$ and $y_{R,i} = \underline{0.206 \times 10^{-2}}$. Hence, from equation (6.14), the stage cut, ϕ, is found to be 0.1151 kmol/kmol and the following table show the results obtained from rigorous analytical solution, simplified approach and the results from Bennett (1996):

Table 6.4 Comparison between analytical solution with the results from numerical solution from (Bennett, 1996) for pyridine/water separation

	Analytical solution [Equation (6.21)]	Simplified approach [Equation (6.24c)]	Numerical solution [*] (Bennett, 1996)
Membrane Area (m^2)	151	146	154
ATU (m^2)	37.96	37.96	37.96
NTU	3.99	3.83	4.06
Pyridine composition in the permeate product (wt%)	8.0	8.0	9.5
Product flowrate (kg/h)	122	122	102
Retentate flowrate (kg/h)	878	878	898

[*]Note: The result from (Bennett, 1996) allow 15°C feed temperature drop and reheat to 70°C.

It was found that membrane area and NTU determined from the rigorous analytical solution with the assumption of constant temperature has only 1.75% less than the one determined with the allowance for temperature drop. Although the permeate composition is underestimated and retentate flow rate is overestimated, the membrane area estimated is still reasonable. For the simplified approach, the area estimated is 5% smaller than the numerical solution and 3.3% smaller than the rigorous analytical solution. Despite such deviation, for preliminary considerations, the membrane area prediction from simplified approach is still quite reasonable. It should be noted that in the simplified approach, the evaluation of stage cut is based on the rigorous analytical solution provided in equation (6.14).

Example 6.2 MIBK/water separation

Another example of modeling a continuous organophilic pervaporation unit is for the removal of MIBK from an effluent stream (1000kg/h) of a MIBK production plant. The required target MIBK concentration reduction is from 1 wt% to 10ppm, before discharged into a general water system. A pure PDMS membrane with thickness of 50µm was used to evaluate the membrane area requirement for a 70°C feed temperature. The following are the parameters for the calculations:

Henry's law constant at 70°C for MIBK in water, $P_i^{sat}\gamma_i^{\infty}$ = 3438 cmHg kmol/kmol

MIBK feed side mass transfer coefficient at 70°C, k_l = 0.09 m/h (=2.5 × 10^{-5} m/s)

MIBK permeability in PDMS membrane (70°C), $\hat{P}_{m,i}$ = 2.613 × 10^{-7} kmol/m²/h/cmHg/m

Water permeability in PDMS membrane (70°C), $\hat{P}_{m,j}$ = 5.482 × 10^{-8} kmol/m²/h/cmHg/m

Operating permeate pressure, P_p = 0.903 cmHg (=12.03 mbar)

The results from analytical solutions and numerical solutions are tabulated in Table 6.5.

Table 6.5 Comparison between analytical solution with the results from a numerical solution (Bennett, 1996) for MIBK/water solution

	Analytical solution [Equation (6.21)]	Simplified approach [Equation (6.24c)]	Numerical solution * (Bennett, 1996)
Membrane Area (m²)	102	101	111
ATU (m²)	14.34	14.34	14.34
NTU	7.11	7.06	7.74
MIBK composition in the permeate product (wt%)	18.2	18.2	18.9
Product flowrate (kg/h)	55	55	53
Retentate flowrate (kg/h)	945	945	947

*Note: The result from Bennett (1996) allows 15°C feed temperature drop and reheats to 70°C.

From Table 6.5, the membrane area determined from the analytical solution is about 8% smaller than the one determined by the numerical solution, which allows for the temperature drop. It is interesting to note that in the case of MIBK/water separation, the difference between the area that estimated with the simplified approach and rigorous analytical solution is less than 1%.

6.6.4 Factors that influence pervaporation unit design

From the design point of view, it is important to recognize how the process parameters and membrane selection influence the scale-up and design process. From the analytical solutions obtained from the previous section, the factors that influence the membrane area requirement and the quality of the permeate can be identified from ATU, NTU, $\bar{y}_i$ and θ functions:

$$\text{ATU} = f\left(F_f, K_i, P_i^{sat}\gamma_i^\infty\right) \text{ or} = f\left(m_l, t_b, K_i, P_i^{sat}\gamma_i^\infty\right) \tag{6.48a}$$

$$\text{NTU} = f\left(E, \Theta_i, \Theta_j, P_p, P_i^{sat}\gamma_i^\infty, P_j^{sat}\gamma_j, x_{f,i}, x_{R,i}\right) \tag{6.48b}$$

$$\bar{y}_i = f\left(E, \Theta_i, \Theta_j, P_p, P_i^{sat}\gamma_i^\infty, P_j^{sat}\gamma_j, x_{f,i}, x_{R,i}\right) \tag{6.48c}$$

$$\theta = f\left(E, \Theta_i, \Theta_j, P_p, P_i^{sat}\gamma_i^\infty, P_j^{sat}\gamma_j, x_{f,i}, x_{R,i}\right) \tag{6.48d}$$

From equations (6.48a)-(6.48d), the influencing factors can be categorized as membrane characteristics (K_i, E, Θ_i and Θ_j), component volatility ($P_i^{sat}\gamma_i^\infty$ and $P_j^{sat}\gamma_j$), operating process parameters (F_f, m_l, t_b, P_p), and the degree of separation ($x_{f,i}$ and $x_{R,i}$).

In this section, the influence of process conditions and membrane systems upon the design of a pervaporation unit are studied for, Class A (Pyridine/water) and class C (MIBK/water) systems.

6.6.4.1 The effect of permeate pressure

The driving force of pervaporation is realized by the lowering of the permeate pressure, hence, the operating permeate pressure will affect the throughput and quality of the permeate of a pervaporation plant. This affects NTU and not ATU. From equations (6.46)-(6.49), the permeate pressure affects the magnitude of NTU, $\bar{y}_i$ and θ. Figs. 6.6 - 6.11 show the effect of permeate pressure, P_p, upon NTU, concentration in the permeate product and mass cut-

stage for the two chosen systems. The calculations are based on the assumption of unity for the desorption factors and 70°C.
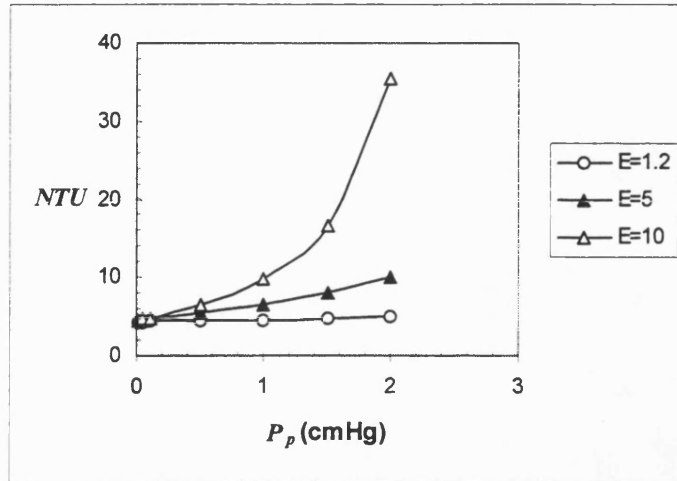
Fig. 6.6 The effect of permeate pressure upon NTU required for pyridine/water separation at 70°C ($w_{f,i}$ = 0.05, $w_{R,i}$ = 0.0005)
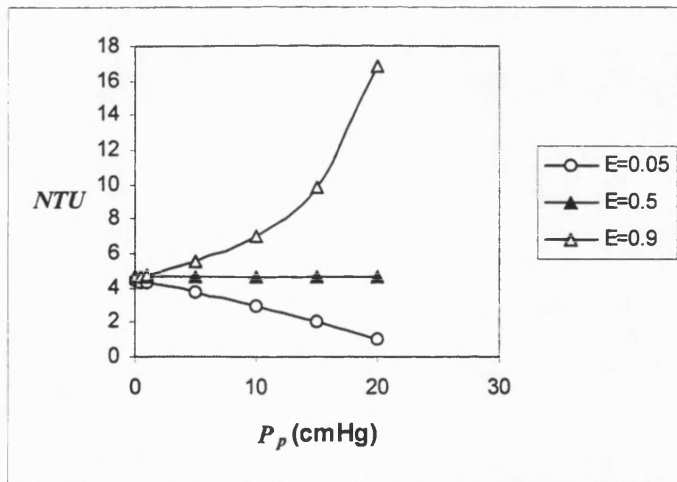
Fig. 6.7 The effect of permeate pressure upon NTU required for MIBK/water separation at 70°C ($w_{f,i}$ = 5×10^{-3}, $w_{R,i}$ = 5×10^{-5})
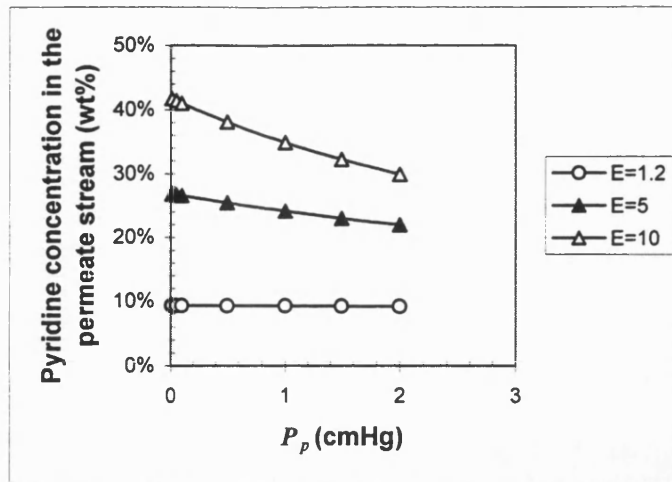
Fig. 6.8 The effect of permeate pressure upon pyridine concentration

in permeate stream for pyridine/water separation at 70°C

($w_{f,i}$ = 0.05, $w_{R,i}$ = 0.0005)
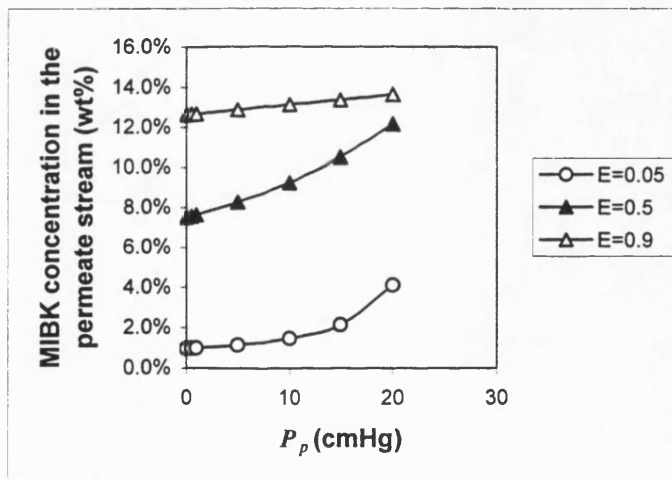
Fig. 6.9 The effect of permeate pressure upon MIBK concentration

in permeate stream for MIBK/water separation at 70°C

($w_{f,i}$ = 5×10^{-3}, $w_{R,i}$ = 5×10^{-5})
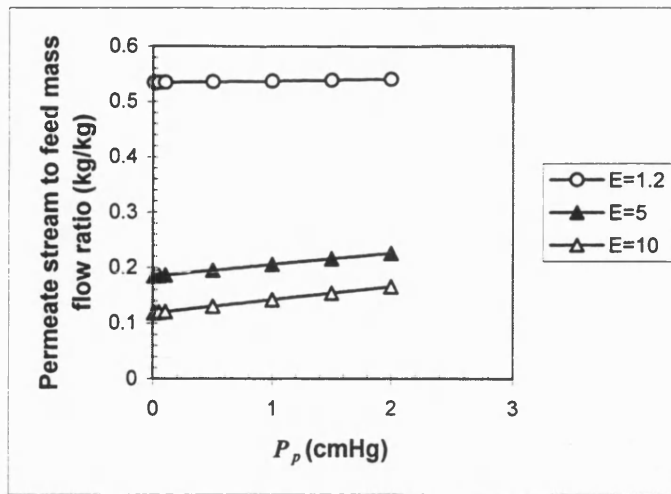
Fig. 6.10 The effect of permeate pressure upon ratio of permeate stream to feed flowrate for pyridine separation at 70°C ($w_{f,i}$ = 0.05, $w_{R,i}$ = 0.0005)
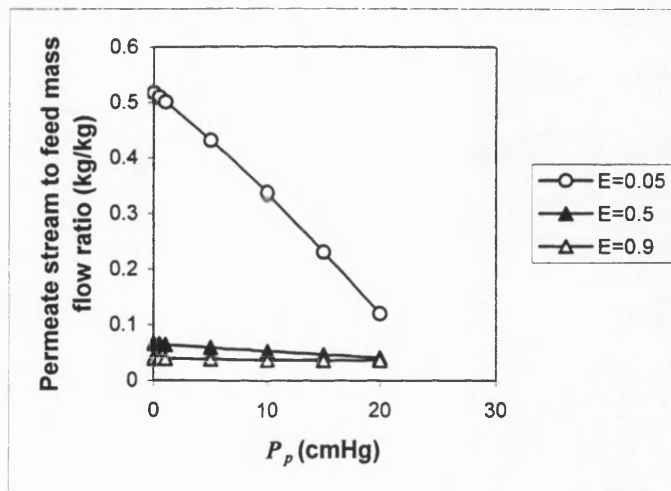
Fig. 6.11 The effect of permeate pressure upon ratio of permeate stream to feed ratio for MIBK separation at 70°C ($w_{f,i}$ = 5×10^{-3}, $w_{R,i}$ = 5×10^{-5})

From Fig. 6.6, the permeate pressure sensitivity of NTU for class A system increases with an increase of E. According to the engineering analysis in Chapter 4, for class A systems with high values of E, the separation factor is higher but the performance will decline with a steeper slope as permeate pressure increases. Such a decline of separation demands a greater number of transfer units to reach the target residue concentration. However, it should be noted that if E increases whilst K_j is constant then the permeability of the organic K_i is

211

increasing and ATU is inversely proportional to K_i. Nevertheless, in order to obtain a reasonable permeate quality and a reduction of membrane area usage, the effect of permeate pressure on module design should be shown due regard for class A membrane systems, especially those with a high E value. However, the observations for a class C membrane system in Fig. 6.7 is totally opposite to the class A system and higher operating permeate pressure is allowed. There is an increase of the MIBK flux to water flux ratio as permeate pressure increases; the separation performance is enhanced. It is interesting to note that at $E =$ 0.5, the NTU is relative constant over a wide range of permeate pressure.

For class A membrane system, due to the increase of NTU and the decline of permeate quality as permeate pressure increases, more water has to be drawn across the membrane if the unit is to reach the target retentate concentration. Hence, the permeate product to feed mass flow increases as the permeate pressure increases (see Fig. 6.10). The magnitude of this ratio decreases as the value of E increases. However, the opposite effect is observed in Fig. 6.11 for the class C membrane system. For a class C membrane system, owning to the increase of separation performance as the permeate pressure increases, the water flux is greatly reduced when the unit is operated at higher permeate pressure. Hence, the permeate product to feed mass ratio decreases as permeate pressure increases.

6.6.4.2 The effect of difficulty of separation

The difficulty of separation is defined as the ratio of feed to retentate concentration ($w_{f,i}/w_{R,i}$) and in general, from Fig. 6.12 – 6.17, the higher the difficulty of separation, the greater the demand of number of transfer units, and the poorer the quality of permeate. Hence the greater the permeate product to feed mass flow ratio. From Fig. 6.12 – 6.13, the NTU is approximately proportional to the logarithm of the separation difficulty. A similar effect can be observed from permeate quality and mass cut-stage in Fig. 6.14 – 6.17. With respect to the increase of E the slopes increase for NTU and mass-cut-stage and decrease for permeate quality. This is so for both class A and class C membrane systems.
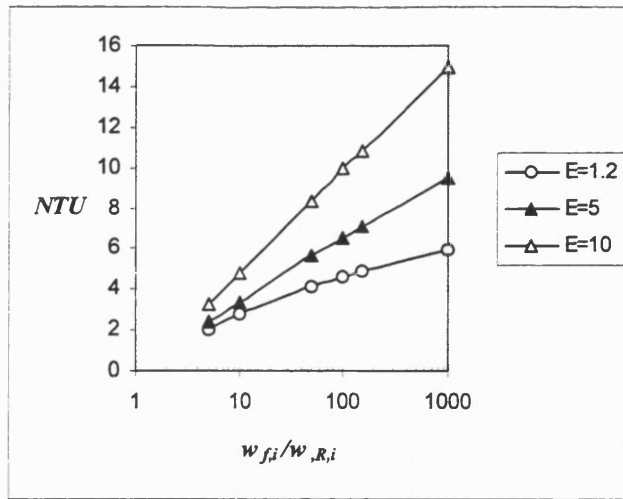
Fig. 6.12 The effect of pyridine separation difficulty upon NTU at 70°C

($w_{f,i}$ =0.05, P_p =1cmHg)
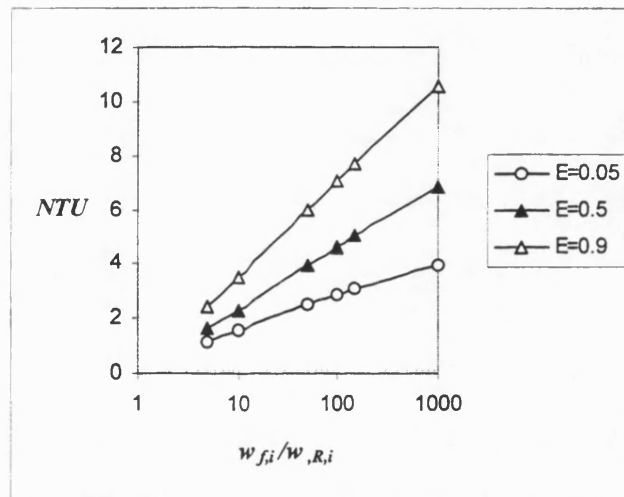
Fig. 6.13 The effect of MIBK separation difficulty upon NTU at 70°C

($w_{f,i}$ = 5×10^{-4}, P_p =10cmHg)
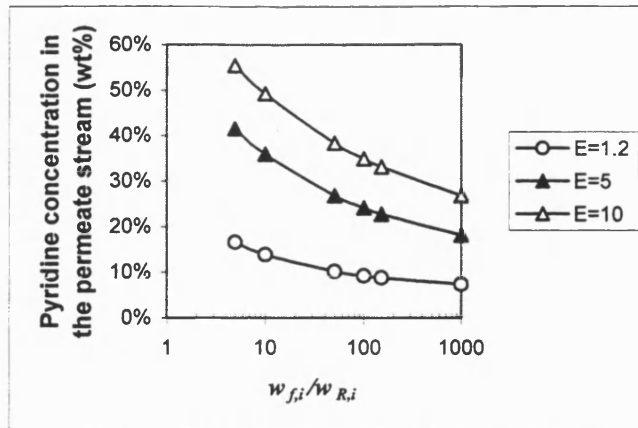
Fig. 6.14 The effect of pyridine separation difficulty upon pyridine

concentration in the permeate at 70°C

($w_{f,i}$ =0.05, P_p =1cmHg)
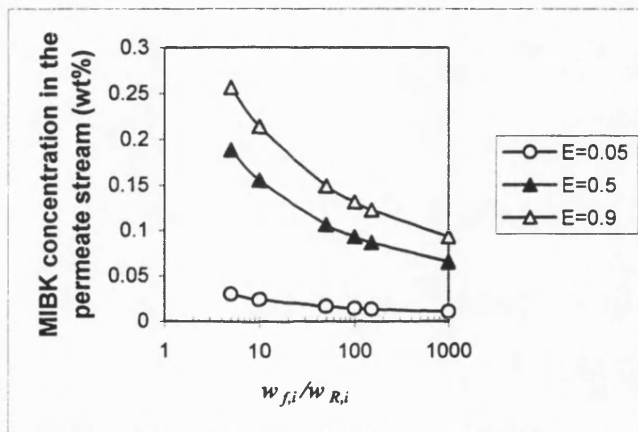
Fig. 6.15 The effect of MIBK separation difficulty upon pyridine

concentration at the permeate at 70°C

($w_{f,i}$ = 5×10⁻⁴, P_p =10cmHg)
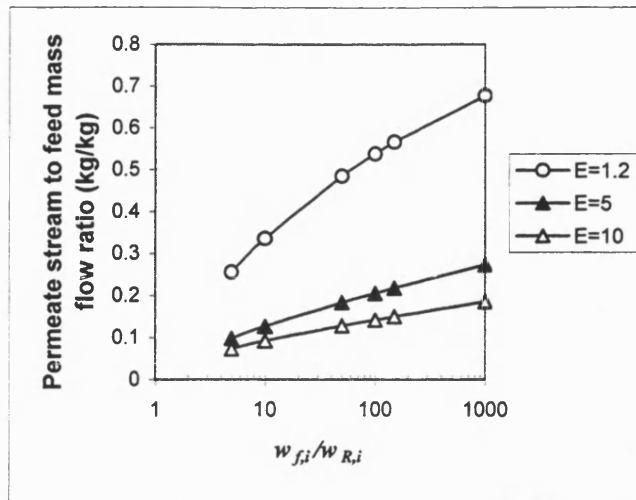
Fig. 6.16 The effect of pyridine separation difficulty upon permeate stream to feed ratio

at 70°C ($w_{f,i}$ =0.05, P_p =1cmHg)
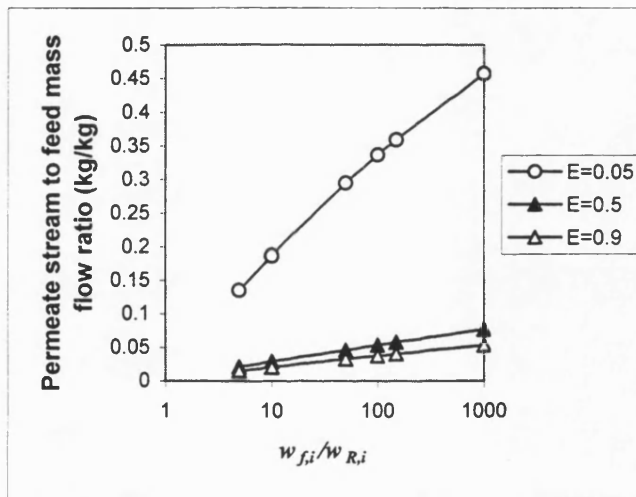
Fig. 6.17 The effect of MIBK separation difficulty upon permeate stream to feed at 70°C

($w_{f,i}$ = 5×10^{-4}, P_p =10cmHg)

6.6.4.3 The effect of the magnitude of E

In Chapter 4 and 5, E is an engineering analysis parameter that is used to determine the performance profile of organophilic pervaporation. Recall equation (4.34) in Chapter 4, E is dependent upon the mass transfer coefficients and the ratio of partition coefficients.

$$E = \frac{K_i \Theta_i}{K_j \Theta_j} = E^* \frac{\Theta_i}{\Theta_j} = \varepsilon_{bl} E^*_{mem} \frac{\Theta_i}{\Theta_j} \tag{4.34}$$

Hence, a membrane system with high ε_{bl} and high E^*_{mem} would exhibit a higher E and subsequently a high α^*_{PV}.

Consider a membrane system with $E \gg 1$ (implies $\alpha^*_{PV} \gg 1$), parameters that are used to evaluate stage cut from equations (6.15)-(6.18) have the following limits: $\beta \to 1$; $\lambda \to E/\alpha^*_{PV}$; $\hat{a} \to 1/(D_j \alpha^*_{PV}/E-1)$; $\hat{b} \to -1$. Thus, stage-cut at $E \gg 1$ becomes:

$$\phi \to 1 - \left(\frac{y_{R,i}}{y_{f,i}} \right)^{\hat{a}} \tag{6.49a}$$

Both $y_{R,i}$ and $y_{f,i}$ can be solved from equation (6.10).

For those membrane systems with $E \gg 1$, (and hence high value of α^*_{PV}), a large amount of the solute is removed from the initial segment of membrane area. Hence, the larger E, the larger the decrease of solute driving force across the subsequent segments of membrane area. So it is reasonable to assume that the total flux at most of the segments of the membrane is quasi constant. Thus, the approximation in equation (6.20d) is valid, i.e. $\frac{1}{A} \int_0^A y dA \cong \frac{1}{Q} \int_0^Q y dq = \bar{y}_i$. This enables one to use equation (6.21) to evaluate membrane area. As $E \gg 1$ (implies $\alpha^*_{PV} \gg 1$), $\lambda \to E/\alpha^*_{PV}$ and hence, from equation (6.22) $\pi \to 1$ and as $\beta \to 1$ the analytical solution for membrane area in equation (6.23) becomes:

$$A \to \frac{F_f \phi(1-\bar{y}_i)}{K_j P_j^{sat} \gamma_j (1-1/D_i)} = \frac{F_f}{K_i P_i^{sat} \gamma_i} \times \alpha_{PV}^* \frac{\phi(1-\bar{y}_i)}{(1-1/D_i)}$$ (6.49b)

where $\alpha_{PV}^* = \dfrac{K_i P_i^{sat}}{K_j P_j^{sat}}$

From equation above, $NTU \to \alpha_{PV}^* \dfrac{\phi(1-\bar{y}_i)}{(1-1/D_i)}$ as $E \gg 1$ (6.49c)

In general, from Fig. 6.19 - 6.23, NTU and permeate quality increases with an increase of E values, and the mass cut-stage decreases as E increases. If a membrane system possesses a higher value of E, it implies a higher separation can be achieved by the membrane and better feed side mass transfer performance of the module. However, NTU would inevitably increase. Unless the membrane possesses a high value of organic mass transfer coefficient (K_i) hence a lower ATU that is able to compensate the increase of NTU, the membrane area requirement will bound to increase dramatically. In practice, the cost for membrane, casing, pumps and permeate quality will be critical to the implementation of a design. Hence a judgement on whether to select a membrane system with high E value or not will depend on the specification and requirement of separation.

It is interesting to note from Fig. 6.18 that for a class A system, the sensitivity of NTU towards feed concentration is low for a constant separation difficulty and permeate pressure when E is less than 5. Such an effect is even more evident in a class C system. From Fig. 6.20-6.21, the permeate quality increases sharply when E is under 10 and 0.3 for class A and class C membrane systems respectively. On contrary, the permeate stream to feed mass flow ratio decreases sharply when E is more than 5 and 0.3 for class A and class C membrane systems respectively. From Fig. 6.19 – 6.23, the effect of separation difficulty overwhelms the effect of feed concentration, regardless the type of membrane system.
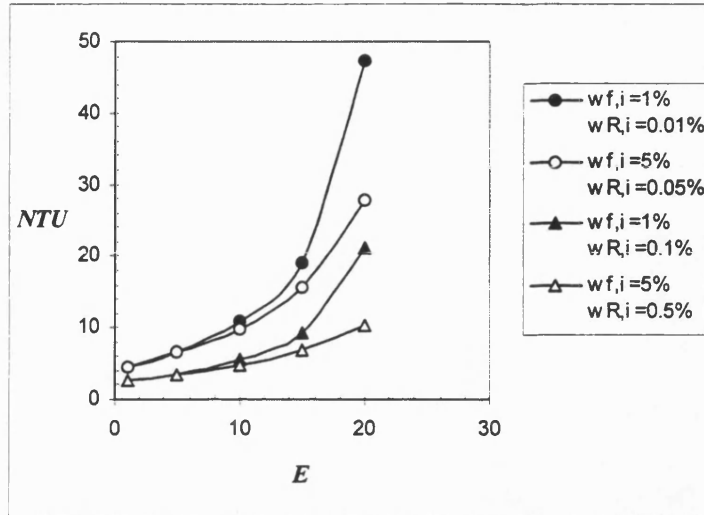
Fig. 6.18 The effect of E upon NTU in pyridine separation at 70°C (P_p =1cmHg)
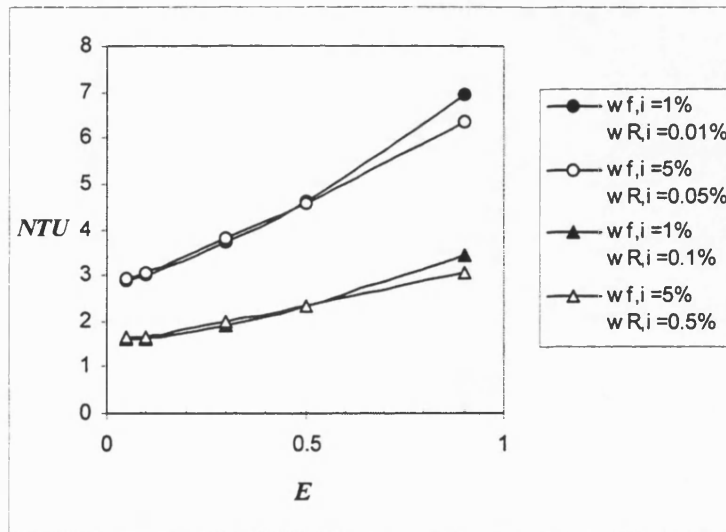
Fig. 6.19 The effect of E upon NTU in MIBK separation at 70°C (P_p =10cmHg)
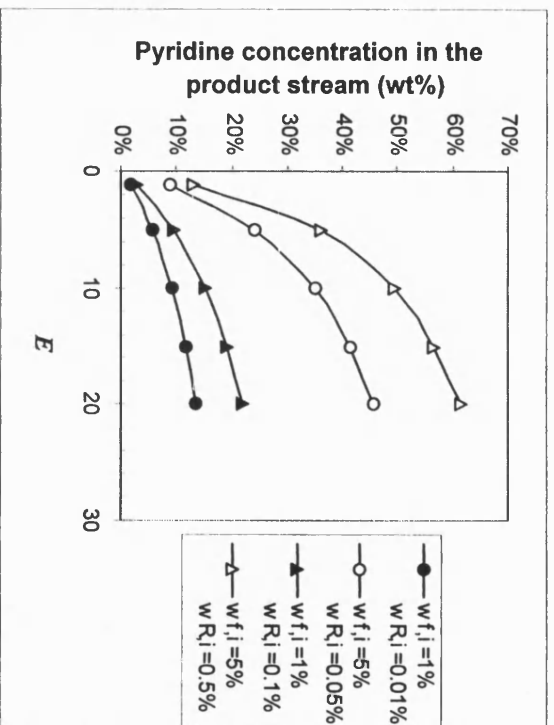
Fig. 6.20 The effect of E upon pyridine concentration in permeate
product in pyridine separation at 70°C(P_p =1cmHg)
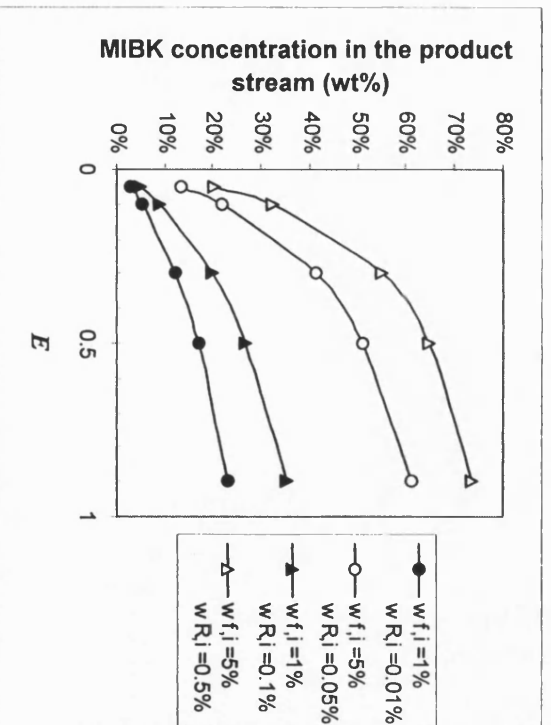
Fig. 6.21 The effect of E upon MIBK concentration in permeate
product in MIBK separation at 70°C(P_p =10cmHg)
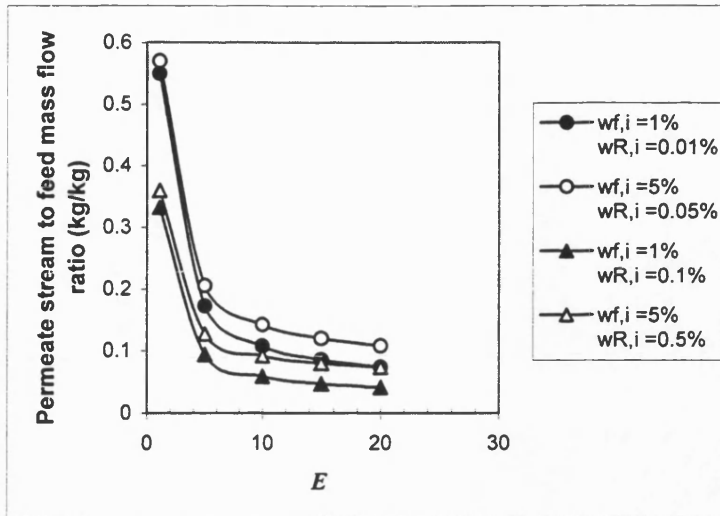
Fig. 6.22 The effect of E upon ratio of permeate stream to feed flowrate for pyridine separation at 70°C (P_p =1cmHg)
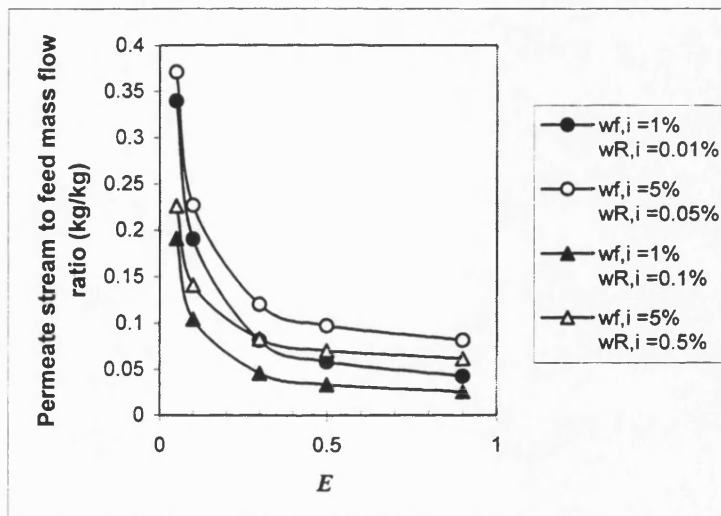
Fig. 6.23 The effect of E upon ratio of permeate stream to feed flowrate for MIBK separation at 70°C (P_p =10cmHg)

6.6.4.4 The effect of membrane permeability

From the definition of ATU in Table 6.2, ATU is inversely proportional to the mass transfer coefficient of the solute and the Henry constant of solute in the liquid feed. The rise of feed temperature would reduce ATU significantly. According to Bennett (1996), the permeability and selectivity of a membrane can be improved by the functionalisation of PDMS membrane. A case study of pyridine/water separation was used to investigate the effect of this functionalisation upon ATU with the assumption of negligible boundary layer resistance and the use of a membrane of thickness 25μm at 70°C. Such an effect is illustrated in a plot of ATU against ideal membrane selectivity at ultimate vacuum (α^{*}_{PV}) as shown in Fig. 6.23.
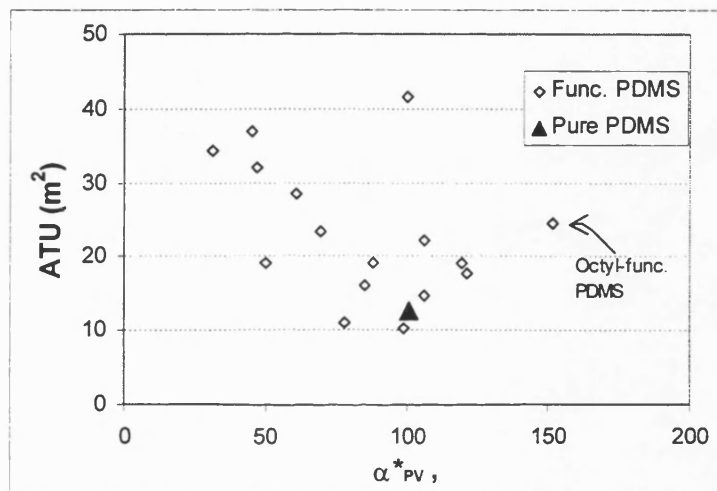
Fig. 6.24 The effect of PDMS functionalisation upon ATU and ideal selectivity for pyridine/water separation at 70°C

From Fig. 6.24, the octyl-functionalised PDMS shows a higher selectivity towards pyridine compared to pure PDMS, however, due to the lower membrane permeability towards pyridine in the octyl-functionalised PDMS membrane compared to pure PDMS, its ATU value is relatively higher than the one of pure PDMS. Hence, the high selectivity of octyl-functionalised PDMS is due to the high water resistance instead of higher organic permeability in the membrane. Overall, for ATU, the key membrane parameter is K_i whilst for NTU it is α^{*}_{PV}.

6.6.4.5 The effect of boundary layer resistance

The effect of boundary layer resistance upon the design of a module is very important when a volatile VOC is to be removed. Flux decrease and poorer separation often occur when the overall mass transfer is dominated by the boundary layer resistance. Fig. 6.25 shows the effect of boundary layer mass transfer effects upon membrane area requirement in the design of a pervaporation plant that is fed by an 1 wt% aqueous pyridine stream at 1000kg/h with a retentate requirement contain of 300ppm. The calculation assumes a constant operating temperature of 70°C and permeate pressure of 0.903 cmHg (=12mbar). The two cases considered are modules with liquid feed mass transfer coefficient, k_l. (a) 2.5×10^{-5} m/s and (b) 2.5×10^{-4} m/s.
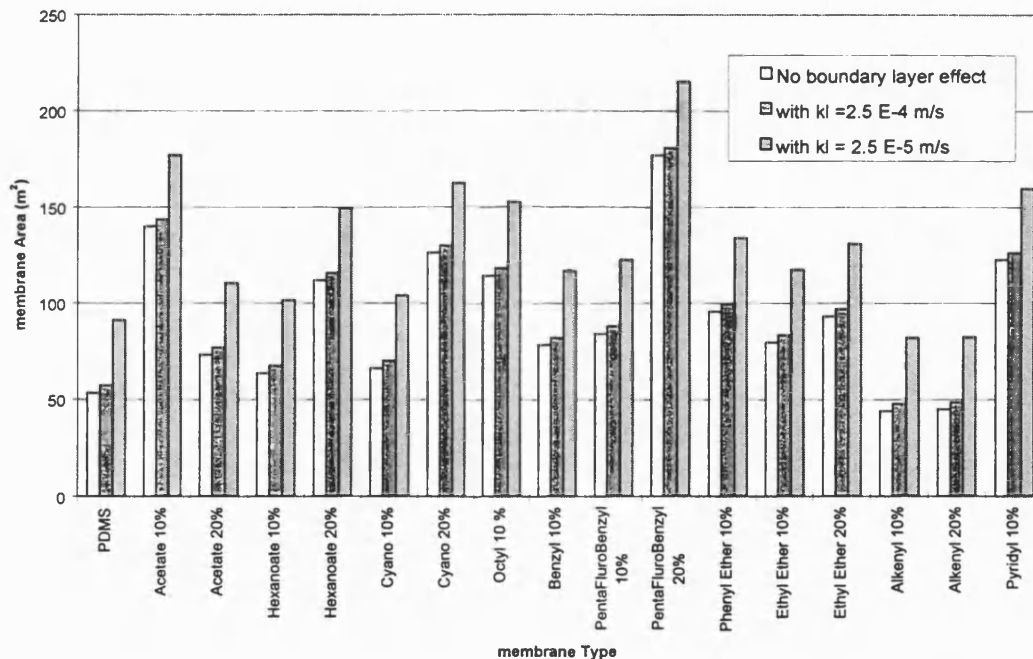
Fig. 6.25 The effect of boundary layer resistance upon membrane area requirement for pyridine/water separation.

As expected, Fig. 6.25 shows that the membranes with lower organic permeability are less sensitive to the magnitude of K_i . This is due to the low contribution of boundary layer resistance to the total resistance in low permeability membranes.

6.6.4.6 The effect of the composite nature of the membrane

In Chapter 5, a commercial PDMS composite membrane was tested for the separation of pyridine/water and MIBK/water. According to the definition of ATU, it is inversely proportional to the mass transfer coefficient and the feed liquid Henry's law constant ($P_i^{sat}\gamma_i^\infty$) of the organic. For a composite membrane, with the use of the resistance in series model, ATU can be written as follow:

$$ATU = \frac{F_f}{K_i P_i^{sat} \gamma_i^\infty} = \frac{F_f}{P_i^{sat} \gamma_i^\infty}\left(R_{bl} + R_{mem,i} + R_{sup,i}\right) \tag{6.50}$$

Composite membranes are required to provide the mechanical strength towards the membrane, however, due to the relatively thick porous support the resistance due to the filling of pores and permeability of the substructure matrix cannot be ignored. Hence, a relatively high ATU will be observed in composite membranes compared to the normalised thickness of a homogeneous membrane. The E value is also affected by the composite nature of the membrane since E is defined as:

$$E = \frac{K_i \Theta_i}{K_j \Theta_j} = \left(\frac{R_{mem,j} + R_{sup,j}}{R_{bl} + R_{mem,i} + R_{sup,i}}\right)\frac{\Theta_i}{\Theta_j} \tag{6.51}$$

Hence, a different NTU, a different organic concentration in the permeate and a different cut-stage will be observed for a composite membrane compared to a homogeneous membrane. The following is a case study involving a batch pervaporation unit plant using (a) a composite membrane and (b) a homogeneous membrane.

Example 6.3: Pyridine/water separation

A batch pervaporation unit is to be designed to handle 1000kg of 5wt% aqueous pyridine in a batch tank and the required residual pyridine concentration is 0.05wt%. A lab-scale PDMS homogeneous membrane (25μm) and a commercial PDMS composite membrane were considered for the preliminary evaluation of the membrane area requirement of the process. The mass transfer characteristics of the PDMS homogeneous membrane were obtained from Bennett (1996) and for the composite membrane, the mass transfer resistances were obtained from Fig. 5.12 in Chapter 5.

Table 6.6 The mass transfer characteristics of a PDMS homogeneous membrane and a commercial PDMS composite membrane towards pyridine and water at 70°C

Type of Membrane Characteristics*	PDMS homogeneous membrane	Commercial PDMS composite membrane
$R_{mem,i}$ (m^{2}hcmHg/kmol)	70.76	28.3
$R_{mem,j}$ (m^{2}hcmHg/kmol)	537.66	215.06
$R_{sup,i}$ (m^{2}hcmHg/kmol)	-	187.76
$R_{sup,j}$ (m^{2}hcmHg/kmol)	-	1287.83
Θ_i	1	0.8
Θ_j	1	1.9

*Note: Subscript i refer to pyridine and j refers to water

Assume that a cross-flow module is used and the feed flow can be operated to Re > 10^5. A relevant Sherwood correlation for the feed side mass transfer coefficient, k_l is given by Karlsson and Tragargh (1993) as follow:

$$Sh = 0.023Re^{0.8}Sc^{0.33}$$ (6.52)

Assume a channel height of 20mm. The feed side mass transfer coefficient, k_l , evaluated from equation (6.48) was found to be 23.12m/h (= 6.423×10^{-3}m/s) for Re = 2×10^5. Hence, the overall mass transfer coefficient and E number for both membranes are as shown below:

Table 6.7 Overall mass transfer coefficients and E number of different membranes

Type of Membrane / Overall mass transfer coefficients	PDMS homogeneous membrane	Commercial PDMS composite membrane
$K_i \times 10^3$ (kmol/m^{2}h/cmHg)	14.109	4.626
$K_j \times 10^3$ (kmol/m^{2}h/cmHg)	1.86	0.665
E	7.586	2.927

From Table 6.7, the mass transfer coefficients and E values for the homogeneous membrane were found to be much larger than those of the composite membrane. According to Fig. 6.6 giving the permeate pressure effect upon NTU, the optimum operating permeate pressure range is between 0 and 1 cmHg for the current separation specification and feed concentration. Hence, an operating permeate pressure of 0.5cmHg was chosen and the NTU, pyridine concentration and residual mass in the batch tank were evaluated for both membranes. The results are in Table 6.8.

Table 6.8 The result of a preliminary design for both membranes

Type of Membrane / Design Results	PDMS homogeneous membrane	Commercial PDMS composite membrane
NTU	5.254	5.083
Pyridine concentration in the permeate product (wt%)	32.7	32.0
Product recovered (kg)	151	155
Residue in the batch tank (kg)	848.5	845

From table 6.8, the NTU, pyridine concentration in the permeate product, product recovered were very close for both membranes. However, due to the relatively low mass transfer coefficients of the composite membrane compared to the homogeneous membrane, with the same batch time (t_b), the membrane area required by the composite membrane would be very much larger than the one obtained for the homogeneous membrane. From the definition of ATU for batch pervaporation (Table 6.1), a plot of ATU against $1/t_b$ can be made for both membranes as shown in Fig. 6.26.
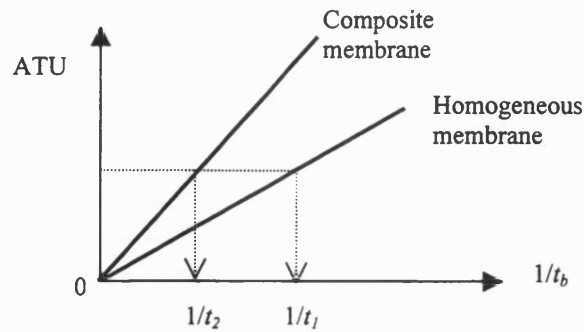
Fig. 6.26 A plot of ATU against $1/t_b$ for homogeneous and composite membranes

In Fig. 6.26, t_1 is the batch time for pervaporation with the homogeneous membrane. Provided the operating conditions are the same, an equal ATU can be obtained by using the composite membrane with a longer batch time, t_2. The following is a relationship between mass transfer coefficients and batch time for different membranes achieving the same ATU:

$$\frac{\left(K_i\right)_{\text{Type 1 membrane}}}{\left(K_i\right)_{\text{Type 2 membrane}}} = \frac{\left(t_b\right)_{\text{Type 2 membrane}}}{\left(t_b\right)_{\text{Type 1 membrane}}} \tag{6.53}$$

With the information in Table 6.7, a pervaporation unit with the PDMS homogeneous membrane has an ATU of 25.9m^2 per transfer unit for one hour of batch processing time. Knowing that the solute mass transfer coefficient of the homogeneous membrane is about three times higher than that of the composite membrane, the required batch process time for a pervaporation unit with the composite membrane same ATU as the homogeneous membrane is about three hours. Hence, the effect of the composite nature of the membrane increases the ATU for a fixed batch time or ATU can be lowered by applying a longer batch processing time.

6.7 Two-stage Pervaporation Process Scheme and Batch Process Strategies

The design of a pervaporation system depends on the nature of the stream to be treated, the desired compositions of permeate and retentate streams and the properties of the available membranes. Ideally, a pervaporation system should be designed and operated such that as the streams pass through a single bank of pervaporation modules one may achieve both sufficiently concentrated permeate and the target retentate concentration. However, it is frequently the case that either the permeate stream or the retentate stream emerging from the module bank does not meet the required specification. Hence, either one or both streams will need to pass through a second module bank before reaching the target concentration and often the recycling of streams between module banks will be necessary. The following is a two-stage pervaporation process configuration that was custom-designed to treat 5wt% pyridine. The flowrate of the aqueous feed is 500kg/h. The outlet streams are the permeate at more than 50wt% and the retentate discharged to a biological treatment plant at a concentration of 300ppm. The membrane type used in the module is the GKSS PDMS-PSF composite membrane and the operating permeate pressure is 1cmHg (=13.32mbar). The mass balance and membrane area determination is calculated based on the composite membrane characteristics shown in table 6.6 and the analytical solution of ATU and NTU. The permeate from the second module bank is recycled, mixed and heated. The total membrane required calculated was 323m^2 (see Fig. 6.27)
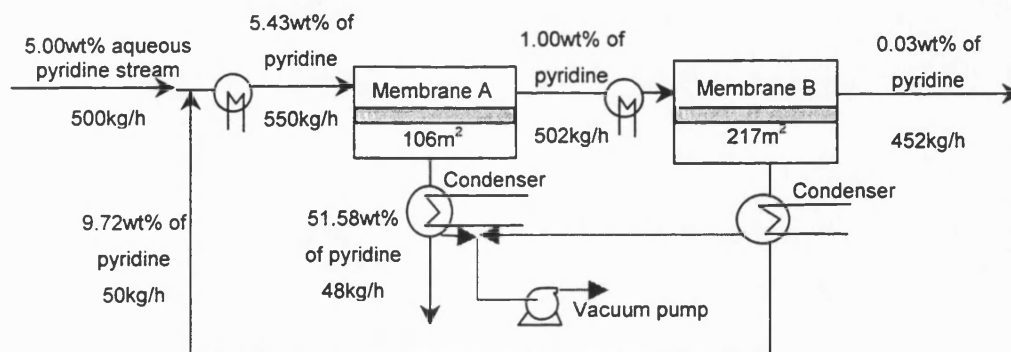
Fig. 6.27 Two-stage pervaporation process scheme

6.7.1 Batch process strategies

In a large industrial plant, the unit operations are usually operated in a continuous mode and constant feed streams with constant composition and large flow rates are frequently encountered. Hence, a custom-designed pervaporation system is acceptable in large industrial plants. However, in small industries, especially those with streams whose flow rate or composition is a variable, or batch pervaporation may well be used. A holding tank for feed awaiting treatment is used and if the feed concentration or residual concentration requirement changes, batch process time can be changed.

Provided a variable permeate concentration arising from other changes is acceptable, process strategy A, as shown in the Fig. 6.28, is recommended. In the first operation of process strategy A, the feed stream overflows the holding tank into the process tank. When the process tank is full, the second operation is initiated by starting up the batch mode pervaporation process. The stream from the process tank is preheated before entering the pervaporation unit. As the batch time increases, the concentration in the process tank drops as well as that of the permeate that is condensed and collected as product. When the concentration in the process tank achieves the discharge requirement, permeate collection is discontinued and the process stops. At this point, the third operation is initiated by draining the depleted residue from the process tank. The timing of each operation can be programmed and the process made automatic.

Process Strategy A

First Operation: Filling of process tank from holding tank
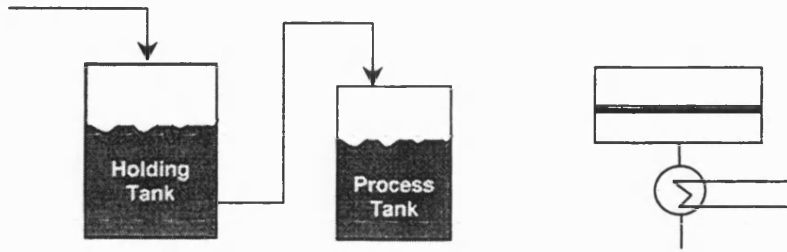
Second Operation: batch pervaporation processing step to reach required residue concentration
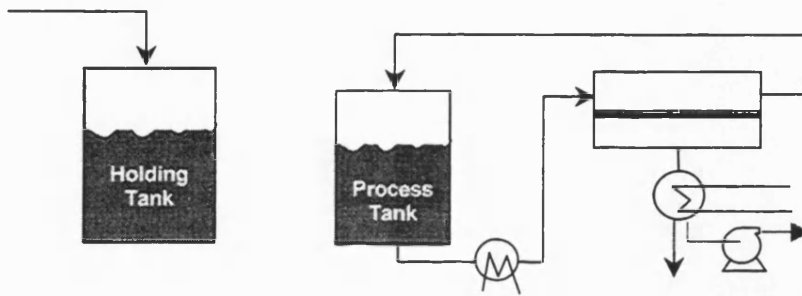
Third Operation: draining the treated residue from process tank
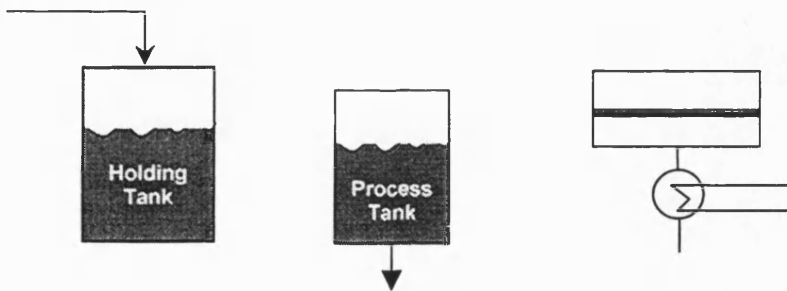
Fig 6.28 Procedures for process strategy A

Batch process strategy A assumes that a variable permeate concentration is acceptable. This can be a disadvantage. Hence, process strategy B (see Fig. 6.29) is devised to achieve two objectives..

In process strategy B, the first operation is to transfer the feed solution from holding tank to process tank. When the process tank is full, the second operation is initiated by the starting up of the pervaporation unit and permeate is condensed as product. The stream from the process tank is preheated before entering the pervaporation unit. As pervaporation process proceeds, the permeate concentration of the preferentially permeating component drops from an initially very high concentration to a low value. This second operation continues until the average total permeate concentration equals the required permeate concentration. During the next operation, the feed concentration of the preferentially permeating component drops, but the residue is still at a value too high for discharge. At this point, further processing will cause undesirable dilution of the permeate and therefore the condensed permeate is transferred back to the holding tank. Processing continues until the concentration of the solution in the process tank has reached the desired target residue concentration. At this point, the process is discontinued and the depleted residue is discharged from the process tank.

Process Strategy B

First Operation: Filling of process tank from holding tank
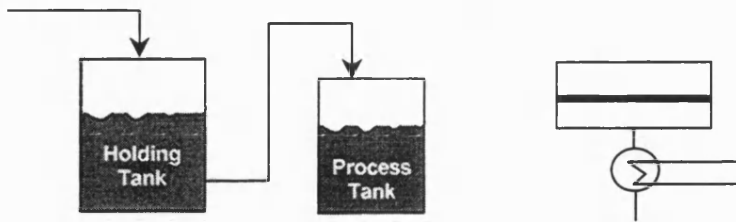
Second Operation: batch pervaporation processing step to obtain the required average permeate concentration
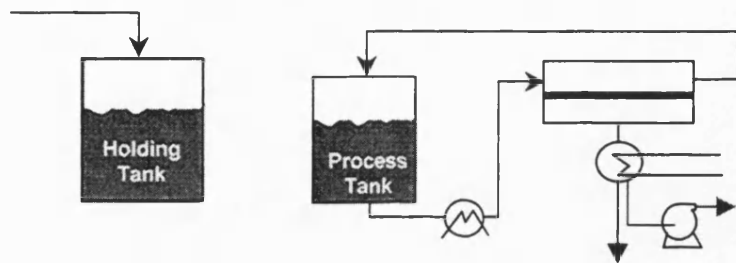
Third Operation: batch pervaporation processing step to reach required residue concentration
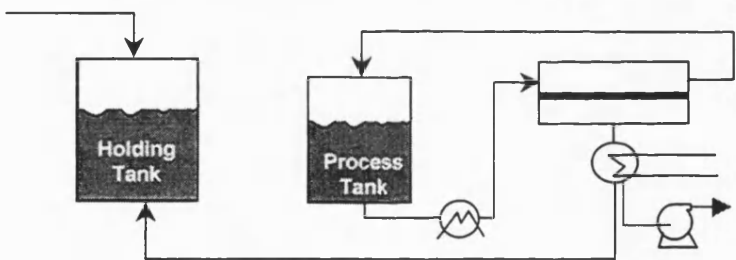
Fourth Operation: draining the depleted residue from process tank
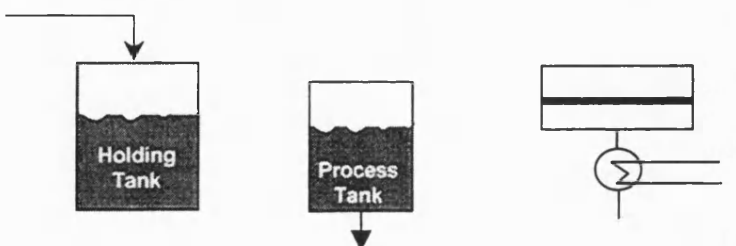
Fig 6.29 Procedures of process strategy B

6.7.2 Case study: wastewater produced from a pharmaceutical plant

Wastewater contains pyridine from batch processes is produced in a pharmaceutical plant daily. Assume that the pyridine concentration in the waste stream varies from 0.25-10wt%, averaging about 0.5 – 5wt%, at a flow rate of 1500-3500kg/day. To make the pyridine recovery viable, concentration of the pyridine has to be greater than 50wt%. Simultaneously, reduction of the pyridine concentration in the discharge stream to less than 1000ppm, and preferably less than 500ppm, is needed.

Assume that a cross-flow pervaporation system with GKSS PDMS-PSF composite membranes is to be designed to produce an enriched-pyridine (> 50wt%) permeate product and a residue with 300ppm of pyridine. Due to the widely fluctuating flow rates and concentration, batch mode pervaporation is to be implemented. A process tank that can hold 1000kg and a single bank of membrane modules with 200m^2 are used. According to the analytical solution for batch mode pervaporation, the batch time can be evaluated as the following function:

$$t_b = \text{Membrane Area} \times \frac{m_1}{K_i P_i^{sat} \gamma_i^{\infty}} \times NTU\left(E, \Theta_i, \Theta_j, P_p, P_i^{sat} \gamma_i^{\infty}, P_i^{sat} \gamma_j, x_{f,i}, x_{R,i}\right) \qquad (6.54)$$

With equation (6.54), the residual concentration in the process tank, $x_{R,i}$, the pyridine concentration of the permeate, amount of permeate collected and mass of the treated residue can be calculated against time. Results are shown in Fig. 6.30 –6.31.

As the process time increases, the pyridine concentration in the residue process tank drops as well as the pyridine concentration of the permeate product. From Fig. 6.30, the pyridine concentration in the permeate product that corresponds to the target pyridine of the residue is unacceptable (i.e. <50wt%). Hence, batch process strategy B will be implemented.
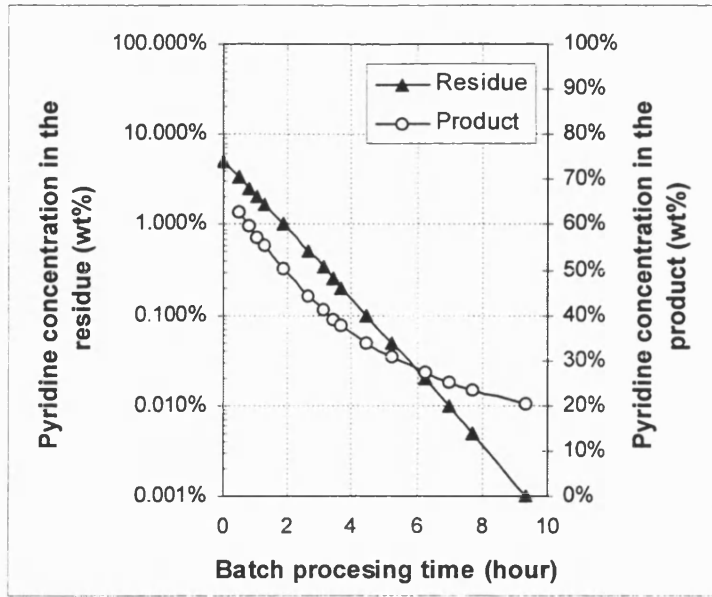
Fig. 6.30 The change of concentration of pyridine in residue and permeate product
with respect to batch processing time
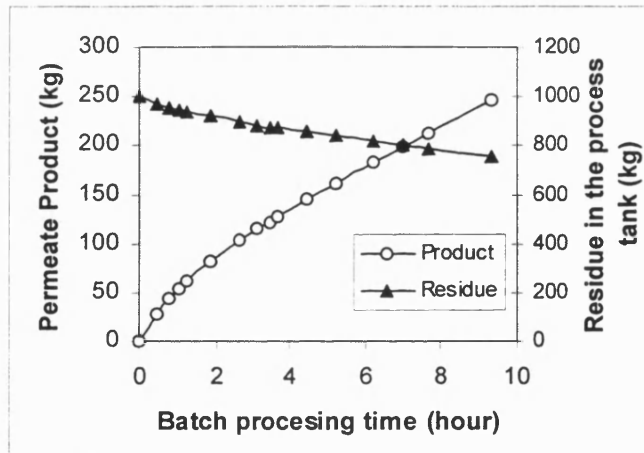
Fig. 6.31 The permeate product collected and the remaining residue in the
process tank with respect to batch processing time

In order to meet both the specification of the permeate pyridine concentration and target pyridine concentration in the residue, process operation times (see Table 6.9) of process strategy B are evaluated from Fig. 6.30-6.31.

Table 6.9 Time schedule for each cycle of each operation in batch process strategy B

Batch Process Strategy B	Time /cycle
First Operation:	5 min
Transfer from holding tank to process tank	
Second Operation:	2 hours
Main pervaporation step	
Average pyridine concentration in permeate end-product = 50wt%	
Pyridine concentration in the process tank drops from 5 to 0.9 wt%	
End-product collected = 82 kg/cycle	
Third Operation:	3hours36min
Secondary pervaporation step	
Pyridine concentration in process tank drops from 0.9 to 0.03 wt%	
Residue in the process tank = 835 kg/cycle	
Fourth Operation:	5min
Discharge of treated feed solution	
Total Treatment Cycle Time:	5hours46min

Assume that the working hours for each day is 20 hours, the pervaporation system above can treat up to 4000kg/day.

6.8 Chapter Conclusions

Based on the comprehensive transport model that was derived in Chapter 4, and assuming no local mixing in both feed and permeate and constant operating temperature, analytical solutions for membrane area were derived for continuous and batch mode pervaporation. The analytical solutions for membrane area were verified by comparing them with the results from numerical solutions that allowed temperature to drop. The predicted design from the analytical solution is reasonable. For preliminary design, the analytical solutions form a good basis for optimization. In addition, a simplified approach was developed to estimate the membrane area and its approximation is within 10% error when compared to numerical solutions that allow feed temperature drop to 15°C.

A relationship between membrane area requirement of continuous and batch mode pervaporation units was also found using the analytical solutions. Provided the key operating conditions are the same, this relationship can be used in scale up and retrofitting batch pervaporation units.

Area per transfer unit (ATU) and number of transfer units (NTU) were defined in order to characterize the performance of a pervaporation unit. The ATU was found to be dependent on mass transfer coefficient and feed stream Henry's law constant of the preferential component. This implies a high flux membrane and higher feed temperature would reduce the membrane area requirement significantly.

The analytical solutions for ATU and NTU were compared with gas/vapour-membrane separation unit design and their similarities noted. Based on the analytical solutions, the effect of permeate pressure, separation difficulty, E value, boundary layer resistance and composite nature of the membrane upon pervaporation unit design were investigated and discussed. In general, the increase of separation difficulty would cause an increase of NTU and of cut-stage and decrease the permeate concentration of the enriched-component. The response of permeate concentration of the enriched-component with operating permeate pressure coincides with the class behaviour found in the engineering analysis result given in Chapter 4. The increase of boundary layer resistance causes a lower E and a higher ATU.

Most of the functionalised PDMS membranes were found to either have a high permeability for the target organic with a low selectivity, or are highly selective with a low membrane permeability. Both inevitably increase the membrane area required.

To optimize the membrane design, a membrane with high selectivity and high permeability of the target organic should be researched. Due to the composite nature of the membrane, mass transfer resistance of the organic was greatly increased by the support layer for the one type of commercial membrane used. Hence, the membrane performance is not as good as the homogeneous membrane and the membrane area requirement is found to be greater. The extent of increase was to a surprising. Work is required to examine the performance of other support layers.

In order to achieve the required target of retentate concentration for discharge but at the same time obtaining a permeate product with acceptable concentration of an enriched-component, a two-stage pervaporation system is outlined. With the analytical solution for ATU and NTU, a mass balance for the two-stage pervaporation flowsheet is performed. Due to the custom-design nature of a two-stage *continuous* mode pervaporation system, it is inflexible to flow rates and fluctuations. In order to counter such a problem, *batch* process strategies are devised. The system contains a holding tank and a process tank with a single stage pervaporation system in which a control system is used to direct liquid flows in the apparatus according to various processing operations. With the analytical solution for the membrane requirement of a batch mode pervaporation system, one can estimate the process cycle time for each operation and hence obtain the capacity of system.

Chapter 7

Application to Hydrophilic Pervaporation

7.1 Chapter Objectives

- Application of the transport equation and engineering analysis to hydrophilic pervaporation

- Application of ATU and NTU design concept to hydrophilic pervaporation

7.2 Implication of Engineering Analysis to Hydrophilic Pervaporation

Although the main focus of the thesis is on organophilic pervaporation, the implications of the present study for hydrophilic pervaporation are briefly presented in this chapter. Hydrophilic pervaporation has been commercialized since 1980 for the dehydration of organics into high purity products. In GFT's hydrophilic pervaporation plants, high performance PVA-PAN composite membranes are mounted. The effect of permeate pressure upon the performance of this glassy PVA-PAN hydrophilic membrane was experimentally studied by Wesslein et al (1990) for the separation of ethanol-water mixtures. In the study, three different operating permeate pressures were used and their performance at 60°C are shown in Fig. 7.1-7.2.
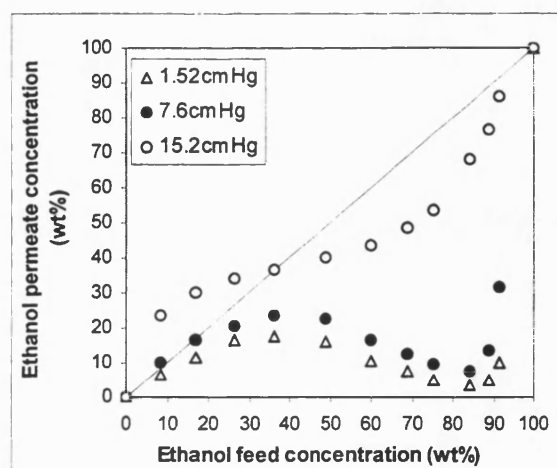
Fig.7.1 Ethanol concentration in permeate as a function of ethanol feed concentration. Data obtained with PVA-PAN membrane at 60°C from Wesslein et al (1990)
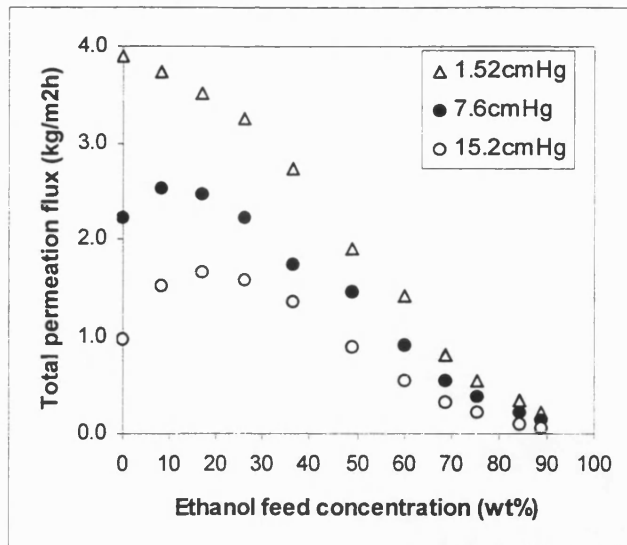
Fig. 7.2 Total permeation flux as a function of ethanol feed concentration. Data obtained with PVA-PAN membrane at 60°C from Wesslein et al (1990)

From Fig. 7.1, the degree of separation achieved is a strong function of both feed composition and permeate pressure. The pervaporation process is water selective under most operating conditions, but it is ethanol-selective at low ethanol feed concentrations when permeate pressures exceeds 8cmHg. This phenomenon was discussed in the beginning of Chapter 4; the membrane does not actually change from water selective to ethanol selective.

In order to understand the effect of permeate pressure upon performance of hydrophilic pervaporation, Fick's first law was used to derive the mass transport equation for hydrophilic pervaporation. In deriving equations for hydrophilic pervaporation, binary feed mixture is assumed and according to Chapter 7, component i (solute) is referring to water and component j (solvent) will be used to refer to organic solvent.

As discussed in Chapter 3, swelling and coupling effects are common features in hydrophilic pervaporation and the steady state partial flux can be expressed as follows:

$$J_i = -D_{m0,i} \exp\left(\tau_{ij} C_{mj} + \tau_i C_{mi}\right) \frac{dC_{mi}}{dz} \tag{7.1}$$

where: $D_{m0,i}$ is the concentration independent diffusion coefficient of component i in the membrane, C_{mi}, C_{mj} are the local concentration of component i and j in the membrane respectively, z is the differential thickness of the membrane, τ_i is the swelling factor due to component i and τ_{ij} is the coupling effect due to component j. If the coupling effect was negligible compared to the swelling effect, then by integrating equation (7.1) over the thickness of δ_m the steady state component flux can be evaluated as follows:

$$J_i = \frac{D_{m0,i}}{\tau_i \delta_m}\left[\exp(\tau_i C_{m1,i}) - \exp(\tau_i C_{m2,i})\right]$$ (7.2)

where, $C_{m1,i}$, $C_{m2,i}$ are the concentrations of component i and in the membrane adjacent to the feed side and permeate side respectively. Assume that the relationship between the feed partial vapour pressure and component concentration in the membrane can be described by Henry's law, equation (7.3) is then further modified into the following:

$$J_i = \frac{D_{m0,i}}{\tau_i \delta_m}\left[\exp(\tau_i S_i^f p_{f,i}) - \exp(\tau_i S_i^p p_{p,i})\right]$$ (7.3)

Where S_i^f and S_i^p are the sorption and desorption coefficient for the feed and permeate interface of the membrane. According to Taylor's expansion series, the exponential terms can be expressed as follow:

$$\exp(x) = 1 + x + \frac{x^2}{2!} + \frac{x^3}{3!} + \frac{x^4}{4!} + \ldots \qquad \text{for } -1 < x < 1$$ (7.4)

Hence, by assuming the third or higher terms in the series are negligible compared to the first two terms (Greenlaw et al, 1977), equation (7.3) can be simplified as the following:

$$J_i = K_i\left(p_{f,i} - \Theta_i p_{p,i}\right)$$ (7.5)

Where $K_i = \dfrac{D_{m0,i} S_i^f}{\delta_m} \left[1 + \dfrac{\tau_i S_i^f}{2} \left(p_{f,i} + \Theta_i p_{p,i} \right) \right]$ and (7.6)

$\Theta_i = S_i^p / S_i^f$

It is interesting to note the similarity of this transport equation for hydrophilic pervaporation with the one for organophilic pervaporation. If the swelling effect is negligible i.e. $\tau_i \rightarrow 0$, the overall mass transfer coefficient, K_i, would be permeate pressure independent. Thus, the partial flux equation (7.5) would reduce to the one for organophilic pervaporation in the absence of boundary layer and support layer resistances. Although equations (7.5)-(7.6) were oversimplified and unable to model the data in Fig. 7.1-7.2, this does provide a qualitative insight into hydrophilic pervaporation transport in response to permeate pressure that might be useful with other data.

Now assume that both boundary layer and support layer effects are negligible compared to the selective layer, the separation factor for water solute can be written as follows:

$$\alpha_{PV} = E^* \, \frac{p_{f,i} - \Theta_i p_{p,i}}{p_{f,j} - \Theta_i p_{p,j}}$$ (7.7)

Where $E^* = \dfrac{K_i}{K_j} = \dfrac{D_{m0,i} S_i^f}{D_{m0,j} S_j^f} \times \dfrac{2 + \tau_i S_i^f \left(p_{f,i} + \Theta_i p_{p,i} \right)}{2 + \tau_j S_j^f \left(p_{f,j} + \Theta_j p_{p,j} \right)}$ (7.8)

From equation (7.8), the ultimate enhancement factor, E^*, is a product of the enhancement factor that can be achieved as in pervaporation in the absence of swelling effect and the swelling effect term. The swelling effect term is a function of partial vapour pressures on the feed side and permeate side. Hence, the K_i and K_j are not merely affected by concentration but also the swelling effect. In an attempt to model the data in Fig. 7.1-7.2, Wijmans and Baker (1993) assumed both K_i and K_j were functions of feed concentration only and $\Theta_i = \Theta_j$ =1. Due to these assumption, Wijmans and Baker (1993) were unable to model the data for higher permeate pressure.

In this Chapter, data from Fig. 7.1-7.2 were used to derive an empirical mass transport equation for hydrophilic pervaporation. To simplified the transport model equation, $\Theta_i = \Theta_j$ =1 was assumed. The overall mass transfer coefficients for various ethanol feed concentration and permeate pressure can be evaluated as shown in Fig. 7.3 - 7.4.
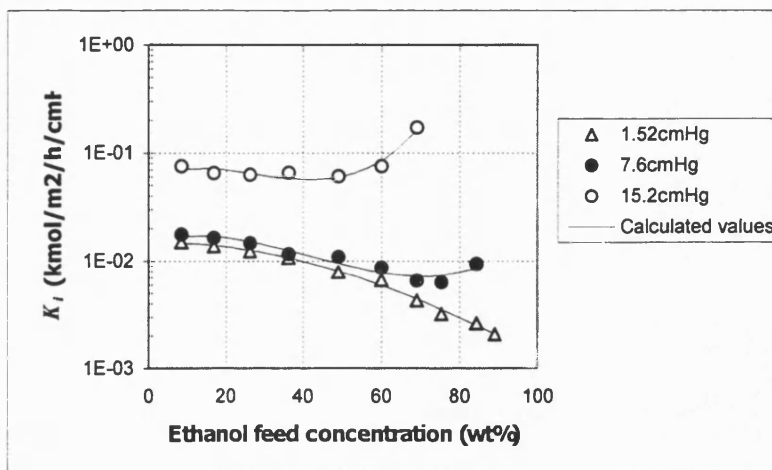
Fig. 7.3 Mass transfer coefficient of water (K_i) in PVA-PAN membrane at 60°C
and the model equation for K_i Data obtained from Fig. 7.1-7.2.
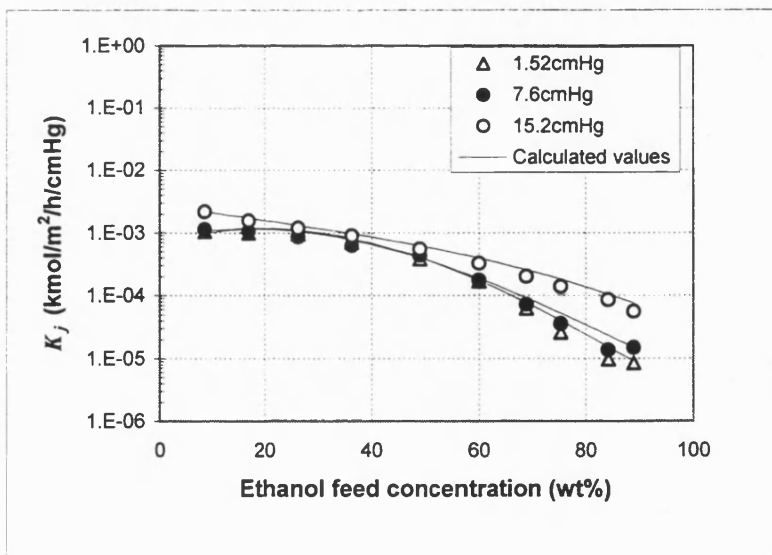
Fig. 7.4 Mass transfer coefficient of ethanol (K_j) in PVA-PAN membrane at 60°C
and the model equation for K_j. Data obtained from Fig. 7.1-7.2.

The calculated values for K_i and K_j are based on the following curve fitting equations in relation to weight fraction of ethanol, $w_{f,j}$ and permeate pressure, P_p (cmHg) via regressions:

Water:

$$\ln K_i = \left[\left(-1392.9 + 1236.7 p_p + 13.7 p_p^2\right) + \left(-525.2 + 495.3 p_p - 15.6 p_p^2\right)w_{f,j} \right.$$
$$\left. + \left(-789.3 - 1612.8 p_p + 35.9 p_p^2\right)w_{f,j}^2 + \left(-1392.9 + 1236.7 p_p + 13.7 p_p^2\right)w_{f,j}^3\right] \times 10^{-3}$$

$$\dots\dots\dots\dots\dots\dots(7.9)$$

Ethanol:

$$\ln K_j = \left[\left(-7239.9 - 54.296 p_p + 9.362 p_p^2\right) + \left(5701.2 + 216.69 p_p - 50.995 p_p^2\right)w_{f,j} \right.$$
$$\left. + \left(-16095 - 651.32 p_p + 115 p_p^2\right)w_{f,j}^2 + \left(4649.2 + 528.41 p_p - 64.742 p_p^2\right)w_{f,j}^3\right] \times 10^{-3}$$

$$\dots\dots\dots\dots\dots\dots(7.10)$$

Applying equations (7.9)-(7.10), E values can be calculated and thus, the permeate composition and total flux can be evaluated by using equation (4.27) in Chapter 4. The calculated values and experimental data of Wesslein et al (1990) are compared in Fig. 7.5 - 7.6.
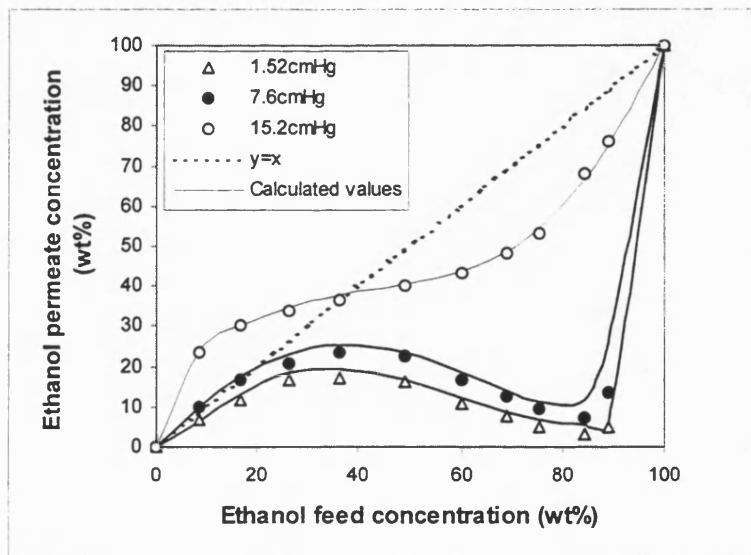
Fig. 7.5 Comparison of experimental ethanol permeate concentration data from Wesslein et al (1990) with data calculated with equations (7.9)-(7.10).
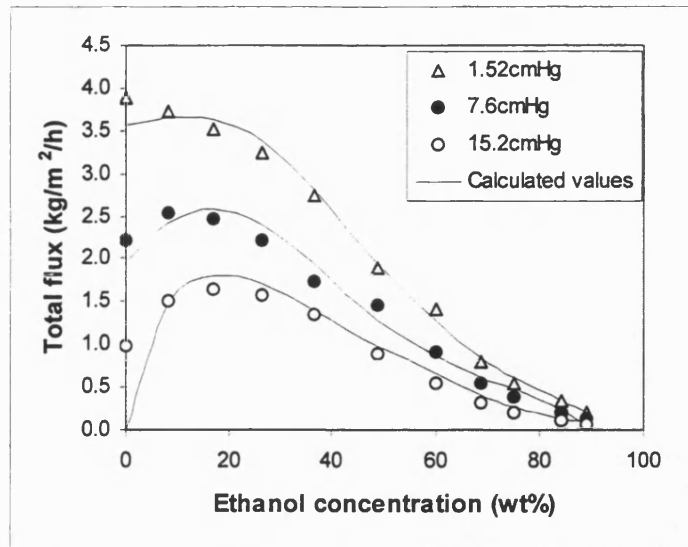
Fig. 7.6 Comparison of experimental total permeation flux data from Wesslein et al (1990) with data calculated with equations (7.9)-(7.10).

Since equations (7.9)-(7.10) were obtained by curve fitting the experimental mass transfer coefficients, excellent fits between experimental and calculated data were observed in Fig. 7.5-7.6. From Fig. 7.6, the calculated permeation flux for pure water at 15.2cmHg permeate pressure is zero because the vapour pressure of water at 60°C is only 14.9cmHg. It is important to note that the permeation flux becomes sensitive to the feed temperature when the permeate pressures is close to the feed vapour pressure. For instance, at 15.2cmHg permeate pressure, the driving force for permeation increases from 0.4 cmHg to 1.2 cmHg as feed temperature increases from 61°C to 62°C for pure water.

According to Chapter 4, the performance profile of organophilic pervaporation in response to permeate pressure can be predicted by evaluating E and y_i^* from the following equations:

$$E = \frac{K_i \Theta_i}{K_j \Theta_j} \qquad (4.19) \qquad \text{and} \qquad y_i^* = \frac{Ef_i}{Ef_i + f_j} \qquad (4.22)$$

where $f_i = p_{f,i} / \Theta_i$ and $f_j = p_{f,j} / \Theta_j$.

243

Knowing that K_i and K_j can be evaluated from equations (7.9) & (7.10), the E and y_i^* coordinates can then be determined by assuming $\Theta_i = \Theta_j = 1$. As these coordinates plotted on the performance behaviour plane (Table 4.3 from Chapter 4) as shown in Fig. 7.7, the performance profile of water-ethanol-PVA-PAN hydrophilic pervaporation system is found to be class B type.
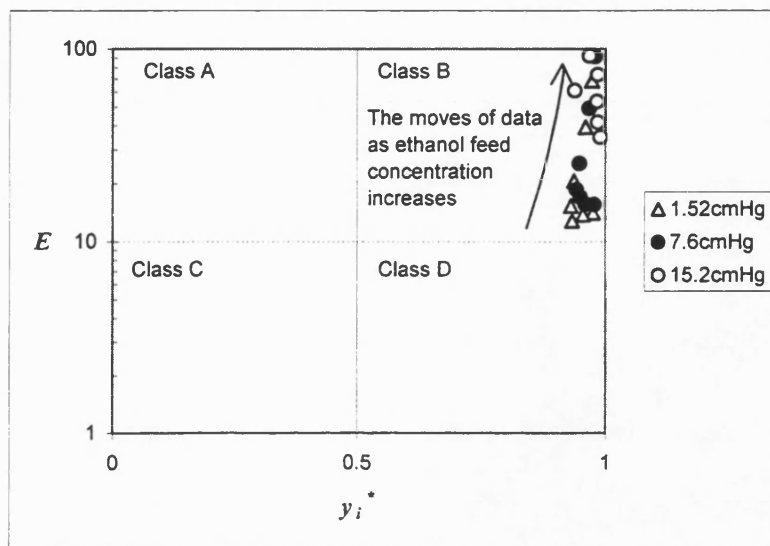
Fig. 7.7 The performance behaviour class location of water-ethanol-PVA-PAN system on E - y_i^* classification plane where y_i^* refers to *water* permeate concentration at ultimate vacuum.

From Fig. 7.7, the increase of ethanol feed concentration leads to significant increase in the E values. Hence, the performance would be more pressure sensitive as ethanol feed concentration increases. Although the experimental data in Fig. 7.1-7.2 covers only three different permeate pressures, the performance profile in response to permeate pressure was found to be reasonably in agreement with expected class B behaviour (see from Fig. 7.8-7.11). From Fig. 7.8, the separation factor decreases as permeate pressure increases. A relatively constant ethanol flux was observed in Fig. 7.11 over a range of permeate pressure, however, the water flux decreases significantly, thus giving the decrease in separation factor observed in Fig. 7.8. From Chapter 4, for pervaporation system with $E>1$, the upper bound of optimum operating permeate pressure can be estimated the solute partial pressure ($p_{f,i}$). In the case of hydrophilic pervaporation of water-ethanol mixture with PVA-PAN membrane, for ethanol concentration of 75wt% and 89wt%, their upper bound of optimum permeate

pressures were estimated as 8 and 10cmHg respectively and these estimations were confirmed experimentally in Fig. 7.8 -7.11.
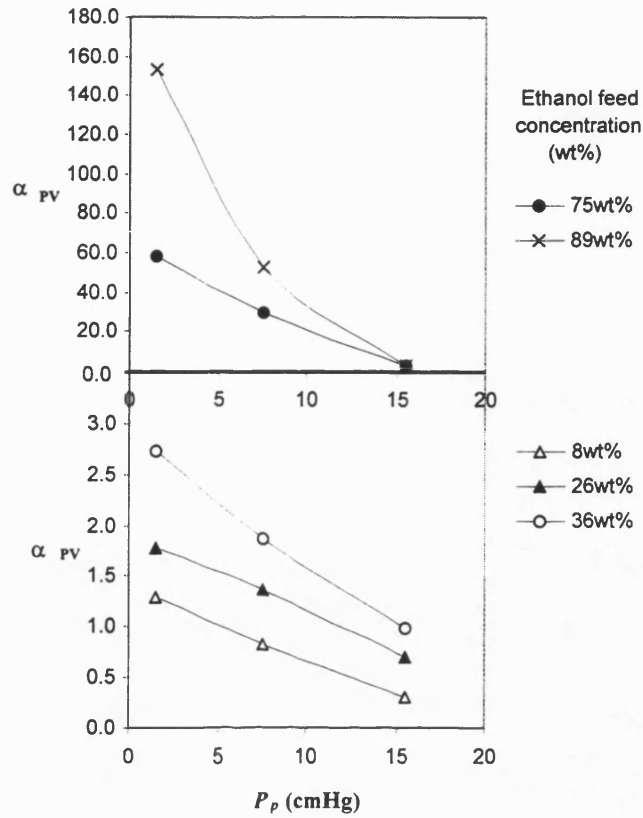
Fig. 7.8 Separation factor towards water in response to permeate pressure of a water-ethanol-PVA-PAN system at 60°C. Data obtained from Wesslein et al (1990).
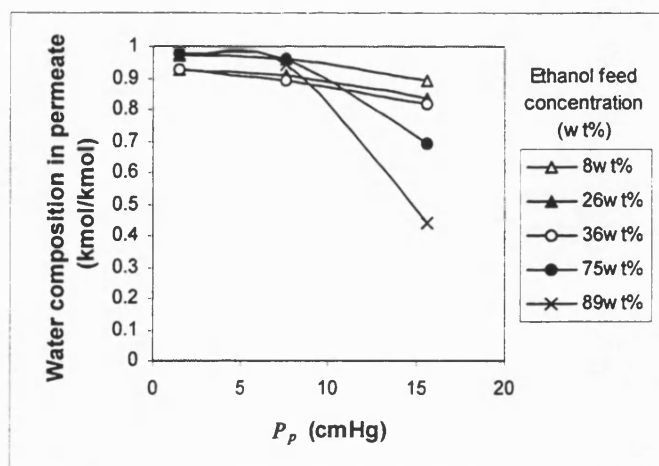
Fig. 7.9 Water permeate composition in response to permeate pressure of a water-ethanol-PVA-PAN system at 60°C. Data obtained from Wesslein et al (1990).
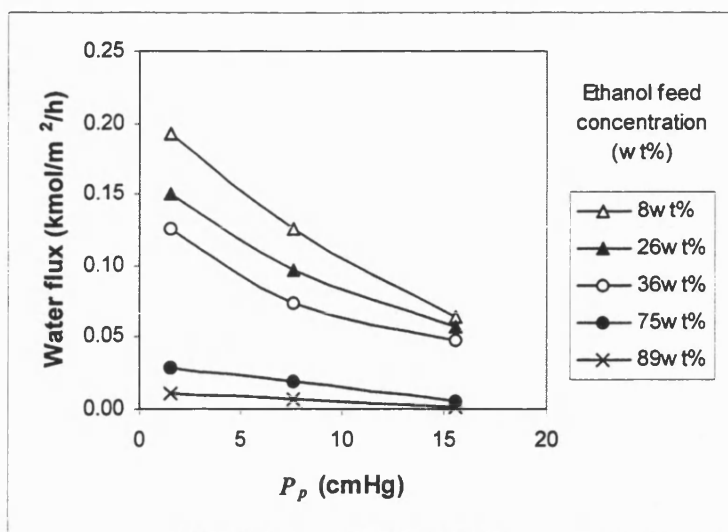
Fig. 7.10 Water flux in response to permeate pressure of a water-ethanol-PVA-PAN

system at 60°C. Data obtained from Wesslein et al (1990).
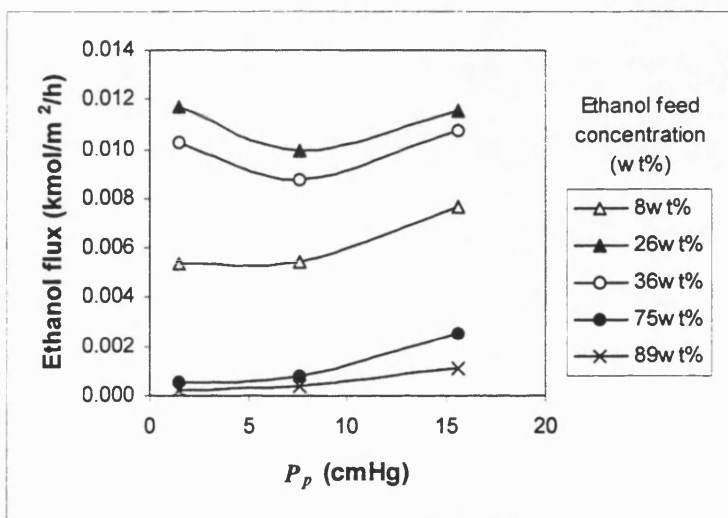
Fig. 7.11 Ethanol flux in response to permeate pressure of a water-ethanol-PVA-PAN

system at 60°C. Data obtained from Wesslein et al (1990).

7.3 Implication of Design Concept to Hydrophilic Pervaporation

In Chapter 6, the ATU and NTU design concepts were based on the assumption of a constant mass transfer coefficient over a range of feed concentration. However, in hydrophilic pervaporation, due to swelling and coupling effects, the mass transfer coefficient was found to be a strong function of feed concentration and permeate pressure. Hence, in general analytical solutions for ATU and NTU can only apply to organophilic pervaporation. For hydrophilic pervaporation, ATU and NTU analytical solutions for limiting cases can be derived under the following assumptions. Assume that the boundary layer and support layer resistances are negligible and the operating permeate pressure in the unit is close to zero (i.e. $P_p \rightarrow 0$), if the coupling effect is negligible, the transport equation for hydrophilic pervaporation in equation (7.3) can be reduced to the following:

$$J_i = \frac{D_{m0,i}}{\tau_i \delta_m} \left[\exp\left(\tau_i S_i^f p_{f,i} \right) - 1 \right]$$ (7.11)

If a pervaporation unit is used to dehydrate the organic from composition $x_{f,i}$ to $x_{R,i}$ and the cut-stage was so low then the retentate flow rate is approximately equal to the feed flow rate (i.e. $F_R \approx F_f$). Hence, the differential mass balance can be written as:

$$-F_f \frac{dx_i}{da} = J_i$$ (7.12)

If that the operating temperature, activity coefficients and sorption coefficients are constant over the concentration range of $x_{f,i}$ to $x_{R,i}$, the membrane area requirement can be solved and obtained as follow:

$$A = \frac{F_f}{K_i^* P_i^{sat} \gamma_i} \ln \left[\frac{1 - \exp\left(- \tau_i S_i^f P_i^{sat} \gamma_i x_{f,i} \right)}{1 - \exp\left(- \tau_i S_i^f P_i^{sat} \gamma_i x_{R,i} \right)} \right]$$ (7.13)

where $K_i^* = \dfrac{D_{m0,i} S_i^f}{\delta_m}$ (7.14)

Hence, from equation (7.14), the definition of ATU and NTU for this limiting case of hydrophilic pervaporation can be defined as follow:

$$ATU = \frac{F_f}{K_i^* P_i^{sat} \gamma_i}$$

(7.15)

$$NTU = \ln\left[\frac{1 - \exp\left(-\tau_i S_i^f P_i^{sat} \gamma_i x_{f,i}\right)}{1 - \exp\left(-\tau_i S_i^f P_i^{sat} \gamma_i x_{R,i}\right)}\right]$$

(7.16)

From equation (7.15), the ATU is dependent on the mass transfer coefficient and Henry constant of solute. While NTU is a function of separation difficulty, sorption coefficient and swelling effect. The format of ATU and NTU in equation (7.16) was found to be similar to the one in organophilic pervaporation. However, due to the concentration and permeate pressure dependence of the mass transfer coefficients of hydrophilic pervaporation, analytical solutions are difficult to obtain. In order to evaluate the membrane area requirement for hydrophilic pervaporation, the differential mass and energy balance has to be solved numerically. Hence, the application of the concept of ATU and NTU in hydrophilic pervaporation is very limited.

7.4 Chapter Conclusions

In this chapter, hydrophilic pervaporation was analyzed qualitatively by applying the principles and equations from Chapter 4 and 6. It was found that, in hydrophilic pervaporation, the transport equation was complicated by the swelling and coupling. Hence, if the format of the mass transport equation that was derived in Chapter 4 is applied to hydrophilic pervaporation, the mass transfer coefficient would be feed concentration and permeate pressure dependent. Experimental data of the ethanol-water-PVA-PAN membrane system from Wesslein et al (1990) were used to verified such a claim and the predicted results for pervaporation performance were in agreement with the experimental data. The application of the E-y_i^* classification plane to predict the performance profile in response to permeate pressure was used. The E values (with respect to water as the target) were generally greater than the E values observed previously for organophilic pervaporation membranes (with the organic as target).

In designing a hydrophilic pervaporation unit, analytical solutions for ATU and NTU were derived for one limiting special case. Due to the dependency of mass transfer coefficients of hydrophilic pervaporation on feed concentration and permeate pressure, analytical solutions for ATU and NTU at permeate pressure greater than zero were unable to be derived. Hence, the membrane area requirement has to be solved numerically, thus making the ATU and NTU design concept of limited use for hydrophilic pervaporation.

Part V   *Conclusions*

Chapter 8

Conclusions and Recommendations for Further Work

8.1 Overall Conclusions

8.1.1 Mass transport mechanisms

In the comprehensive review of mass transport within pervaporation systems the feed side boundary layer resistance was shown to be of great importance. In some cases it can be the dominant resistance to mass transfer. Convective and diffusional flux profiles in the boundary layer were also mathematically analyzed. It was shown that convective transport is generally negligible compared to diffusive transport as the Peclet number is much smaller than unity.

In general, the mass transport mechanism for the removal of trace organic contaminants from aqueous streams, using organophilic composite membranes, can be considered as a series of mass transfer steps, i.e. boundary layer transport, selective layer transport and the support layer transport. The concentration profiles generated in each step can be approximated ideally as a linear decrease of concentration. Due to the low organic component feed concentration and low water sorption within the membrane, the convective flow term is usually negligible. Furthermore, owing to the low feed concentration, membrane swelling and flux coupling are generally very low. It is evident that the solution-diffusion model can describe the mass transport in the dense selective layer of the membrane more successfully than the pore flow model. Organic component sorption may be successfully described by Henry's law and membrane diffusion coefficient treated as being quasi constant. The effect of two dimensional diffusion in the selective layer caused by the impermeable support matrix can be assumed to be negligible for most commercial membranes, hence, one dimensional diffusion can be used for the selective layer. This greatly simplifies the mathematical treatment of mass transport and justifies the use of the resistances in series model.

In the present study, a comprehensive transport model was derived, accounting for the resistances of the boundary layer, the selective layer and the support layer. In addition, it could also account for the effect of permeate pressure and the adverse effect caused by the desorption factor at elevated permeate pressure. It should be noted that the transport model can not be applied in other areas of pervaporation, particularly when feed concentrations are high and especially for the dehydration of organic solvents using hydrophilic membranes. In these cases, significant departure from ideality may occur.

8.1.2 Engineering analysis of component transport and the classification of performance behaviour with respect to permeate pressure

In the present study, a mathematical treatment definition was introduced, namely, the enhancement factor, E', to account for the effect of the operating conditions, module design, membrane material and the composite nature of the membrane. The enhancement factor, E', enables one to account for the enhancement achieved by the chosen pervaporation modules and operating condition from ordinary vapour-liquid equilibrium separation. For $E' > 1$, organophilic pervaporation separation is better than vapour liquid equilibrium separation. For $E' < 1$, the separation achieved by organophilic pervaporation is less effective than that achieved by vapour-liquid equilibrium.

In order to model the effect of permeate pressure upon performance, a comprehensive permeation model that includes the mass transfer in (1) the boundary layer, (2) the membrane and (3) the support layer was introduced. The model derived also accounts for the non-linearity of the partition coefficient by introducing a partition coefficient ratio Θ_i which is the ratio of the partition coefficient for the upstream interface to the one for the downstream side of the membrane.

With the derived transport model, a distinction can be made between intrinsic membrane properties (E^*_{mem}), effectiveness of the module (ε_{bl}) and the operating conditions. A comparison between pervaporation and gas permeation was presented. Explicit solutions for performance such as permeate pressure, feed composition and membrane permeability were

obtained. This will enable engineers to use literature pervaporation data to calculate performance at different operating conditions.

By calculus analysis of the derived transport model with respect to permeate pressure, performance parameters such as permeate composition, partial fluxes and separation factor profile of pervaporation was investigated. This analysis has led to the classification of pervaporation system behaviour in a manner that is similar to Geldart's classification of powder behaviour for fluidisation system. A classification plane with y_i^* (permeate concentration obtained at ultimate vacuum) as its x-axis and E (the product of the ratio of overall mass transfer coefficients and the ratio of partition coefficient ratios) as its y-axis was presented.

According to the this analysis, A, B, C and D type of pervaporation system exists. It has been found that the most favorable system is type B which is less pressure sensitive than type A and gives both high permeation flux and a high quality of separation. In order to estimate the optimum operating permeate pressure range, simple approximations were introduced for both systems with $E < 1$ and $E > 1$. The only parameter that needed for the approximation is the knowledge of feed side vapour pressures.

A summary for aqueous -organic-PDMS system from the present study and literature cases is shown in Table 5.6.

Table 5.6 Classification for aqueous-organic-PDMS systems

Feed	Class
Aqueous-pyridine	Class A
Aqueous-MIBK	Class A or B or C; depends on membrane type and concentration.
Aqueous-phenol	Class A
Aqueous-ethanol	Class C up to at least 50 wt% ethanol feed
Aqueous-chloroform	Mainly class D, but in class B if ε_{bl} tends to 1

8.1.3 Experimentation and model verification

In order to verify the validity of the transport model and the predictions offered by the engineering analysis, pervaporation experimentation was carried out and data from the literature were also used to confirm the usability of the model and analysis. In general, the transport model prediction was in agreement with the experimental data. The usefulness of evaluating the dimensionless term E and y_i^* were tested and found to be in agreement with the experimental results on performance profile classification. In addition, the optimum operating permeate pressure range determined by the approximation method was also found to be reasonable when it is compared to experimental results. A method to determine the mass transfer coefficient and desorption factor was demonstrated, and for high boilers like phenol it was found to be important.

In evaluating the mass transfer coefficient of the commercial composite membrane, the support layer was found to be the dominant resistance in both pyridine and MIBK pervaporation experiments due to the thin selective layer. The actual values of the support layer resistance is unlnown because the PDMS used by the manufacturer (GKSS) will have different permeability than that made at Bath University. Nevertheless the surface layer resistance seems to dominate.

8.1.4 Analytical design tool

Based on the comprehensive transport model, assuming (1) there is no local mixing on both feed side and permeate side, (2) constant operating temperature and permeate pressure, analytical solutions for the membrane area were determined for both continuous and batch modes. The analytical solutions for membrane area requirement were also verified by comparing them with the design result from numerical solution with allowable temperature drop. The prediction from the analytical solution gave reasonable results suitable for a preliminary design. A relationship between membrane area requirement for the continuous mode with that for the batch mode pervaporation unit was also found.

By analogy to the design of gas strippers, Area per transfer unit (ATU) and Number of transfer unit (NTU) were defined in order to characterize performance. The ATU was found

to be dependent on mass transfer coefficient and feed stream Henry constant of the preferential component. This implies a high flux membrane and higher feed temperature would reduce the membrane area requirement significantly.

The analytical solutions for ATU and NTU were compared with gas/vapour-membrane separation unit design and their similarity was observed. Based on the analytical solutions, the effect of permeate pressure, separation difficulty, E value, boundary layer resistance and composite nature of the membrane upon pervaporation unit design were investigated and discussed. In general, the increase of separation difficulty would cause the increase of NTU and cut-stage and give a decrease in permeate concentration of the enriched-component. The response of permeate concentration of the enriched-component towards the operating permeate pressure coincides with the class behaviour found in the engineering analysis. The increase of boundary layer resistance causes a lower E and a higher ATU. Most of the functionalised PDMS membranes were found to have a high permeability for the target organic but be low in selectivity. Hence the use of highly selective membranes with low permeability would inevitably increase the membrane area required. To optimize the membrane design, a membrane with high selectivity and high permeability of the target organic should be researched.

In order to achieve the required target of retentate concentration for discharge but at the same time obtaining a permeate product with acceptable concentration of an enriched-component, a two-stage pervaporation system was outlined based on batch process strategies. The system contains a holding tank and a process tank with a single pervaporation system in which a control system is used to direct liquid flows in the apparatus according to various processing operations. With the analytical solution for the membrane requirement, one can evaluate the process cycle time for each operation obtains the capacity of system. Hence the ATU and NTU concept is a useful tool to devise new process schemes.

8.1.5 Implication to hydrophilic pervaporation

Although the focus of the present study was on organophilic pervaporation, the transport model and engineering analysis was tested for hydrophilic pervaporation. Due to the evident swelling and coupling effect, modification of the mass transfer coefficient is necessary but

the overall format is retained. The mass transfer coefficient was found to be feed concentration and permeate pressure dependent. Experimental data for the water-ethanol-PVA-PAN membrane system from Wesslein et al (1990) were used to verified such a claim and the predicted result for pervaporation performance was in agreement with the experimental data. The application of E-y_i^* classification plane to predict the performance profile in response to permeate pressure were found to be applicable to hydrophilic pervaporation. The permeate pressure range that gives reasonable performance could be estimated using the method derived for organophilic pervaporation. The optimum operating permeate range could also be estimated by the method is developed for orgnophilic pervaporation.

In designing a hydrophilic pervaporation unit, analytical solutions for ATU and NTU were derived for limiting and special cases. Due to the dependency of mass transfer coefficients of hydrophilic pervaporation on feed concentration and permeate pressure, analytical solution for ATU and NTU at permeate pressure greater than zero were not derived.

8.2 Recommendations for Further Work

8.2.1 Engineering analysis and transport model

1. Establishment of a wide membrane system class database: In the literature, there are a lot of membrane systems that have not been classified. By determining the mass transfer coefficients of a particular system, performance behaviour with respect to permeate pressure can be classified.

2. Development of a multi-component transport model for organophilic pervaporation: a transport model for multi-component transport model can be derived and engineering analysis can be performed for organophilic pervaporation. Useful dimensionless numbers should be derived to predict the performance profiles

8.2.2 Experimentation investigations and re-design of experimental rigs

1. Investigation of the influence of the support layer: Experimental investigation and characterization of support materials, particularly their permeability towards organics and water can be determined by pervaporation experiments. Various support materials can be used to perform pervaporation experiments, e.g. Celgard, PVDF, PTFE, ceramic support and metal mesh.

2. Building automated pervaporation rigs: An automated pervaporation experimental rig should be built with online permeate concentration measurement by gas chromatography, on-line measurement of permeate collected by differential weight balance and computer controlled valves and pumps. Such an automated system can provide efficient and fast membrane testing, membrane system classification, transport properties determination and also provide a facility for long term (aging) tests.

3. Experimental sorption and diffusion measurements: Sorption isotherm and diffusion coefficient for each pure and functionalised PDMS membrane can experimentally be investigated by building an vapour-sorption measurement rigs with on-line measurement of the weight of organics and water absorbed into the membrane sample. The history of sorption and desorption can be determined in such experiments.

8.2.3 Membrane and module design

1. Production of the double side coated composite membrane: From the present study, the major transport resistance of the commercially available membrane was found to be the hydrophilic support layer. Due to the reduction of available selective membrane surface area at the permeate side, the mass transfer of organics through the composite membrane and the overall selectivity are significantly compromised due to the hydrophilic nature and the significant thickness of the support layer. At the same time, production of thin selective layers may cause the domination of the feed-side mass transport resistance. According to Bennett (1996), the improvement of selectivity can be achieved by functionalisation of PDMS, however a decrease in permeability is observed. Hence, instead of preventing pores filling, a double side coated composite membrane for flat

256

sheet and hollow fibre membrane is suggested as shown in Fig. 8.1 – 8.2. The suggested composite membrane consists of a hydrophobic porous support, e.g. Celgard polypropylene, with thickness at least $50\mu m$ and a selective layer coated on both side of the composite membrane. Instead of preventing the material from filling the pores, the pores of the support is filled with pure PDMS membrane material. However, the porosity of the support has to be greater than 35%. Pure PDMS material is coated on the permeate side of the porous support while the functionalised PDMS with enhanced selectivity will be coated at its feed side surface. Such a type of membrane will not be restricted to a flat sheet membrane; a hollow fibre double side coated composite membrane can be formed. In order to fill the pores of the commercially available hydrophobic porous support with PDMS membrane material, PDMS solution is injected into the bores of the hollow fibres and high pressure is exerted on the bore-side of the membrane. After the pores are filled, the desired selective material is then coated on both sides of the hollow fibre.
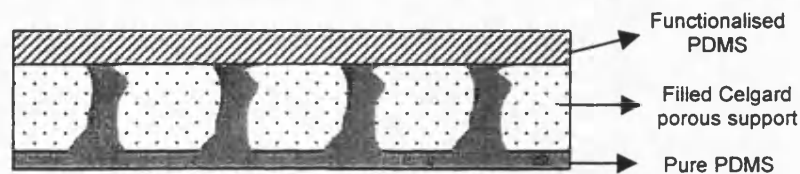
Fig. 8.1 Double-side coated flat sheet composite membrane
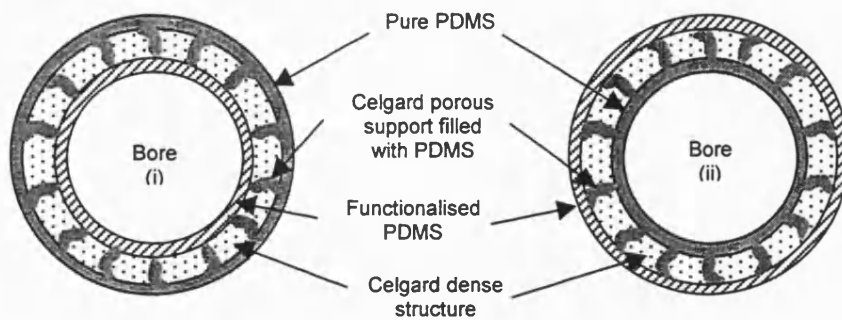
Fig. 8.2 Two types of double-side coated tubular/hollow-fibre composite membrane:
(i) bore-side feed and shell-side permeate, (ii) bore-side permeate and shell-side feed

4. Production of various membrane modules for various classes of membrane system: From the present study, the separation performance of class A membrane systems is usually a significant decline as the permeate pressure increases, but often, the boundary layer resistance is not as significant as the membrane resistance. In contrast, for class C membrane systems, the separation performance is improved as the permeate pressure increases. Hence, a relatively higher permeate pressure is allowed in such systems compared to class A systems. Often, however, the boundary layer resistance is significant for class C. For these reasons, the following membrane module designs can be produced as shown in Fig. 8.3-8.4 for each membrane systems.
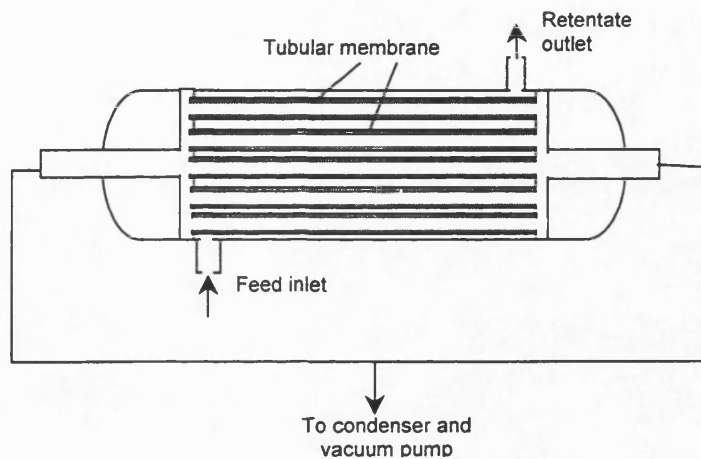
Fig. 8.3 Tubular membrane module configuration for class C membrane system
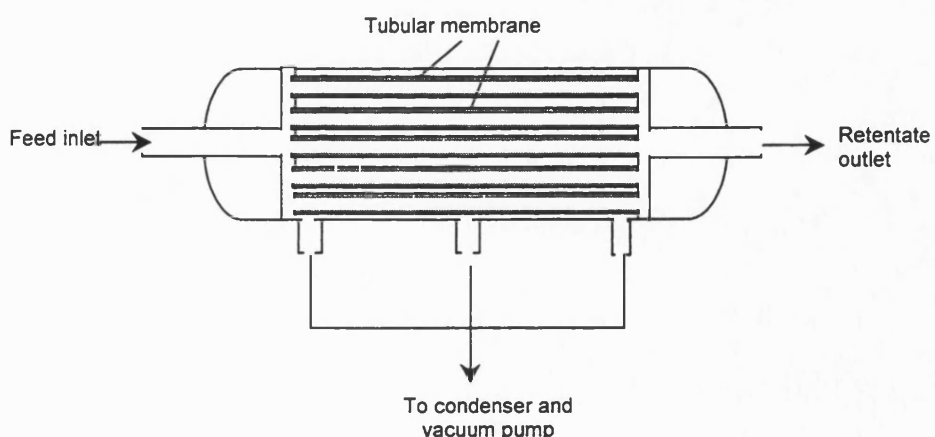
Fig. 8.4 Tubular membrane module configuration for class A membrane system

5. Researching new and improved membrane module design by CFD investigation: For class A, permeate pressure affects the performance behaviour of the pervaporation system. With the use of computational fluid dynamics (CFD), different configurations and design of membrane modules and the number of openings for the permeate exit can be optimized to achieve low permeate pressure operation.

5.2.4 Scale-up study and experimental verification of batch process strategy

1. Experimental verification of batch process strategy: In the present study, two batch process strategies were devised. Hence, by building a pilot scale batch pervaporation unit, process strategy schemes can be verified experimentally and the treatment cycle time can be investigated and determined.

2. Other batch process strategies for multiple stage pervaporation membrane system: Other batch process strategies can be devised with the incorporation of decanter or additional process tanks to perform the similar task of a multi-stage pervaporation system.

Appendix A1

Mathematical Derivation and Analysis

A1.1 Derivation of equation (4.32) & (4.33)

The separation factor and permeate composition can be defined as in equation (4.31) and (4.6) respectively:

$$\alpha_{PV} = \alpha_{PV}^{*} \frac{1 - P_p y_i / f_i}{1 - P_p (1 - y_i) / f_j} \tag{4.31}$$

$$y_i = \frac{\alpha_{PV} x_{b,i}}{(\alpha_{PV} - 1) x_{b,i} + 1} \tag{4.6}$$

By substituting (4.6) into (4.31) one obtains:

$$\alpha_{PV} = \alpha_{PV}^{*} \frac{\alpha_{PV} (1 - P_p / f_i) + 1/\pi_f}{\alpha_{PV} + (1 - P_p / f_j) / \pi_f} \tag{A1.1}$$

Where $\pi_f = \dfrac{x_{b,i}}{1 - x_{b,i}}$

Hence, rearranging equation (A1.1) one can form a quadratic equation:

$$\alpha_{PV}^2 - [\alpha_{PV}^{*}(1 - P_p / f_i) + (1 - P_p / f_j)/\pi_f]\alpha_{PV} - \alpha_{PV}^{*}/\pi_f = 0 \tag{A1.2}$$

Knowing that $E = \dfrac{K_i \Theta_i}{K_j \Theta_j} = \pi_f \alpha_{PV}^{*} \dfrac{f_j}{f_i}$, equation (A1.2) one can then be rewritten as:

260

$$\alpha_{PV}^2 - \left\{ \alpha_{PV}^* + \left[(1-E)\cdot\left(P_p/f_j\right)-1\right]\cdot\left(1/\pi_f\right)\right\}\cdot\alpha_{PV} - \alpha_{PV}^*/\pi_f = 0 \tag{4.32}$$

Rearrange equation (4.32) and form:

$$\left(\frac{\alpha_{PV}}{\alpha_{PV}^*}\right)^2 - \left\{1+\frac{1}{\pi_f\alpha_{PV}^*}\left[(1-E)\cdot\frac{P_p}{f_j}-1\right]\right\}\cdot\left(\frac{\alpha_{PV}}{\alpha_{PV}^*}\right)-\frac{1}{\pi_f\alpha_{PV}^*}=0 \tag{A1.3}$$

Knowing that there is only one solution where $\alpha_{PV} > 0$, the explicit solution can be readily obtained as follows:

$$\alpha_{PV} = \frac{\alpha_{PV}^*}{2}\left\langle 1+\frac{1}{\pi_f\alpha_{PV}^*}\left[(1-E)\cdot\frac{P_p}{f_j}-1\right]\right.$$
$$\left. +\left\{\left\{1+\frac{1}{\pi_f\alpha_{PV}^*}\left[(1-E)\cdot\frac{P_p}{f_j}-1\right]\right\}^2+\frac{4}{\pi_f\alpha_{PV}^*}\right\}^{0.5}\right\rangle \tag{4.33}$$

A1.2 Calculus analysis of pervaporation performance

To perform calculus analysis upon performance parameters, first and second derivative functions of these parameters need to be derived. Provided the feed concentration is unchanged and the mass transfer coefficients and desorption factors are permeate pressure independent which often is the case in organophilic pervaporation; the performance parameters can be treated as a function of permeate pressure only. Hence, the derivatives are ordinary differential equations. Results at $P_p = 0$ are presented. Hence, the effect and limitation of dimensionless group E and y_i^* upon the performance in response to permeate pressure can be derived as shown in Table A1 at the end of this appendix.

A1.2.1 Derivative functions of permeate composition of solute (y_i):

According to equation (4.18), the relationship between permeate composition for a binary mixture in pervaporation can be expressed as:

$$\frac{y_i}{1-y_i} = E \frac{f_i - P_p y_i}{f_j - P_p(1-y_i)} \tag{4.18}$$

Hence the first and second order derivatives can be obtained by differentiating equation (4.18) with respect to permeate pressure P_p. This yields:

$$\frac{dy_i}{dP_p} = \frac{(1-E) \cdot y_i \cdot (1-y_i)}{P_p \cdot (1-E) \cdot (2y_i - 1) + f_i + E \cdot f_j} \tag{A1.4}$$

$$\frac{d^2 y_i}{dP_p^2} = \frac{2 \cdot (1-E)}{P_p \cdot (2y_i - 1) \cdot (1-E) + f_i + E \cdot f_j} \cdot \left(1 - 2y_i - P_p \frac{dy_i}{dP_p}\right) \cdot \frac{dy_i}{dP_p} \tag{A1.5}$$

At $P_p = 0$, equations (A1.4) and (A15) reduced to:

$$\left(\frac{dy_i}{dP_p}\right)_{P_p=0} = \frac{(1-E) \cdot y_i^* \cdot (1-y_i^*)}{f_i + E \cdot f_j} \tag{A1-6}$$

$$\left(\frac{d^2 y_i}{dP_p^2}\right)_{P_p=0} = y_i^*(1-y_i^*)(1-2y_i^*)\left(\frac{1-E}{f_i + E \cdot f_j}\right)^2 \tag{A1.7}$$

where y_i^* is the organic mole fraction in the permeate at $P_p = 0$ and it can be evaluated from equation (4.22)

$$y_i^{\bullet} = \cfrac{1}{1 + \cfrac{K_j P_j^{sat} \gamma_j x_{b,j}}{K_i P_i^{sat} \gamma_i x_{b,i}}} = \cfrac{1}{1 + \cfrac{f_j}{E f_i}} \qquad (4.22)$$

A1.2.2 Derivative functions of partial fluxes (J_i, J_j)

The partial fluxes of solute and solvent can be expressed as:

Solute partial flux: $\quad J_i = K_i \Theta_i \left(f_i - P_p y_i \right)$ $\qquad$ (A1.8)

Solvent partial flux: $\quad J_j = K_j \Theta_j \left[f_j - P_p (1 - y_i) \right]$ $\qquad$ (A1.9)

From equation (A1.8)-(A1.9), the first and second order derivatives are obtained as follows:

$$\frac{dJ_i}{dP_p} = -K_i \Theta_i \cdot \left(y_i + P_p \frac{dy_i}{dP_p} \right) \qquad (A1.20)$$

$$\frac{dJ_j}{dP_p} = -K_j \Theta_j \cdot \left(1 - y_i - P_p \frac{dy_i}{dP_p} \right) \qquad (A1.21)$$

$$\frac{d^2 J_i}{dP_p^2} = -K_i \Theta_i \cdot \left(2 \frac{dy_i}{dP_p} + P_p \frac{d^2 y_i}{dP_p^2} \right) \qquad (A1.22)$$

$$\frac{d^2 J_j}{dP_p^2} = K_j \Theta_j \cdot \left(2 \frac{dy_i}{dP_p} - P_p \frac{d^2 y_i}{dP_p^2} \right) \qquad (A1.23)$$

At $P_p = 0$, equations (A1.20)-(A1.23) are reduced to:

$$\left(\frac{dJ_i}{dP_p}\right)_{P_p=0} = -K_i\Theta_j \cdot y_i^*$$

(A1.24)

$$\left(\frac{dJ_j}{dP_p}\right)_{P_p=0} = -K_j\Theta_j \cdot \left(1-y_i^*\right)$$

(A1.25)

$$\left(\frac{d^2J_i}{dP_p^2}\right)_{P_p=0} = -2K_i\Theta_i \cdot \left(\frac{dy_i}{dP_p}\right)_{P_p=0}$$

(A1.26)

$$\left(\frac{d^2J_j}{dP^2}\right)_{P=0} = K_j\Theta_j \cdot \left(\frac{dy_i}{dP}\right)_{P=0}$$

(A1.27)

From equation (A1.26) and (A1.27), it can be shown that $\left(\dfrac{d^2J_i}{dP_p^2}\right)_{P_p=0} \times \left(\dfrac{d^2J_j}{dP_p^2}\right)_{P_p=0} < 0$.

Hence, if the profile of J_i is maximum then the other would be minimum.

A1.2.3 Derivative functions of separation factor (α_{PV})

The separation factor of a binary system was defined as:

$$\alpha_{PV} = \frac{y_i}{1-y_i} \cdot \frac{x_{b,j}}{x_{b,i}}$$

(A1.28)

and the first and second order derivatives obtained as follows:

$$\frac{d\alpha_{PV}}{dP_p} = \frac{x_{b,j}}{x_{b,i}} \cdot \frac{1}{\left(1-y_i\right)^2} \cdot \frac{dy_i}{dP_p}$$

(A1.29)

$$\frac{d^2\alpha_{PV}}{dP_p^2} = \frac{x_{b,j}}{x_{b,i}} \cdot \frac{1}{(1-y_i)^2} \cdot \left(\frac{1}{1-y_i} \left(\frac{dy_i}{dP_p} \right)^2 + \frac{d^2y_i}{dP_p^2} \right)$$

(A1.30)

At $P_p = 0$, equations (A1.29) and (A1.30) reduce to:

$$\left(\frac{d\alpha_{PV}}{dP_p} \right)_{P_p=0} = \frac{x_{b,j}}{x_{b,i}} \cdot \frac{(1-E) \cdot y_i^*}{f_i + E \cdot f_j}$$

(A1.31)

$$\left(\frac{d^2\alpha}{dP_p^2} \right)_{P_p=0} = \frac{x_{b,j}}{x_{b,i}} \cdot \left(\frac{1-E}{E \cdot f_j + f_i} \right)^2 \cdot y_i^*$$

(A1.32)

Table A1 Summary of calculus analysis of performance at various downstream pressure P_p with respect to permeate pressure

E	y_i^*	Class of system	$\left(\dfrac{dy_i}{dP_p}\right)_{P_p=0}$	$\left(\dfrac{d^2y_i}{dP_p}\right)_{P_p=0}$	$\left(\dfrac{d^2J_i}{dP_p^2}\right)_{P_p=0}$	$\left(\dfrac{d^2J_j}{dP_p^2}\right)_{P_p=0}$	$\left(\dfrac{d\alpha_{PV}}{dP_p}\right)_{P_p=0}$	$\left(\dfrac{d^2\alpha_{PV}}{dP_p^2}\right)_{P_p=0}$
		Class A						
	< 0.5	$\dfrac{J_i^*}{f_i} > \dfrac{J_j^*}{f_j}$		+ ve				
		$J_i^* < J_j^*$						
$E > 1$		**Class B**	- ve		+ ve	- ve	- ve	+ ve
	> 0.5	$\dfrac{J_i^*}{f_i} > \dfrac{J_j^*}{f_j}$		- ve				
		$J_i^* > J_j^*$						
		Class C						
	< 0.5	$\dfrac{J_i^*}{f_i} < \dfrac{J_j^*}{f_j}$		+ ve				
		$J_i^* < J_j^*$						
$E < 1$		**Class D**	+ ve		- ve	- ve	+ ve	+ ve
	> 0.5	$\dfrac{J_i^*}{f_i} < \dfrac{J_j^*}{f_j}$		- ve				
		$J_i^* > J_j^*$						

Appendix A2

Membrane Permeabilities

The membrane permeabilities of pure PDMS and functionalised PDMS membrane materials that are provided by (Bennett, 1996) are shown Table A2.1

Table A2.1 Permeabilities of pure and functionalised PDMS membrane (Bennett, 1996):

Component Systems		Phenol/water[1]		Chloroform/water[2]		Pyridine/water[3]		MIBK/water[4]	
Permeability of organic (i) and water (j)		$\hat{P}_{m,i}$ $\times 10^8$ kmolm^{-2}h^{-1} cmHg^{-1}m^{-1}	$\hat{P}_{m,j}$ $\times 10^8$ kmolm^{-2}h^{-1} cmHg^{-1}m^{-1}	$\hat{P}_{m,i}$ $\times 10^8$ kmolm^{-2}h^{-1} cmHg^{-1}m^{-1}	$\hat{P}_{m,j}$ $\times 10^8$ kmolm^{-2}h^{-1} cmHg^{-1}m^{-1}	$\hat{P}_{m,i}$ $\times 10^8$ kmolm^{-2}h^{-1} cmHg^{-1}m^{-1}	$\hat{P}_{m,j}$ $\times 10^8$ kmolm^{-2}h^{-1} cmHg^{-1}m^{-1}	$\hat{P}_{m,i}$ $\times 10^8$ kmolm^{-2}h^{-1} cmHg^{-1}m^{-1}	$\hat{P}_{m,j}$ $\times 10^8$ kmolm^{-2}h^{-1} cmHg^{-1}m^{-1}
Functional Group[5]	Load %								
Pure PDMS	0	99.10	3.82	6.95	5.87	35.35	4.62	26.16	5.53
Acetate-	10	126.74	6.29	3.34	6.03	12.02	3.56		
	20	349.85	17.54	7.20	13.76	23.23	6.25		
Di-Acetate-	10	113.48	3.51	4.71	5.90				
	20	146.74	6.07						
	30	157.32	12.78						
Hexanoate-	10	160.10	4.65	8.37	5.63	29.93	3.78		
	20	225.30	5.73	3.71	5.08	15.59	3.37	13.52	6.58
Cyano-	10	163.77	4.29	5.11	5.52	27.65	4.29		
	20	234.20	7.27	2.18	7.40	12.41	5.46		
Octyl-	10	56.61	1.40	4.11	2.42	18.02	1.54	16.69	2.41
Benzyl-	10	104.46	3.20	5.65	4.14	24.97	2.75		
PentaFluro-Benzyl-	10	60.07	2.73	3.79	3.05	23.16	2.56	20.51	3.59
	20			2.00	3.43	10.64	1.43		
Phenyl Ether-	10	65.87	2.97	4.43	4.67	19.89	2.45		
Ethyl Ether-	10	141.73	3.39	6.10	5.38	23.17	3.47		
	20	206.62	4.64	6.33	6.12	19.04	3.70	14.28	5.05
Alkenyl-	10	192.01	7.45	11.37	10.11	42.68	5.74	61.45	19.15
	20	47.39	3.70	6.04	6.18	40.29	6.93		
Amino-[6]	10	202.45	4.82						
	20	243.83	4.84	4.42	11.13				
Amido-[7]	10	132.24	3.97						
Pyridyl-	10	257.19	5.15			13.80	3.89		
Cyano-[7]	10	118.81	3.99	4.55	5.05				
	20	113.91	6.36	5.18	7.32				
Tridecyl-	6.67							22.67	2.86
	10							15.07	1.79
Branched Heptyl-	10							14.21	2.25
	12.5							13.23	2.23

Notes for Table A2.1:

1. 5wt% aqueous phenol solution at 70°C.

2. 0.3wt% aqueous chloroform solution at 25°C.

3. 2wt% aqueous pyridine solution at 70°C.

4. 0.75wt% aqueous MIBK solution at 70°C.

5. Most functionalised PDMS membrane are manufactured via substitution reaction of PHMS with alkene.

6. Functionalisation via crosslink the PDMS silanol with tri-methoxy or tri-ethoxy-silane that contain functional group.

7. Functionalisation via crosslinking the PDMS silanol with tri-alkoxy-silane that contain functional group.

In order to convert the $D_{m,i}S_i^a$ of each systems provided by Bennett (1996) into a permeabilities that are based on a partial pressure driving force, the following conversion equation was used: $\hat{P}_{m,i} = D_{m,i}S_i^f = \dfrac{D_{m,i}S_i^a \rho_m}{M_i P_i^{sat}}$ where ρ_m is the density of the membrane ($\sim$970kg/m^3).

Appendix 3

Physical Properties and Constants

The values of all physical constants necessary to complete all calculation procedures described within chapters 4-7 are listed below.

A3.1 Water Density and Viscosity, ρ_w & μ_w

The density and viscosity of water, measured at 1 atm, are given by the following empirical equations (Weast, 1980):

$$\rho_w, \ \text{kg/m}^3 = (999.83952 + 16.945176 \ T - 7.9870401 \times 10^{-3} \ T^2 - 46.170461 \times 10^{-6} \ T^3 + 105.56302 \times 10^{-9} \ T^4 - 280.54253 \times 10^{-12} \ T^5) / (1 + 16.879850 \times 10^{-3} \ T) \tag{A3.1}$$

$$0 - 20°C: \ \log_{10}\mu_w = \frac{1301}{998.333 + 8.1855 \ (T - 20) + 0.00585 \ (T - 20)^2} - 3.30233 \tag{A3.2}*$$

$$20 - 100°C: \ \log_{10}\frac{\mu_w}{\mu_{wT=20}} = \frac{1.3272 \ (20 - T) - 0.001053 \ (T - 20)^2}{T + 105} \tag{A3.3}*$$

Where: T = Temperature, C

* Units of μ_w in equation (A3.2) & (A3.3) = Centipoise. To convert to kg/ms, multiply by 0.001.

A3.2 Saturated Vapour Pressure, P_i^{sat}

Component saturated vapour pressures are evaluated using the Antoine equation:-

$$\log_{10}(P_i^{sat}) = A_i - \frac{B_i}{T + C_i} \tag{A3.4}$$

Where: P_i^{sat} = Saturated vapour pressure, mmHg   T = Temperature, °C

A_i, B_i, C_i = Antoine Constants

Values of A_i, B_i and C_i for all components are displayed in Table A3.1 (Gmehling et al, 1978).

269

Table A3.1 Antoine Coefficients

Component	A_i	B_i	C_i
Water	8.07131	1730.630	233.426
Ethanol	8.11220	1592.864	226.184
Phenol	6.93051	1382.650	159.493
Chloroform	6.95465	1170.966	226.232
Pyridine	7.01328	1356.930	212.655
MIBK	6.67272	1168.408	191.944

To convert from mmHg to Pa, multiply by 133.32237.

A3.3 Activity coefficients

The activity coefficients of phenol, chloroform, pyridine and MIBK are evaluated using modified UNIFAC method (Reid et al, 1987) and the activity coefficients that are used in the calculation in Chapter 5-7 are shown in Table A3.2. Due to low concentration of organics, in all cases, the activity coefficient of water is taken as 1.

Table 3.2 Activity coefficients estimated by modified UNIFAC method for dilute phenol/water, chloroform/water, pyridine/water and MIBK/water systems

(Reid et al, 1987)

Component	Temperature	Wt%	Activity coefficient, γ_i
Phenol	70°C	5.00	20.9
Chloroform	25°C	0.30	864
Pyridine	70°C	2.00	10.0
		2.50	8.94
		5.00	8.043
MIBK	70°C	0.25	210.7
		0.50	207.4
		0.75	204.2

For the sake of comparison, the activity coefficients for ethanol(1) and water(2) were estimated according to van Laar equations (Wijmans and Baker, 1993):

$$\ln(\gamma_1) = A_{12} \left[A_{21}x_2 / (A_{21}x_1 + A_{12}x_2) \right]^2 \tag{A3.5}$$

$$\ln(\gamma_2) = A_{21} \left[A_{12}x_1 / (A_{12}x_1 + A_{21}x_2) \right]^2 \tag{A3.6}$$

Where the van Laar constants for 30°C and 60°C are shown in Table A3.3:

Table A3.3 Coefficients for van Laar equation used in calculations:

	A_{12}	A_{21}
Ethanol(1) / water (2) at 30°C	1.5232	1.0388
Ethanol(1) / water (2) at 60°C	1.6276	0.9232

A3.4 Temperature Independent Properties

The following values for temperature independent properties were used:

Component molecular mass, M_i, (Weast, 1980):

Water:	18.02	Chloroform:	119.39	MIBK:	100.16
Phenol:	94.11	Pyridine:	79.10	Ethanol:	46.069

Gas Constant, R, = 8.314 kJ/kmolK (Brodkey and Hershey, 1988)

PDMS density, ρ_m, = 970 kg/m^3 (Nijhuis, 1990)

This value for ρ_m is used for all functionalised and unfunctionalised PDMS membranes at all temperatures.

A3.5 UK Occupational limits (The Royal Society of Chemistry, 1996)

Chloroform:	10ppm
MIBK:	50-100ppm
Phenol:	5ppm
Pyridine:	5ppm

Appendix A4

Derivation of Membrane Area Requirement

A4.1 Derivation of analytical solution of stage cut and membrane area

According to *Rayleigh equation*, the stage cut and the relationship between compositions were expressed as equation (6.5)

$$\ln(1-\phi) = \int_{x_{f,i}}^{x_{R,i}} \frac{dx_i}{y_i - x_i} \tag{6.5}$$

To solve the integral above analytically, a swap of variable is introduced. i.e. integrate equation (6.5) with respect to y_i instead of x_i. From equation (6.10), the relationship between y_i and x_i can be expressed in dimensionless groups as follows:

$$x_i = \frac{C_3 y_i (y_i + C_1)}{y_i + C_2} \tag{6.10}$$

where:

$$C_1 = \frac{D_j + E - 1}{1 - E} \quad \text{(A4.1)}; \quad C_2 = \frac{ED_i}{D_j - ED_i} \quad \text{(A4.2)}; \quad C_3 = \frac{1 - E}{D_j - ED_i} \quad \text{(A4.3)}$$

$$E = \frac{K_i \Theta_i}{K_i \Theta_j} \quad \text{(4.19)}; \quad D_i = \frac{P_i^{sat} \gamma_i}{\Theta_i P_p} \quad \text{(6.11)}; \quad D_j = \frac{P_j^{sat} \gamma_j}{\Theta_j P_p} \quad \text{(6.12)}$$

From equation (6.10) , all C_1, C_2 and C_3 are virtually constants based on our assumptions made previously, hence, the derivative of equation (6.10) with respect to y_i can be obtained as below:

$$\frac{dx_i}{dy_i} = \frac{C_3 [(y_i + C_2)(2y_i + C_1) - y_i(y_i + C_1)]}{(y_i + C_2)^2} \tag{A4.4}$$

By substituting equations (A4.4) and (6.10) into equation (6.5), the integral was transformed into a function of y_i as shown in equation (A4.5) with boundary values of y_i corresponds to the feed and retentate as $y_{f,i}$ and $y_{R,i}$ respectively. Hence, the integral form of equation (6.5) is:

$$\ln(1-\phi) = \int_{y_{of}}^{y_{oR}} \frac{C_3}{(1-C_3)} \cdot \frac{(y_i + C_2)(2y_i + C_1) - y_i(y_i + C_1)}{y_i(y_i + C_2)\left(y_i + \frac{(C_2 - C_1 C_3)}{1 - C_3}\right)} dy_i \qquad (A4.5)$$

Knowing that $\dfrac{C_2 - C_1 C_3}{1 - C_3} = -1$, the analytical solution for cut-stage can be evaluated as:

$$\phi = \frac{Q}{F_f} = 1 - \left(\frac{y_{R,i}}{y_{f,i}}\right)^{\hat{a}} \left(\frac{1 - y_{R,i}}{1 - y_{f,i}}\right)^{\hat{b}} \left(\frac{\beta - y_{R,i}}{\beta - y_{f,i}}\right) \qquad (6.14)$$

where :

$$\hat{a} = \frac{\beta}{1 - \lambda / D_j} - 1 \qquad (6.15) \qquad\qquad \hat{b} = \frac{1 - \beta}{1 - \lambda / D_j} - 1 \qquad (6.16)$$

$$\beta = \frac{\alpha_{PV}^*}{\alpha_{PV}^* - 1} \qquad (6.17) \qquad\qquad \lambda = \frac{E - 1}{\alpha_{PV}^* - 1} \qquad (6.18)$$

$$\alpha_{PV}^* = E \times \frac{D_i}{D_j} = \frac{K_i P_i^{sat} \gamma_i}{K_j P_j^{sat} \gamma_j} \qquad (A4.6)$$

Knowing that the mass transfer equation (6.3) can be transformed into the following:

$$y_i \frac{dq}{da} = K_i P_i^{sat} \gamma_i \left(x_i - \frac{y_i}{D_i}\right) \qquad (A4.7)$$

By substituting equation (6.10) into equation (A4.7), it yields:

$$y_i \frac{dq}{da} = K_i P_i^{sat} \gamma_i \left(\frac{C_3 y_i (y_i + C_1)}{y_i + C_2} - \frac{y_i}{D_i}\right) \qquad (A4.8)$$

Rearrange equation (A4.8) and integrate both side of the equation:

$$\int_0^Q D_i(y_i + C_2) dq = \int_0^A K_i P_i^{sat} \gamma_i [(D_i C_3 - 1) y_i + (D_i C_3 C_1 - C_2)] da \qquad (A4.9)$$

Since D_i, C_1, C_2 and C_3 are considered as constants according to the assumptions, equation (A4.9) can be simplified as follow:

$$D_i \left(\int_0^Q y_i dq + C_2 Q \right) = K_i P_i^{sat} \gamma_i \left[(D_i C_3 - 1) \int_0^A y_i da + (D_i C_3 C_1 - C_2) A \right]$$ (A4.10)

Let $\dfrac{1}{A} \int_0^A y_i da = \bar{y}_i^a$ and thus the total membrane area requirement can be obtained as follow:

$$A = \frac{F_f \phi (\bar{y}_i + C_2)}{K_i P_i^{sat} \gamma_i \left[(C_3 - 1/D_i) \bar{y}_i^a + (C_1 C_3 - C_2/D_i) \right]}$$ (A4.11a)

By substituting equation (A4.1)-(A4.3) into equation (A4.11), the analytical solution can be expressed in terms of β and λ as follow:

$$A = \frac{F_f \beta \phi (\beta - \bar{y}_i)}{K_i P_i^{sat} \gamma_i (\beta - 1)(1 - \pi / D_i)}$$ (6.21)

$$\text{where} \quad : \pi = \frac{\beta - \left[\dfrac{\alpha_{PV}^*}{E} \lambda (1 - \bar{y}_i^a) + \bar{y}_i^a \right]}{\beta - 1}$$ (A4.11b)

Assume that the total flux throughout the membrane is quasi constant (the argument of the assumption will be discussed in the next section), then

$$\bar{y}_i^a = \frac{1}{A} \int_0^A y_i da \cong \frac{1}{Q} \int_0^Q y_i dq = \frac{x_{f,i} - (1 - \phi) x_{R,i}}{\phi} = \bar{y}_i$$ (6.20d)

Hence, (A4.11b) can be rewritten as:

$$\pi = \frac{\beta - \left[\dfrac{\alpha_{PV}^*}{E} \lambda (1 - \bar{y}_i) + \bar{y}_i \right]}{\beta - 1}$$ (6.22)

From the knowledge of $\alpha^* = \dfrac{K_i P_i^{sat} \gamma_i}{K_j P_j^{sat} \gamma_j}$ and $\beta = \dfrac{\alpha_{PV}^*}{\alpha_{PV}^* - 1}$, equation (6.21) can also be written in terms of mass transfer coefficient of water as follow:

$$A = \frac{F_f \phi(\beta - \bar{y}_i)}{K_j P_j^{sat} \gamma_j \beta(1 - \pi / D_i)}$$ (6.23)

A4.2   The argument of the assumption of constant total flux through the membrane and its effect on area determination

In the derivation of the analytical solution in (6.21), a quasi-constant total flux is assumed. Thus the relationship in equation (6.20d) hold. In this section, the validity of such assumption is tested.

Let the difference between the two integrals be:

$$\Delta = \frac{1}{Q} \int_0^Q y_i dq - \frac{1}{A} \int_0^A y_i da$$ (A4.12)

If Δ is found to be large, then the relationship in equation (6.20d) will not hold.

Knowing that $\dfrac{dq}{da} = J_t$ (see equation (6.3) in page 184), substitute $da = dq / J_t$ into equation (A4.12) and gives:

$$\Delta = \frac{1}{Q} \int_0^Q y_i dq - \frac{1}{Q} \int_0^Q \frac{y_i}{J_t} dq$$ (A4.13)

Let the mean total flux $\bar{J}_t = Q/A$ and substitute into equation (A4.13) and yields:

$$\Delta = \frac{1}{Q} \int_0^Q (1 - \bar{J}_t / J_t) y_i dq$$ (A4.14)

If the local total flux is quasi constant, $\bar{J}_t \cong J_t$ and thus, $\Delta \cong 0$. Due to the fact that large part of the membrane is for polishing the retentate and high concentration of solvent, it is reasonable to assume that the total flux is quasi constant along the membrane area.

Despite the total flux is not quasi constant along the membrane. For pervaporation system with $E \gg 1$ and $\alpha^*_{PV} \gg 1$, the value of the product of $\dfrac{\alpha_{PV}\lambda}{E} \cong 1$, thus from equation (A4.11b), $\pi \cong 1$. Even though the total flux is not quasi constant along the membrane and with a very small E, due to the low operating permeate pressure (i.e. $1/D_i$ is very small), the effect that caused by using $\bar{y}_i$ instead of $\bar{y}_i^a$ in determining of membrane area according to equation (6.21) is small. The difference of membrane area determined by using numerical method and analytical solution based on this assumption was demonstrated in the case study of *examples 6.1&6.2* in Chapter 6 and the difference was found to be small.

References

Abed-Ali, S.S., Brisdon, B.J., England, R. (1989). Poly(Organosiloxanes) Containing Crown Ether Functionalities. *Macromolecules*, 22, 3969-3973.

Aoki, T., Yamagiwa, K., Yoshino, E., Oikawa, E. (1993). Temperature Sensitive Ethanol Permselectivity of Poly(dimethylsiloxane) Membrane by the Modification of its Surface with Copoly(N-isopropylacrylamide / 1H, 1H, 2H, 2H-perfluorododecyl acrylate). Polymer, 34(7), 1538-1540.

Aptel, P., Neel, J. (1986). Pervaporation. In *Synthetic membranes: science, engineering, and application*, ed. Bungay, P. M., Lonsdale, H. K., depinho, M. N. pp403-436. Dordrecht, Holland: Reidal, D. Publishing Company.

Asada, T. (1992). Future of Pervaporation. *Proceedings of 6th Conf. on Pervaporation Processes in the Chemical Industry*. ed. R Bakish., pp. 554-558.

Ashworth, A.J., Brisdon, B.J., England, R., Reddy, B.S.R., Zafar, T. (1991). The Permselectivity of Polyorganosiloxanes containing Ester Functionalities. *Journal of Membrane Science*, 56, 217-228.

Athayde, A.L., Markiewicz, G., Miller, B., Wijmans, J.G. (1995). Removal and Recovery of Volatile Organic Compounds from Water by Pervaporation - Opportunities and Applications. *Proceedings of 7th Conf. on Pervaporation Processes in the Chemical Industry*. ed. R Bakish., pp. 338-348.

Athayde, A.L., Baker, R.W., Daniels, R., Le, M.H., Ly, J.H. (1997). Pervaporation for Wastewater Treatment. *Chemtech*, 27(1), 34-39.

Atkins T. (1996) Physical Chemistry, Chichester, New York, Bris bane, Toronto, Singapore, John Wiley and Sons Co.

Baudot, A., Marin, M. (1997) Pervaporation of aroma compounds: Comparison of membrane performances with vapour liquid equilibria and engineering aspects of process improvement. *Trans. IChemE*, Vol. 75, Part C, 117-142

Baker, R.W., Wijmans, J. G. (1993) Process for Recovering Organic Components from Liquid Streams. US Patent No. 5266206.

Baker, R.W. (1996) Membrane Technology, *Kirk Othmer Encyclopedia of Chemical Technology*. McGraw Hill Corp.

Baker, R. W., Wijmans, J. G., Athayde, A. L., Daniel, R., Ly, J. H., Le, M. (1997) *Journal of Membrane Science*, Vel. 137, p159

Barber, T.A., Miller, B.D. (1994). Pervaporation Technology: Fundamentals and Environmental Applications. *Chemical Engineering*, 101(9), 88-90.

Barrer, R. M., Barrie, J. A., Rogers, M.G. (1962) Permeation through a membrane with mixed bounary conditions, *Trans. Faraday. Soc.*, 58, 2473-2483

Beaumelle, D., Marin, M., Gibert, H. (1993). Pervaporation with Organophilic Membranes: State of the Art. *Trans. IChemE*, 71(Part C), 77-89.

Bell, C.M., Gerner, F.J., Strathmann, H. (1988). Selection of Polymers for Pervaporation Membranes. *Journal of Membrane Science*, 36, 315-329.

Bengtson, G., Pingel, H., Boddeker, K.W. (1991). Recovery of ABE Fermentation Products by Integrated Pervaporation. *Proceedings of 5th Conf. on Pervaporation Processes in the Chemical Industry*. ed. R Bakish., pp. 508-510.

Benedict, M (1947), Multistage separation processes, *J. AIChE*, Vol. 43, No.2, 41-61

Bennett, M. (1994) PhD First Year Report, University of Bath, UK.

Bennett, M. (1996) PhD Thesis, University of Bath, UK

Bennett, M, Brisdon B. J., England, R and Field, R. W. (1997) Performance of PDMS and organofunctionalised PDMS membranes for the pervaporative recovery of organics from aqueous stream, *Journal of Membrane Science.*, 137, 63-88

Binning, R. C., Lee, R. J., Jennings, J.F., Marin, E. C. (1961) Separation of Liquid Mixtures by Permeation. *Ind. & Eng. Chem.* Vol. 53, p45

Bird, R. B., Stewart, W.E., Lightfoot, E. N. (1960). *Transport Phenomena,* John Wiley and Sons, New York, NT.

Bitter, J.G.A. (1991). Transport Mechanisms in Membrane Separation Processes. New York: Plenum Press.

Blume, I., Bos, A., Schwering, P.J.F., Mulder, M.H.V., Smolders, C.A. (1991). Transport Phenomena of Vapour and Liquid Permeants in Elastomeric Membranes. *Proceedings of 5th International Conference on Pervaporation Processes in the Chemical Industry.* ed. R.Bakish., pp. 190-204.

Blume, I., Baker, R. W. (1987) Separation and Concentration of Organics from Water Using Pervaporation, *Proceedings of Second International Conference on Pervaporation Process in the Chemical Industry,* Bakish Materials Corp., p111

Blume, I., Pinnau, I. (1990). Composite membranes, method of preparation and use; US Patent 4963165

Blume, I., Wijmans, J.G., Baker, R.W. (1990). The Separation of Dissolved Organics from Water by Pervaporation. *Journal of Membrane Science,* 49, 253-286.

Blume, I., Schwering, P.J.F., Mulder, M.H.V., Smolders, C.A. (1991). Vapour Sorption and Permeation Properties of Polydimethylsiloxane Films. *Journal of Membrane Science,* 61, 85-97.

Boddeker, K.W., Bengtson, G., Bode, E. (1990). Pervaporation of Low Volatility Aromatics from Water. *Journal of Membrane Science,* 53, 143-158.

Boddeker, K.W., Bengtson, G. (1991). Selective Pervaporation of Organics from Water. In: Pervaporation Membrane Separation Processes. Huang, R.Y.M. ed., pp. 437-460. Amsterdam: Elsevier.

Boddeker, K.W., Pingel, H., Dede, K. (1992). Continuous Pervaporation of Aqueous Phenol on a Pilot Plant Scale. *Proceedings of 6th Conf. on Pervaporation Processes in the Chemical Industry.* ed. R Bakish., pp. 514-519.

Bode, E., Busse, M., Ruthenberg, K. (1993). Considerations on interface resistances in the process of permeation of dense membranes. *Journal of Membrane Science,* 77, 69-84.

Bode, E., Hoempler, C. (1996). Transport resistances during pervaporation through a composite membrane: experiments and model calculations. *Journal of Membrane Science*, 113, 43-56

Borges, C.P., Mulder, M.H.V., Smolders, C.A. (1992). Composite Hollow Fiber for Removal of VOCs from Water by Pervaporation. *Proceedings of 6th International Conference on Pervaporation Processes in the Chemical Industry.* ed. R.Bakish., pp. 207-222.

Brisdon, B.J., Watts, A.M. (1985). Synthesis of Organofunctional Siloxanes Containing Metal-Ligating Side-Chains. *J. Chem. Soc. Dalton Trans.*, 2191-2194.

Brodkey, R.S., Hershey, H.C. (1988). Transport Phenomena A Unified Approach. New York: McGraw-Hill.

Brun, J.P., Larchet, C., Melet, R., Bulvestre, G. (1985). Modeling of the Pervaporation of Binary Mixtures through Moderately Swelling, Non-Reacting Membranes. *Journal of Membrane Science,* 23, 257-283.

Brun, J.P., Larchet, C., Bulvestre, G., Auclair, B. (1985). Sorption and Pervaporation of Dilute Aqueous Solutions of Organic Compounds through Polymer Membranes. *Journal of Membrane Science,* 25, 55-100.

Bruschke, H.E.A. (1991). State-of-Art of Pervaporation. Proceedings of 5th Conf. on Pervaporation Processes in the Chemical Industry. ed. R Bakish., pp. 2-6.

Burslem, R.H., Naylor, T.D., Field, R.W. (1992). The Performance and Stability of Polyacrylate Membranes. *Proceedings of 6th International Conference on Pervaporation Processes in the Chemical Industry*. ed. R.Bakish., pp. 17-34.

Burslem, R. H. (1996). PhD Thesis, *The University of Bath*, UK.

Cartwright, P. (1994) Membranes Meets Environmental Challenges. *Chemical Engineering*, September, p85.

Castello, M. J., Fane, A. G., Hogan, P.A., Schofield, R.W. (1993) The effect of shell side hydrodynamics on the performance of axial flow hollow fibre modules. *Journal of Membrane Science*, 80, 1-11

Chilton, T. H., Colburn, A.P. (1935). Distillation and absorption in packed columns, A convinient design and correlation method. *Ind. Eng. Chem.*, 27, p255

Côté, P., Lipski, C. (1988). Mass Transfers Limitations in Pervaporation for Water and Wastewater Treatment. *Proceedings of Third International Conference on Pervaporation Processes in Chemical Industry*, 449-462.

Crank, J. (1975). The Mathematics of Diffusion. Second Edition. Oxford: Clarendon Press.

Cussler, E.L. (1984). Diffusion: Mass Transfer in Fluid Systems. Cambridge: Cambridge University Press.

Dotremont, C., Brabants, B., Geeroms, K., Mewis, J., Vandecasteele, C. (1995). Sorption and Diffusion of Chlorinated Hydrocarbons in Silicalite Filled PDMS Membranes. *Journal of Membrane Science*, 104, 109-117.

Drioli, E., Zhang, S., Basile, A. (1993). On the Coupling Effect in Pervaporation. *Journal of Membrane Science*, 81, 43-55.

Drioli, E., Zhang, S., Basile, A. (1993). Recovery of Pyridine from Aqueous Solution by Membrane Pervaporation. *Journal of Membrane Science*, 80, 309-318.

Ebert, K. (1995). Thin film composite membranes of glassy polymers for gas separation: preparation and characterization, *Dissertation*, University of Twente, Netherland.

Fang, Y., Pham, V.A., Mahmud, H., Santerre, J.P., Narbaitz, R.M., Matsuura, T. (1995). Application of Surface Modifying Macromolecules for the Preparation of Membranes with High Surface Hydrophobicity to Extract Organic Molecules from Water by Pervaporation. *Proceedings of 7th International Conference on Pervaporation Processes in the Chemical Industry*. ed. R.Bakish., pp. 349-362.

Favre, E., Nguyen, Q.T., Schaetzel, P., Clement, R., Neel, J. (1993). Sorption of Organic Solvents into Dense Silicone Membranes. *Journal of the Chemical Society Faraday Transactions*, 89(24), 4339-4346.

Favre, E., Nguyen, Q.T., Schaetzel, P., Clement, R., Neel, J. (1994). Sorption, Diffusion and Vapor Permeation of Various Penetrants through Dense Polydimethylsiloxane Membranes: a Transport Analysis. *Journal of Membrane Science*, 92, 169-184.

Feng, X., Huang, R.Y.M. (1992). Separation of Isopropanol from Water by Pervaporation using Silicone Based Membranes. *Journal of Membrane Science*, 74, 171-181.

Feng, X., Huang, R.Y.M. (1994). Concentration Polarisation in Pervaporation Separation Processes. *Journal of Membrane Science*, 92, 201-208.

Feng, X., Huang, R.Y.M. (1996). Estimation of activity energy for permeation in pervaporation process. *Journal of Membrane Science*, 118, 127-131.

Feng, X., Huang, R.Y.M. (1997). Liquid separation by membrane pervaporation: a review. *Ind. Eng. Chem. Res.* 36, 1048-1066

Field, R.W., Burslem, R. (1992). The Effect of Concentration Polarisation upon the Performance of Pervaporation Membranes. *Proceedings of 6th International Conference on Pervaporation Processes in the Chemical Industry.* ed. R.Bakish., pp. 275-289.

Fleming, H.L. (1990). Membrane Pervaporation: Separation of Organic/Aqueous Mixtures. *Separation Science and Technology,* 25(13-15), 1239-1255.

Fleming, H. I. , Slater, C. S. (1992) Pervaporation : In Handbook of Membrane., by Ho, W. and Sikdar, K. pp105

Flory, P.J. (1953). Principles of Polymer Chemistry. New York: Cornell University Press.

Freitas Dos Santos, L. M., Blundo, Lo. G. (1999) Treatment of Pharmaceutical Industry Proces Wastewater Using the Extractive Membrane Bioreactor. *Environmental Progress,* Vol 18., No 1., Spring, p34 -39

Fujita, H. (1961). Diffusion in Polymer-Diluent Systems. *Advanced Polymer Science,* 3, 1-23.

Gabelman, A., and Hwang, S-T. (1999). Hollow fiber membrane contactors, *Journal of Membrane Science,* 159, 61-106.

Geankoplis, C. J. (1982). Mass Transport Phenomena, 5th Printing. New York: Holt, Rinehart and Winston Inc.

Gekas, V., Hallstrom, B. (1987). Mass Transfer in the Membrane Concentration Polarisation Layer Under Turbulent Crossflow. I. Critical Literature Review and Adaptation of Existing Sherwood Correlations to Membrane Operations. *Journal of Membrane Science,* 30, 153-170.

Gilliland, E. R., Baddour, R. F., Russell, J. L. (1958). Rates of flow through microporous solids, *AIChE. J.* 4, p90.

Gmehling, J., Onken, U., Artt, W. (1978). Vapour-Liquid Equilibrium Data Collection. Frankfurt: Dechema.

Goe, G.L. (1982). Pyridine and Pyridine Derivatives. In: Kirk - Othmer Encyclopedia of Chemical Technology. 3rd ed. vol 19. ed. Mark, H.F., Othmer, D.F., Overberger, C.G., Seaborg, G.T., Greyson, M., Eckroth, D. New York: John Wiley & Sons.

Goethaert, S., Dotremont, C., Kuijpers, M., Michiels, M., Vandecasteele, C. (1993). Coupling Phenomena in the Removal of Chlorinated Hydrocarbons by means of Pervaporation. *Journal of Membrane Science,* 78, 135-145.

Gooding, C.H., Hickey, P.J., Crowder, M.L. (1991). Mass Transfer Characteristics of a New Pervaporation Module for Water Purification. *Proceedings of 5th International Conference on Pervaporation Processes in the Chemical Industry.* ed. R.Bakish., pp. 237-249.

Graham, T. (1866). London Edinburgh Dublin Phil. Mag. Sci. Serie 4 32 p401

Gref, R., Nguyen, Q.T., Neel, J. (1992). Influence of Membrane Properties on System Performances in Pervaporation under Concentration Polarisation Regime. *Separation Science and Technology,* 27(4), 467-491.

Greenlaw, F.W., Prince, W.D., Shelden, R.A., Thompson, E.V. (1977). Dependence of Diffusive Permeation Rates on Upstream and Downstream Pressures. I. Single Component Permeat. *Journal of Membrane Science,* 2, 141-151.

Greenlaw, F.W., Prince, W.D., Shelden, R.A., Thompson, E.V. (1977). Dependence of Diffusive Permeation Rates on Upstream and Downstream Pressures. II. Two Component Permeat. *Journal of Membrane Science,* 2, 333-348. *Journal of Membrane Science,* 2, 333-348.

Guo, C.J., Kee, D.D. (1992). Effect of Molecular Structure on Diffusion of Organic Solvents in Rubbers. *Chemical Engineering Science*, 47, 1525-1532.

Gudernatsch, W., Menzel, Th., Strathmann, H. (1991a) Influence of composite membrane structure on pervaporation. *Journal of Membrane Science*, 61, 19-30

Gudernatsch, W., Kimmerle, K. (1991b). New Capillary Module for Pervaporation. *Proceedings of 5th International Conference on Pervaporation Processes in the Chemical Industry*. ed. R.Bakish., pp. 259-269.

Habib, A.G. (1989). Methyl Isobutyl Ketone. Encyclopedia of Chemical Processing and Design vol. 21. ed. McKetta, J.J. New York: Marcel Dekker Inc. pp. 50-63.

He, G., Huang, X., Xu, R., Zhu, B. (1996). An improved resistance model for gas permeation in composite membranes. *Journal of Membrane Science*, 118, 1-7.

Heintz, A., Funke, H., Lichtenthaler, R.N. (1991). Sorption and Diffusion in Pervaporation Membranes. *Pervaporation Membrane Separation Processes*. ed. R.Y.M. Huang. Amsterdam: Elsevier pp. 279-320.

Heintz, A., Stephan, W. (1994). A Generalised Solution-Diffusion Model of the Pervaporation Process through Composite Membranes. Part II. Concentration Polarization, Coupled Diffusion and the Influence of the Porous Support Layer. *Journal of Membrane Science*, 89, 153-169.

Henis., J. M. S. , Tripodi, M. K. (1981) Composite hollow fiber membranes for gas separation: The resistance model approach, *Journal of Membrane Science.*, 8, 233

Hennepe, H.J.C.te, Bargeman, D., Mulder, M.H.V., Smolders, C.A. (1987). Zeolite Filled Silicone Rubber Membranes. Part 1. Membrane Preparation and Pervaporation Results. *Journal of Membrane Science*, 35, 39-55.

Hennepe, H.J.C.te, Boswerger, W.B.F., Bargeman, D., Mulder, M.H.V., Smolders, C.A. (1994). Zeolite Filled Silicon Rubber Membranes Experimental Determination of Concentration Profiles. *Journal of Membrane Science*, 89, 185-196.

Hennepe, H.J.C.te, Smolders, C.A., Bargeman, D., Mulder, M.H.V. (1991). Exclusion and Tortuosity Effects for Alcohol / Water Separation by Zeolite Filled PDMS Membranes. *Separation Science and Technology*, 26(4), 585-596.

Hickey, P.J., Gooding, C.H. (1994). The Economic Optimisation of Spiral Wound Membrane Modules for the Pervaporative Removal of VOC's from Water. *Journal of Membrane Science*, 97, 53-70.

Hino, T., Ohya, H., Hara, T. (1991). Removal of Halogenated Organics from their Aqueous Solutions by Pervaporation. *Proceedings of 5th Conf. on Pervaporation Processes in the Chemical Industry*. ed. R Bakish., pp. 423-436.

Huang, R.Y.M., Rhim, J.W. (1991). Separation Characteristics of Pervaporation Membrane Separation Processes. *Pervaporation Membrane Separation Processes*. ed. R.Y.M. Huang. Amsterdam: Elsevier, pp.111-180.

Hwang, S-T. and Thorman, J. M., (1980) The continuous membrane column, *J. AIChE.*, Vol. 26, No. 4, 558-566.

Ji, W., Hilaly, A., Sikdar, S.K., Hwang, S.T. (1994). Optimisation of Multicomponent Pervaporation for Removal of Volatile Organic Compounds from Water. *Journal of Membrane Science*, 97, 109-125.

Ji, W., Sikdar, S.K., Hwang, S.T. (1994). Modeling of Multicomponent Pervaporation for Removal of Volatile Organic Compounds from Water. *Journal of Membrane Science*, 93, 1-19.

Jian, K., Pintaro, P. N., (1996). Separation of dilute organic/water mixtures with asymmetric poly(vinylidene fluoride) membranes. *Journal of Membrane Science*, 117, 117-133

Jian, K., Pintaro, P. N., (1997). Asymmetric PVDF hollow fiber membranes for organics/water separation, *Journal of Membrane Science*, 135, 41-53

Jordt, F., Ohlrogge, K., Hapke, J. (1997). A Liquid Ring Vakuum Pump Combined with Pervaporation Unit to Ensure a Steady Capacity. *Euromembrane '97- Progress in Membrane Science and Technology, Third International Symposium*. (Oral Presentation).

Joyce, P.C., Devine, K.M., Slater, C.S. (1995). Separation of Pyridine / Water Solutions using Pervaporation. *Separation Science and Technology*, 30(10), 2145-2158.

Kaka, K. M., Fane, A. G., Ma, R. (1992). *Proceeding of Engineering and Membrane Processes*, Germany.

Karlsson, H.O.E., Tragardh, G. (1993). Pervaporation of Dilute Organic-Waters Mixtures. A Literature Review on Modeling Studies and Applications to Aroma Compound Recovery. *Journal of Membrane Science*, 76, 121-146.

Kaschmekat, J., Wijmans, J. G., Baker, R. W., Blume, I (1988). Separation of Organic Solvents from Water. *Proceedings of Third Conference on Pervaporation Processes in the Chemical Industry*. ed. R Bakish., pp. 405.

Kaschmekat, J., Baker, R. W., Wijmans, J. G. (1990). Membrane Module, US Patent No. 5069793.

Kataoka, T., Tsuru, T., Nakao, S., Kimura, S. (1991a) Membrane transport properties of pervaporation and vapor permeation in ethanol-water system using polyacylonitrile and cellulose acetate membranes. *Journal of Chemical Engineering Japan*, 24, p334

Kataoka, T., Tsuru, T., Nakao, S., Kimura, S. (1991b) Permeation equations developed for prediction of membrane performance in pervaporation, vapor permeation and reverse osomosis based on solution-diffusion model. *Journal of Chemical Engineering Japan*, 24, p326

Kedem, O. (1989). The Role of Coupling in Pervaporation. *Journal of Membrane Science*, 47, 277-284.

Kesting, R. E. (1985) *Synthetic membranes: A structural prospective*, 2nd Ed., John Wiley and Sons Corp. New York.

Kondo, M., Sato, H. (1994). Treatment of Wastewater from Phenolic Resin Process by Pervaporation. *Desalination*, 98, 147-154.

Koningsveld, R., Kleinjtens, L.A. (1971). Liquid-Liquid Phase Separation in Multicomponent Polymer Systems. X. Concentration Dependence of the Pair Interaction Parameter in the System Cyclohexane-Polystyrene. *Macromolecules*, 4, 637-641.

Koops, G.H., Smolders, C.A. (1991). Estimation and Evaluation of Polymeric Materials for Pervaporation Membranes. In: Pervaporation Membrane Separation Processes. Huang, R.Y.M. ed., pp. 253-278. Amsterdam: Elsevier.

Lamer, T., Rohart, M.S., Voilley, A., Baussart, H. (1994). Influence of Sorption and Diffusion of Aroma Compounds in Silicone Rubber on their Extraction by Pervaporation. *Journal of Membrane Science*, 90, 251-263.

Lapack, M.A., Tou, J.C., McGuffin, V.L., Enke, C.G. (1994). The Correlation of Membrane Permselectivity with Hildebrand Solubility Parameters. *Journal of Membrane Science*, 86, 263-280.

Lee, C. H. (1975). Theory of reverse osmosis and some other membrane permeation proceses. *J. Appl. Polym. Sci.* 19, p83.

Lee, Y.M., Bourgeois, D., Belfort, G. (1989). Sorption, Diffusion and Pervaporation of Organics in Polymer Membranes. *Journal of Membrane Science*, 44, 161-181.

Lee, Y.M., Bourgeois, D., Belfort, G. (1989). Sorption, Diffusion and Pervaporation of Organics in Polymer Membranes. *Journal of Membrane Science*, 44, 161-181.

Lee, Y.T., Iwamoto, K., Sekimoto, H., Seno, M. (1989). Pervaporation of Water-Dioxane Mixtures with Poly(Dimethylsiloxane-co-Siloxane) Membranes Prepared by a Sol-Gel Process. *Journal of Membrane Science*, 42, 169-182.

Lee, G.T., Krovvidi, K.R., Greenberg, D.B. (1989). Pervaporation of Trace Chlorinated Organics from Water through Irradiated Polyethylene Membrane. *Journal of Membrane Science*, 47, 183-202.

Lipnizki, L., Haussmans, S., Ten, P. K., Field, R. W., Laufenberg, G. (1999). Organophilic Pevaporation: Prospects and Performance. *Chemical Engineering Journal*, 73, 113-129.

Lipski, C., Cote, P. (1990). The use of Pervaporation for the Removal of Organic Contaminants from Water. *Environmental Progress*, 9(4), 254-261.

Lipski, C., Cote, P., Fleming, H. (1991). Transverse Feed Flow for Hollow Fibres Significantly Improves Mass Transfer at Low Energy Consumption. *Proceedings of 5th International Conference on Pervaporation Processes in the Chemical Industry*. ed. R.Bakish., pp. 134-142.

Lipski, C, Cote, P. (1992). Supported Pervaporation Membrane and Module containing Arrays of Membrane. US Patent No. 5167825

Liu, M.G., Dickson J.M., Côté, P. (1996). Simulation of a Pervaporation System on the Industrial Scale for Waste Water Treatment Part I: Extended Resistance-in-Series Model. *Journal of Membrane Science*, 111, 227-241.

Long, R. B. (1965). Liquid permeation through plastic films. *Ind. Eng. Chem. Fundam.*, 4, 445-451

Lopez, J. L., Matson, S. L., Marchese, J., Quinn, J. A. (1986). Diffusion through composite membrane: two-dimensional analysis., *Journal of Membrane Science*, 27, p301

Matson, S. L., Lopez, J. and Quinn, J. A., (1983).Separation of gases with synthetic membranes. *Review Article No.13, Chem. Eng. Sci.* Vol. 38, No.4, 503-524

Matsumoto, Y., Kondo, M., Fujita, T. (1992). Transport Mechanism in PEBA Membrane. *Proceedings of 6th Conf. on Pervaporation Processes in the Chemical Industry.* ed. R Bakish., pp. 55-65.

Mauro, A. (1960). Some properties of ionic and non ionic semi-permeable membranes, Circulation, 21, p845

McCray, S. B., Friesen, D. T., Newbold, D. D., Ray, R., Millard, D. L. (1995). Tube-side-feed hollow fiber modules for pervaporation. In *Proceedings of the 7th International conference on pervaporation processes in Chemical Industry,* (Ed.) Bakish, R., Bakish Material Corp. New Jersey.

Meckl (1994) Dissertation, *University of Heidelberg*, Germany.

Michaels, A.S. (1995). Effects of Feed-Side Solute Polarisation on Pervaporative Stripping of Volatile Organic Solutes from Dilute Aqueous Solution: a Generalised Analytical Treatment. *Journal of Membrane Science*, 101, 117-126.

Molina, C., Steinchen, A., Charbit, G., Charbit, F. (1997). Model for pervaporation:application to ethanolic solutions of aroma. *Journal of Membrane Science*, 132, 119-129.

Moulin, P., Serra, C., Rouch, C., Clifton, M. J., Aptel, P. (1996). Mass transfer improvement by secondary flows: Dean vortices in coiled tubular membranes, *Journal of Membrane Science*, 114, 235-244.

Mulder, M.H.V., Franken, T., Smolders, C.A. (1985). Preferential Sorption Versus Preferential Permeability in Pervaporation. *Journal of Membrane Science*, 22, 155-173.

Mulder, M.H.V. (1991). Thermodynamic Principles of Pervaporation. *Pervaporation Membrane Separation Processes.* ed. R.Y.M. Huang. Amsterdam: Elsevier pp. 225-252.

Mulder, M.H.V., Smolders, C.A. (1991). Mass Transport in Pervaporation Processes. *Separation Science and Technology*, 26(1), 85-95.

Mulder, M.H.V., Smolders, C.A. (1984). On the Mechanism of Separation of Ethanol/Water Mixtures by Pervaporation. I. Calculations of Concentration Profiles. *Journal of Membrane Science*, 17, 289-307.

Naylor, R. W. and Backer, P. O. (1955) Enrichment calculations in gaseous diffusion: Large separation factor, *J. AIChE*, Vol. 1, No. 1, 95-99

Neel, J. (1991). Introduction to Pervaporation. *Pervaporation Membrane Separation Processes.* ed. R.Y.M. Huang. Amsterdam: Elsevier pp. 1-110.

Nguyen, T.Q. (1987). Modeling of the Influence of Downstream Pressure for Highly Selective Pervaporation. *Journal of Membrane Science*, 34, 165-183.

Nguyen, T.Q., Nobe, K. (1987). Extraction of Organic Contaminants in Aqueous Solutions by Pervaporation. *Journal of Membrane Science*, 30, 11-22.

Nijhuis, H.H. (1990). Removal of Trace Organics from Water by Pervaporation. A Technical and Economic Analysis. Ph.D. Thesis, University of Twente, Enshede, The Netherlands.

Nijhuis, H.H., Mulder, M.H.V., Smolders, C.A. (1991). Removal of Trace Organics from Aqueous Solutions. Effect of Membrane Thickness. *Journal of Membrane Science*, 61, 99-111.

Nijhuis, H.H., Mulder, M.H.V., Smolders, C.A. (1993). Selection of Elastomeric Membranes for the Removal of Volatile Organics from Water. *Journal of Applied Polymer Science*, 47, 2227-2243.

Noezar, L., Nguyen, Q.T., Clement, R., Neel, J. (1995). High Performance Polymer Blend Membranes for Alcohol - Ether Separation. *Proceedings of 7th International Conference on Pervaporation Processes in the Chemical Industry.* ed. R.Bakish., pp. 45-51.

Okada, T., Matsuura, T. (1991). A New Transport Model for Pervaporation. *Journal of Membrane Science*, 59, 133-150.

Okada, T., Matsuura, T. (1992). Theoretical and Experimental Study of Pervaporation on the Basis of Pore Flow Mechanism. *Proceedings of 6th International Conference on Pervaporation Processes in the Chemical Industry.* ed. R.Bakish., pp. 137-152.

Page, C. A., Fouda, A. E. R. Tyagi, R., Matsuura, T. (1994) Pervaporation performance of polyetherimide membranes spin- and dip-coated eith polydimethylsiloxane, *Journal of Applied Polymer Science*, Vol., 54, 975-989

Pan, C. Y. and Habgood, H. W. (1974) An analysis of the single-stage gaseous permeation process, *Ind. Eng. Chem., Fundam.,* Vol. 13, No. 4, 323-331

Pan, C. Y. and Habgood, H. W. (1978) Gas separation by permeation Part 1. Calculation methods and parametric analysis., *Can. J. Chem. Eng.* Vol. 56, 197-209

Pan, C. Y., (1983), Gas separation by permeators with high flux asymmetric membranes, *J. AIChE*, Vol. 29, No. 4, 545-553

Paul, D. R. (1974a). Diffusive transport in swollen polymer membranes, in H. B. Hopfenberg (Ed.), Permeability of plastic films and coatings, Pergamon, New York.

Paul, D. R. (1974b). Further comment on the relation between hydraulic permeation and diffusion. *J. Appl. Polym. Sci.,* 12, p1221

Perry, R.H., Green, D.W., Maloney, J.O. (1984). Perrys Chemical Engineers Handbook. 6th ed. New York: McGraw-Hill.

Peters, M.S., Timmerhaus, K.D. (1982). Plant Design and Economics for Chemical Engineers, New York: McGraw-Hill.

Psaume, R., Aptel, P., Aurelle, J.C., Mora, J.C., Bersillon, J.L. (1988). Pervaporation: Importance of Concentration Polarisation in the Extraction of Trace Organics from Water. *Journal of Membrane Science*, 36, 373-384.

Radovanovic, P., Thiel, S.W., Hwang, S.T. (1990). Transport of Ethanol-Water Dimers in Pervaporation through a Silicone Rubber Membrane. *Journal of Membrane Science*, 48, 55-65.

Raghunath, B., Hwang, S.T. (1992). Effect of Boundary Layer Mass Transfer Resistances in the Pervaporation of Dilute Organics. *Journal of Membrane Science*, 65, 147-161.

Rautenbach, R., Albrecht, R. (1985). The Separation Potential of Pervaporation Part 1. Discussion of Transport Equations and Comparison with Reverse Osmosis. *Journal of Membrane Science*, 25, 1-23.

Rautenbach, R., Albrecht, R. (1989). Membrane Processes. Chichester, New York, Bris bane, Toronto, Singapore, John Wiley & Sons.

Rautenbach, R., Klatt, S. (1991). Treatment of Phenol Contaminated Waste water by a RO-PV Hybrid Process. *Proceedings of 5th Conf. on Pervaporation Processes in the Chemical Industry*. ed. R Bakish., pp. 392-408.

Rautenbach, R., Klatt, S., Vier, J. (1992). State of the Art of Pervaporation, 10 Years of Industrial PV. *Proceedings of 6th Conf. on Pervaporation Processes in the Chemical Industry*. ed. R Bakish., pp. 2-15.

Reid, R.C., Prausnitz, J.M., Poling, B.E. (1987). The Properties of Gases and Liquids. 4th ed. New York: McGraw-Hill.

Rhim, J.W., Huang, R.Y.M. (1989). On the Prediction of Separation Factor and Permeability in the Separation of Binary Mixtures by Pervaporation. *Journal of Membrane Science*, 46, 335-348.

Riley, R. L., Grabowsky, R. L., (1980). Preparation of gas separation membranes; U. S. Patent 4243701
Rogers, C. E., Stannett, V., Szwarc, M. (1960). The sorption, diffusion, and permeation of organic vapors in polyethylene. *J. Polymer Sci.* 45, 61-85

Rosenbaum, S., Cotton, O. (1969). Steady-state distribution of water in cellulose acetate membrane. *J. Polymer Sci.* 7, p101

Royal Society of Chemistry (1996). Website information from http://www. rsc.bids.ac.uk/

Sander, U., Soukup, P. (1988) Design and Operation of Pervaporation Plant for Ethanol Dehydration. *Journal of Membrane Science*, Vol 36, 463-475

Schnabel, S., Moulin, P., Nguyen, T. Q., Roizard, D., Aptel, P. (1998). Removal of volatile organic components (VOCs) from water by pervaporation: separation improvement by Dean vortices, 142, 129-141

Schofield, W., McCray, B., Ray, R.J., Newbold, D.D. (1991). Opportunities for Pervaporation in the Water Treatment Industry. *Proceedings of 5th Conf. on Pervaporation Processes in the Chemical Industry*. ed. R Bakish., pp. 409-420.

Sferrazza, R.A., Escobosa, R., Gooding, C.H. (1988). Estimation of Parameters in a Sorption-Diffusion Model of Pervaporation. *Journal of Membrane Science*, 35, 125-136.

Shaban, H.I. (1995). Separation of Binary, Ternary and Multicomponent Organic/Water Mixtures. *Gas Separation and Purification*, 9(2), 75-79.

Shanley, A., Ondrey, G., Moore, S. (1994). Pervaporation finds its Niche. Chemical Engineering, 101(9), 34-37.

Shelden R. A., Thompson, V. (1978) Dependence of diffusive permeation rates on the upstream and downstream pressure III. Membrane selectivity and implications for separation processes, *Journal of Membrane Science*, 4, 115-127

Shelden R. A., Thompson, V. (1984) Dependence of diffusive permeation rates on the upstream and downstream pressure IV. Computer simulation of non-ideal systems, *Journal of Membrane Science*, 19, 39-49

Shieh, J. J., Huang, R.Y.M. (1998) A pseudophase-change solution-diffsion model for pervaporation. II. Binary mixture permeation. *Separation Science and Technology*, 33, 933-957

Shimizu, S., Watanabe, N., Kataoka, T., Shoji, T., Abe, N., Morishita, S., Ichimura, H. (1993). Pyridine and Pyridine Derivatives. *Ullmans Encyclopedia of Industrial Chemistry*, Vol A 22 ed. Elves, B., Hawkins, S., Russey, W., Schulz, G. Weinheim: VCH Publishers Inc, pp. 399-430.

Siegel, H., Eggersdorfer, M. (1993). Ketones. *Ullmans Encyclopedia of Industrial Chemistry*, Vol A 15 ed. Elves, B., Hawkins, S., Russey, W., Schulz, G. Weinheim: VCH Publishers Inc, pp. 77-94.

Singh, R. (1998) Industrial Membrane Separation Processes, *ChemTech*, April, 33-44

Slater, C. S., Hickey, P. J. (1989). Pervaporation R&D: a chronological and geographic prospective. In *Proceedings of the 4th International conference on pervaporation processes in Chemical Industry*, (Ed.) Bakish, R., Bakish Material Corp. New Jersey.

Slater, C.S., Hickey, P.J., Juricic, F.P. (1990). Pervaporation of Aqueous Ethanol Mixtures through Polydimethylsiloxane Membranes. *Separation Science and Technology*, 25(9&10), 1063-1077.

Sourirajan, S., Matsuura, T. (1985). *Reverse Osmosis/Ultrafiltration process principles*, National research Council Canada: Ottawa.

Saltonstall, C. W. (1987) Calculation of the membrane area requirement for gas separation., *Journal of Membrane Science* . Vol. 32, 185-193

Stern, S. A. and Walawender, W. P. (1969), Analysis of membrane separation parameters, *Separation. Sc.*, Vol. 4, No. 2, 129-159

Stern, S. A. and Walawender, W. P. (1972), Analysis of membrane separation parameters. II. Counter-current and co-current flow in a single permeation stage., *Separation Sc.*, Vol. 7, No. 5, 553-584

Strathmann, H., Bell, C. M., Gudernatsch, W., Kimmerle, K. (1988) Die Entwicklung von losungsmittelselektiven Membranen und ihre Anwendung in der Gastrennung und Pervaporation, *Chem. Ing. Technik.*, 60, 590-603

Sturken, K. (1994). PhD Thesis, Technische Universitat Hamburg, Hamburg, Germany.

Takegami, S., Yamada, H., Tsujii, S. (1992). Pervaporation of Ethanol/Water Mixture using Novel Hydrophobic Membranes containing Polydimethylsiloxane. *Journal of Membrane Science*, 75, 93-105.

Ten, P. K. (1997) First year PhD Report, The University of Bath, UK.

Ten, P. K., Field, R. W., Brisdon, B. J., England, R., and Bennett, M. (1998) "A Simplified Method for the Determination of Intrinsic Selectivity in Pervaporation." *IChemE Research Event 1998, Newcastle*, IChemE, UK

Ten, P. K. and Field, R. W. (1998) "Organophilic Pervaporation" in Membrane Workshop "Membrane processes call on expanded limits." *Nordic Network in Membrane Technology*, 1998, Trondheim, Norway.

Ten, P. K., Field, R. W. (2000) Organophilic pervaporation: an engineering science analysis of component transport and the classification of behaviour with reference to the effect of permeate pressure. *Chemical Engineering Science*, Vol. 55, p1425-1445

Tyagi, R.K., Fouda, A.E., Matsuura, T. (1995). A Pervaporation Model: Membrane Design. *Chemical Engineering Science*, 50(19), 3105-3114.

UK Environmental (1995). Website information from *http://www.environmental.gov.uk/*
Van der Scheer (1986). Composite dense membranes; US Patent 4581043.

Van Krevelen, D. W. (1976). Properties of Polymers - Their estimation and correlation with chemical structure, Elsevier, Amsterdam.

Vankelecom, I.F.J., Depre, D., Beukelaer, S.D., Uytterhoeven, J.B. (1995). Influence of Zeolites in PDMS Membranes: Pervaporation of Water / Alcohol Mixtures. *Journal of Physical Chemistry*, 99, 13193-13197.

Vankelecom, I.F.J., Scheppers, E., Heus, R., Uytterhoeven, J.B. (1994). Parameters Influencing Zeolite Incorporation in PDMS Membranes. *Journal of Physical Chemistry*, 98, 12390-12396.

Volkov, V.V., Bokarev, A.K., Zheleznov, A.V., Selinskaya, Y.A., Rakhimov, V.M., Borisov, M.Y., Zakhovaev, I.R. (1995). Removal of High Boiling Organic Compounds from their Aqueous Solutions by Pervaporation. *Proceedings of 7th Conf. on Pervaporation Processes in the Chemical Industry*. ed. R Bakish., pp. 397-407.

Wakeman, W. A. and Mason, E. A. (1979) Diffusion through Multiperforate Laminae. *Ind. Eng. Chem. Fundam.*, 118, p301

Watson, J.M., Payne, P.A. (1990). A Study of Organic Compound Pervaporation through Silicone Rubber. *Journal of Membrane Science*, 49, 171-205.

Watson, J.M., Zhang, G.S., Payne, P.A. (1992). The Diffusion Mechanism in Silicone Rubber. *Journal of Membrane Science*, 73, 55-71.

Weast, R. C., Astle, M. J. (1980). *CRC Handbook of Data on Organic Compound.* Boca Raton, Fla. CRC Press.

Weller, S. and Steiner, W. A. (1950a) Engineering aspects of separation of gases: Fractional permeation through membranes., *Chem. Eng. Prog.*, Vol. 46, No. 11, 585-590.

Weller, S. and Steiner, W. A (1950b) Separation of gases by fractional permeation through membranes., *J. Applied Physics*, Vol. 21, 279-282

Wesslein, M., Heintz, A., Lichtenthaler, R. N. (1990). Pervaporation of liquid mixtures through poly(vinyl alcohol) membranes. I. Study of water containing binary systems with complete and partial miscibility, *Journal of Membrane Science*, 52, p169

Wickramasinghe, S. R., Semmens, M.J., Cussler, E. L. (1993) Hollow fiber modules made with hollow fiber fabric. *Journal of Membrane Science*, 84, 1-14

Wijmans, J.G., Baker, R.W. (1993). A Simple Predictive Treatment of the Permeation Process in Pervaporation. *Journal of Membrane Science*, 79, 101-113.

Wijmans, J.G., Baker, R.W. (1995). The solution-diffusion model: a review. *Journal of Membrane Science*, 107, p1.

Wijmans, J.G., Kaschemekat, J., Davidson, J.E., Baker, R.W. (1990). Treatment of Organic Contaminated Wastewater Streams by Pervaporation. Environmental Progress, 9(4), 262-268.

Wijmans, J. G., Athayde, A. L., Daniel, R., Ly, J. H., Kumaruddin, H. D., Pinnau, I. (1996) *Journal of Membrane Science,* Vol. 109, p135

Wu, P., Field, R.W. (1998). Experimental and modeling study of composite pervaporative membranes, *ICMST' 98*, June., Beijing.

Xie, H.A., Ping, Z.H., Nguyen, Q.T., Neel, J. (1992). Dehydration of Highly Corrosive Liquids by Pervaporation. *Proceedings of 6th Conf. on Pervaporation Processes in the Chemical Industry.* ed. R Bakish., pp. 361-367.

Yamaguchi, T., Yamahara, S., Nakao, S., Kimura, S. (1994). Preparation of Pervaporation Membranes for Removal of Dissolved Organics from Water by Plasma-Graft Filling Polymerization. *Journal of Membrane Science*, 95, 39-49.

Yeom, C. K., Lee, K. H. (1997). A study on desorption resistance in pervaporation of single component through dense membrane. *J. Appl. Polymer Sci.*, 63, 221-232

Young, M.L., Bourgeois, D., Belfort, G. (1989). Sorption, Diffusion and Pervaporation of Organics in Polymer Membranes. *Journal of Membrane Science*, 44, 161-181.

Zhu, C.L., Yang, C.W., Fried, J.R., Greenberg, D.B. (1983). Pervaporation Membranes - A Novel Separation Technique for Trace Organics. *Environmental Progress*, 2, 132-138.

Zhang, S.Q., Fouda, A.E., Matsuura, T. (1992). A Study on Pervaporation of Aqueous Benzyl Alcohol Solution by Polydimethylsiloxane Membrane. *Journal of Membrane Science*, 70, 249-255.

Zielinski, J.M., Duda, J.L. (1992). Predicting Polymer-Solvent Diffusion Coefficients using Free Volume Theory. *Journal of the American Institute of Chemical Engineering*, 38, 405-415.